Integrated heat, air, moisture and pollutant (IHAMP) modeling, Part I: State-of-the-art HAM models of building constructions

EBC

Energy in Buildings and Communities Programme

Integrated Heat, Air, Moisture and Pollutant (IHAMP) Modeling

A simulation tool for indoor air qualty design and control in buildings

PART I: State-of-the-art HAM models of building constructions

Dr.ir. Jos van Schijndel, Supervisor

Sander Goesten, (MSc student)

Eindhoven University of Technology

April, 2016

Inhoud

1. Summary

This report is the PART I of a series of reports for the IEA EBC Annex 68. The overall objective is the development of an Integrated Heat, Air, Moisture and Pollution (IHAMP) model for the built environment in MatLab/SimuLink and Comsol.

The methodology consists of four steps:
Step 1. Benchmark existing state-of-the-art HAM models of building constructions using Comsol.
Step 2. Benchmark existing state-of-the-art HAMC models of building zones using HAMBase.
Step 3. Integrate concentration modeling in (1) i.e. HAMC for constructions
Step 4. Integrate (2) and (3) using SimuLink for building zones and constructions

PART I presents the results of Step 1. Benchmark existing state-of-the-art HAM models of building constructions using Comsol.

2. Appendix MSc Report Sander Goesten

Technische Universiteit Eindhoven University of Technology

Hygrothermal simulation model: Damage as a result of insulating historical buildings

Author:
A.J.P.M. Goesten
0830241

Supervisors:
dr. ir. H.L. Schellen
dr. ir. A.W.M. van Schijndel
ir. K. Kompatscher

Master Thesis
Unit **Building Physics and Services (BPS)**
Master **Architecture, Building and Planning (ABP)**
January 2016

Preface

This is my master thesis for the study at the unit Building Physics and Services of the Eindhoven University of Technology. In this report, a hygrothermal simulation model is described and validated which addresses the damage types that may result after insulating historical buildings.

I would like to thank my supervisors dr.ir. Henk Schellen, dr.ir. Jos van Schijndel and ir. Karin Kompatscher for their guidance during this project. Also, I would like to thank all my family members for their support and all my fellow students who collaborated with me during my study.

Summary

Many historical buildings are insulated to improve thermal comfort and to decrease the energy demand. In several cases, the insulation can only be applied at the internal side of the existing construction to preserve the historical appearance. However, insulating historical buildings may result in damage, such as: condensation, mold growth, frost damage, salt damage and thermal cracks. However, thermal cracks are not discussed in this report.

Condensation may cause damage to paint or wallpaper. Condensation occurs when the vapor pressure exceeds the saturation pressure. Condensation can occur at the surface of a construction or inside the construction.

Molds in a building increase the risk of adverse health effects, respiratory symptoms, respiratory infections and allergic sicknesses. Mold can survive dry situations, but only grows when the surface relative humidity is above a certain threshold, which is 80% or higher for the indoor mold species. Wood rotting fungi are the main cause of wood decay. The wood rotting process by fungi requires a relative humidity at the surface of the wood higher than 95% or a moisture content of the wood higher than 20 mass percent.

Frost damage occurs when the moisture in the capillary pores of the material freezes and the volumetric moisture content is above 91%. This causes a high mechanical tension in the material, which can cause micro cracks when this pressure exceeds the tensile strength of the material. Frost damage occurs after several freeze-thaw-cycles.

Physical salt damage occurs when salts crystallize inside the material which causes a pressure higher than the tensile strength of the material. An accumulation of micro cracks occurs due to crystallization-dissolution-cycles of the salts.

In this report, a hygrothermal simulation model is developed and validated which addresses the damage types that may result after insulating historical buildings. This simulation model is described in the manual *Heat, Air and Moisture transport in Building Constructions* version *2015* (HAM-BC 2015). The manual is added in Annex A.

The validation of HAM-BC 2015 has been validated by three means, namely with the HAMSTAD-benchmarks, empirical validation with measured data from a French climate chamber study, and empirical validation with measured data from a historical school building in Estonia.

INDEX

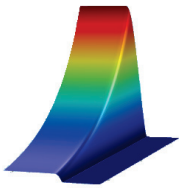

Nomenclature

a_w	water activity [-]
c	specific heat capacity [J/(kg·K)]
c_l	specific heat capacity of liquid water [J/(kg·K)] ≈ 4200 (J/kg·K)
c_p	specific heat capacity of air [J/(kg·K)]
D_v	diffusion coefficient [m^2·s]
e	stored heat per unit volume [J/m^3]
E	irradiation [W/m^2]
g	gravity [m/s^2] = 9.81 m/s^2
g	mass flux of moisture [$kg/(m^2·s)$]
g_a	air flux in mass [$kg/(m^2·s)$]
g_v	water vapor flow rate [$kg/(m^2·s)$]
h	height [m]
h_c , h_i , h_e	(combined) surface coefficient of heat transfer [$W/(m^2·K)$]
h_{cv}	surface coefficient of convective heat transfer [$W/(m^2·K)$]
h_r	surface coefficient of radiative heat transfer [$W/(m^2·K)$]
k_a	air permeability [kg/(s·m·Pa)] ~ [s]
k_m	moisture permeability [kg/(s·m·Pa)] ~ [s]
L	latent heat [J/kg] = evaporation $2.5·10^6$ J/kg
Le	Lewis number [-]
Lp_c	logarithmic capillary pressure [Pa]
M_g	molar weight [kg/mol]
M_w	molar weight of water [kg/mol] = 0.018 kg/mol
p_a	air pressure [Pa]
p_c	capillary pressure [Pa]
p_r	protective pore ratio [-]
p_s	water vapor pressure of solution [Pa]
p_{sat}	saturation pressure [Pa]
p_v	vapor pressure [Pa]
p_w	water vapor pressure of pure water [Pa]
q	heat flux [W/m^2]
Q	quantity of heat [J]
r	radius [m]
R	universal gas constant [J/(kg·K)] = 8.314 J/(kg·K)
R_a	gas constant of dry air [J/(kg·K)] = 287.1 J/(kg·K)
R_h	horizontal rainfall intensity [$l/(m^2·h)$]
RH	relative humidity in [%]
R_v	gas constant of vapor [J/(kg·K)] = 462 J/(kg·K)
R_{wdr}	wind-driven rain intensity [$l/(m^2·h)$]
t	time [s] or [h]
T	temperature [°C] or [K]
U	wind velocity [m/s]
w	moisture content [kg/m^3]
w_{cap}	capillary moisture content [kg/m^3]
x, y, z	direction [-]

α	absorption factor [-]
β_{air}	air convection exchange coefficient [s/m] = 0.1 s/m
β_p , β_i , β_e	surface coefficient of vapor transfer [s/m]
δ_a	vapor permeability coefficient of air [kg/(s·m·Pa)] ~ [s] = $1.8 \cdot 10^{-10}$ s
δ_v	vapor permeability coefficient [kg/(s·m·Pa)] ~ [s]
ε	emissivity factor [-]
η	viscosity of water [Pa·s]
θ	angle [-] or [◦]
λ	thermal conductivity coefficient [W/(m^2·K)]
μ	vapor diffusion resistance factor [-]
ξ	hygroscopic vapor differentiation capacity [kg/m^3]
Ξ	(capillary) moisture differentiation capacity [kg/(m^3·Pa)]
ρ	specific density [kg/m^3]
ρ_a	specific density of air [kg/m^3] = 1.2 kg/m^3
ρ_w	specific density of water [kg/m^3] = 1000 kg/m^3
σ	Stefan-Boltzmann constant [W/(m^2·K^4)] = $5.67 \cdot 10^8$ W/(m^2·K^4)
σ	surface tension of the liquid interface or vapor interface [N/m]
φ	relative humidity in [-]

Subscript

a	air or ambient
e	external / outdoor
i	internal / indoor
inf	infiltration of air
latent	latent heat
rad	radiation
rain	rain
s	surface
sol	solar
t	total

COMSOL Symbols

a	absorption coefficient
c	diffusion coefficient
d_a	damping or mass coefficient
e_a	mass coefficient
f	source term
g	boundary flux/source
n	outward unit normal vector
q	boundary absorption/impedance term
t	time
u	dependent variables
α	conservative flux convection coefficient
β	convection coefficient
γ	conservative flux source
Ω	computational domain

1. Introduction

Monuments and other historical buildings are insulated with the goal to decrease the energy demand and to improve thermal comfort. Applying insulation improves thermal comfort because it prevents low surface temperature and downdraught. Downdraught occurs when air is cooled down by a cold surface, which causes an increase of the air density; and therefore, the vertical velocity accelerates downwards, which leads to thermal discomfort. [Schellen 2010]

To preserve the historical appearance of the facade, in many cases the insulation can only be applied at the internal side of the construction. In the Netherlands, it is generally forbidden to make large changes to the exterior of monuments. However, insulating the external construction at the inside may cause damage to the construction. According to [Schellen and Stappers 2008], [Vereecken 2013] and [Zagorskas et al. 2014], the insulating of historical buildings leads in many cases to damage.

According to [Qiu 2003], around 80% of the damages at the external constructions of buildings are related to moisture; therefore the development of a hygrothermal simulation model is important, because this makes it possible to predict damages to historical buildings. Predictions about the occurrence of damage can aid in finding prevention measures to preserve the historical buildings for future generations.

1.1 Goal

The goal of this research project is the development and validation of a hygrothermal simulation model, which has the ability to determine several indicators related to damage as a result of insulating historical buildings. The damage types which are implemented are condensation, mold growth and wood decay, frost damage and salt damage.

1.2 Methodology

To achieve the goal of this project, it is necessary to gain knowledge about the damage types which may result from insulating historical buildings. The second chapter is a literature study about these damage types, in which damage indicators for condensation, mold growth and wood decay, frost damage and salt damage are defined.

The hygrothermal simulation model is a further development of the model from [Uittenbosch 2012]. A manual of the hygrothermal simulation model is made, which explains how the model is implemented in Matlab and COMSOL Multiphysics. The manual is called **Heat, Air and Moisture transport in Building Construction** version **2015** (HAM-BC 2015). This manual can be found in Annex A.

HAM-BC 2015 is validated with the HAMSTAD-benchmarks by inter-model comparison and analytical verification. Thereafter, the model is empirical validated with the dataset from the climate chamber study described in [Rafidiarison et al. 2015]. Furthermore, HAM-BC 2015 is empirical validated with the dataset from the historical school building in Estonia monitored by [Klõšeiko et al. 2015], which consists of four insulated wall configurations. The damage indicators are determined for the simulated configurations of the historical school building.

1.3 Outline

Chapter 2 describes the damage types which may result from insulating existing envelopes of historical buildings. This includes the determination of several damage indicators related to these damage types. **Chapter 3** explains the general theory behind the hygrothermal simulation model HAM-BC 2015. **Chapter 4** contains the validation of HAM-BC 2015. The validation of the hygrothermal simulation model with the HAMSTAD-benchmarks is described in section 4.1. The empirical validation with the dataset obtained from measurements in a climate chamber in France is described in section 4.2. In section 4.3, the empirical validation of HAM-BC 2015 with the measured dataset from a historical school building in Estonia is shown. **Chapter 5** consists of the conclusions and the recommendations for further improvement or expansion of the hygrothermal simulation model.

Annex A contains the manual for the application of HAM-BC 2015 in COMSOL Multiphysics and Matlab. **Annex B** describes the transformation of the formulas in section 3.1 into the heat and moisture balance equations described in section 3.3. **Annex C** contains additional information and results from the validation of HAM-BC 2015 with the HAMSTAD-benchmarks, which were briefly described and summarized in section 4.1. **Annex D** gives additional information and results about the validation with the dataset from the climate chamber study described in section 4.2. **Annex E** describes more information and results from the validation described in section 4.3, *i.e.* the empirical validation using the measurement data from the historical school building in Estonia.

2. Damage as a result of insulating historical buildings

In this chapter, the damage types are described which may result from insulating existing envelopes of historical buildings, including the physical processes and mechanisms which cause these damages. Damage types related with insulating existing external construction are according to [Vereecken 2013]:

1) Condensation
2) Mold growth and wood decay
3) Frost damage
4) Salt damage
5) Thermal cracks

These five damage types are now discussed shortly. In the other sections of this chapter, the specific types of damages are discussed in more detail.

Condensation can occur at the surface of the construction or within the construction. Condensation may cause material degradation.

Applying insulation decreases the risk of **mold growth**, due to the increase of surface temperature; and therefore, the decrease of the relative humidity at the surface [Schellen 2010]. However, the risk of mold growth increases when the ventilation and infiltration rate is decreased due to air-tightness measures in the renovation project: the result is that the indoor relative humidity increases, because the moisture from indoor sources of water vapor is slower removed. Indoor sources of water vapor are for example people, cooking, shower, laundry and plants. Avoiding thermal bridges is important to prevent mold growth. Internal condensation near a wooden construction increases the chance on **wood decay** by fungi significantly. Wood rotting fungi are the main cause of wood decay [Vereecken 2013].

The risk of **frost damage** may increase with the use of internal insulation, which leads to the situation that the external wall becomes colder and the drying process will be slowed down during the winter, which leads to an increase of the amount of freeze-thaw-cycles. According to [Hens et al. 2007], frost damage occurs rarely, and can be easily prevented by the implementation of materials which are not frost sensitive. However, the materials of many historical buildings are not tested on frost sensitivity; and therefore it must be assumed that frost damage may occur.

Building materials with a high concentration of salt solutions are vulnerable to **salt damage**. By the evaporation of the liquid in the solution, the dissolved salt will crystallize. If the salt crystallization occurs inside the material, this can cause a pressure of several hundred bars, which can cause physical damage [Voerman 2013].

The risk on **thermal cracks** increases when the insulation is applied at the internal side of the construction or when the cavity is filled with insulation [Meeusen 2006]. However, thermal cracks will not be discussed in this report.

Explanatory remark: If the reference is placed just before the dot of a sentence, the reference is used for the sentence. When a reference is located under a paragraph, the reference is used for the information in the whole paragraph.

Location of the insulation

There are three ways to insulate an existing construction, namely applying the insulation at the external side, filling an existing cavity with insulation or applying insulation at the internal side of the construction. Each choice has its advantages and disadvantages.

Thermal bridges can occur in all three cases. Thermal bridges are parts of the construction where the insulation layer is interrupted or where the thermal resistance of the construction is significantly lower than the thermal resistance of the rest of the construction. According to [Stappers and Schellen 2011], the negative consequences of thermal bridges are:
a) Increase of heat loss.
b) Lower surface temperatures at the inside; therefore, higher relative humidity at the surface with higher chance of condensation and mold growth.
c) Temperature difference between the thermal bridge and the rest of the construction, which may lead to thermal cracks.

Also, it is important to prevent air gaps or cracks between the insulation material and the construction, because this increases the transmission losses of the wall. [Vereecken 2013] found U-values which were 2.5 times higher than expected, caused by the air flows in the air gaps. It is important that the insulation is applied thoroughly, because when air can flow behind the insulation layer, than the insulation layer will be disabled, because this air flow causes convection and leads to higher heat loss [Stappers and Schellen 2011]. Many moisture problems are related to convective vapor transport of the humid air which transports from inside to outside [Stappers and Schellen 2011]. When there are air cracks or air gaps between insulation parts, than the hot humid indoor air may flow easy and condensate on cold surfaces.

External Insulation

The Dutch monument regulations mostly forbid major changes to the outside appearance of monuments, which makes applying insulation at the outside of the existing construction in many cases not possible. Monuments with plasterwork on the outside are in many cases allowed to be insulated at the outer surface of the construction, because the appearance can be retained if the same kind of plaster with the same color is applied [Schellen and Stappers 2008]. External insulation has the disadvantage that the thickness of the construction at the outside is increased, which makes it sometimes necessary to change the details at the roof and the windows [Voerman 2013].

An advantage of applying insulation material at the outside is that the heat accumulating ability of the construction is preserved, which means that the indoor air temperature will fluctuate less in the summer. During the winter, the chance of internal condensation or moisture accumulation in the construction decreases. Also the chance of thermal cracks in the original construction will decrease, because the temperature of the construction will be more constant due to the insulation layer at the outside. [Voerman 2013]

Cavity Insulation

The cavity wall was introduced in the 1930s as a solution against rain penetration. Before the 1970s the cavity was not filled with insulation material. According to [Meeusen 2006], by filling an existing empty cavity wall with insulation, the chance on frost damage and thermal cracks will increase, because the external wall has a lower average temperature in the winter and a higher temperature in the summer than before insulating. Also, the temperature of the external wall will fluctuate more. [Meeusen 2006] [Aarle 2013]

According to [Meeusen 2006], there will be no damage occurring from filling the existing air cavity, when two conditions are met. The first requirement is that the outer skin of the construction must not show signs of frost damage. The second requirement is that the outer skin of the construction must not be a vapor barrier by the appliance of wall tiles or glazing. [Meeusen 2006]

Cavity ventilation does have insignificant effect on the removal of water vapor. [Meeusen 2006] concluded that a ventilated cavity is not required, except when the external leaf of a cavity wall has a vapor barrier on the outside, such as tiles, glazing or certain vapor-tight paint. According to [Meeusen 2006], cavity ventilation has little effect on the drying process of the outer leaf of the wall construction. [Hens et al. 2007] state that the cavity ventilation in a cavity wall has no real purpose relating the moisture tolerance, because a complete fill of a cavity wall is equally moisture tolerant as a partial fill. Some reports and articles state the opposite and are referring to imbibition experiments where a wall is subjected to water in a box; however, a normal façade is not subjected to these boundary conditions in reality, but is only subjected to rain [Hens et al. 2007]. According to [Meeusen 2006], there is no reason against the filling of existing cavity walls if the material of the wall is frost resistant.

Internal Insulation

According to [Voerman 2013] and [Zagorskas et al. 2014], in many cases of insulating historical buildings, it is chosen to place the insulation at the interior side of the wall, for preserving the historical appearance of the facade. By insulating an existing envelope at the inside, the temperature of the masonry fluctuates more throughout the year than before the appliance of the insulation. This means that the wall is subjected to more shrinkage and expansion than before, which increases the chance of thermal cracks [Vereecken 2013] [Stappers and Schellen 2011].

By insulating at the inside, the masonry will be colder in the winter, because the heat from the indoor environment is subjected to a larger thermal resistance. This decreases the drying process in the winter, which causes a higher moisture content of the masonry [Stappers and Schellen 2011] [Zagorskas et al. 2014]. The increased moisture content and the lower temperature increase the risk of frost damage [Schellen et al. 2008]. With the increase of the moisture content, it is possible that wood decay will occur at wooden beam ends of floors or wood rot of wooden window frames [Stappers and Schellen 2011] [Zagorskas et al. 2014].

Indoor environment

The renovation of buildings may be accompanied with changes in the indoor environment by different heating, ventilation and air conditioning systems or different temperature and relative humidity set points. These changes may influence the boundary conditions of the construction. In the past the heating was done by fireplace or other primitive forms of heating, which have all in common that thermal comfort was mainly achieved by radiant heat. Nowadays, most heating systems heat up the entire air mass in the room with radiators or convectors, which lead to convective air flows. Convection is caused by the fact that hotter air has a smaller density than colder air, whereas air with low density (hot air) flows to the areas with higher densities (cold air). [Monumentenwacht 2014]

According to [Schellen 2010], the requirements for the conservation of the Dutch *Rijkscollectie* in museums are:

- Relative humidity between 48% and 55%
- Air temperature between 20°C and 25°C
- Air temperature fluctuations smaller than 3°C per day

The four damage types which are discussed in this report are further explained in the next sections of this chapter.

2.1 Condensation

Condensation can occur at the surface of a construction or inside a construction. Condensation occurs when the vapor pressure (p_v) exceeds the saturation pressure (p_{sat}) – in other words: when the relative humidity is 100%. The saturation pressure is dependent of the ambient or the surface temperature. The equation for relative humidity is:

$$\text{Relative Humidity} = \frac{p_v}{p_{sat}} \cdot 100\% \tag{2.1}$$

A specific type of internal condensation is the so-called *summer condensation*. Summer condensation happens when the wet wall is dried by solar irradiation, whereas the temperature of the external side will increase, which leads to an inward moisture flux. If the vapor resistance of a layer at the inside of the construction is too high, than summer condensation may occur between the insulation layer and the vapor retarding layer. By vapor tight insulation material – such as XPS – no summer condensation will occur, because the insulation layer acts like a vapor barrier in both directions. [Vereecken 2013]

The Glaser method is a commonly used method to determine if a certain construction is sensitive for internal condensation. However, the Glaser method has some flaws. According to [Vydra 2007], [Ramos et al. 2010], [Magrini et al. 2014] and [Mumovic et al. 2006], the flaws of the Glaser method are:

a) the use of one-dimensional calculations;
b) the use of constant boundary conditions (steady state);
c) the fact that the Glaser method only takes vapor diffusion into account and disregards convective vapor transport;
d) the neglecting of heat transfer by convection;
e) the disregarding of sorption, capillary suction and migration of liquid water;
f) the assumption that the liquid moisture is only caused by condensation of water vapor;
g) not taking solar irradiation and rain into account;
h) the disregarding of the dependence of the thermal conductivity on the moisture content. In reality the thermal conductivity changes with changes in moisture content. Also the dependence of the vapor resistance factor on the relative humidity is not taken into account;
i) the neglecting of the influence of latent heat on the temperature distribution and the saturation pressures. Evaporation will lead to a sudden temperature drop in the construction. When vapor condenses to water, than the temperature suddenly increases.

By increasing the vapor resistance at the warmer side, the chance on condensation decreases. That is the reason that vapor retarding layers are applied. A rule of thumb is that the vapor retarder must be applied on the warm side. According to [Stappers and Schellen 2011], the water resisting layer on the outside must be more vapor-open than the vapor retarder on the inside. Unintentional perforations of the vapor retarder can lead to a decrease of the effect of the vapor retarder. Moisture problems can also be caused by bad connections between two vapor retarders or between a vapor retarder with another construction. [Voerman 2013]

It is possible that by insulating a historical building at the inside of the construction, the chance of condensation on the external surface increases, because the internal insulation shields off the external surface from the (commonly) higher indoor temperature. Hence the external surface temperature can be lower than before the appliance of insulation. This dew phenomenon is caused by a low outdoor temperature and the emission of long wave radiation

between the construction surface and the sky during night [Aelenei and Henriques 2008]. Dew occurs during the night, because there is no solar irradiation which balances out the radiation losses [Ramos et al. 2010]. According to [Aelenei and Henriques 2008] and [Camuffo and Giorio 2002], only constructions facing largely the sky have this dew problem.

2.2 Mold Growth

In general, applying insulation and increasing the air tightness makes it more difficult for mold to grow, because those measures increase the indoor surface temperature, and so the relative humidity decreases. However, the chance of mold growth will increase when the moisture generated by the occupants is not sufficiently extracted from the indoor environment. [Viitanen et al. 2010]

The dampness in a building promotes the growth of mold, dust mites and insects. [Mudarri and Fisk 2007], [Singh et al. 2010] and [Adan and Samson 2011] state that dampness increases the risk of adverse health effects, respiratory symptoms, respiratory infections and allergic sicknesses. The World Health Organization showed that approximately 25% of the social housing dwellings in Europe are exposed to increased health risks related to indoor molds, *i.e.* 45 million occupants. Approximately 4.6 million of the 22 million US asthma cases in 2007 were related to dampness. According to [Adan and Samson 2011], 15% of the Dutch building stock has problems with mold. Approximate 20% of the social housing building stock in Belgium has problems with mold, while in Germany this was about 30% and in the United Kingdom was between 20-25%. In the coastal region of Israel there were mold problems in approximate 45% of the dwellings. [Adan and Samson 2011]

Suitable environment for mold growth

More than 100,000 species of fungi are known, of which around 100-150 species can be found indoors. Indoor molds can only grow on the surface of materials, with the exception of the wood degrading species of basidiomycetes. [Adan and Samson 2011]

According to [Adan and Samson 2011] and [Vereecken and Roels 2012], there are several conditions required for mold growth:

1) Infection by fungal spores
2) Optimal surface temperatures, because molds cannot regulate their internal temperature
3) Sufficient nutrients in the substrate
4) Suitable moisture conditions
5) No fungi-killing substances
6) Suitable PH
7) Enough oxygen

Temperatures, substrate, spores, PH and oxygen are almost always sufficient available for mold growth in heated buildings. Indoor mold species can grow with the temperature range which is considered comfortable for building occupants. Mold can find a suitable substrate even on materials with a low porosity – such as glass and metal – when there is dust accumulated on the material surface. [Menetrez and Foarde 2003] and [Singh et al. 2011] state that large amounts of molds can be found in humidifiers, air conditioning units and ventilation ducts when they are not sufficient cleaned. Therefore, it is assumed in this report that there is everywhere sufficient substrate for mold growth.

The spores of fungi are transported by air currents, rain, insects and transport of goods [Harris 2001]. The spores infest a substrate and produces hyphae. The hyphae become a mycelium

which creates spores. A colony of *Serpula lacrymans* with a surface area of one square meter can produce 50 million spores per minute during several days. [Bos and Hesselink 1996]

Moisture is the only mold growth condition which can be addressed in heated buildings. Almost all indoor molds have a condition of growth between the RH-range of 80% to 100% [Adan and Samson 2011].

Instead of relative humidity, the variable *water activity* is used in biologic science. Water activity gives information about water in liquid form. Water activity ranges from 0 to 1, where 1 is pure water. Water activity can only be measured directly when the solution is in equilibrium with the ambient air. In the case that equilibrium exist between the air and the solution and no net transfer of water exist between solution and air, the relative humidity is the same as the water activity. [Adan and Samson 2011]

$$a_w = \frac{p_s}{p_w} \tag{2.2}$$

a_w = water activity [-]
p_s = water vapor pressure of solution [Pa]
p_w = water vapor pressure of pure water [Pa]

Growth rate isopleths of two molds are shown in figure 2.1. Isopleths are contour plots of growth rates of molds as a function of temperature and humidity – depicted in relative humidity or in water activity – under steady state conditions. Many molds have their optimal growth rate at a water activity larger than 0.90. [Adan and Samson 2011]

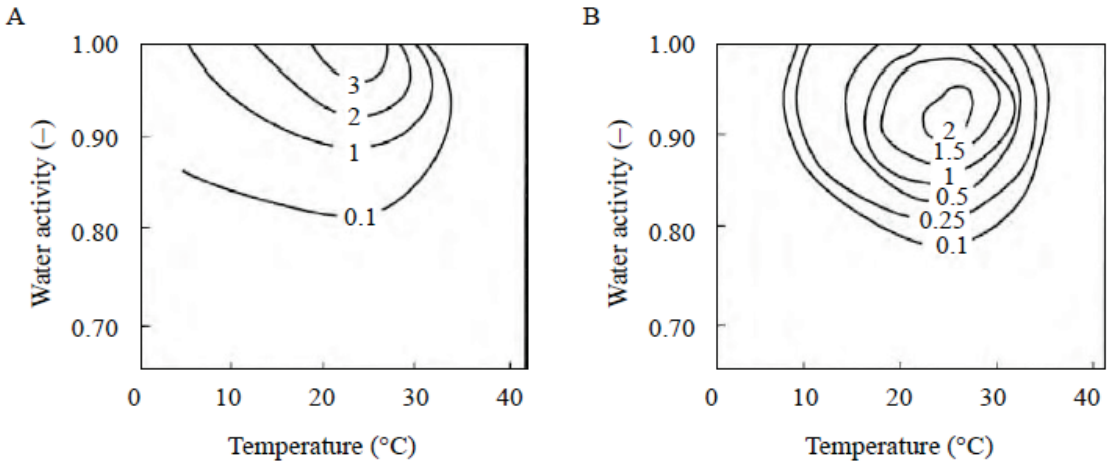

Figure 2.1: Mold growth of (A) Penicillium martensii and (B) Aspergillus versicolor on agar as a function of water activity and temperature. The numbers at the isopleths are in mm/day. Source: [Adan and Samson 2011]

Mold will stop growing when the relative humidity decreases below the threshold, but the mold does not necessarily die. Mold starts growing again when the threshold is exceeded. Thus short peaks of the relative humidity can cause mold growth. These peaks can be caused by household activities such as showering, cooking, cooling and heating. For example, the fungi *Cladosporium cladosporioides* can start growing again after one hour following two weeks of relative humidity below the threshold. [Adan and Samson 2011]

[Viitanen and Ojanen 2007] state that the temperature range 0°C - 50°C is suitable for mold growth. According to [Viitanen and Ojanen 2007], the RH-threshold can be described with the equation:

$$\begin{cases} \mathrm{RH_{crit}} = -0.00267 \cdot \mathrm{T}^3 + 0.160 \cdot \mathrm{T}^2 - 3.13 \cdot \mathrm{T} + 100 & for \;\; T < 20℃ \\ \mathrm{RH_{crit}} = 80\% & for \;\; T \geq 20℃ \end{cases} \tag{2.3}$$

[Hens 1999] considered the equation:

$$\mathrm{RH_{crit}} = 0.033 \cdot \mathrm{T}^2 - 1.5 \cdot \mathrm{T} + 96 \tag{2.4}$$

The equation for the critical relative humidity of [Viitanen and Ojanen 2007] is based on several fungi species when grown on a wooden substrate. The equation of [Hens 1999] is based on the mold *Aspergillus versicolor*, which has the lowest isopleth for germination of all molds which are commonly found indoors. Both equations are plotted in figure 2.2.

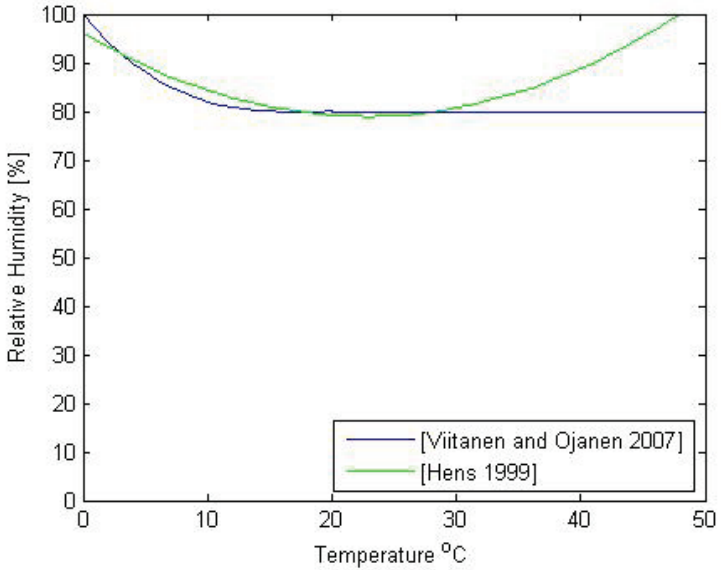

Figure 2.2: Isopleths based on [Viitanen and Ojanen 2007] and [Hens 1999].

The damage indicator for mold growth in HAM-BC 2015 will be the percentage of time that the relative humidity exceeds the 80%. In comparison with [Viitanen and Ojanen 2007] and [Hens 1999], the mold growth will be overestimated in the temperature range below 20°C.

Temperature Ratio

The RH-threshold is defined in the IAE-Annex 14 as the surface relative humidity which is based on the conditions for mold growth of the specie *Aspergillus versicolor,* because it has the lowest isopleths. The temperature ratio is based on this mold specie. When the temperature ratio is higher than 0.7, than the mold risk is considered below 5%.

$$\text{Temperature Ratio} = \frac{T_{surface} - T_{external}}{T_{internal} - T_{external}} \tag{2.5}$$

According to [Vereecken 2013], the temperature ratio does not take into account:

- Wind driven rain
- Capillary moisture transport
- Ventilation rate
- Internal moisture production
- Convective vapor transport
- Transient boundary conditions

A temperature ratio of 0.73 is consistent with the value based on an 80% threshold of relative humidity, when using January conditions in the Netherlands [Adan and Samson 2011]. However, the Dutch regulations demand a minimal value of 0.65, which is lower than the value corresponding to a relative humidity of 80%. According to [Vereecken 2013], the temperature ratio underestimates the risk on mold growth.

Time-of-Wetness

Mold does not necessarily die when the relative humidity is below the threshold value, but starts growing again when the threshold is exceeded again. [Hens 1999] states that mold growth was found when only 10% of the time during a measurement period of 30 months was higher than 80%. Hence, humidity peaks cannot be neglected. For this reason the Time-of-Wetness (TOW) is defined, which is the amount of time that the relative humidity is higher than the RH-threshold divided by the total cycle time of 24 hours.

$$\mathrm{TOW} = \frac{\text{cyclic period (RH} \geq 80\%)}{\text{cyclic period (wet + dry)}} \tag{2.6}$$

A TOW-value of 0.2 has the meaning that the relative humidity is 4.8 hours above the RH threshold in 24 hours. No real criterion is defined about the TOW-value, but a TOW below 0.5 retards the mold growth significantly. [Vereecken and Roels 2012] [Hens 1999]

Wood Decay

The rotting process of wood can be caused by fungi, bacteria and insects. Applying insulation at an existing construction can lead to an increase of periods which are suitable for growth of wood rotting fungi. Bacteria and insects are not significantly affected by applying insulation at existing constructions. Bacteria can attack the wood when there is a very low oxygen level, but when only bacteria attack the wood, it can take more than 100 years to rot the wood under anaerobic conditions [Adan and Samson 2011]. The typical time to decay of several wood-rot fungi and bacteria are depicted in figure 2.3. Fungi are the most important causes of wood decay, because molds are capable of degrading cellulose and lignin, while bacteria cannot destroy lignin [Bos and Hesselink 1996]. Wood exists of 40% to 60% of cellulose, 10% to 30% is made of hemicelluloses and 15% to 30% exists of lignin [Bos and Hesselink 1996]. According to [Klaassen 2014], wood decay by erosion bacteria is important for wooden foundation piles where there is a very low oxygen level and large liquid water movement in the piles. However, foundation piles are not discussed in report, but only insulating the external constructions of historical buildings.

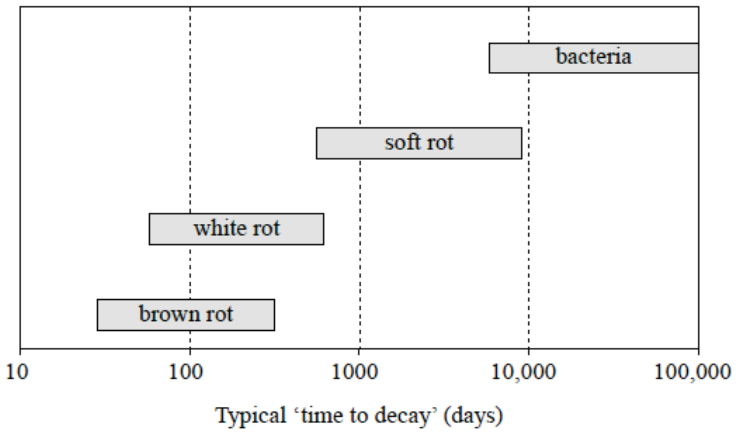

Figure 2.3: Typical "time to decay" of several wood decay types. Soft rot, white rot and brown rot are caused by fungi. Source: [Adan and Samson 2011]

According to [Morelli and Svendsen 2013], the critical moisture content for the start of wood decay by fungi is 0.2 kg/kg. According to [Viitanen et al. 2010], wood decay occurs with mass moisture contents above 25% with a temperature between 0°C and 45°C. According to [Adan and Samson 2011], brown rot on pine wood and spruce sapwood is initiated when the moisture content is higher than 25% or if the relative humidity at the surface of the wood is higher than 95%. Wood rot only occurs when the wood is wet. Wood rotting mold can survive dry situations, but only attacks the wood when it becomes wet [Adan and Samson 2011].

Every type of mold needs a humid environment, even the so-called *dry rot fungi*. The "dry rot" refers to the fact that these molds absorb the moisture from the vicinity of the material surface. Therefore, the material surface is dry. This has led to the wrong conclusion that dry rot fungi do not require a humid environment, but nowadays it is known that dry rot fungi has the same humidity requirements. [Adan and Samson 2011]

The growth of the mycelia has not to be necessarily on the same location as the humid area. According to [Bos and Hesselink 1996], *Serpula lacrymans* are in many cases found at 250 centimeters distance from their moisture source. An extreme example, the fungus *Serpula lacrymans* can grow from the moisture in a cellar, but destroys wood on the second floor [Adan and Samson 2011].

[Bos and Hesselink 1996] draw attention to the fact that several historical buildings have no crawl spaces under their wooden ground floor, which permits the ground water for reaching the underside of the ground floor, thus increasing the risk on wood decay.

Prevention of wood decay

Wood decay can be prevented by using wood preservatives, for example CCA. CCA consist of copper, chromium and arsenic. In certain situations these coatings can aggravate the situation, because they decrease the drying ability of the material. Another disadvantage is that arsenic and chromium enters the environment, because CCA has a leaching rate of 5% in 25 years. Also there are concerns that children get sick when they come in contact with CCA-treated wood. [Adan and Samson 2011]

[Morelli and Svendsen 2013] investigated a possible solution for prevention of wood decay of wooden beam ends in masonry when the building is insulated. Their solution was to make a gap in the insulation at the level of the wooden beam end, so that the drying process of the wood and masonry was not changed. This leads to a lower humidity at the wooden beam end. However, without insulation at the beam end the transmission loss was increased 2 to 3 times.

It is advised by [Stappers and Schellen 2011] that ground floors are insulated at the underside of the floor, because this increases the temperature of the wooden beams of the existing floor, which decreases the risk of mold growth and wood decay. Besides, this leads to the possibility to ventilate the crawl space. When the insulation material is applied to the soil of the crawl space, it is not possible to ventilate the crawl space, because in that case the effect of the thermal resistance of the insulation material is reduced to zero. [Stappers and Schellen 2011] advise to apply a plastic foil on the soil of the crawl space, because this prevents the evaporation of soil moisture.

Damage indicators for damage by fungi

The damage indicator for mold growth will be the percentage of the time that the relative humidity of the internal surface exceeds the 80%. Wood decay will be indicated by the amount of

time that the relative humidity of the wood surface exceeds the 95% or when the moisture content of the wood exceeds the 20 mass percent.

2.3 Frost Damage

Frost damage occurs when the moisture in the capillary pores of the material freezes. The density of H_2O decreases when it is freezing, which leads to a volume increase of 9%. When the volumetric moisture content is below 91%, than the volume increase of H_2O can be "absorbed" by the empty pores. An internal pressure on the surface of the pores occurs when there are no unfrozen voids which can "absorb" the volume change. This occurs when the volumetric moisture content is above 91%. Micro cracks are developed when the hydraulic pressure exceeds the tensile strength of the material. Hydraulic pressures can be caused by the volume increase by ice formation, stress due to supercooling, pressures at the interfaces between ice and water and also stresses between ice crystals of different sizes. It takes a couple of freeze-thaw cycles before frost damage occurs. Frost damage is not a fatigue mechanism, but a summation of micro damages caused by the preceding freeze-thaw cycles. Frost damage leads to a decrease of the material strength and decrease of adhesion. Examples of frost damage are cracks, spalling and chipping of the surface, stone splinters, swelling and bending of material. Frost damage at reinforced concrete can lead to steel corrosion. [Aarle 2013] [Bekke 2001] [Pakkala et al. 2014] [Kruschwitz and Bluhm 2005] [Scherer 2006]

Figure 2.4: Example of frost damage of masonry.

The surface tensions in surrounding pore walls are larger in a smaller pore than in a bigger pore; therefore, a higher pressure occurs inside the smaller pore. Hence the freezing temperature in a smaller pore is lower than a bigger pore [Kruschwitz and Bluhm 2005]. The water in the relatively bigger pores will freeze first. The volume increase by the phase change will increase the pressure in the other pores. Above a certain maximal pressure (p_{max}) also the water in the small pores will freeze [Bekke 2001].

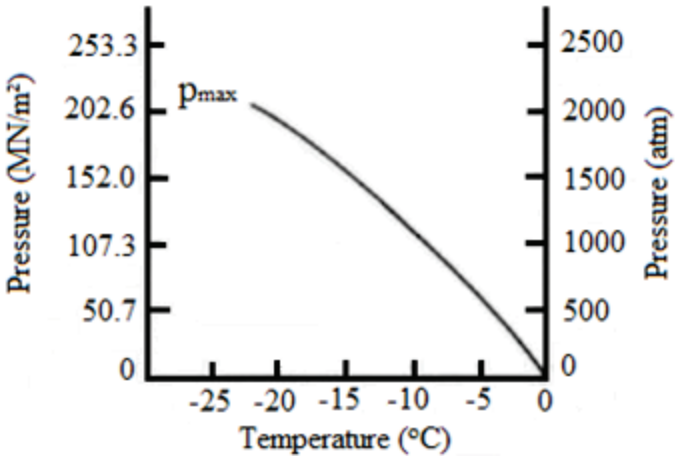

Figure 2.5: Ice pressure as function of temperature. Source: [Bekke 2001]

An increase of the concentration of dissolved salts in the liquid pore water lowers the freezing point, because osmotic pressure will occur [Lisø et al. 2006] [Pakkala et al. 2014].

When the average pore radius is below 0.65 micrometer than the material is sensitive for frost damage. When the average pore radius is between 0.65 and 1.65 micrometer than it is not certain if or if not the material is sensitive to frost damage. When the average pore radius is larger than 1.65 micrometer, than the material is considered frost proof [Bekke 2001]. Frost damage does not occur when the material is frost proof, but the walls of historical buildings are in many cases not frost-proof.

[Cai and Liu 1998] state that there is no significant more damage when the temperature goes below -10°C in comparison with the interval of 0°C and -10°C. The concrete investigated in [Cai and Liu 1998] with a mass ratio of 0.65 sustained 133 freeze-thaw cycles when the lowest temperature was -5°C. The concrete did endure 12 freeze-thaw-cycles before frost damage occurred when the lowest temperature was -10°C.

An important parameter is the protective pore ratio. The protective pore ratio (pr) is the ratio between the pores which are not capillary connected and the total pores. According to [Pakkala et al. 2014], after 307 to 400 freeze-thaw-cycles there was frost damage of exposed concrete samples with pr $\leq$ 0.10 when rain or sleet occurred for a maximum of two days before freezing when the temperature is lower than -5°C. For freeze-thaw cycles with temperatures lower than -10°C, it required between 140 to 200 freeze-thaw cycles before frost damage occurred. [Pakkala et al. 2014]

Frost damage will be indicated by the amount of effective freeze-thaw-cycles ($T \leq 0°C \cap w_{cap} \geq 91\%$ volume). The caused pressure increase by freezing and the amount of mass loss will not be implemented in the hygrothermal simulation model.

2.4 Salt Damage

Esthetical and physical salt damage are caused by the crystallization of salts. Efflorescence occurs when salt crystallizes on the material surface which leads to white or gray stains and stripes. When salt crystallizes inside the pores than that is called subflorescence or cryptoflorescence [Bekke 2001] [Pavlíková et al. 2011].

Efflorescence is only an esthetical problem and it can be washed off by the rain. Efflorescence occurs when the evaporation of the water is slower than the supply flux of water for the salt

solutions. *Solution* is the chemical term for a mix of two different chemical substances. The evaporation process causes the salt solutions in the material to be transported to the surface. The salts in the salt solution will crystallize at the material surface when the water in the salt solution evaporates. [Merillou et al. 2012]

Physical salt damage occurs when subflorescence leads to granular disintegration, honeycombing and contour scaling. Granular disintegration occurs when subflorescence occurs near the surface, which causes the detachment of grains of stone. Honeycombing is a type of granular disintegration with a characteristic shape. Contour scaling occurs when entire plaques become detached. Subflorescence occurs when evaporation is faster than the salt migration by for example capillary suction. That is why the salts do not reach the material surface. The salts crystallize in the pores, which generates internal mechanical stresses higher than the tensile strength. This causes cracks under the surface and the detachment of stone grains or entire plaques. [Merillou et al. 2012] In figure 2.6, the four types of salt damage are shown.

Figure 2.6: Photographs of salt damages: (a) thin efflorescence, (b) granular disintegration, (c) honeycombing and (d) contour scaling. Source: [Merillou et al. 2012].

Salt crystallization of the salt solutions in the materials induces mechanical stresses due to the expansion of the salt crystal volume. Micro cracks occur when the pressure caused by the crystallization of the salts inside the material becomes higher than the tensile strength of the material. There is an accumulation of micro cracks when the salt solutions undergo several cycles of crystallization and dissolution because of wetting and drying cycles. The wetting leads to dissolution, while the drying results in crystallization of salts which are present in the pores. [Watt and Colston 2000] [Fassina et al. 2002] [Kubik and Kucharczyk 2008]

A larger penetration depth leads to more severe damage; however, if the penetration depth is larger, than it takes more time before damage occurs, due to the fact that the drying process takes more time than the drying process near the surface [Hees and Brocken 2004]. Only salts which have a significant volume change cause damage. [Pavlíková et al. 2011] state that most physical salt damages are caused by sulfates, nitrates and chlorides. But even non-destructive salts can cause efflorescence.

A crucial variable which influences salt crystallization is the ambient relative humidity. Soluble salts will take up moisture from the air when the ambient relative humidity exceeds the equilibrium value of relative humidity of that specific salt. When the ambient relative humidity is below the threshold than the salt will be solid. A relative humidity higher than the threshold relative humidity causes the salt to absorb vapor and will dissolve. When the specific equilibrium relative humidity of the salt is lower than 50%, these salts will not crystallize in normal building indoor environment. When the equilibrium relative humidity is between 50% and 75% these salts crystallize rarely. When the equilibrium relative humidity is above 75% than the salt will crystallize easily. [Watt and Colston 2000] [Pavlíková et al. 2011]

Salinity and critical relative humidity

Salt damage depends on three physical properties of the material: salt content, porosity and mechanical strength [Merillou et al. 2012]. Salts in a material can be inherent in the material; deposited by rising damp; originating from salts used to de-ice roads; formed by reaction with atmospheric pollutants or created by the metabolic activity of microbes [Scherer 2004]. Another term for salt content is salinity. According to [Voerman 2013], historical masonry has in many cases inherently a high concentration of sulfates. [Pavlíková et al. 2011] state that the behavior of a salt in a porous material depends on the moisture content, solubility of the salt, temperature and humidity.

A classification of salinity has been determined in the project EUREKA EU-1270, which distinguishes five different salinity classes. The percentages by mass related to these classes are depicted in table 2.1. The *percentage by mass* is the mass of the salts divided by the mass of the total solution. These are according to [Pavlíková et al. 2011]:

Class 0: Very low concentration of salts: No harm for masonry.
Class 1: Low salinity: Small danger of damage.
Class 2: Medium salinity: The life time of plaster and paint are slightly reduced.
Class 3: High salinity: The life time of paint and plasters are significantly reduced. The salt content causes wet areas on the wall.
Class 4: Extreme high salinity: The construction is expected to be damaged in a very short time.

Table 2.1: Classification of salinity in mass percentages. Source: [Pavlíková et al. 2011].

Salt	Class 0	Class 1	Class 2	Class 3	Class 4
Chlorides	0% - 0.01%	0.01% - 0.03%	0.03% - 0.09%	0.09% - 0.28%	> 0.28%
Nitrates	0% - 0.01%	0.01% - 0.05%	0.05% - 0.15%	0.15% - 0.50%	> 0.50%
Sulfates	0% - 0.02%	0.02% - 0.08%	0.08% - 0.24%	0.24% - 0.77%	> 0.77%

The salt content in a material influences the water sorption of the material, which can lead to wet places on the wall surface under influence of the relative humidity. The critical relative humidity – according to [Bekke 2001] – for several salts is shown in table 2.2.

Table 2.2: Salts and their corresponding critical relative humidity. Source: [Bekke 2001].

Salt	Source	RH critical
$MgCl_2\ 6H_2O$	mortar	33%
$CaCl_2\ 6H_2O$	de-icing salt	31%
$K_2CO_3\ 2H_2O$	water glass	43%
$Ca(NO_3)\ 4H_2O$	cement, groundwater	54%
$NaNO_3$	groundwater	75%
NaCl	de-icing salt, groundwater	76%
Na_2SO_4	de-icing salt, air pollution	82%
$MgSO_4\ H_2O$	mortar, air pollution	65%
$MgSO_4\ 7H_2O$	mortar	90%
$NaCO_3$	groundwater	95%
$NaCO_4\ 10H_2O$	de-icing salt, groundwater	94%

The indicator for salt damage in HAM-BC 2015 will be the amount of crystallization-dissolution cycles for the sulfates $MgSO_4$ (H_2O) and $MgSO_4$ (7 H_2O), which have

respectively 65% and 90% as critical relative humidity. Sulfates are chosen because these are main causes for physical salt damage. Salt migration will not be simulated.

2.5 Damage Indicators

The defined damage indicators are:

Condensation is indicated with the percentage of the time that the relative humidity exceeds the 99%. The value 99% is chosen instead of 100% to cope with the inaccuracy of the model and the (measured) input.

Mold growth will be indicated by the percentage of the time that the relative humidity of the indoor surface exceeds the 80%. **Wood decay** will be indicated by the amount of simulation time steps that the relative humidity at the wood surface exceeds the 95% or when the moisture content of the wood exceeds the 20 mass percent.

Frost damage will be indicated by the amount of effective freeze-thaw-cycles ($T \leq 0°C \cap w_{cap} \geq 91\%$ volume). Also, the total freeze-thaw cycles ($T \leq 0°C$) is determined. The pressure increase caused by freezing and the amount of mass loss will not be implemented in the simulation model.

The indicator for **salt damage** will be the amount of crystallization-dissolution cycles for the sulfates $MgSO_4$ (H_2O) and $MgSO_4$ (7 H_2O), which have respectively 65% and 90% as critical relative humidity. Sulfates are chosen because these are main causes for physical salt damage. Salt migration will not be simulated.

The term "*indicators*" is used, because essential and crucial mechanism in the field of physics and biology are excluded, with the result that the model cannot predict damage precisely. Those missing mechanisms or variables are – for example – substrate quality for fungi, amount of fungi spores; ice volume expansion, salinity and tensile strength of materials.

These indicators are implemented in HAM-BC 2015. The next chapter describes the theory behind the hygrothermal simulation model. The manual of HAM-BC 2015 is added in Annex A. The damage indicators are used in section 4.3.

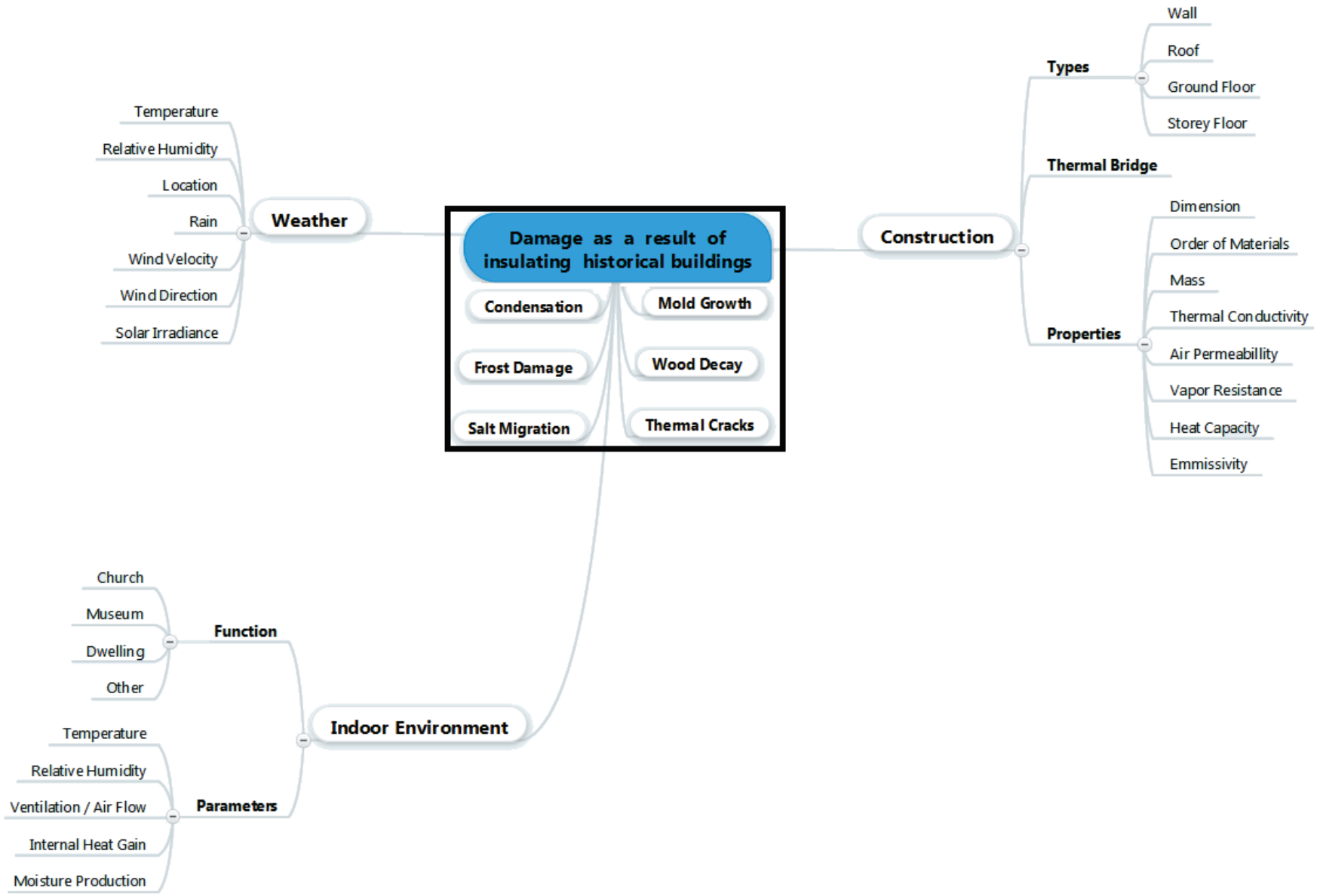

Figure 2.7: Mind map of the damage types as a result of insulating historical buildings and the important parameters related to these problems.

3. Hygrothermal Simulation Model

In this chapter, the general theory behind the hygrothermal simulation model **HAM-BC 2015** is described. HAM-BC 2015 is the abbreviation of **Heat, Air and Moisture transport in Building Constructions** version **2015**. HAM-BC 2015 has the ability to calculate heat transport by conduction and convection inside a material, including the influence of rain, solar irradiation and latent heat related to evaporation and condensation. Additionally, the radiation transfer with other surfaces or the sky can be added, but this is not described in this report. HAM-BC 2015 has the ability to calculate the moisture transfer by diffusion, convection and capillary suction – including the influence of rain. Also the dependence of material properties on the humidity, temperature, and moisture content can be implemented. HAM-BC 2015 can simulate constructions in 1D, 2D and 3D. The implementation of HAM-BC 2015 in Matlab and COMSOL Multiphysics 5.0 is described in Annex A.

The first section of this chapter describes the general physics related to heat, air and moisture transport in building constructions. In the second section, the choice of the potential for the calculation of moisture transport is discussed. The main structure of HAM-BC 2015 is described in section three of this chapter.

3.1 General Physics

This section describes the general physics and general equations for heat, air and moisture transport in building constructions. The equations without references come from [Uittenbosch 2012].

A scalar is a variable with only a value or magnitude, while a vector has a value or magnitude in a certain direction. The change of a certain scalar variable or scalar function in a direction is described by the gradient (grad):

$$\text{grad}\, f = \nabla \cdot f = \left(\frac{\partial}{\partial \text{x}} \cdot f \,, \frac{\partial}{\partial \text{y}} \cdot f \,, \frac{\partial}{\partial \text{z}} \cdot f \right) \tag{3.1}$$

∇ = grad = gradient
f = certain scalar function or scalar variable
∂ = derivative
x = distance in x direction
y = distance in y direction
z = distance in z direction

The equivalent of a gradient for a scalar is for a vector the divergence (div):

$$\text{div}\, f = \nabla \cdot \vec{f} = \left(\frac{\partial}{\partial \text{x}} \cdot f_{\text{x}} + \frac{\partial}{\partial \text{y}} \cdot f_{\text{y}} + \frac{\partial}{\partial \text{z}} \cdot f_{\text{z}} \right) \tag{3.2}$$

∇ = div = divergence
$\vec{f}$ = certain vector function or vector

Air and vapor in building physics can be considered as ideal gasses due to the small temperature and pressure range in building physics [Wit 2009]. For ideal gasses the following equation applies:

$$p = \frac{\rho \cdot R \cdot T}{M_g} \tag{3.3}$$

p = pressure [Pa]
ρ = density [kg/m^3]
R = universal gas constant [J/(mol·K)] = 8.315 J/(mol·K)
T = absolute temperature [K]
M_g = molar mass [kg/mol]

The molar mass (M_g) for vapor is 0.018 kg/mol and the molar mass for dry air is 0.029 kg/mol. By R/M_g, the gas constant of vapor (R_v) is 462 J/(kg·K) and the gas constant of dry air (R_a) is 287.1 J/(kg·K).

Air flux

Convective heat and vapor transport with air as medium in building materials are caused by air pressure differences, whereby the air flows from the location with a higher air pressure to the location with a lower air pressure. These air pressure differences can be caused by temperature differences, because hotter air has a lower density than colder air. Air pressure differences can also be caused by wind. Important factors related to convection are the air permeability of the construction, air pressure differences, temperature differences, wind velocity, building height and external shielding from wind [Al-Homaud 2004]. Infiltration can be caused by wind, which leads to over pressure at one façade, which leads to an air flow from outside to inside. Exfiltration is when the air flows from the indoor environment to the outdoor environment. Convection occurs through building materials, but even more through cracks. [Stappers and Schellen 2011]

$$\vec{g_a} = -k_a \cdot (\text{grad } p_{air} + \rho_a \cdot g) \quad (3.4)$$

$\vec{g_a}$ = air flux [kg/(m^2·s)]
k_a = air permeability [kg/(s·m·Pa)] ~ [s]
p_{air} = air pressure [Pa]
ρ_a = specific density of air [kg/m^3]

The gravity in equation 3.4 is not taken into account in HAM-BC 2015, because it is not applicable in the *Coefficient Form PDE.*

HAM-BC 2015 contains two convection methods: the simple convection method and the sophisticated convection method. The simple convection method uses the total pressure difference between outdoor and indoor as the value for air pressure (p_{air}) in equation 3.4 at each location in the construction. The sophisticated convection method calculates first the local air pressure at each location in the construction and uses this value for the air pressure (p_{air}) in equation 3.4. The sophisticated convection method uses equation 3.5 as boundary condition for the calculation of the air flux. Equation 3.5 is based on the air convection boundary conditions used in Delphin 5:

$$g_a = \beta_{air} \cdot (p_{air\ surface} - p_{ambient\ air}) \quad (3.5)$$

g_a = air flux at surface [kg/(m^2·s)]
β_{air} = air convection exchange coefficient [s/m] = 0.1 s/m
$p_{ambient\ air}$ = air pressure of the ambient air [Pa]
$p_{air\ surface}$ = air pressure inside the material near the surface [Pa]

Contrary to building materials in modern buildings, the materials in historical buildings are in most cases more soft, flexible and porous. Historical constructions have a higher air permeability than modern buildings; therefore, convective moisture transport in historical

constructions can play a more prominent role than in new buildings [Voerman 2013]. The air permeability of a material depends on the amount of pores and the pore structure of the material. Also, the interface between different materials is important for the air permeability [Uittenbosch 2012]. The air tightness of a construction can only be achieved by implementing air tight materials thoroughly, thus by preventing small gaps and perforations [Voerman 2013]. Making constructions more air tight, can be achieved by plastering the inside leaf [Hens et al. 2007].

Heat flux

Heat is the kinetic energy of the molecules [Wit 2009]. Heat transport can occur by conduction, convection and radiation. Conduction is heat transport by molecules that do not move compared to each other in macroscopic viewpoint. Conduction is the same as thermal diffusion. The heat flux by conduction is described by Fourier's law:

$$\vec{q} = -\lambda \cdot \text{grad } T \tag{3.6}$$

q = heat flux [W/m^2]
λ = thermal conductivity coefficient [W/(m·K)]
T = temperature [°C] or [K]

The thermal conductivity coefficient of insulation materials gives the apparent thermal conductivity. In this coefficient also convection and radiation inside the pores of the material are integrated. Thermal insulation materials work by resisting heat flux by the numerous microscopic dead air-cells or cells with fluorocarbon gas. Air-based insulation cannot exceed the thermal resistance of stagnant air. To increase the thermal resistance further, it is necessary to use, for example, fluorocarbon gas in the pores of the insulation material. Plastic foam insulation (EPS and XPS) uses fluorocarbon gas. The dead cells with air or fluorocarbon gas provide the thermal resistance by reducing the conductive, radiation and convective heat transport. The convective heat transfer is decreased because these cells entrap dead air, so preventing any flow through the material. The conductive, radiative and convective heat transfer through the material is described in the (apparent) thermal conductivity coefficient. [Al-Homaud 2004]

The heat necessarily to heat up a material with a mass of 1 kg with 1K is called the *specific heat capacity* or just *specific heat*. A change of the stored heat per unit volume is proportional with the change in temperature:

$$\Delta e = \rho \cdot c \cdot \Delta T \tag{3.7}$$

e = stored heat per unit volume [J/m^3]
c = specific heat capacity [J/(kg·K)]
ρ = specific density [kg/m^3]

Equation 3.7 could be described as an energy balance, which leads to:

$$\rho \cdot c \cdot \frac{\partial T}{\partial t} = -\frac{\partial}{\partial x} \cdot q_x - \frac{\partial}{\partial y} \cdot q_y - \frac{\partial}{\partial z} \cdot q_z \tag{3.8}$$

∂ = derivative
t = time [s]

The combining of equations 3.6 and 3.8 leads to the heat conduction equation:

$$\rho \cdot c \cdot \frac{\partial T}{\partial t} = \text{div } \lambda \cdot \text{grad } T \tag{3.9}$$

The heat storage is not only determined by the dry material itself, but is also determined by the moisture inside the material. The heat storage in the moisture is determined by the moisture content [kg/m^3] multiplied by the heat capacity of water [J/(kg·K)]. This leads to:

$$(\rho \cdot c + c_l \cdot w) \cdot \frac{\partial T}{\partial t} = \text{div}\,\lambda \cdot \text{grad}\,T \tag{3.10}$$

c_l = specific heat capacity of liquid water [J/(kg·K)] ≈ 4200 J/(kg·K)
w = moisture content [kg/m^3]

Heat transfer by convection is heat transport by fluids (liquid and gasses). In this hygrothermal simulation model the convective heat transport by air is taken into account. The influence of the air flux on heat is based on the mass air flux multiplied by the specific heat capacity of air, which describes how much heat energy there is internalized per temperature increase. When heat transport by air convection is included in equation 3.10, the following equations is attained:

$$(\rho \cdot c + c_l \cdot w) \cdot \frac{\partial T}{\partial t} = \text{div}\,\lambda \cdot \text{grad}\,T - c_p \cdot \vec{g_a} \cdot \text{grad}\,T \tag{3.11}$$

c_p = specific heat capacity of air [J/(kg·K)] ≈ 1042 J/(kg·K)
$\vec{g_a}$ = air flux in mass [kg/(m^2·s)]

The specific heat capacity of air is dependent on the pressure – which is depicted in figure 3.1 – where in pores the pressure is higher than in the outdoor and indoor environment. Just as [Uittenbosch 2012], the value 1005 J/(kg·K) is used for the boundary conditions and the value 1042 J/(kg·K) for the convective heat transport in the material.

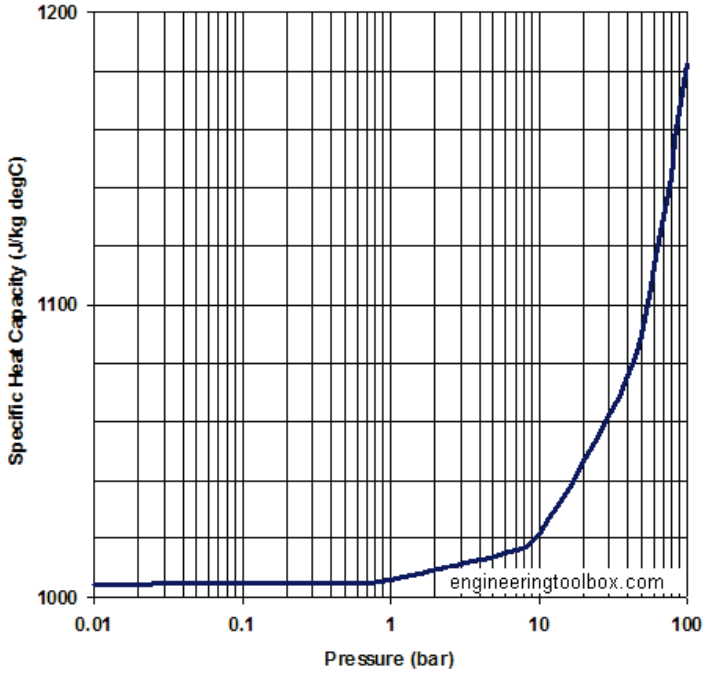

Figure 3.1: Relationship of the specific heat capacity of air [J/(kg·K)] and the pressure [bar]. Source: engineeringtoolbox.com.

Latent Heat

Hitherto, only sensible heat is discussed, *i.e.* heat which humans or sensors can perceive as heat because of the temperature change it causes. Besides sensible heat, there also exists latent heat. Latent heat can be absorbed or transported without causing a temperature change. During evaporation the heat from the surrounding is absorbed by the water, which causes that the sensible temperature is decreased, because sensible heat is converted into latent heat. Latent heat in vapor is transformed into sensible heat when the vapor condensates which cause a (small) temperature increase. When condensation occurs, the latent heat will be transformed in sensible heat. [Wit 2009]

According to [Wit 2009], the latent heat for evaporation at 0°C is approximate $2.5 \cdot 10^6$ J/kg and at 100°C it is approximate $2.26 \cdot 10^6$ J/kg. HAM-BC 2015 uses constant the value $2.5 \cdot 10^6$ J/kg. The evaporation of water causes that sensible heat change into latent heat, which explains the fact that wet surfaces tend to cool down when the water evaporates. To implement the latent heat in the equations, the mass of water vapor must be known. Inserting the latent heat part in equation 3.11, the heat balance equation becomes:

$$(\rho \cdot c + c_l \cdot w)\frac{\partial T}{\partial t} = \text{div}\,\lambda\,\text{grad T} - c_p \cdot \vec{g_a}\,\text{grad T} + L \cdot \text{div}\,\frac{\delta_a}{\mu}\,\text{grad p}_\text{v} - \text{L} \cdot 0.62 \cdot 10^{-5} \cdot \vec{g_a}\,\text{grad p}_\text{v} \quad (3.12)$$

L= latent heat for evaporation and condensation [J/kg] ≈ $2.5 \cdot 10^6$ J/kg
δ_a = vapor permeability of air [kg/(s·m·Pa)] = $1.8 \cdot 10^{-10}$ kg/(s·m·Pa)
μ = vapor diffusion resistance factor [-]
p_v = partial water vapor pressure [Pa]

The latent heat when water freezes or ice melts has the value $3.34 \cdot 10^5$ J/kg; however, this is not taken into account by HAM-BC 2015, because this requires the knowledge of the ice volume fraction. [Aarle 2013]

Boundary conditions heat

HAM-BC 2015 has the ability to simulate boundary conditions related for heat transport including conduction, convection, latent heat, solar irradiance and rain.

$$q_t = h_c \cdot (T_a - T_s) + q_{\text{inf}} + q_{\text{latent}} + q_{\text{rad}} + q_{\text{sol}} + q_{\text{rain}} \quad (3.13)$$

q_t = total heat flux at the surface [W/m^2]
h_c = combined surface coefficient for heat transfer [W/(m^2·K)]
T_a = ambient temperature [°C] or [K]
T_s = surface temperature [°C] or [K]
q_{inf} = heat flux caused by infiltration of air [W/m^2]
q_{latent} = heat flux caused by latent heat [W/m^2]
q_{rad} = heat flux caused by radiation [W/m^2]
q_{sol} = heat flux caused by solar irradiation [W/m^2]
q_{rain} = heat flux caused by rain [W/m^2]

The (combined) surface heat coefficient (h_c) for internal surface (h_i) and external surface (h_e) is the combination of the surface coefficient of radiative heat transfer (h_r) with the surface coefficient of convective heat transfer (h_{cv}). [Wit 2009]

The surface coefficient of convective heat transfer (h_{cv}) is dependent on the difference between air and surface temperature and the air velocity near the surface [Bekke 2001] [Wit 2009]. The relationship between the air velocity near the surface and the value of the surface coefficient of convective heat transfer is depicted in figure 3.2.

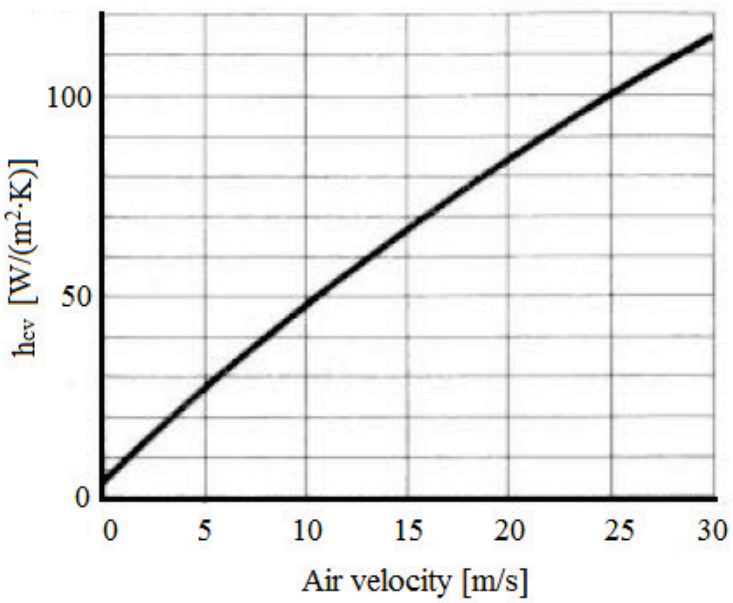

Figure 3.2: Relationship of the air velocity [m/s] near the surface and the surface coefficient of convective heat transfer (h_{cv}) in [W/(m^2·K)]. Based on [Bekke 2001].

Thermal radiation is the heat transport by the propagation of electromagnetic waves. Thermal radiation is related to the thermal movement of molecules. The radiant power emitted, transferred or received is called the radiant flux. The term *irradiance* is used for the radiant flux on a surface. Irradiance [W/m^2] can be absorbed, reflected or transmitted. [Wit 2009]

Solar irradiation is implemented with the equation based on [Li 2008]:

$$q_{sol} = \alpha \cdot E^0_{sol} \cdot \cos(\theta) = \alpha \cdot E_{sol} \tag{3.14}$$

α = absorption factor for solar irradiation [-]
θ = angle between the normal of the material surface and the solar rays (or measurement plane)
E^0_{sol} = solar irradiation to a plane normal of the solar irradiation [W/m^2]
E_{sol} = solar irradiation on a horizontal plane [W/m^2]

Heat transport by radiation between material surface and the sky is not simulated and described in this report. The equations for heat transfer by radiation between the sky and construction surface are described in [Aelenei and Henriques 2008]. The emissivity factor shows to which extent the material emits infra-red radiation. [Stappers and Schellen 2011]

According to [Uittenbosch 2012], the heat flux caused by **rain** is described by:

$$q_{\text{rain}} = \vec{g}_{\text{rain}} \cdot c_l \cdot (T_{\text{rain}} - T_s) \tag{3.15}$$

q_{rain} = heat flux caused by rain [W/m^2]
g_{rain} = rain flux [kg/(m^2·s)]
c_l = specific heat of liquid water [J/(kg·K)] ≈ 4200 J/(kg·K)
T_{rain} = temperature of rain [°C] or [K]
T_s = surface temperature [°C] or [K]

The heat boundary condition for **infiltration of air** is:

$$q_{\text{inf}} = c_p \cdot \vec{g_a} \cdot (\text{T}_a - \text{T}_s) \tag{3.16}$$

q_{inf} = heat flux by infiltration of air [W/m^2]
c_p = specific heat capacity of air [J/(kg·K)] = 1005 J/(kg·K)
$\vec{g_a}$ = air flux in mass [kg/(m^2·s)]
T_a = ambient temperature [°C] or [K]
T_s = surface temperature [°C] or [K]

The boundary condition related to **latent heat** for diffusion and convection is:

$$q_{\text{latent}} = L \cdot \beta_p \cdot (\text{p}_{\text{v}_a} - \text{p}_{\text{v}_s}) + L \cdot 0.62 \cdot 10^{-5} \cdot \vec{g_a} \cdot (\text{p}_{\text{v}_a} - \text{p}_{\text{v}_s}) \tag{3.17}$$

q_{latent} = heat flux by latent heat [W/m^2]
L = latent heat [J/kg] ≈ 2.5·10^6 J/kg for evaporation and condensation
$p_{v\,a}$ = ambient water vapor pressure [Pa]
$p_{v\,s}$ = surface water vapor pressure [Pa]

Moisture transport

The word "*moisture*" is used for water vapor and liquid water in a medium (material, air or soil). Bulk water and flowing water are not considered moisture [Adan and Samson 2011].

The absolute humidity can be described with the humidity ratio or the vapor pressure. The absolute humidity ratio (x_v) is the mass of vapor in the air divided by the mass of dry air [kg $_{vapor}$/kg $_{dry\ air}$]. The vapor pressure [Pa] and [N/m^2] can be used to describe the absolute humidity, because of the relationship between the amount of moisture in air and the pressure in the air caused by vapor.

$$\text{p}_\text{v} = \rho_\text{a} \cdot \text{x}_\text{v} \cdot \text{R}_\text{v} \cdot \text{T} \tag{3.18}$$

p_v = vapor pressure [Pa]
ρ_a = specific density of air [kg/m^3]
x_v = humidity ratio [kg $_{vapor}$ / kg $_{dry\ air}$]
R_v = gas constant of vapor [J/(kg·K)] = 462 J/(kg·K)
T = absolute temperature [K]

The air pressure – which is always approximate 10^5 Pa (1 atmosphere) – can be determined by:

$$\text{p}_a = \rho_\text{a} \cdot \text{R}_a \cdot \text{T} \tag{3.19}$$

p_a = air pressure [Pa] ≈ 10^5 Pa
ρ_a = specific density of air [kg/m^3]
R_a = gas constant of dry air [J/(kg·K)] = 287.1 J/(kg·K)
T = absolute temperature [K]

According to [Wit 2009], the relationship between the absolute humidity ratio (x_v) and the vapor pressure (p_v) can also be **estimated** by:

$$\text{x}_\text{v} \approx \frac{\text{p}_\text{v}/\text{R}_\text{v} \cdot \text{T}}{\text{p}_\text{a}/\text{R}_\text{a} \cdot \text{T}} \approx 0.62 \cdot 10^{-5} \cdot \text{p}_\text{v} \tag{3.20}$$

x_v = humidity ratio [kg $_{vapor}$ / kg $_{dry\ air}$]
p_v = vapor pressure [Pa]
p_a = air pressure [Pa] ≈ 10^5 Pa

R_a = gas constant of dry air [J/(kg·K)] = 287.1 J/(kg·K)
R_v = gas constant of vapor [J/(kg·K)] = 462 J/(kg·K)
T = absolute temperature [K]

Instead of absolute humidity, the humidity can also be described with the relative humidity. The equation for relative humidity is:

$$RH = \frac{p_v}{p_{sat}} \cdot 100\% = \varphi \cdot 100\% \quad (3.21)$$

RH = relative humidity [%]
φ = relative humidity [-]
p_v = vapor pressure [Pa]
p_{sat} = saturation pressure [Pa]

The saturation pressure is dependent on the temperature, for which HAM-BC 2015 uses the equation:

$$p_{sat} = \exp\left(65.8094 - \frac{7066.27}{T} - 5.976 \cdot ln(T)\right) \quad (3.22)$$

p_{sat} = saturation pressure [Pa]
T = absolute temperature [K]

The main hygric properties of a material are the vapor permeability, the moisture retention curve and the capillary suction of liquid water. [Voerman 2013]

Vapor transport by diffusion
Moisture transport in building constructions can occur in liquid form or in gaseous form (vapor). Each phase has its own transport mechanisms. The hygroscopic properties are about moisture in gas phase with vapor diffusion and convective vapor transport as transport mechanisms. Vapor diffusion is caused by differences between the partial vapor pressures at different locations. Partial vapor pressure is the pressure that is caused by water vapor in air. The air pressure as a result of oxygen, nitrogen, carbon dioxide and other gasses has no influence on the vapor pressure. The vapor is transported by diffusion from a location with a high vapor pressure to a location with a lower vapor pressure. [Al-Homaud 2004] [Stappers and Schellen 2011] The vapor transport can be described with Fick's law:

$$\vec{g_v} = -\delta_v \cdot \text{grad } p_v \quad (3.23)$$

g_v = water vapor flow rate [kg/(m^2·s)]
δ_v = vapor permeability of the material [kg/(s·m·Pa)] ~ [s]
p_v = partial water vapor pressure [Pa]

The goal of a vapor retarding foil is to diminish the transport of vapor through the construction. In cold climates with heated buildings the indoor environment is warmer and more humid than the outside air. For this reason, the moisture will be transported from the warmer and more humid indoor environment to the colder and drier outdoor environment. In general, the vapor retarding layer material is implemented at the warm side of the insulation material. Therefore, in cold climates – such as in West- and North-Europe – the vapor retarder is applied at the side of the insulation near the indoor environment [Al-Homaud 2004]. The permeability of a material [perm] describes the extent to which vapor can transport through the material. As stated by [Al-Homaud 2004]: "*The lower the permeability, the better the material is as vapor retarder.*" There is a distinction between vapor barriers ($\leq$ 1 perm) and vapor retarders (1 - 10 perm) [Al-Homaud 2004]. The value 1 perm is equal to $5.7 \cdot 10^{-11}$ kg/(m^2·s·Pa) [Voerman 2013].

The vapor diffusion resistance factor is in many cases used for notating the material property related to vapor diffusion. The relationship between the vapor permeability and the vapor diffusion resistance factor is:

$$\delta_v = \frac{\delta_a}{\mu} \tag{3.24}$$

δ_v = vapor permeability of the material [kg/(s·m·Pa)] ~ [s]
δ_a = vapor permeability of air [kg/(s·m·Pa)] ~ [s] = $1.8 \cdot 10^{-10}$ [s]
μ = vapor diffusion resistance factor [-]

The temperature gradient influences the vapor transport, which is important for summer condensation. When the influence of the temperature gradient on the vapor flux is included in 3.22, this lead to:

$$\vec{g}_v = -\frac{\delta_a}{\mu} \cdot \text{grad } p_v - \frac{\delta_a}{\mu} \cdot \varphi \cdot \frac{\partial p_{sat}}{\partial T} \cdot \text{grad } T \tag{3.25}$$

Moisture retention curve

The moisture storage term describes the relation between the moisture content and the relative humidity in the material. The moisture content describes the ratio between the amount of moisture and the volume or mass of the material. The moisture content with the symbol **w** describes the ratio between the mass of moisture [kg] in the volume of material [m^3]. The relationship between relative humidity (φ) and moisture content (w) is called the differentiation capacity (ξ). This lead to the equation:

$$\xi \cdot \frac{\partial \varphi}{\partial t} = \text{div } \frac{\delta_a}{\mu} \cdot \text{grad } p_v - \frac{\delta_a}{\mu} \cdot \varphi \cdot \frac{\partial p_{sat}}{\partial T} \cdot \text{grad } T \tag{3.26}$$

ξ = hygroscopic vapor differentiation capacity related to relative humidity [kg/m^3]

The moisture retention curve is the material dependent relationship between the relative humidity and the moisture content. An example of the moisture retention curve is shown in figure 3.3.

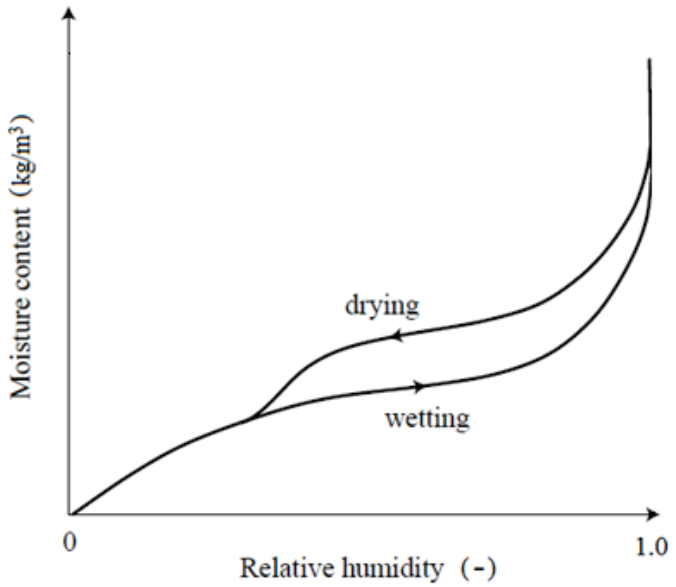

Figure 3.3: Example of a moisture retention curve for both desorption (drying) and adsorption (wetting). Source: [Adan and Samson 2011] (modified)

A difference exists between the values of desorption during drying and adsorption during the wetting of the material – which is also visible in figure 3.3. This difference is called hysteresis. One theory about the cause of hysteresis is described by [Steeman et al. 2009]. This theory states that during the drying (desorption) of the material, the water in the small pores blocks the water in a neighboring larger pore; and therefore, preventing the evaporation of the water in the large pore. According to this theory as described by [Steeman et al. 2009], the water in the larger pore only evaporates after the relative humidity has dropped sufficiently to evaporate the water inside the smaller pores. During adsorption, the vapor first condensates in the smaller pores, because of the capillary pressure and the condensation occur only in the larger pores after a higher relative humidity. It takes the most time to get the large pore wet, but the largest pores take the most time to become dry – which causes the different shapes of the curves. [Steeman et al. 2009]

HAM-BC 2015 can only use one moisture retention curve at a time.

Convective vapor transport

Moisture transport by convection (advection) means in building physics that vapor is transported with air. When convection is added in equation 3.26, this results in:

$$\xi \cdot \frac{\partial \varphi}{\partial \mathrm{t}} = \mathrm{div}\ \frac{\delta_a}{\mu} \cdot \mathrm{grad}\ \mathrm{p_v} - \frac{\delta_a}{\mu} \cdot \varphi \cdot \frac{\partial \mathrm{p}_{sat}}{\partial \mathrm{T}} \cdot \mathrm{grad}\ \mathrm{T} - 0.62 \cdot 10^{-5} \cdot \vec{g_a} \cdot \mathrm{grad}\ \mathrm{p_v} \qquad (3.27)$$

The value $0.62 \cdot 10^{-5}$ in the convection part of equation 3.27 comes from the relationship between the absolute humidity ratio and the vapor pressure as stated in equation 3.20. The result of multiplying the vapor pressure with $0.62 \cdot 10^{-5}$ is the absolute humidity ratio with the dimension [$kg_{\ moisture}$ / $kg_{\ dry\ air}$]. When the absolute humidity ratio is multiplied with the air mass flux (g_a) in [kg/(m^2·s)], the moisture flux by convection in [$kg_{\ moisture}$/(m^2·s)] is achieved.

Capillary pores and capillary pressure

Liquid moisture is transported in building constructions by capillary forces, gravity and pressure differences. Capillary transport is caused by capillary suction [Stappers and Schellen 2011]. Gravity is neglected in HAM-BC 2015; therefore, only the liquid moisture transport by capillary pressure is described by capillary suction and pressure differences.

The pores are important for heat and moisture transport in solid materials. Pores consist of two types, namely closed pores and open pores. The open pores are capillary connected which each other [Wit 2009]. The volume fraction which consists of open pores is called the open porosity. The capillary pressure is negative, because the capillary pressure acts like suction. Therefore, the capillary pressure is many times described as capillary suction. According to [Wit 2009], the swelling and shrinking of porous materials is generated by changes of the capillary pressure in the pore water. When the relative humidity increases, the capillary pressure becomes less negative; therefore, the internal pressure increases which lead to swelling [Wit 2009].

The capillary pressure in a single capillary pore is given by the equation 3.28 from [Wit 2009] and [Voronina et al. 2013]:

$$\mathrm{p_c} = -\frac{2 \cdot \sigma \cdot \cos(\theta)}{\mathrm{r}} \qquad (3.28)$$

p_c = capillary pressure [Pa]
σ = surface tension of the liquid interface or vapor interface [N/m]
θ = contact angle between the liquid/air and liquid/solid interface [-] or [°]
r = capillary radius [m]

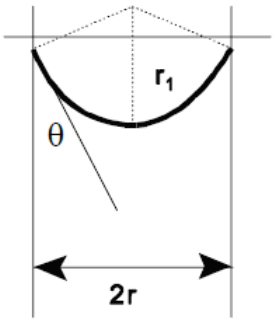

Figure 3.4: Impression of a capillary with the meniscus and the contact angle (θ) of the meniscus of the water front with the capillary wall. [Wit 2009]

The molecules in a liquid perform forces on each other (cohesion), whereby in the liquid these forces outweigh each other, with the result that the net force is zero. However, at the surface of the liquid at the pore walls or capillary walls, the net force is not (always) zero, but instead an inwards resulting force in the liquid occurs. Capillary attraction is caused by the fact that a liquid in a capillary has this *surface tension*, when this is higher than the cohesion forces of the liquid itself. [Wit 2009]

According to [Wit 2009], materials with a contact angle with water smaller than 90° are called hydrophilic materials; whereas, materials which have a contact angle larger than 90° are called hydrophobic. The capillary suction is larger as the radius of the capillary is smaller and the contact area is smaller. The contamination of the surface has also a large influence on the contact angle. A greasy surface has a large contact angle, while the contact angle is small when soap is in the water [Wit 2009].

The relation between the capillary pressure in a pore and the relative humidity is described with Kelvin's law:

$$p_c = \rho_w \cdot R_v \cdot T \cdot ln\,(\varphi) \tag{3.29}$$

$$\varphi = \exp\left(\frac{-p_c}{\rho_w \cdot R_v \cdot T}\right) \tag{3.30}$$

p_c = capillary pressure [Pa]
ρ_w = specific density of water [kg/m^3]
R_v = gas constant of vapor [J/(kg·K)] = 462 J/(kg·K)
T = absolute temperature [K]
φ = relative humidity [-]

Water vapor in pores may condensate below the saturation pressure. [Wit 2009]

According to [Wit 2009], the moisture permeability of a homogenous cylindrical capillary pore can be described by:

$$k_m = \rho_w \cdot \frac{r^2}{8 \cdot \eta} \tag{3.31}$$

k_m= moisture permeability [kg/(s·m·Pa)] ~ [s]
ρ_w = specific density of water [kg/m^3]
r = radius [m]
η = viscosity of water [kg/(s·m)] = [Pa·s]

Due to the fact that not all the precise pore sizes of a material are known, the total moisture permeability (k_m) of a material is determined with measurements. Therefore, equation 3.31 is not used in the simulation model. According to [Wit 2009], the moisture permeability increases significantly with the moisture content. Moreover, [Wit 2009] states that the appliance of the moisture permeability as a moisture independent constant *"is very wrong"*. Above the critical moisture content, the moisture transport by vapor diffusion does not dominate the moisture transport. The moisture transport by capillary suction is described by Darcy's Law:

$$\vec{g_l} = -k_m \cdot \text{grad}\,(p_c + \rho_w \cdot g \cdot z) \tag{3.32}$$

k_m= moisture permeability [kg/(s·m·Pa)] ~ [s]
g = gravity [m/s^2] = 9.81 m/s^2
z = vertical height [m]

This leads to the mass balance:

$$\Xi \cdot \frac{\partial p_c}{\partial t} = \text{div}\,(-k_m) \cdot \text{grad}\,(p_c + \rho_w \cdot g \cdot z) \tag{3.33}$$

Ξ = (Capillary) moisture differentiation capacity related to suction [kg/(m^3·Pa)]

Boundary condition moisture
The boundary condition related to vapor transport by **diffusion** is described by:

$$g = \beta_p \cdot (p_{v_a} - p_{v_s}) \tag{3.34}$$

β_p = surface coefficient of vapor transfer [s/m]
$p_{v\,a}$ = ambient water vapor pressure [Pa]
$p_{v\,s}$ = surface water vapor pressure [Pa]

The surface coefficient of vapor transfer and the heat transmission coefficient are in a relation described by the Lewis-equation:

$$\beta_p = (Le)^{n-1} \cdot 0.62 \cdot 10^{-8} \cdot h_{cv} \tag{3.35}$$

Le = Lewis number
n = 0 for laminar flow and n = 1 for turbulent flow
h_{cv} = heat transmission coefficient for convection [W/(m^2·K)]

$$Le = \frac{\lambda}{D_v \cdot \rho \cdot c_p} \tag{3.36}$$

λ = thermal conductivity coefficient [W/(m·K)]
D_v = diffusion coefficient [m^2·s]
ρ = specific density [kg/m^3]
c_p = specific heat capacity [J/(kg·K)]

According to [Li 2008], the relationship between the surface coefficient of vapor transfer (β_p) in [s/m] and the heat transmission coefficient for convection (h_{cv}) in [W/(m^2·K)] can be estimated with the equation:

$$\beta_p = 7.7 \cdot 10^{-9} \cdot h_{cv} \tag{3.37}$$

The boundary condition for moisture transport caused by **infiltration of air** can be described by:

$$g = 0.62 \cdot 10^{-5} \cdot \vec{g_a} \cdot (p_{v_a} - p_{v_s}) \quad (3.38)$$

$\vec{g_a}$ = air flux in mass [kg/(m^2 ·s)]
$p_{v\,a}$ = ambient water vapor pressure [Pa]
$p_{v\,s}$ = surface water vapor pressure [Pa]

Rain can be taken into account in [kg/(m^2 ·s)].

Wind-Driven Rain

[Blocken et al. 2004] describes equation 3.39 as a rough estimation for the horizontal wind-driven rain (WDR) on a vertical plane:

$$R_{wdr} = 0.222 \cdot U \cdot R_h^{0.88} \approx 0.222 \cdot U \cdot R_h \quad (3.39)$$

R_{wdr} = wind-driven rain intensity [l/(m^2 ·h)]
U = upstream horizontal wind velocity component at 10 meter height [m/s]
R_h = horizontal rainfall intensity [l/(m^2 ·h)]

The value 0.222 s/m is an average empirically determined WDR coefficient. The exponent 0.88 can be omitted from the equation 3.39, according to [Blocken et al. 2004]; therefore, this exponent is omitted in HAM-BC 2015.

3.2 Moisture Potential

Several potentials can be used for calculating the moisture transport. [Künzel and Kiessl 1997] advise the use of a potential which is a physical driving force. Also it is important that the chosen potential is everywhere present in the construction which is calculated. [Wit 2009] states that there are five possible potentials for calculating moisture transport in building constructions, which are: the moisture content [kg/m^3], partial water vapor pressure [Pa], capillary pressure [Pa], relative humidity [%] and the logarithmic capillary pressure [Pa].

The **moisture content** has the disadvantage that when a construction is made out of several different materials, each material has a different moisture retention curve, so a discontinuity in the calculation could occur between the moisture content of one material with another material. **Partial vapor pressure** has the disadvantage that it is useless when the vapor condensate to liquid water. The **capillary pressure** has the disadvantage that when the capillary pressure varies between 1 Pa to around 10^9 Pa – and vice versa – that can lead to numerical instability. **Relative humidity** has the disadvantage that when it becomes higher than 100%, the results are not accurate and reliable. Water transport in liquid form cannot be calculated with the use of relative humidity or partial vapor pressure.

According to [Uittenbosch 2012], the logarithmic capillary pressure does not suffer from numerical instability when a material becomes saturated by water. The use of the logarithmic capillary pressure as potential is called the Lp_c-method. The equations in section 3.1 are transformed to the equations with potential Lp_c which are used in HAM-BC 2015. The mathematically transformation is described in Annex B.

The potential of moisture transport in HAM-BC 2015 is the logarithmic capillary pressure:

$$Lp_c = {}^{10}\log(p_c) \quad (3.40)$$

Lp_c = logarithmic capillary pressure [Pa]
p_c = capillary pressure [Pa]

3.3 HAM-BC 2015

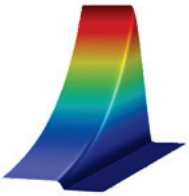

Heat, Air and Moisture transport in Building Constructions version **2015** is implemented in Matlab and COMSOL, which allows the user to change or remove certain parts in accordance with the availability of known parameters. The hygrothermal simulation model developed in this report is a further elaboration of [Schijndel 2006] and [Uittenbosch 2012]. The work of [Uittenbosch 2012] is improved in this project: by implementing solar irradiation, rain flux, damage indicators, additional tools, and a validated sophisticated convection method. Also the tables of the coefficients generated with Matlab were improved by using smaller steps of temperature and logarithmic capillary pressure, which lead to more accurate results in the validation study. [Uittenbosch 2012] uses constant steps of 0.2 Pa for Lp_c and 1°C for temperature, while HAM-BC 2015 uses 0.01 Pa and 0.05°C. The implementation of this hygrothermal simulation model in Matlab and COMSOL is described in the manual HAM-BC 2015, which can be found in Annex A.

COMSOL Multiphysics is used to solve partial differential equations (PDEs). [Russell 1961] states: *"The use of differential equations is necessary whenever a certain set of circumstances produces a tendency to a certain change in the circumstances, and this change, in turn, alters the tendency to change."* For example, the temperature and moisture content influences the variables and material properties which determine the heat, air and moisture transfer. This causes a change of the temperature and moisture content inside the material, which changes the variables and material properties of the material – and from there the cycle continues.

COMSOL uses an iterative approximation method, which means that approximate solutions are determined by several iterations. *Iterations* are the repeating of calculations to decrease the value of the residue. The result of one iteration step is the starting point for the next iteration. The goal of an iterative process is to achieve convergence of the results. This is done by defining a (relative) tolerance which must be achieved between the values of two subsequent calculations. After the difference between subsequent calculations complies with the defined tolerance, the calculation continues with the following time step or gradient.

Boundary conditions in HAM-BC 2015

The total equation for the boundary conditions for heat is:

$$q = h_c \cdot (\mathrm{T}_a - \mathrm{T}_s) + L \cdot \beta_p \cdot (\mathrm{p_{v}}_a - \mathrm{p_{v}}_s) + c_p \cdot \vec{g_a} \cdot (\mathrm{T}_a - \mathrm{T}_s) + L \cdot 0.62 \cdot 10^{-5} \cdot \vec{g_a} \cdot (\mathrm{p_{v}}_a - \mathrm{p_{v}}_s) + g_{\,\mathrm{rain}} \cdot c_l \cdot (\mathrm{T}_{\mathrm{rain}} - \mathrm{T}_s) + \alpha \cdot \mathrm{E_{sol}} \quad (3.41)$$

The total boundary condition for moisture is:

$$g = \beta_p \cdot (\mathrm{p_{v}}_a - \mathrm{p_{v}}_s) + 0.62 \cdot 10^{-5} \cdot \vec{g_a} \cdot (\mathrm{p_{v}}_a - \mathrm{p_{v}}_s) + g_{\,\mathrm{rain}} \quad (3.42)$$

Boundary condition of air flux (sophisticated method) is:

$$g_a = \beta_{air} \cdot (\mathrm{p}_{\,air\,surface} - \mathrm{p}_{\,ambient\,air}) \quad (3.43)$$

Heat and moisture balance equations

This section describes how the heat balance equation and the moisture balance equation are implemented in COMSOL with the help of text-files generated by Matlab.

The equation for heat transfer and temperature change in the material is:

$$(\rho \cdot c + c_l \cdot w)\frac{\partial \mathrm{T}}{\partial \mathrm{t}} = \left(\mathrm{div}\,\lambda + L \cdot \left(\mathrm{div}\,\frac{\delta_a}{\mu} - 0.62 \cdot 10^{-5} \cdot \vec{g_a}\right) \cdot \varphi \cdot \frac{\partial \mathrm{p}_{sat}}{\partial \mathrm{T}} - c_p \cdot \vec{g_a}\right) \cdot \mathrm{grad\ T} + L \cdot \left(\mathrm{div}\,\frac{-\delta_a}{\mu} + 0.62 \cdot 10^{-5} \cdot \vec{g_a}\right) \cdot \mathrm{p}_{sat(\mathrm{T})} \cdot \frac{\varphi}{\rho_w \cdot R_v \cdot T} \cdot \frac{\partial \mathrm{p_c}}{\partial \mathrm{Lp_c}} \cdot \mathrm{grad\ Lp_c} \tag{3.44}$$

The equation for moisture transfer and moisture storage is:

$$\frac{\partial w}{\partial \mathrm{p_c}} \cdot \frac{\partial \mathrm{p_c}}{\partial \mathrm{Lp_c}} \cdot \frac{\partial \mathrm{Lp_c}}{\partial \mathrm{t}} = \left(\mathrm{div}\,\frac{\delta_a}{\mu} - 0.62 \cdot 10^{-5} \cdot \vec{g_a}\right) \cdot \varphi \cdot \frac{\partial \mathrm{p}_{sat}}{\partial \mathrm{T}} \cdot \mathrm{grad\ T} + \left(\left(\left(-\mathrm{div}\,\frac{\delta_a}{\mu} + 0.62 \cdot 10^{-5} \cdot \vec{g_a}\right) \cdot \mathrm{p}_{sat(\mathrm{T})} \cdot \frac{\varphi}{\rho_w \cdot \mathrm{R_v} \cdot \mathrm{T}} \cdot \frac{\partial \mathrm{p_c}}{\partial \mathrm{Lp_c}}\right) - \mathrm{div}\,\mathrm{k_m} \cdot \frac{\partial \mathrm{p_c}}{\partial \mathrm{Lp_c}}\right) \mathrm{grad\ Lp_c} \tag{3.45}$$

ρ = specific density [kg/m^3]
c = specific heat capacity of the material [J/(kg·K)]
c_l = specific heat capacity of water [J/(kg·K)] = 4200 J/(kg·K)
c_p = specific heat capacity of air [J/(kg·K)]
w = moisture content [kg/m^3]
T = absolute temperature [K]
t = time [s]
λ = thermal conductivity [W/(m·K)]
L = latent heat of evaporation [J/kg] = 2.5 · 10^6 J/kg
δ_a = water vapor permeability of air [s]
μ = water vapor resistance factor [-]
g_a = air flux through the material [kg/(m^2·s)]
ϕ = relative humidity [-]
p_{sat} = saturation pressure [Pa]
ρ_w = density of water [kg/m^3] = 1000 kg/m^3
R_v = gas constant of water [J/(kg·K)] = 461.89 J/(kg·K)
p_c = capillary pressure [Pa]
Lp_c = logarithmic capillary pressure [Pa]
k_m = moisture (conductivity) permeability [kg/(s·m·Pa)]

The equations (3.44) and (3.45) combined in matrix form:

$$\begin{bmatrix} (\rho \cdot c + c_l \cdot w) & 0 \\ 0 & \frac{\partial \mathrm{w}}{\partial \mathrm{p_c}} \cdot \frac{\partial \mathrm{p_c}}{\partial \mathrm{Lp_c}} \end{bmatrix} \cdot \begin{bmatrix} \frac{\partial \mathrm{T}}{\partial t} \\ \frac{\partial \mathrm{Lp_c}}{\partial t} \end{bmatrix} =$$

$$\nabla \cdot \left(\begin{bmatrix} \lambda + L \cdot \frac{\delta_a}{\mu} \cdot \varphi \cdot \frac{\partial \mathrm{p}_{sat}}{\partial T} & -L \cdot \frac{\delta_a}{\mu} \cdot \mathrm{p}_{sat(\mathrm{T})} \cdot \frac{\varphi}{\rho_w \cdot R_v \cdot T} \cdot \frac{\partial \mathrm{p_c}}{\partial \mathrm{Lp_c}} \\ \frac{\delta_a}{\mu} \cdot \varphi \cdot \frac{\partial \mathrm{p}_{sat}}{\partial T} & -\mathrm{k_m} \cdot \frac{\partial \mathrm{p_c}}{\partial \mathrm{Lp_c}} - \frac{\delta_a}{\mu} \cdot \mathrm{p}_{sat(\mathrm{T})} \cdot \frac{\varphi}{\rho_w \cdot R_v \cdot T} \cdot \frac{\partial \mathrm{p_c}}{\partial \mathrm{Lp_c}} \end{bmatrix} \cdot \nabla \begin{bmatrix} \mathrm{T} \\ \mathrm{Lp_c} \end{bmatrix} \right) +$$

$$\vec{g_a} \begin{bmatrix} -\left(c_p + L \cdot 0.62 \cdot 10^{-5} \cdot \varphi \cdot \frac{\partial \mathrm{p}_{sat}}{\partial T}\right) & L \cdot 0.62 \cdot 10^{-5} \cdot \mathrm{p}_{sat(\mathrm{T})} \cdot \frac{\varphi}{\rho_w \cdot R_v \cdot T} \cdot \frac{\partial \mathrm{p_c}}{\partial \mathrm{Lp_c}} \\ -0.62 \cdot 10^{-5} \cdot \varphi \cdot \frac{\partial \mathrm{p}_{sat}}{\partial T} & 0.62 \cdot 10^{-5} \cdot \mathrm{p}_{sat(\mathrm{T})} \cdot \frac{\varphi}{\rho_w \cdot R_v \cdot T} \cdot \frac{\partial \mathrm{p_c}}{\partial \mathrm{Lp_c}} \end{bmatrix} \cdot \nabla \begin{bmatrix} \mathrm{T} \\ \mathrm{Lp_c} \end{bmatrix}$$

Implementation of the heat and moisture balance equations in COMSOL and Matlab

The $\frac{\partial T}{\partial t}$, $\frac{\partial LPc}{\partial t}$, ∇T and ∇Lp_c are calculated with COMSOL, while the other parts are implemented in COMSOL as interpolation functions of the text-files generated by Matlab. These functions are implemented in different parameters. HAM-BC 2015 works with *Coefficient Form PDE*, which uses the equations:

$$\begin{cases} e_a \cdot \frac{\partial^2 u}{\partial t^2} + d_a \cdot \frac{\partial u}{\partial t} + \nabla \cdot (-c \cdot \nabla u - \alpha \cdot u + \gamma) + \beta \cdot \nabla u + \mathrm{a} \cdot u = f & in\ \Omega \\ -n \cdot (-c \cdot \nabla u - \alpha \cdot u + \gamma) = g - q \cdot u & on\ \partial\Omega \end{cases}$$

The **u** stands for the dependent variables T and LPc. The **Ω** stands for the computational domain, which is the union of all sub-domains. The domain boundary is symbolized by **∂Ω.** The **n** symbolizes the outward unit normal vector on **∂Ω**. The parameters $\mathbf{e_a}$, **α**, **γ**, **a**, **f**, **q** are zero in HAM-BC 2015. This leads to:

$$\begin{cases} d_a \cdot \frac{\partial u}{\partial t} + \nabla \cdot (-c \cdot \nabla u) + \beta \cdot \nabla u = 0 & in\ \Omega \\ -n \cdot (-c \cdot \nabla u) = g & on\ \partial\Omega \end{cases}$$

The **g** stands for the boundary conditions. The equations (3.44) and (3.45) are implemented in the damping coefficient $\mathbf{d_a}$, diffusion coefficient **c** and convection coefficient **β**.

$$d_a = \begin{bmatrix} (\rho \cdot c + c_l \cdot w) & 0 \\ 0 & \frac{\partial w}{\partial \mathrm{p_c}} \cdot \frac{\partial \mathrm{p_c}}{\partial \mathrm{Lp_c}} \end{bmatrix}$$

$$c = \begin{bmatrix} \lambda + L \cdot \frac{\delta_a}{\mu} \cdot \varphi \cdot \frac{\partial \mathrm{p}_{sat}}{\partial \mathrm{T}} & -L \cdot \frac{\delta_a}{\mu} \cdot \mathrm{p}_{sat(\mathrm{T})} \cdot \frac{\varphi}{\rho_w \cdot \mathrm{R_v} \cdot \mathrm{T}} \cdot \frac{\partial \mathrm{p_c}}{\partial \mathrm{Lp_c}} \\ \frac{\delta_a}{\mu} \cdot \varphi \cdot \frac{\partial \mathrm{p}_{sat}}{\partial \mathrm{T}} & -\mathrm{k_m} \cdot \frac{\partial \mathrm{p_c}}{\partial \mathrm{Lp_c}} - \frac{\delta_a}{\mu} \cdot \mathrm{p}_{sat(\mathrm{T})} \cdot \frac{\varphi}{\rho_w \cdot \mathrm{R_v} \cdot \mathrm{T}} \cdot \frac{\partial \mathrm{p_c}}{\partial \mathrm{Lp_c}} \end{bmatrix}$$

$$\beta = \vec{g_a} \begin{bmatrix} -\left(c_p + L \cdot 0.62 \cdot 10^{-5} \cdot \varphi \cdot \frac{\partial \mathrm{p}_{sat}}{\partial \mathrm{T}}\right) & L \cdot 0.62 \cdot 10^{-5} \cdot \mathrm{p}_{sat(\mathrm{T})} \cdot \frac{\varphi}{\rho_w \cdot \mathrm{R_v} \cdot \mathrm{T}} \cdot \frac{\partial \mathrm{p_c}}{\partial \mathrm{Lp_c}} \\ -0.62 \cdot 10^{-5} \cdot \varphi \cdot \frac{\partial \mathrm{p}_{sat}}{\partial \mathrm{T}} & 0.62 \cdot 10^{-5} \cdot \mathrm{p}_{sat(\mathrm{T})} \cdot \frac{\varphi}{\rho_w \cdot \mathrm{R_v} \cdot \mathrm{T}} \cdot \frac{\partial \mathrm{p_c}}{\partial \mathrm{Lp_c}} \end{bmatrix}$$

All sub formulas in the matrix are separate coefficients, which have the following names:

$$d_a = \begin{bmatrix} \mathrm{B_T}(\mathrm{Lp_c}, \mathrm{T}) & 0 \\ 0 & \mathrm{B_L}(\mathrm{Lp_c}, \mathrm{T}) \end{bmatrix}$$

$$c = \begin{bmatrix} \mathrm{D11}(\mathrm{Lp_c}, \mathrm{T}) & \mathrm{D12}(\mathrm{Lp_c}, \mathrm{T}) \\ \mathrm{D21}(\mathrm{Lp_c}, \mathrm{T}) & \mathrm{D22}(\mathrm{Lp_c}, \mathrm{T}) \end{bmatrix}$$

$$\beta = \vec{g_a} \begin{bmatrix} \mathrm{C11}(\mathrm{Lp_c}, \mathrm{T}) & \mathrm{C12}(\mathrm{Lp_c}, \mathrm{T}) \\ \mathrm{C21}(\mathrm{Lp_c}, \mathrm{T}) & \mathrm{C22}(\mathrm{Lp_c}, \mathrm{T}) \end{bmatrix}$$

The equations for each coefficient are:

$$B_T(Lp_c, T) = (\rho \cdot c + c_l \cdot w)$$

$$B_L(Lp_c, T) = \frac{\partial w}{\partial p_c} \cdot \frac{\partial p_c}{\partial Lp_c}$$

$$D11(Lp_c, T) = \lambda + L \cdot \frac{\delta_a}{\mu} \cdot \varphi \cdot \frac{\partial p_{sat}}{\partial T}$$

$$D12(Lp_c, T) = -L \cdot \frac{\delta_a}{\mu} \cdot p_{sat(T)} \cdot \frac{\varphi}{\rho_w \cdot R_v \cdot T} \cdot \frac{\partial p_c}{\partial Lp_c}$$

$$D21(Lp_c, T) = \frac{\delta_a}{\mu} \cdot \varphi \cdot \frac{\partial p_{sat}}{\partial T}$$

$$D22(Lp_c, T) = -k_m \cdot \frac{\partial p_c}{\partial Lp_c} - \frac{\delta_a}{\mu} \cdot p_{sat(T)} \cdot \frac{\varphi}{\rho_w \cdot R_v \cdot T} \cdot \frac{\partial p_c}{\partial Lp_c}$$

$$C11(Lp_c, T) = -\left(c_p + L \cdot 0.62 \cdot 10^{-5} \cdot \varphi \cdot \frac{\partial p_{sat}}{\partial T}\right)$$

$$C12(Lp_c, T) = L \cdot 0.62 \cdot 10^{-5} \cdot p_{sat(T)} \cdot \frac{\varphi}{\rho_w \cdot R_v \cdot T} \cdot \frac{\partial p_c}{\partial Lp_c}$$

$$C21(Lp_c, T) = -0.62 \cdot 10^{-5} \cdot \varphi \cdot \frac{\partial p_{sat}}{\partial T}$$

$$C22(Lp_c, T) = 0.62 \cdot 10^{-5} \cdot p_{sat(T)} \cdot \frac{\varphi}{\rho_w \cdot R_v \cdot T} \cdot \frac{\partial p_c}{\partial Lp_c}$$

The **B** stands for Buffer, the **D** for Diffusion and **C** for Convection.

Matlab is used to generate tables in text-files, which are imported into COMSOL – as visualized in figure 3.5.

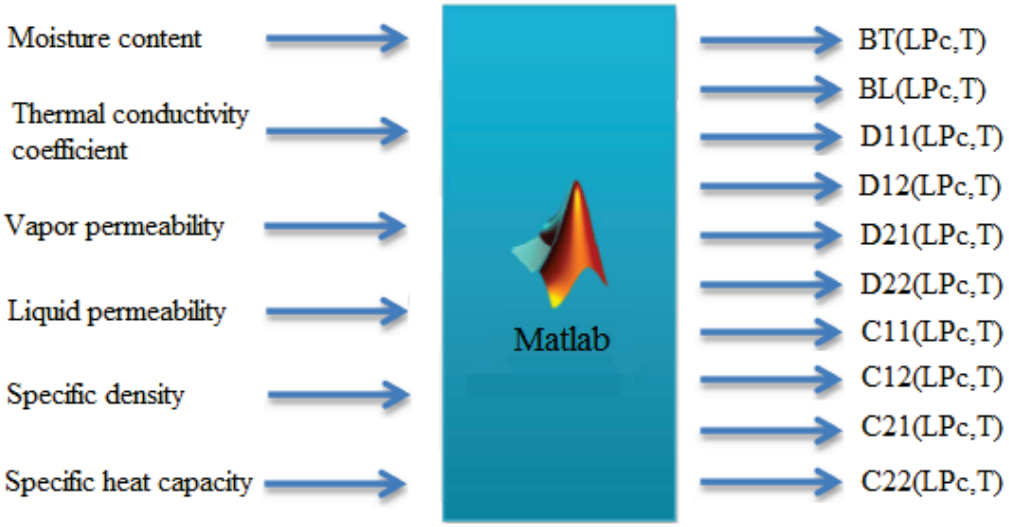

Figure 3.5: Material properties (left) which are implemented in the coefficients (right).

The implementation of the hygrothermal simulation model in Matlab and COMSOL Multiphysics are explained in the manual HAM-BC 2015, which can be found in Annex A.

4. Validation and Verification

HAM-BC 2015 is validated by computer-model-comparison and analytical verification with the HAMSTAD-benchmarks and empirical validation with a dataset obtained from measurements in a climate chamber in France and a dataset with measurements from a historical school building in Estonia.

4.1. HAMSTAD-benchmarks

The European Union initiated in 2000 the research program *Heat, Air and Moisture Standards Development* (HAMSTAD) with the goal to develop benchmarks which could be used for verifying calculation programs for heat, air, and moisture transport in building constructions. HAM-BC 2015 is validated with all five HAMSTAD-benchmarks. Most HAMSTAD-benchmarks are inter-computer-model comparisons, which mean that the results of HAM-BC 2015 are compared with the results of other simulation models. HAMSTAD-benchmark 2 consists of an analytical verification. All benchmarks are one-dimensional heat and moisture transport. In this section, results of the benchmarks are shown. More input and results from the HAMSTAD-benchmarks are shown in Annex C.

HAMSTAD-benchmark 1

Benchmark 1 is an insulated roof with the following configuration: a vapor retarding layer, 100 mm load bearing material and 50 mm insulation material. The complete description of the benchmark is given in [Hagentoft 2002].

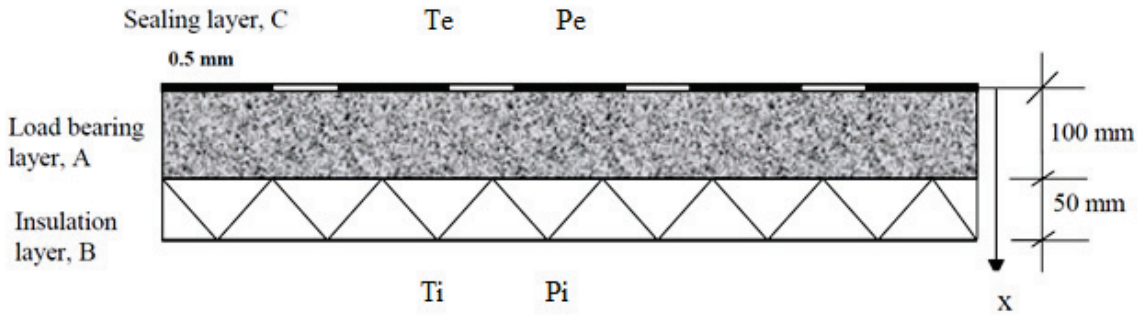

Figure 4.1: Intersection of the insulated roof from HAMSTAD-benchmark 1. [Hagentoft 2002]

The model in HAM-BC 2015 is made with a 1D-geometry. The sealing layer is not modelled, but the effect of the layer is implemented by giving the boundary moisture flux the value zero. The construction is air-tight; and therefore, the convective heat and moisture transport has no influence on the heat and moisture transport. The boundary conditions are transient and the simulation period is 5 years. The boundary conditions are depicted in Annex C.

The computer-model-comparison is done with data from HAMSTAD, which are provided by the Catholic University of Leuven, Belgium (KUL); Eindhoven University of Technology, the Netherlands (TUE); National Research Council, Canada (NRC), University of Technology Dresden, Germany (TUD); Technion-Institute of Technology, Israel (Technion); Chalmers University of Technology, Sweden (CTH); and Institute of Building Physics, Germany (IBP).

In this section only the results of year 1 are shown. All results from benchmark 1 are shown in Annex C. The results of HAM-BC 2015 are in red.

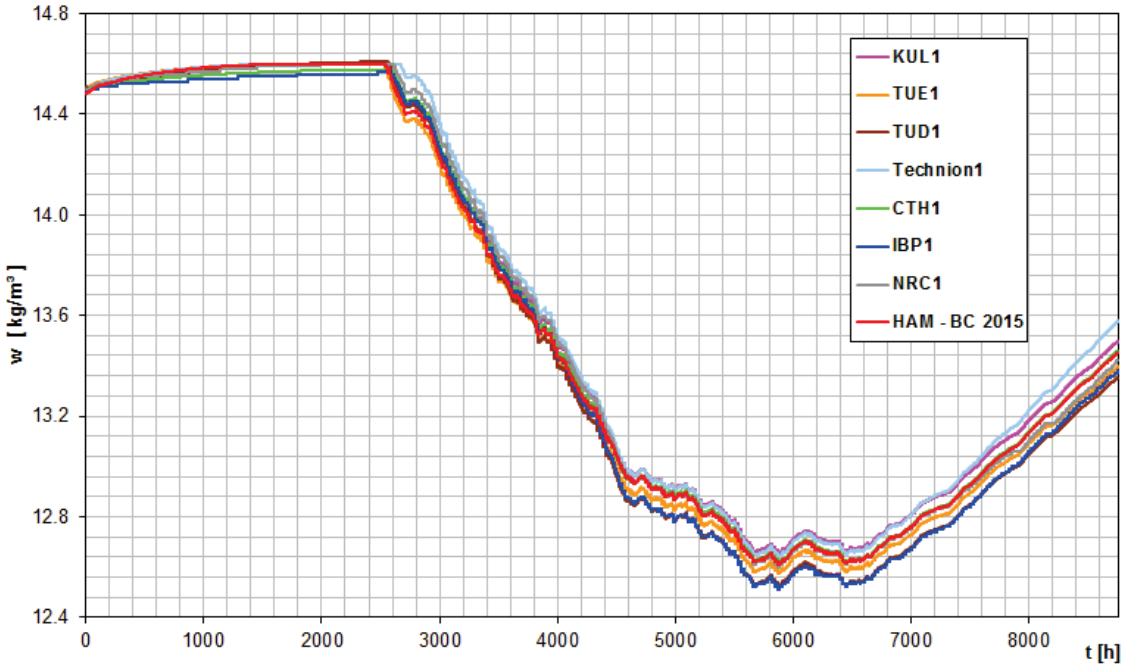

Figure 4.2: Total moisture content [kg/m^3] of the load bearing material in the first year.

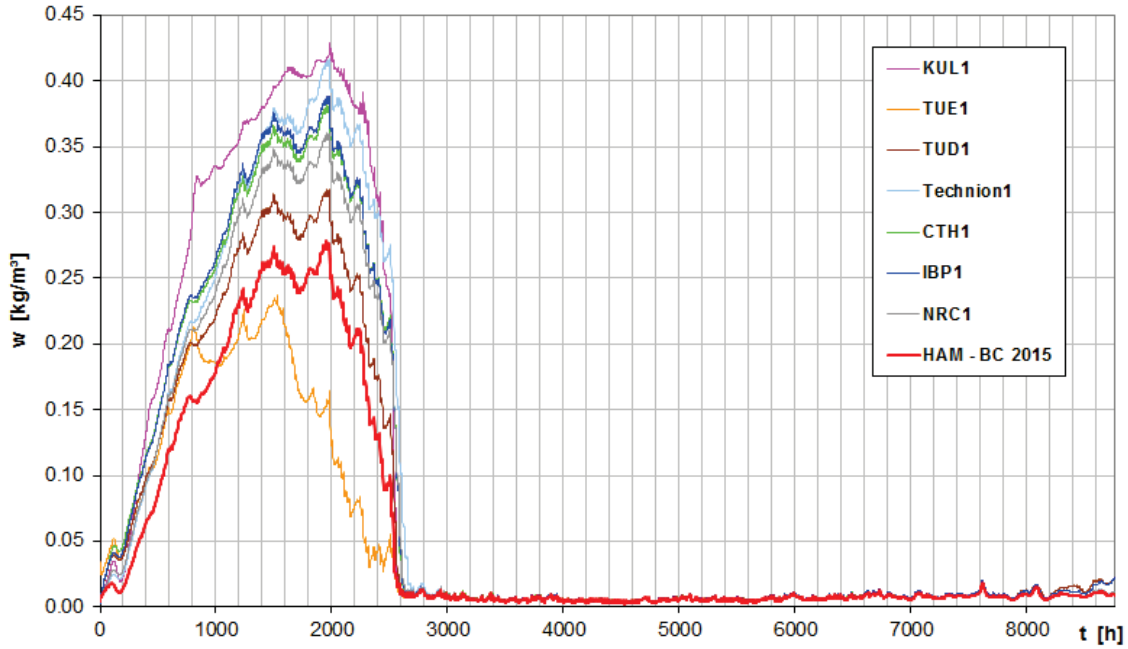

Figure 4.3: Total moisture content [kg/m^3] of the insulation material in the first year.

Figure 4.2 and 4.3 show that the results from HAM-BC 2015 comply with the results from the other models, *i.e.* it shows the same trend and similar values.

HAMSTAD-benchmark 2

The second HAMSTAD-benchmark is about an isotherm drying process of an initially wet 200 mm thick material. The initial conditions are 293 K and a relative humidity of 85%. The indoor boundary conditions are a temperature of 293 K and a relative humidity of 65%. The external side has the boundary conditons consisting of a temperature of 293 K and a relative humidity of 45%. For this benchmark an analytical solution is given. The complete benchmark is described in [Hagentoft 2002]. The model in COMSOL consists of a 1D-geometry.

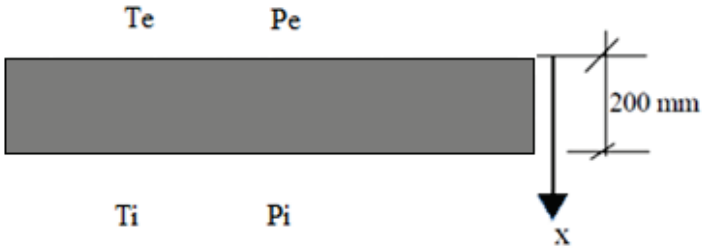

Figure 4.4: The geometry of HAMSTAD-benchmark 2. Modified figure from [Hagentoft 2002]

The results of HAM-BC 2015 are shown in figure 4.5, which depicts the moisture content [kg/m^3] across the thickness at 100 hours, 300 hours and 1000 hours.

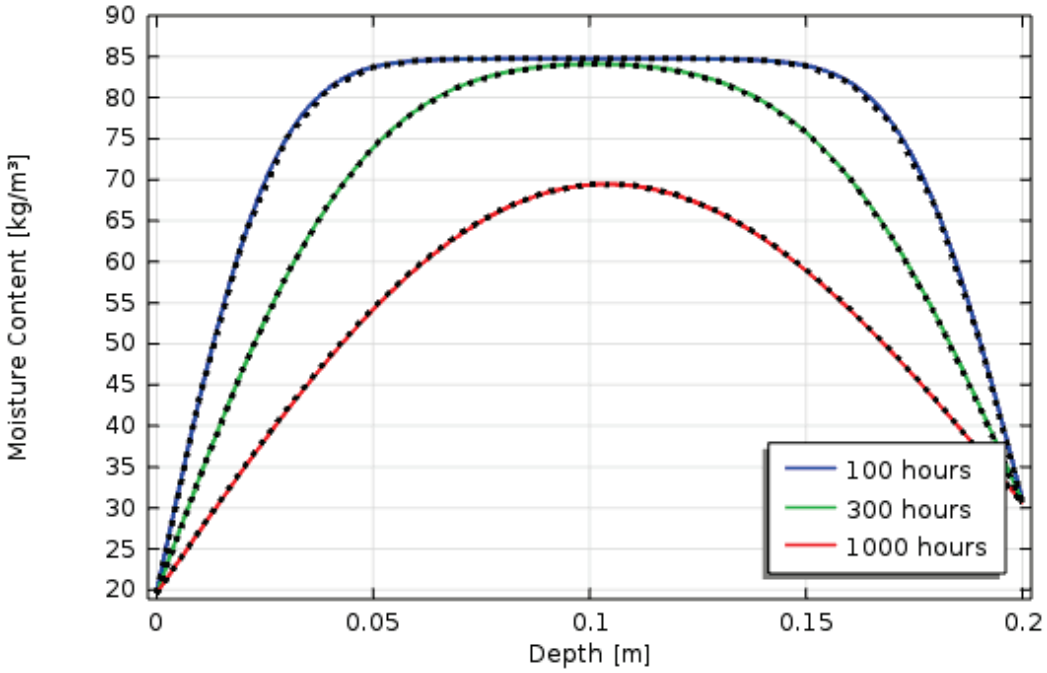

Figure 4.5: Moisture content [kg/m^3] related to the depth [m] measured from the outside after 100 hours, 300 hours and 1000 hours, where the colored graphs are the results of the HAM-BC 2015 and the dotted graphs are the analytical solutions from HAMSTAD-benchmark 2.

HAM-BC 2015 generates the same results as the analytical solution.

HAMSTAD-Benchmark 3

Convective heat and moisture transport is simulated with HAMSTAD-benchmark 3 by inter-computer-model-comparison. A single-plane lightweight construction with a thickness of 200 mm is simulated. The boundary conditions are constant, with the exception of the pressure difference between indoor and outdoor. First there is infiltration of air, caused by a pressure difference of 30 Pa, which at day 20 will be changed linearly to -30 Pa, which value is reached at day 21, *i.e.* to an exfiltration by an air pressure difference of 30 Pa. The complete description of the benchmark is given in [Hagentoft 2002]. A 2D-geometry was used for this benchmark.

The computer-model-comparison is done with the results provided by the National Research Council, Canada (NRC), University of Technology Dresden, Germany (TUD); Technion-Institute of Technology, Israel (Technion) and Chalmers University of Technology, Sweden (CTH).

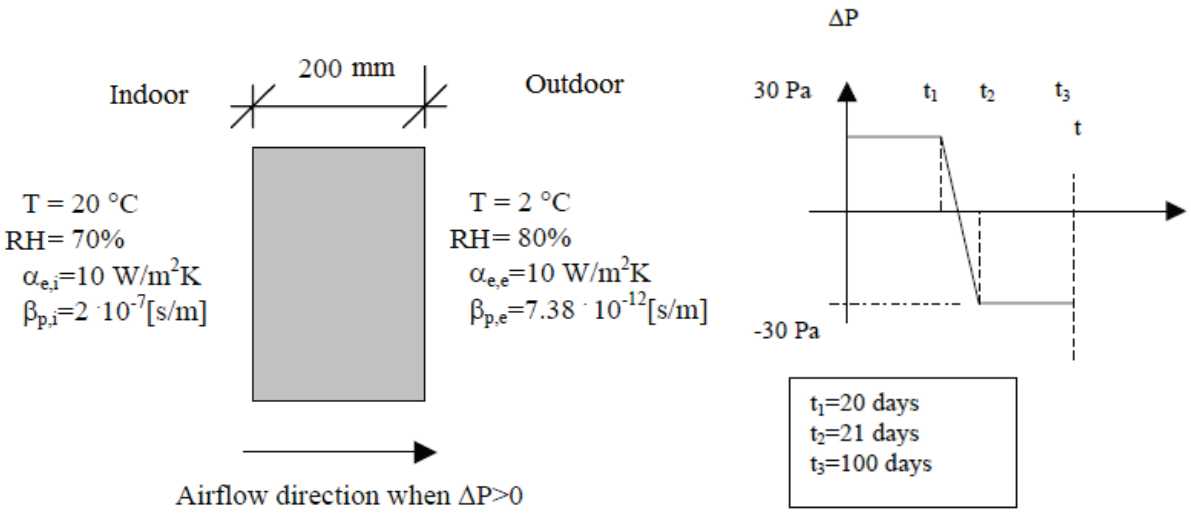

Figure 4.6: Geometry of the construction of benchmark 3 and the air pressure difference. Source: [Hagentoft 2002]. The figure is modified by the current author.

The data for creating the graphs have a time step of 24 hours. The results given in this report are made with the simplified convection method of HAM-BC 2015. The results of HAM-BC 2015 are in red.

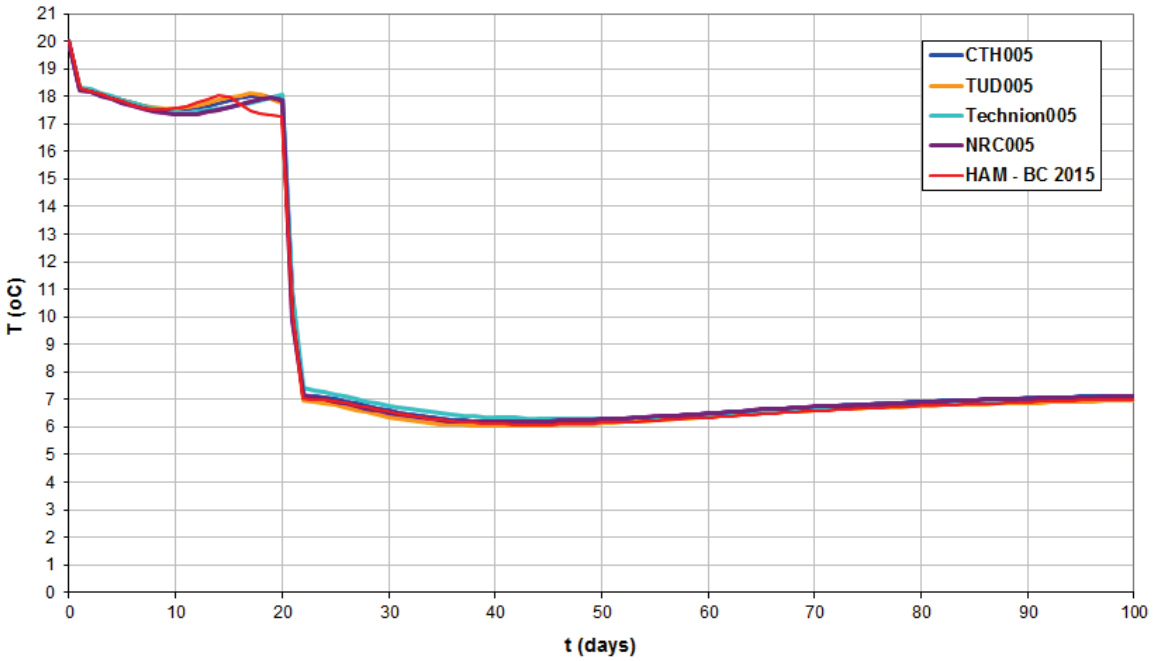

Figure 4.7: Temperature [°C] related to time [days] at 0.05 m.

The moisture content increases at the start with the exfiltration (ΔP = +30 Pa), because the indoor air with the higher absolute humidity in the value of vapor pressure reaches the colder area near the outdoor environment. Both the temperature and moisture content decreases rapidly when the exfiltration (ΔP = +30 Pa) alters to infiltration (ΔP = -30 Pa), which is caused by the fact that the cold and dry air from the outside transports through the construction.

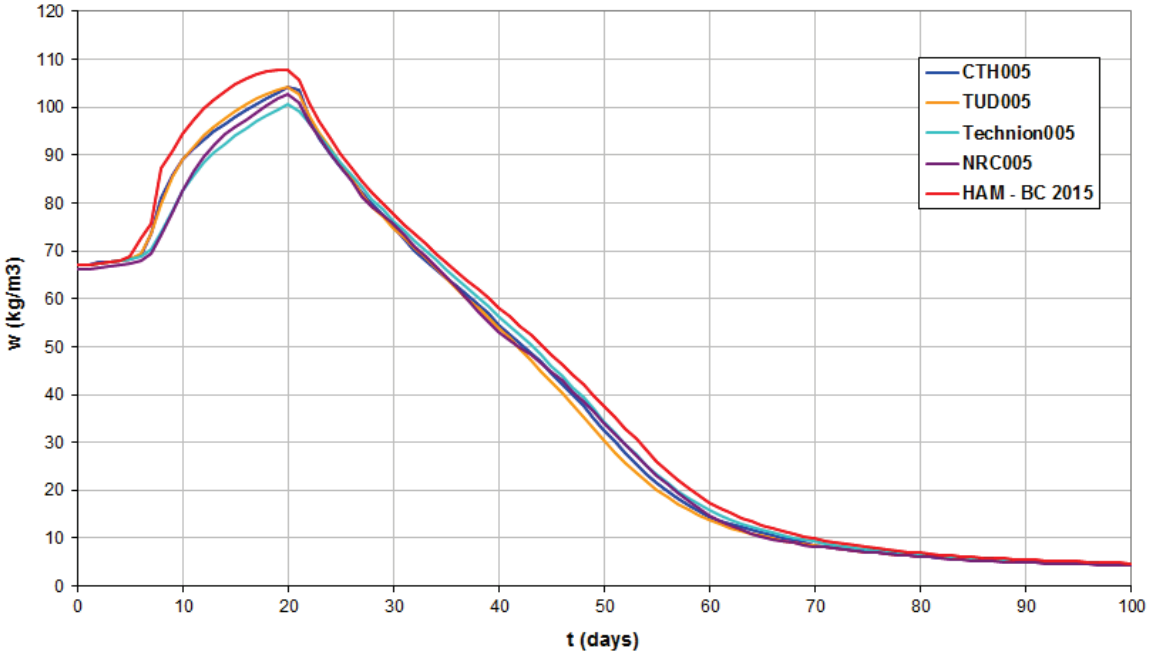

Figure 4.8: Moisture content [kg/m^3] related to time [days] at 0.05 m.

It is visible in figure 4.8 that HAM-BC 2015 computes a larger moisture content between day 8 and day 21 than the other models.

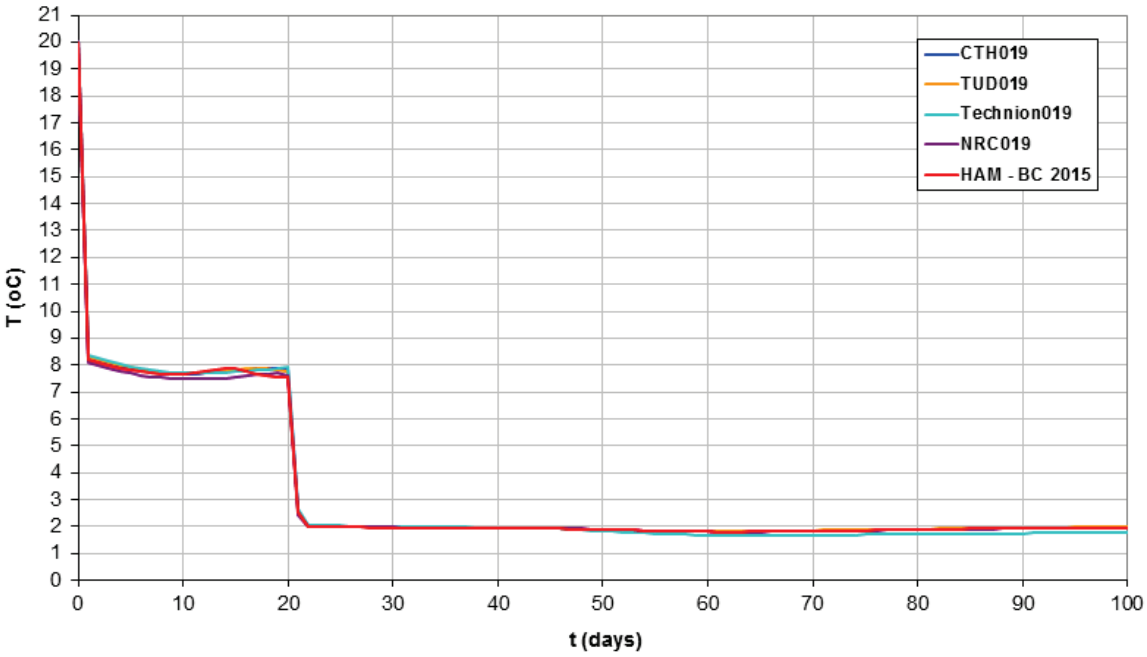

Figure 4.9: Temperature [°C] related to time [days] at 0.19 m.

In figure 4.9, the temperature decreases rapidly after the start of the simulation, which is caused by the fact that at the start of the simulation there is a sudden implementation of an air pressure difference of 30 Pa, while there is no initial air pressure difference. So the air pressure difference changes from 0 Pa to 30 Pa in an instant.

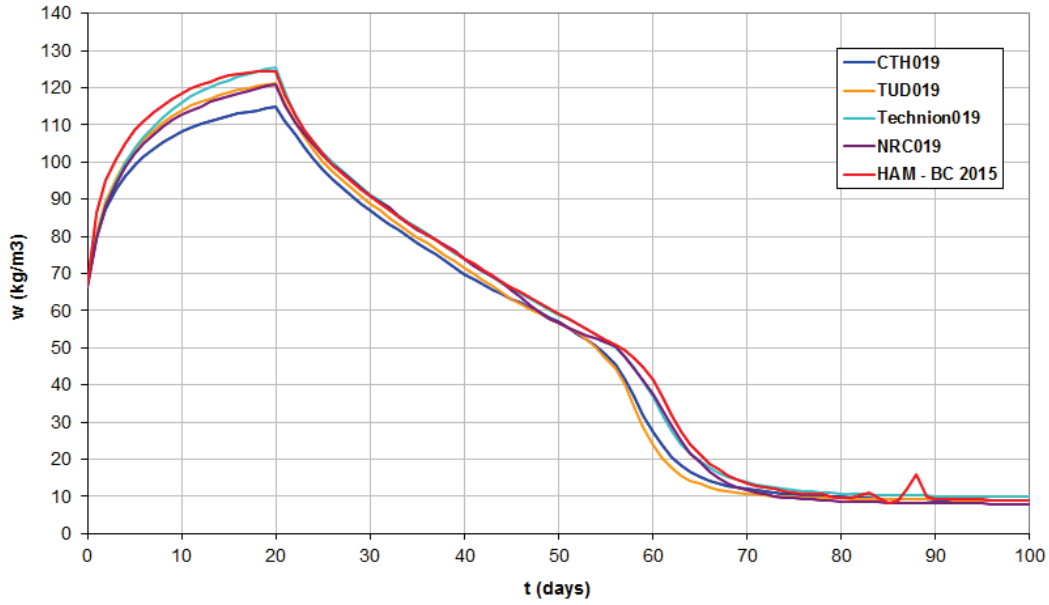

Figure 4.10: Moisture content [kg/m^3] related to time [days] at 0.19 m.

At the depth of 0.19 m, there is a little peak at the moisture content between 85 and 90 days, which is caused by the fact that the simulation uses a time step of 24 hours. This deviation does not occur when the time step is set on 1 hour. The description of benchmark 3 instructed the use of a 24 hour time step.

HAM-BC 2015 improves the results of [Uittenbosch 2012] for benchmark 3, which is mainly achieved by using smaller steps of temperature and logarithmic capillary pressure for the tables of the coefficients generated with Matlab. [Uittenbosch 2012] uses steps of 0.2 Pa for Lp_c and 1°C for temperature, while HAM-BC 2015 uses 0.01 Pa and 0.05°C.

HAMSTAD-benchmark 4

The geometry of benchmark 4 consists of a wall with a plaster at the inside, which is submitted to rain and a high temperature caused by solar irradiation. The structure is airtight; and therefore, no convective heat and moisture transport occurs. The boundary conditions are described in Annex C. The calculation time is 120 days. The complete description of the benchmark is given in [Hagentoft 2002]. The model in COMSOL was made with a 2D-geometry.

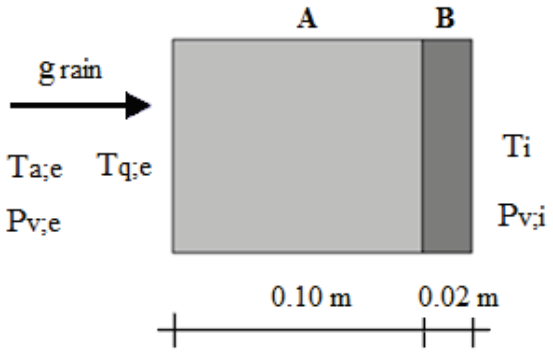

Figure 4.11: Geometry and boundary conditions of HAMSTAD-benchmark 4. Source: HAMSTAD-benchmark 4 description, with some self-made changes.

The computer-model-comparison is done with data provided by the Catholic University of Leuven, Belgium (KUL); National Research Council, Canada (NRC), University of Technology Dresden, Germany (TUD); Technion-Institute of Technology, Israel (Technion); Chalmers University of Technology, Sweden (CTH); and Institute of Building Physics, Germany (IBP).

The temperature at the external surface of the construction is shown in figure 4.12. This shows that HAM-BC 2015 generates similar results as the other models for external surface temperature including the influence of rain and solar irradiation. The sudden increase of the temperature is caused by the solar irradiation. The results of HAM-BC 2015 are in blue.

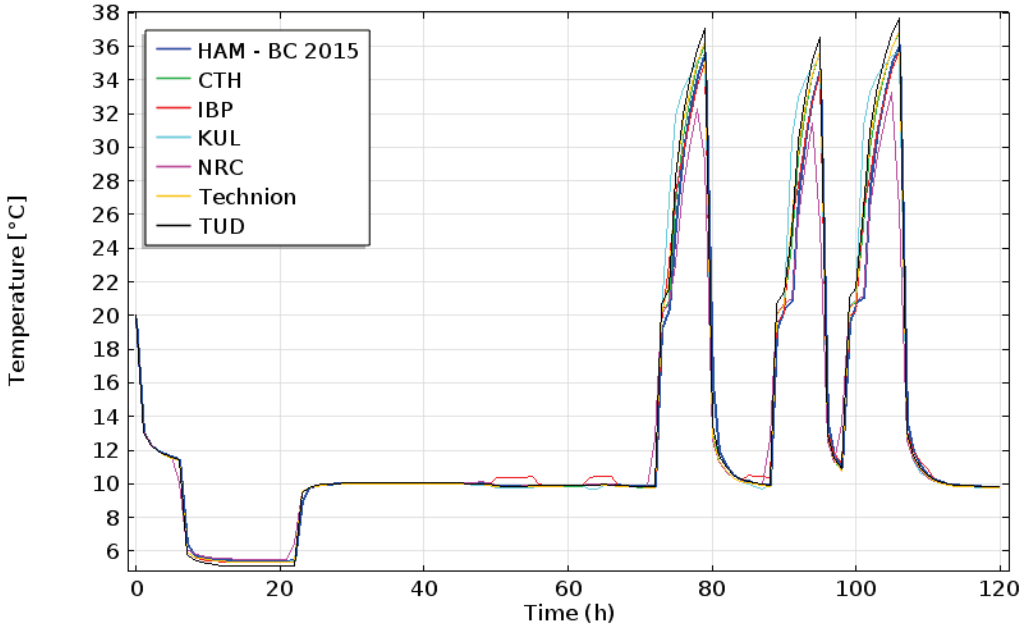

Figure 4.12: Temperature [°C] related to time [hours] at the external surface.

The moisture content at the external surface is shown in figure 4.13, which shows that the influence of the rain flux on the moisture content at the external surface generated by HAM-BC 2015 leads to similar results as the other simulation models.

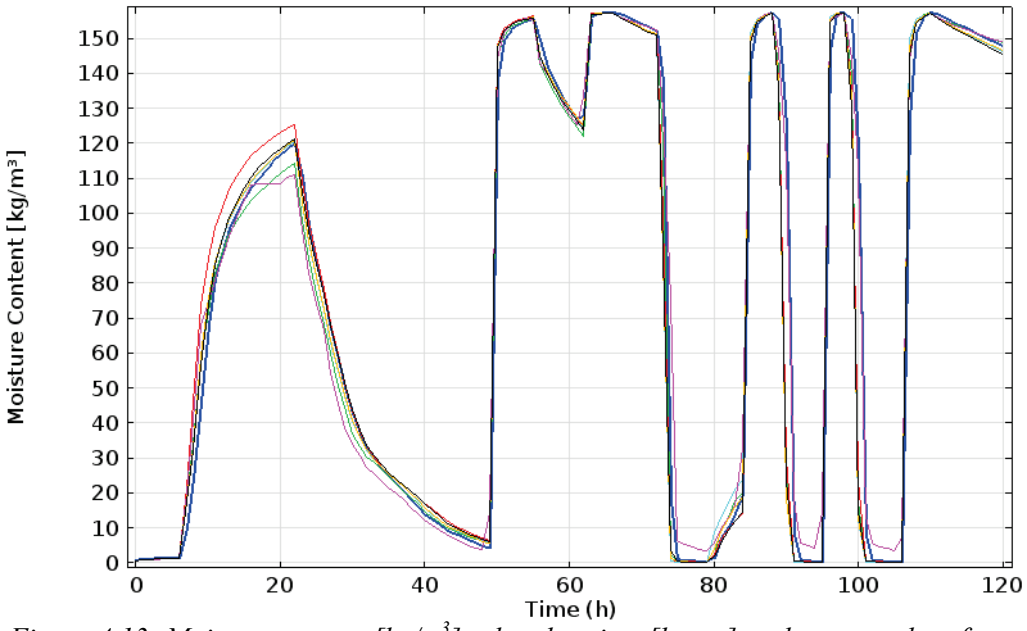

Figure 4.13: Moisture content [kg/m^3] related to time [hours] at the external surface.

Figure 4.14 depicts the moisture content over the depth of the construction at 24 hours, which shows that HAM-BC 2015 lead to similar results as the results of the different models from HAMSTAD.

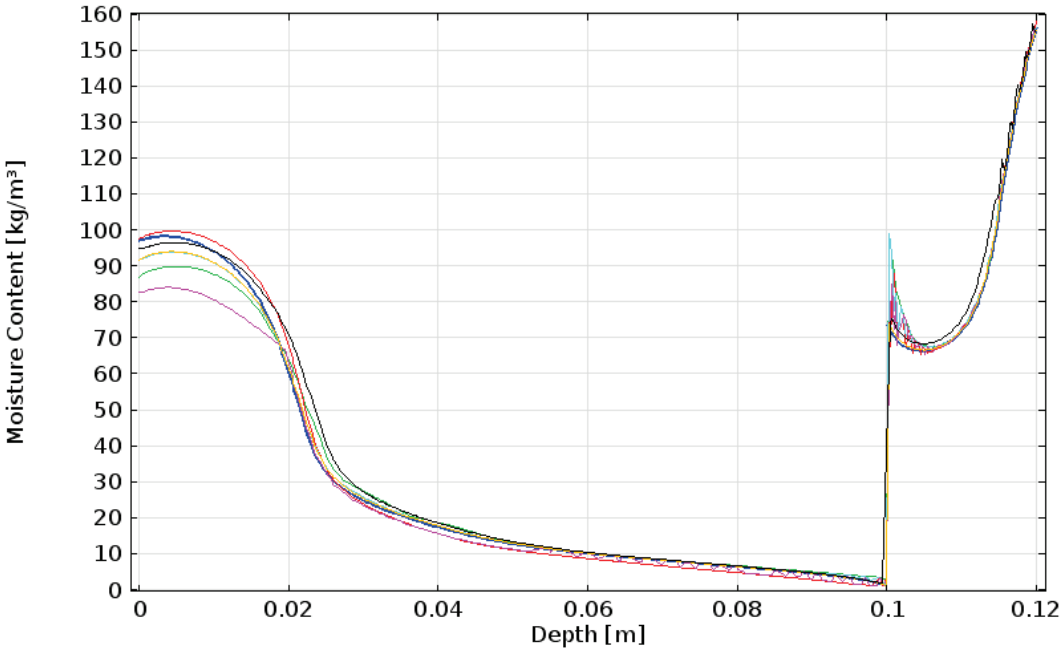

Figure 4.14: Moisture content [kg/m^3] related to depth [m] on 24 hours.

More results from HAMSTAD-benchmark 4 are shown in Annex C.

HAMSTAD-benchmark 5

Benchmark 5 is about a wall with insulation applied at the internal side of the construction. This benchmark was developed by the Technical University of Dresden. It consists at the outside of brick with a width of 365 mm, 15 mm mortar and 40 mm insulation material. The complete description of the benchmark is given in [Hagentoft 2002]. The model was made with a 2D-geometry.

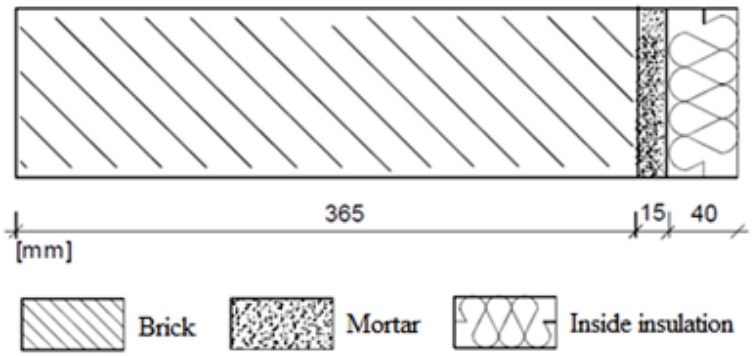

Figure 4.15: Geometry of HAMSTAD-benchmark 5. Source: [Hagentoft 2002].

The boundary conditions are constant and the results are from the last time step, *i.e.* 60 days. The results are the relative humidity and the moisture content of the last time step at 60 days. The results of HAM-BC 2015 are compared with the average values of benchmark 5.

The computer-model-comparison is done with data from HAMSTAD, which are provided by the Catholic University of Leuven, Belgium (KUL); Eindhoven University of Technology, the Netherlands (TUE); National Research Council, Canada (NRC), University of Technology Dresden, Germany (TUD); Technion-Institute of Technology, Israel (Technion); and Chalmers University of Technology, Sweden (CTH).

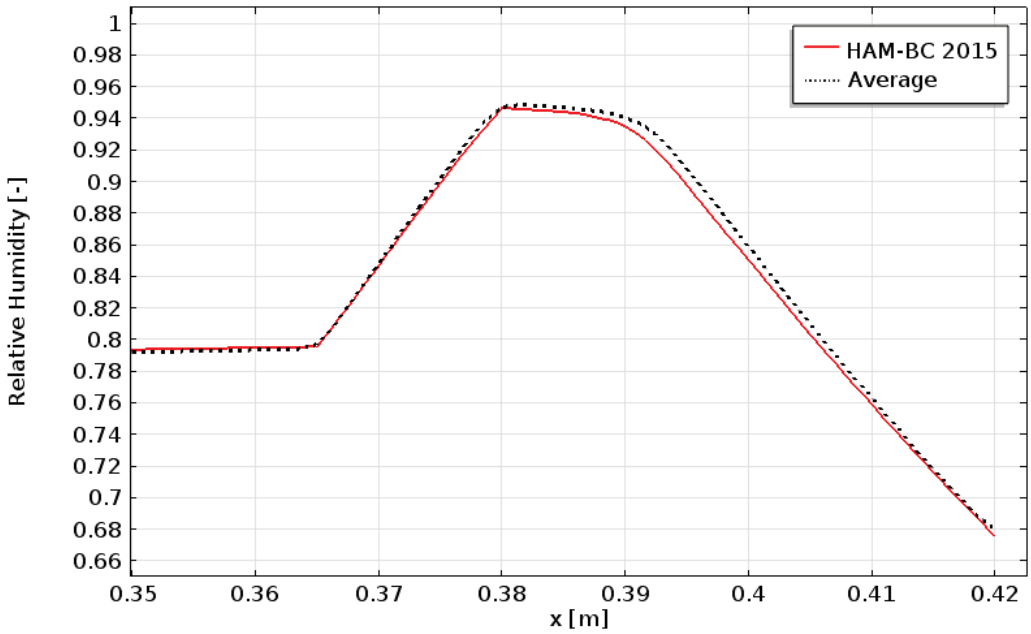

Figure 4.16: Relative humidity [-] related to the depth [m] on day 60. The result from HAM-BC 2015 is in red. The average results of HAMSTAD are depicted with the dotted line.

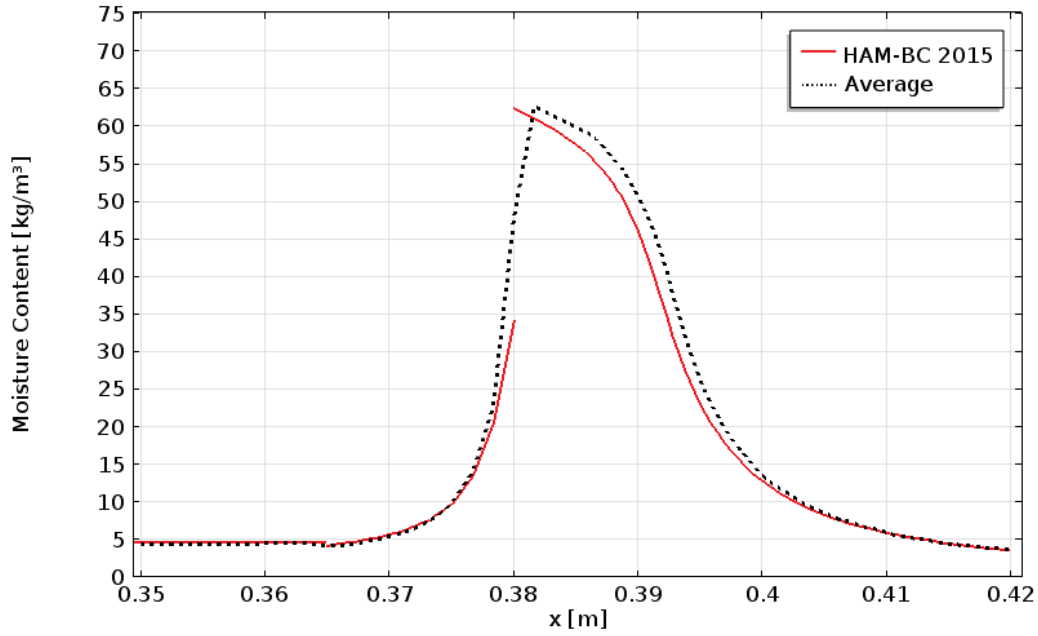

Figure 4.17: Moisture content [kg/m^3] related to the depth [m] on day 60. The result from HAM-BC 2015 is in red. The average results of HAMSTAD are depicted with the dotted line.

In figure 4.17, a part of the graph of HAM-BC 2015 has a gap, due to the fact that each material has its own moisture retention curve. This means that COMSOL generates for each material its own graph; and therefore, the line is not continuous.

4.2 Validation with dataset from climate chamber in France

HAM-BC 2015 is empirical validated with the dataset from [Rafidiarison et al. 2015][1]. The article [Rafidiarison et al. 2015] describes the measurements of four wall configurations in a double climatic chamber for creating a dataset with the purpose to be used for empirically validation of hygrothermal simulation models. The climatic chamber is located at the *Laboratory of Studies and Research on Wood Material* (LERMAB) at the *School of Wood Science and Timber Engineering* (ENSTIB) in the French city Epinal. The two chambers were divided by a wall, which contained four wall configurations. The temperature and relative humidity of the chambers and inside the materials were measured. Also the air pressure difference between the two chambers was determined.

More information about the chamber design, climatic conditions, instrumentation and materials is described in [Rafidiarison et al. 2015]. The investigation of the material properties used in the wall configuration is described in [Vololonirina et al. 2014]. Additional information about the material properties and environmental data are given in Annex D.

Figure 4.18: Photograph of the climate chamber. Source: [Rafidiarison et al. 2015]

The measurements at the material surface and inside the material were done with SHT 75 sensors of the manufacturer Sensirion with an inaccuracy of ±0.3°C and ±1.8% RH. These sensors are also used to determine the ambient air temperatures. The surface temperatures are measured with T-type thermocouples with an inaccuracy of ±0.5°C. This information and more information can be found in [Rafidiarison et al. 2015].

[1] *Helisoa Rafidiarison, Romain Rémond, Eric Mougel, Dataset for validating 1-D heat and mass transfer models within building walls with hygroscopic materials, Building and Environment, Volume 89, July 2015, Pages 356-368, ISSN 0360-1323, http://dx.doi.org/10.1016/j.buildenv.2015.03.008.*

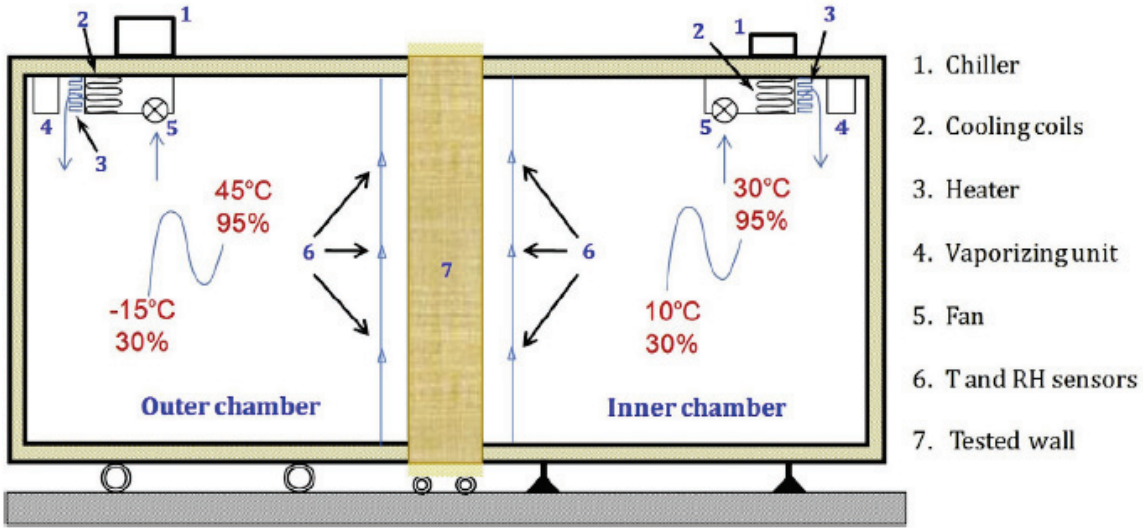

Figure 4.19: Schematic representation of the climate chamber. Source: [Rafidiarison et al. 2015].

The climate conditions are measured at each wall configuration. The climate data measured at wall configuration 1 is shown in graph 4.20. The climate conditions measured at the other wall configurations are shown in Annex D. The term *external* refers to the side of the configuration at the outer chamber.

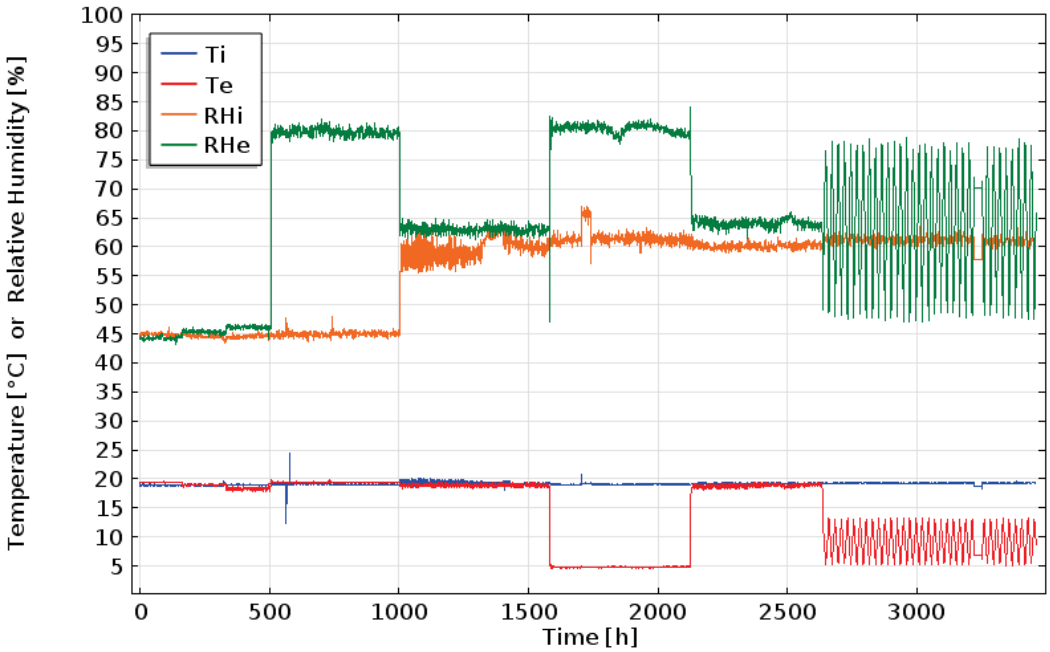

Figure 4.20: Climate data measured at wall configuration 1 with indoor temperature (Ti), external temperature (Te), indoor relative humidity (RHi) and external relative humidity (RHe).

After 2634 hours there is a daily oscillation of the temperature and the relative humidity in the outer chamber. The external vapor pressure – which is not shown in the graph – have at that interval a daily oscillation with a minimum of approximate 700 Pa and a maximum of approximate 760 Pa in the climate data measured at wall configuration 1. Figure 4.20 shows the climate data as used in the simulation of wall configuration 1, whereas for the temperature of the inner chamber at the interval between 1703 hour and 1755 hour a large increase of the temperature was removed, because otherwise this would lead to a singularity error which terminated the simulation process.

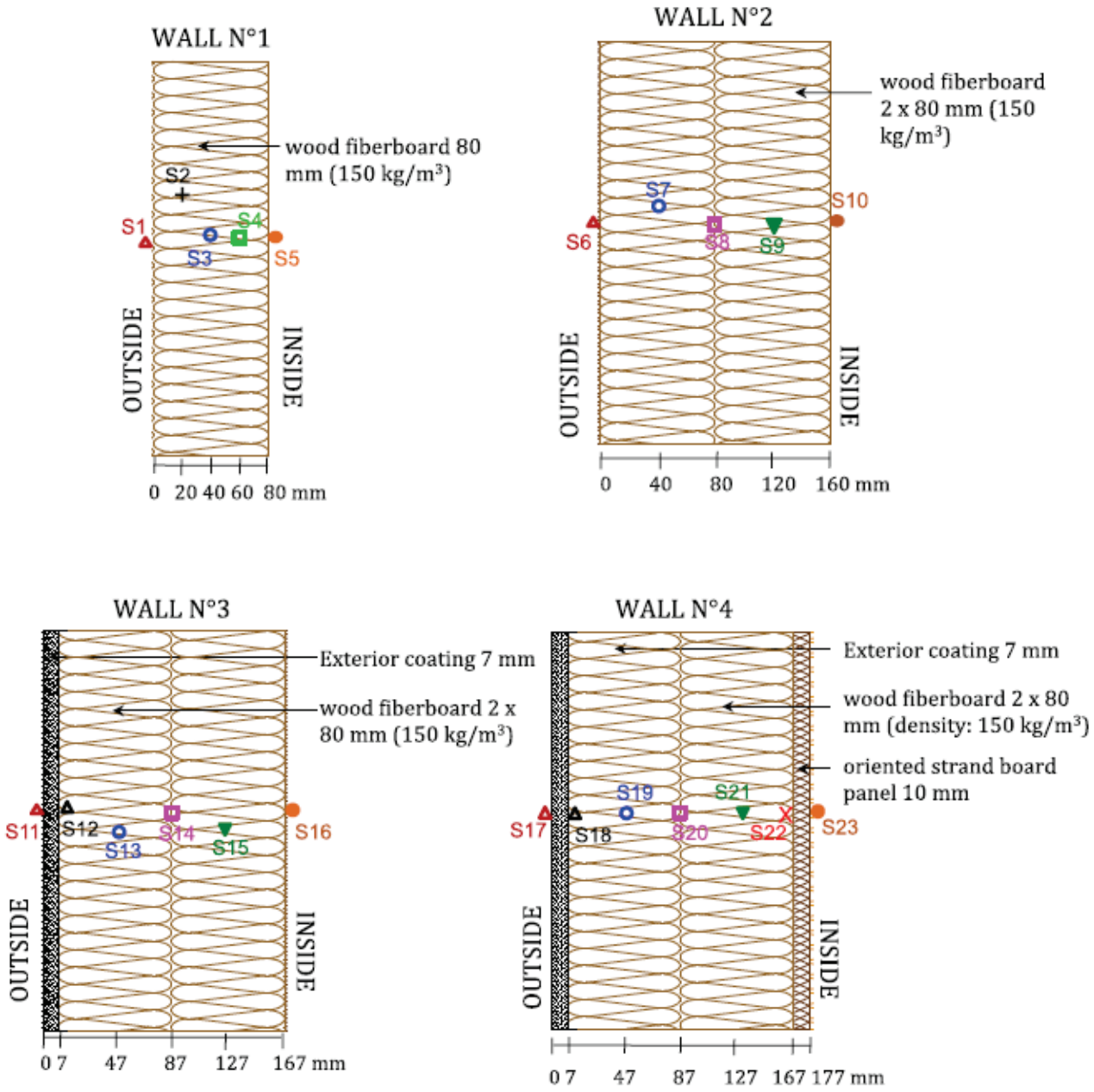

Figure 4.21: Wall configurations 1, 2, 3 and 4. Source: [Rafidiarison et al. 2015].

All simulations of the wall configurations in the climate chamber have a time step of one hour, because both the climate information as the measurement results were given as hourly data. The simulation model interpolates linearly between the known values of the climate and result data. The size of the time steps influences the plotting of the graphs, because the graphs are made by interpolating between the results at each time step.

The simulation results for each wall configuration are separate discussed per paragraph. More results in graphs of the validation study with the dataset from [Rafidiarison et al. 2015] are shown in Annex D. The quality of the simulation is described with the use of the percentage Root Mean Square Error (%RMSE) and the maximum error between the simulation results and the measurement results.

The percentage Root Mean Square Error (%RMSE) is determined by:

$$\%\text{RMSE} = \sqrt{\frac{\sum(V_{meas} - V_{sim})^2}{n}} \cdot \frac{100 \cdot n}{\sum(V_{meas})} \tag{4.1}$$

%RMSE = percentage Root Mean Square Error
V_{meas} = values of the measurement
V_{sim} = values determined with the simulations
n = amount of values

Wall configuration 1

In table 4.1, the percentage Root Mean Square Error and the maximum error are shown of the simulation results of wall configuration 1. The results of the simulation with the sophisticated convection method have lower error values than the results from the simple convection method for the relative humidity, especially for the relative humidity at the internal surface.

Table 4.1: The percentage Root Mean Square Error (%RMSE) and maximum error for the simulation of wall configuration 1. The simulation is done with both the simple convection method and the sophisticated convection method of HAM-BC 2015.

	Temperature				Relative Humidity			
	%RMSE		Maximum Error		%RMSE		Maximum Error	
Location	Simple	Sophisticated	Simple	Sophisticated	Simple	Sophisticated	Simple	Sophisticated
External	7.57	7.52	4.16	4.14	7.07	7.08	9.95	9.93
20 mm	4.05	4.05	2.01	1.98	5.56	5.55	9.71	9.68
40 mm	1.86	1.89	1.44	2.26	5.62	5.59	8.51	8.54
60 mm	4.63	4.67	4.52	4.53	6.18	6.17	6.63	6.56
Internal	3.07	3.04	4.33	4.67	5.52	5.54	10.02	8.41

The graphs in this section are generated with the sophisticated method. The best results were derived at location 40 mm depth, while the worst results were at a depth of 60 mm.

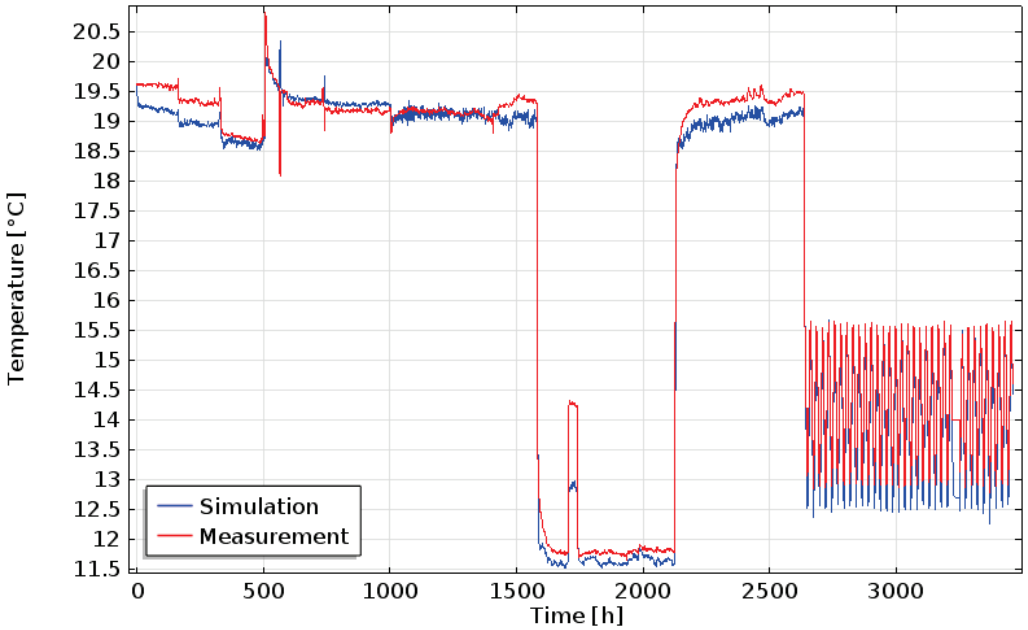

Figure 4.22: Temperature [°C] at the depth 40 mm of wall configuration 1.

It is visible in figure 4.22 that at the interval between 1703 hour and 1755 hour there is a sudden increase of the temperature in the material, which is caused by a sudden temperature increase at the internal temperature. It is visible that the increase according to the simulation model is lower than the peak of the measured value. This is caused by the fact that the sudden temperature increase in the boundary conditions of the simulation model was lowered, because otherwise a singularity-error occurred in COMSOL. This problem is a shortcoming of HAM-BC 2015.

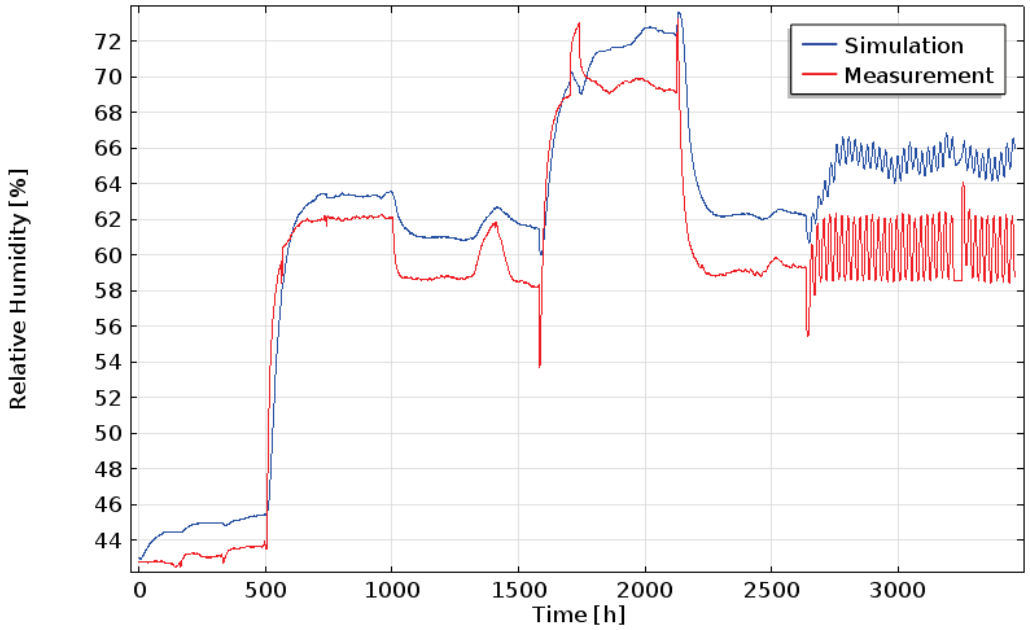

Figure 4.23: Relative Humidity [%] at the depth 40 mm of wall configuration 1.

In figure 4.23, the simulated values are almost always higher than the measured values. In the simulation, the moisture retention curve of the *Wood Fiber Board* from the Delphin-database of materials is used instead of the moisture retention curve from the article [Rafidiarison et al. 2015], because this lead to better results. This is almost certainly caused by the fact that the Delphin-values consist of 100 values, instead of the 6 values from the article.

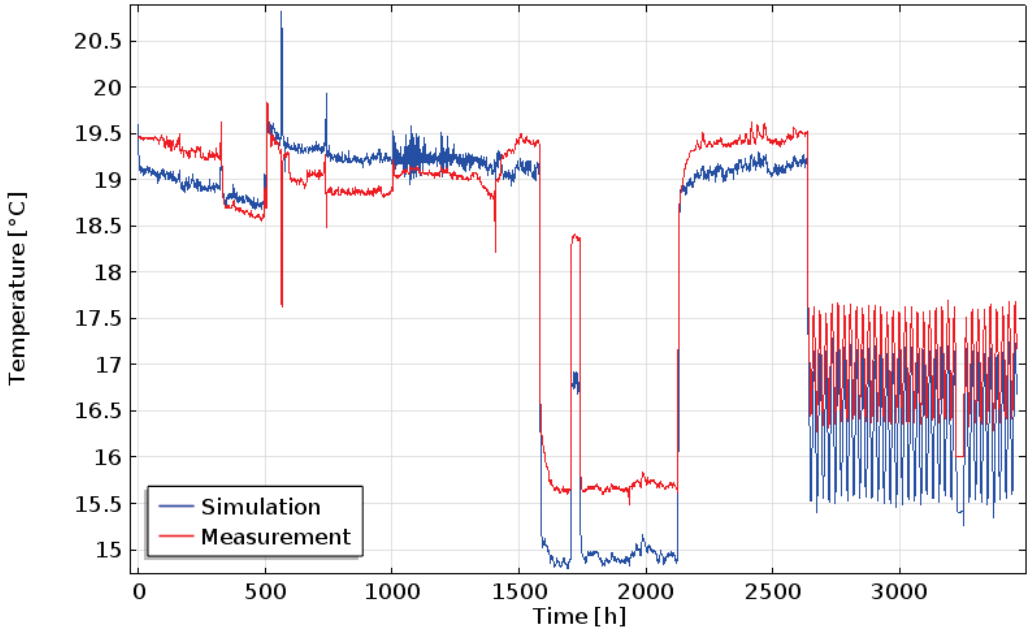

Figure 4.24: Temperature [°C] at the depth 60 mm of wall configuration 1.

Figure 4.24 and 4.25 show the results at depth 60 mm, from which both the graph of temperature and relative humidity show the same trend, but differ from the measurement.

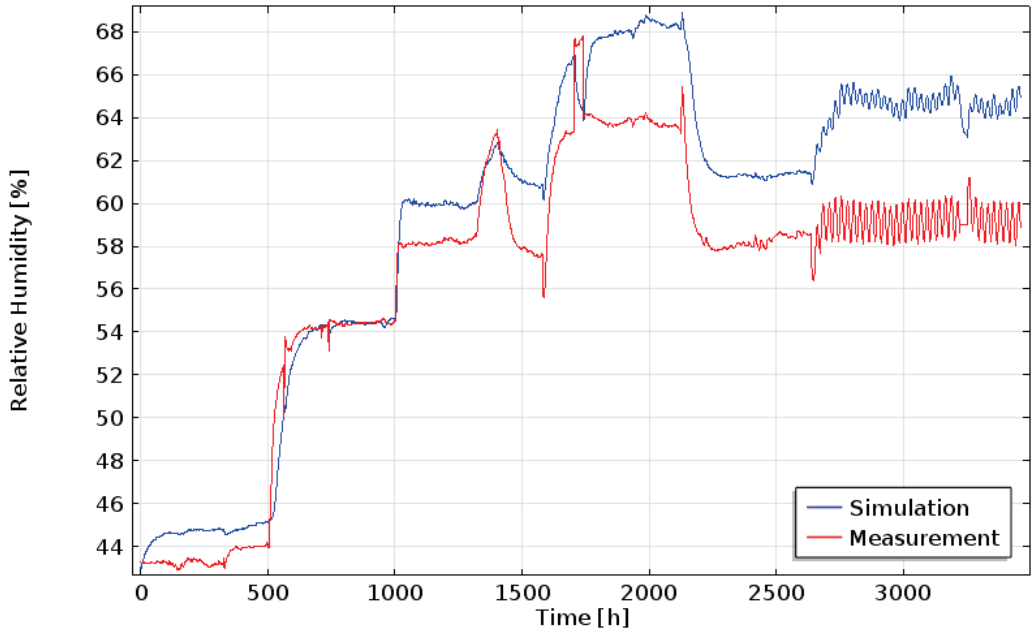

Figure 4.25: Relative Humidity [%] at the depth 60 mm of wall configuration 1.

Wall configuration 2

Wall configuration 2 has a thickness of 160 mm and consists of two layers of wood fiberboard. Wall 2 with both the simple as the sophisticated method is also calculated in a 3D-version, but that lead to similar results. This was also expected, because it is a one-directional transport of heat, air and moisture in a homogenous simulated material. The results are from the 2D-version of the calculation.

Table 4.2: The percentage Root Mean Square Error (%RMSE) and maximum error for the simulation of wall configuration 2. The simulation is done with both the simple convection method and the sophisticated convection method of HAM-BC 2015.

	Temperature				Relative Humidity			
	%RMSE		Maximum Error		%RMSE		Maximum Error	
Location	Simple	Sophisticated	Simple	Sophisticated	Simple	Sophisticated	Simple	Sophisticated
External	7.16	7.13	3.75	3.69	5.79	5.81	16.29	17.19
40 mm	2.57	2.61	2.06	2.09	3.86	4.29	6.39	7.77
80 mm	2.82	2.89	2.39	2.45	3.79	4.61	7.27	8.64
120 mm	2.07	2.08	1.54	1.49	3.95	4.22	4.87	6.02
Internal	2.39	2.38	1.21	1.65	4.86	5.29	7.26	10.4

In table 4.2, it is visible that the simple convection method generates the best results related to relative humidity. The graphs are made with the use of the simple convection method, because this method generated the most accurate results.

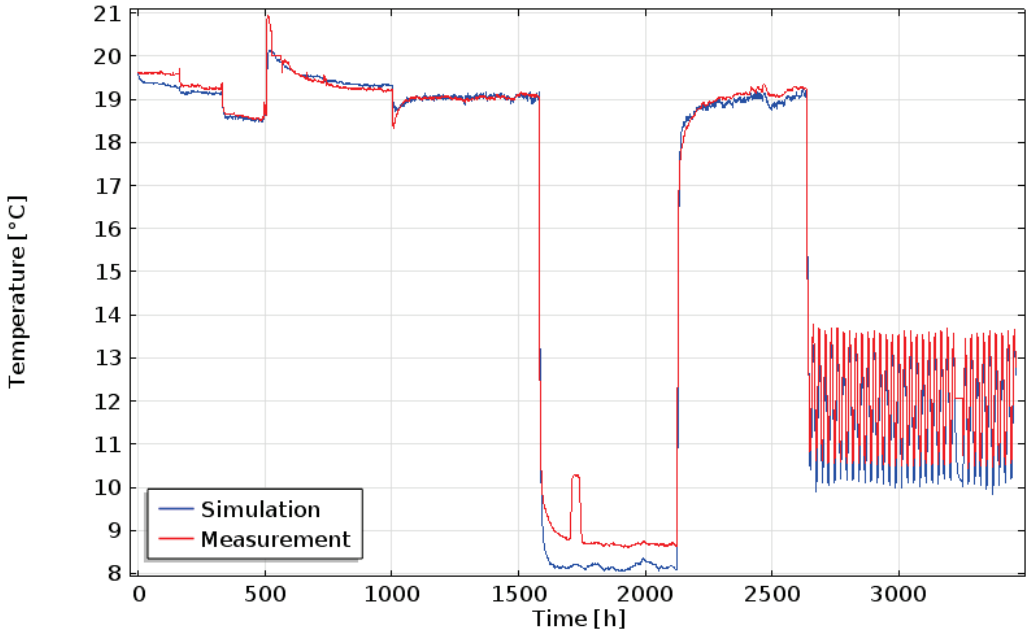

Figure 4.26: Temperature [°C] at the depth 40 mm of wall configuration 2.

The temperature peak at the interval between 1703 hour and 1755 hour is removed to prevent a *singularity*-error, which aborts the simulation. The peak in the measurements and the removal of the peak in the simulation causes that the peak is the largest deviation between the measurements and the simulations.

In the time slot of 2634 hour to 3406 hour with the daily fluctuating boundary conditions are the peaks of the measured temperature and the peaks of the simulated temperature on the same time.

The simulated relative humidity at depth 40 mm – in figure 4.27 – shows a high compliance with the measured relative humidity. The maximum error is 6.39% relative humidity on 1586 hour.

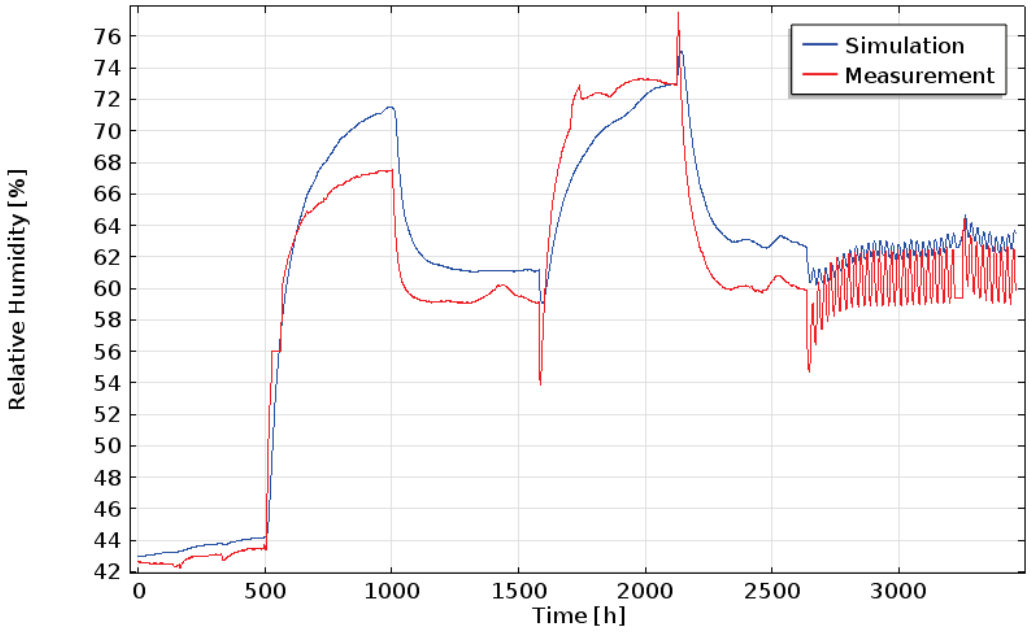

Figure 4.27: Relative Humidity [%] at the depth 40 mm of wall configuration 2.

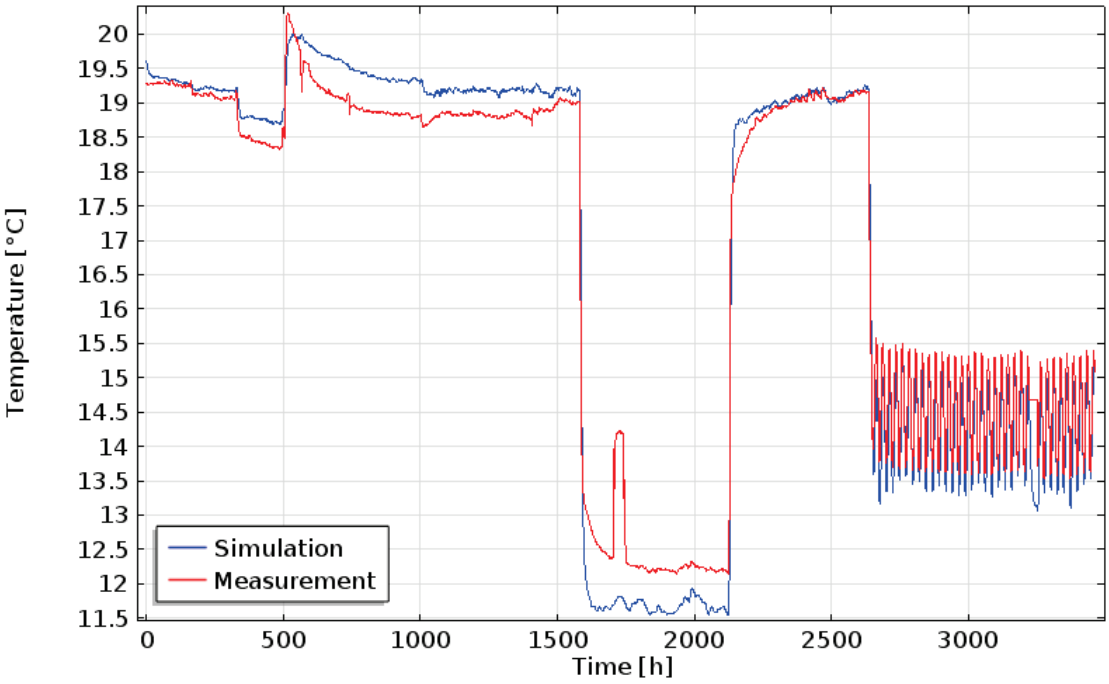

Figure 4.28: Temperature [°C] at the depth 80 mm of wall configuration 2.

Figure 4.28 show a large compliance between the simulation and the measurement, with the exception of the peak at 1703 h to 1755 h. Also a deviation exists of approximate 0.5°C between 563 h and 1495 h; however, the inaccuracy of the sensor related to temperature is 0.3°C.

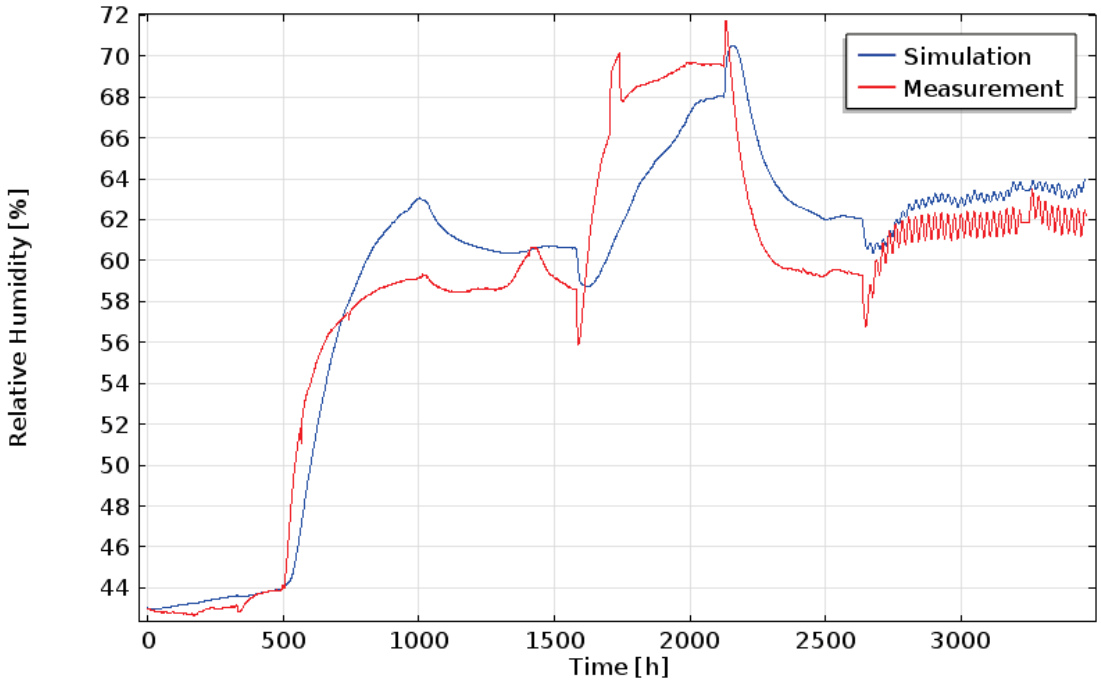

Figure 4.29: Relative Humidity [%] at the depth 80 mm of wall configuration 2.

In figure 4.29 is visible that the simulation and measurements show a large compliance with a maximum error of 7.27% relative humidity near 1709 h.

The effect of the air permeability on the simulation of a single-material construction is investigated with the simulation model of wall configuration 2, because it generated better results than the simulation of wall configuration 1. The simulation model with the simplified method is used and the results are shown in table 4.3. The values of the %RMSE and maximum error are given of the locations in the material were it has the highest values – *i.e.* the worst results. The results at the indoor and outdoor surface are not taken into account, because the air permeability is mainly important for heat and moisture transport inside the material. For the values of %RMSE and maximum error of the temperature this was always at a depth of 40 mm, while the %RMSE of the relative humidity was always on depth 80 mm and the maximum error was on various locations. This variable study was done with the air permeability in the range of $1 \cdot 10^{-4}$ kg/(s·m·Pa) to $1 \cdot 10^{-9}$ kg/(s·m·Pa). The graphs of the relative humidity in the cases of air permeability $1 \cdot 10^{-4}$ kg/(s·m·Pa) and $5 \cdot 10^{-5}$ kg/(s·m·Pa) did not generate the graph shape, which is also visible in the %RMSE and maximum error.

Table 4.3: %RMSE and Maximum Error of the simulation with the simple convection method for several air permeability values (ka) in [kg/(s·m·Pa)] of wall configuration 2.

	Temperature		Relative Humidity	
ka	%RMSE	Max Error	%RMSE	Max Error
1e-4	12.34	7.04	12.14	19.86
5e-5	7.81	4.95	11.96	19.66
1e-5	3.34	2.74	5.76	10.87
5e-6	2.84	2.39	4.11	8.34
1e-6	2.52	2.11	4.48	8.28
5e-7	2.49	2.08	4.55	8.67
1e-7	2.46	2.05	4.61	8.98
5e-8	2.46	2.05	4.62	8.97
1e-8	2.46	2.05	4.62	9.03
5e-9	2.46	2.04	4.63	9.01
1e-9	2.45	2.04	4.63	9.03
0	2.46	2.04	4.62	8.98

Table 4.3 shows that the air permeability is more important for moisture transport than for heat transfer. In comparison with the use of no convectional transport, the value $1 \cdot 10^{-6}$ leads to a decrease of 0.14 %RMSE and 0.7% RH for the simulation of the relative humidity.

Wall configuration 3

Wall configuration 3 consists of an exterior coating of 7 mm at the external side and 160 mm wood fiberboard on the internal side.

In table 4.4, the %RMSE and maximum error are given. It must be mentioned that the first values of the simulation are not taken into account, because of the initial value of the relative humidity was used from the middle of the construction, while according to the measurements in wall configuration 3, there are large differences of the initial values at different locations. The wall configurations 1 and 2 did not have these large differences, probably due to the fact that wall configurations 1 and 2 consisted of one material.

Instead of the material properties given in [Rafidiarison et al. 2015], the material properties of Delphin were used for the coating. The best results were obtained with the moisture retention curve from Delphin of *Gypsum Plaster* multiplied with 6. The multiplying with 6 was done to

get approximate the same values of the 6 data points from the article [Rafidiarison et al. 2015] in the Delphin-properties. The goal was to get the same line-shape of the moisture retention curve with the similar values as given in the article [Rafidiarison et al. 2015]. The moisture permeability and vapor diffusion resistance factor of *Surface coating plaster* was used from the material database of Delphin.

Table 4.4: The percentage Root Mean Square Error (%RMSE) and maximum error for the simulation of wall configuration 3. The simulation is done with both the simple convection method and the sophisticated convection method of HAM-BC 2015.

	Temperature				Relative Humidity			
	%RMSE		Maximum Error		%RMSE		Maximum Error	
Location	Simple	Sophisticated	Simple	Sophisticated	Simple	Sophisticated	Simple	Sophisticated
External	5.69	5.7	4.2	4.19	2.76	2.81	9.47	18.95
07 mm	4.05	4.07	5.98	5.99	7.35	7.36	12.94	12.98
47 mm	1.67	1.69	4.34	4.32	7.33	7.35	12.89	12.89
87 mm	2.86	2.86	2.26	2.25	5.96	5.98	9.69	9.68
127 mm	1.93	1.94	2.97	2.94	5.02	5.03	7.05	7.06
Internal	2.84	2.84	4.18	4.18	1.81	1.81	10.88	11.14

The maximum error of the external surface relative humidity with the sophisticated convection method is 18.95 %, which was caused by a sudden decrease of the relative humidity where the simulation was just a couple minutes later, while on the hourly time step the difference was large; and therefore, that value is not trustworthy. The differences between the simple convection method and the sophisticated method are insignificant. The graphs are made with the simple convection method.

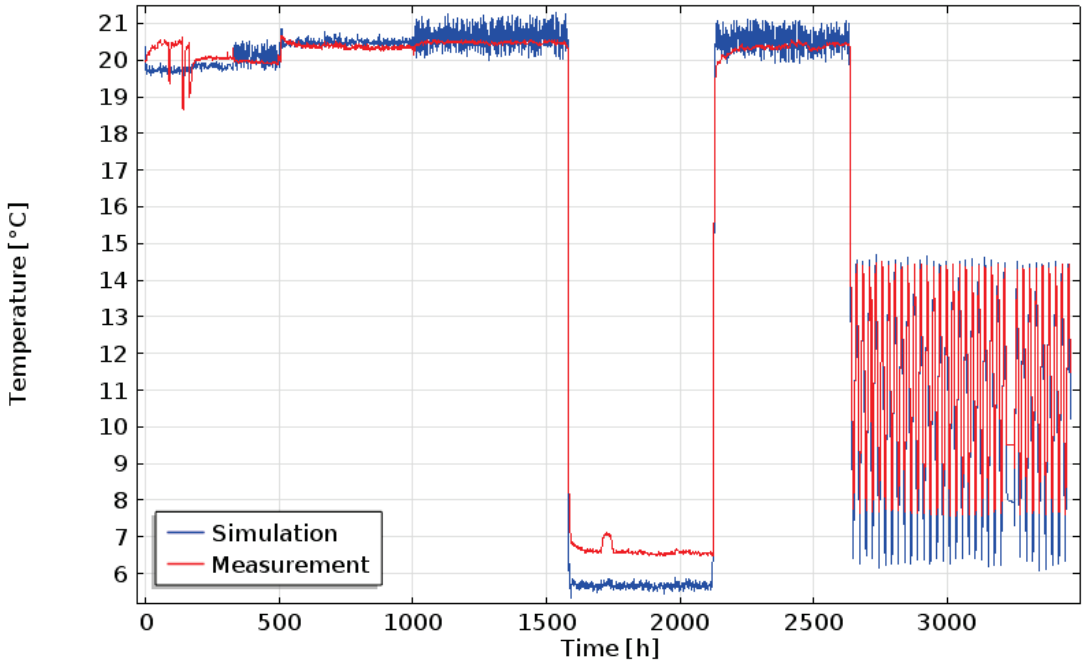

Figure 4.30: Temperature [°C] at the depth 7 mm of wall configuration 3.

In the case of wall configuration 3, the peak around 1600 hours has decreased less than the peak at the internal temperature of wall configuration 1.

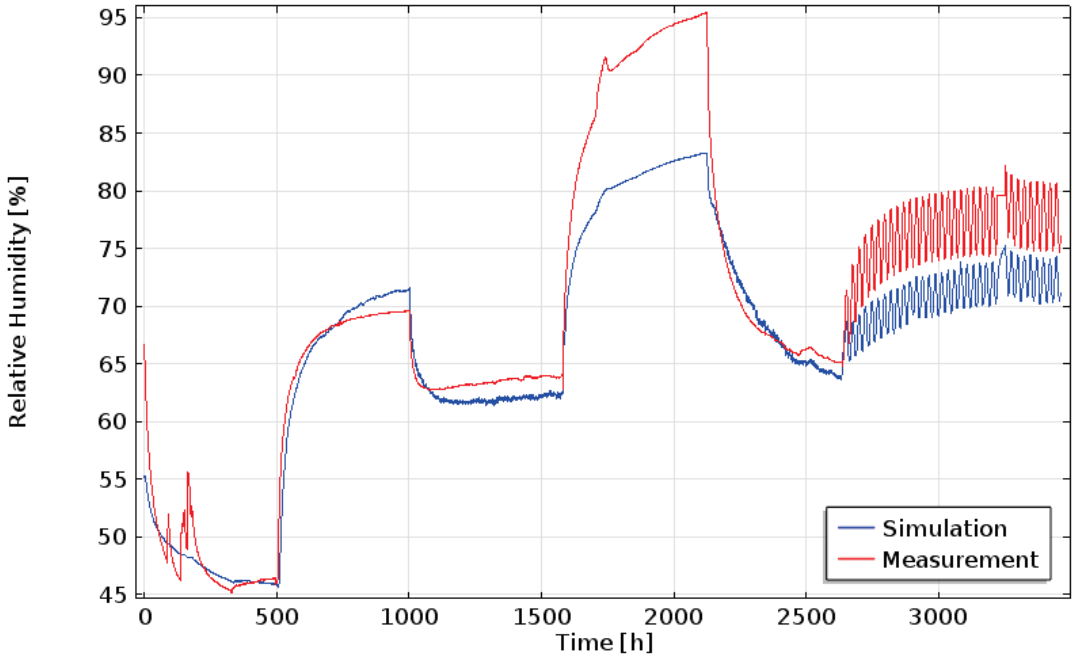

Figure 4.31: Relative Humidity [%] at the depth 7 mm of wall configuration 3.

Figure 4.31 shows the simulated a measured relative humidity at depth 7 mm of wall configuration 3. There is a high deviation between the measured and simulated values between approximate 1600 to 2200 hours of more than 10% relative humidity.

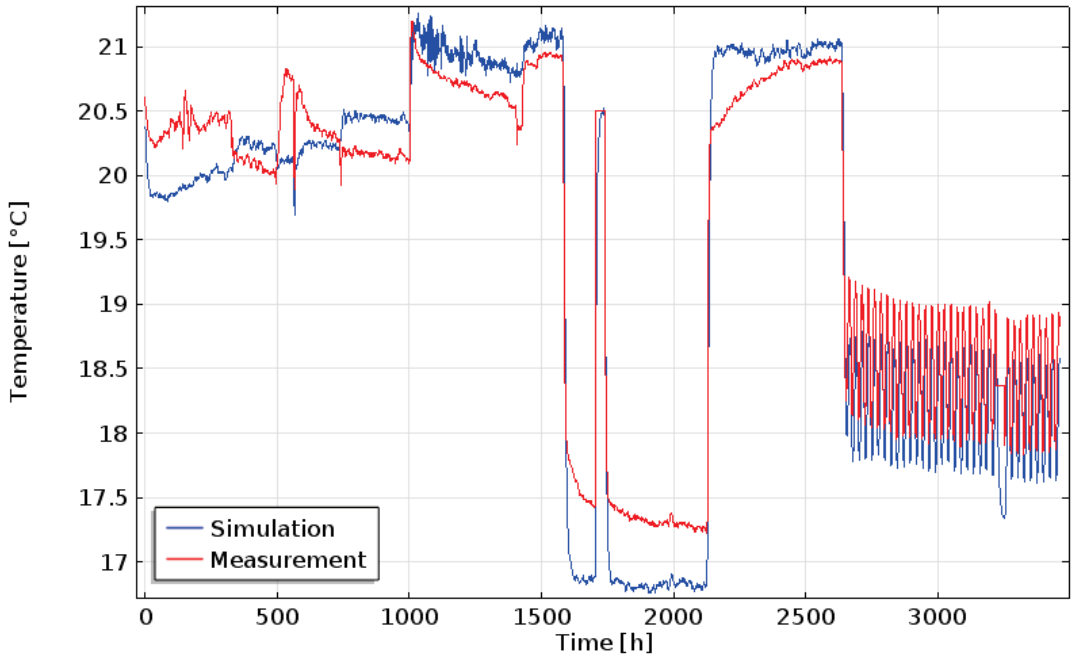

Figure 4.32: Temperature [°C] at the depth 127 mm of wall configuration 3.

The best results in wall configuration 3 were at depth 127 mm for both the temperature as the relative humidity – respectively depicted in figure 4.32 and figure 4.33. The simulation shows the same trend as the measurement data, but with a %RMSE of 5%. As already mentioned, the sensor inaccuracy of relative humidity was 1.8%.

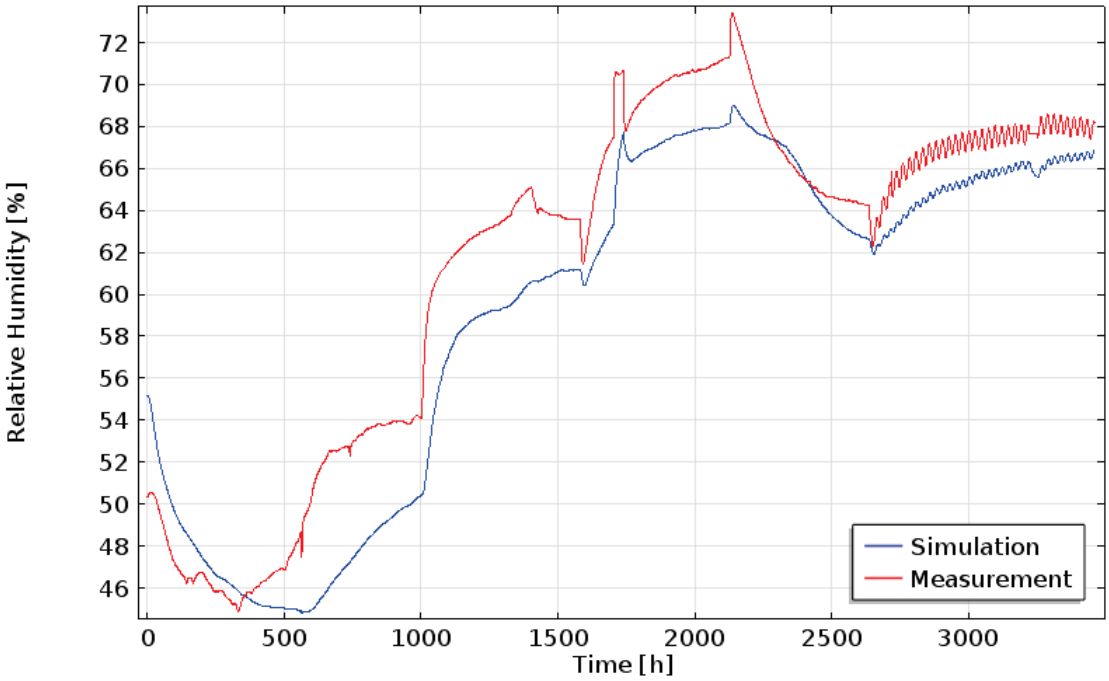

Figure 4.33: Relative Humidity [%] at the depth 127 mm of wall configuration 3.

Wall configuration 4

Wall configuration 4 is shown in figure 4.21. Wall configuration 4 differs from wall configuration 3 that an OSB-board is applied at the side of the internal chamber.

Table 4.5: The percentage Root Mean Square Error (%RMSE) and maximum error for the simulation of wall configuration 4. The simulation is done with both the simple convection method and the sophisticated convection method of HAM-BC 2015.

	Temperature				Relative Humidity			
	%RMSE		Maximum Error		%RMSE		Maximum Error	
Location	Simple	Sophisticated	Simple	Sophisticated	Simple	Sophisticated	Simple	Sophisticated
External	5.70	5.72	4.19	4.18	1.79	1.80	10.04	7.69
07 mm	3.53	3.56	4.55	4.57	3.20	3.19	6.36	6.50
47 mm	1.89	1.91	1.32	1.32	5.39	5.39	6.91	6.92
87 mm	2.32	2.33	1.26	1.26	6.00	6.01	7.16	7.17
127 mm	3.72	3.72	1.92	1.93	7.82	7.82	10.19	10.20
167 mm	3.83	3.83	2.21	2.17	8.89	8.89	11.36	11.35
Internal	3.69	3.69	3.69	3.65	2.24	2.28	7.69	7.70

The difference between the simple convection method and the sophisticated convection method is small, except the maximum error at the external surface regarding to the relative humidity. The sophisticated convection method has in that location a smaller maximum error. For this reason, the graphs of the sophisticated convection are used in this report.

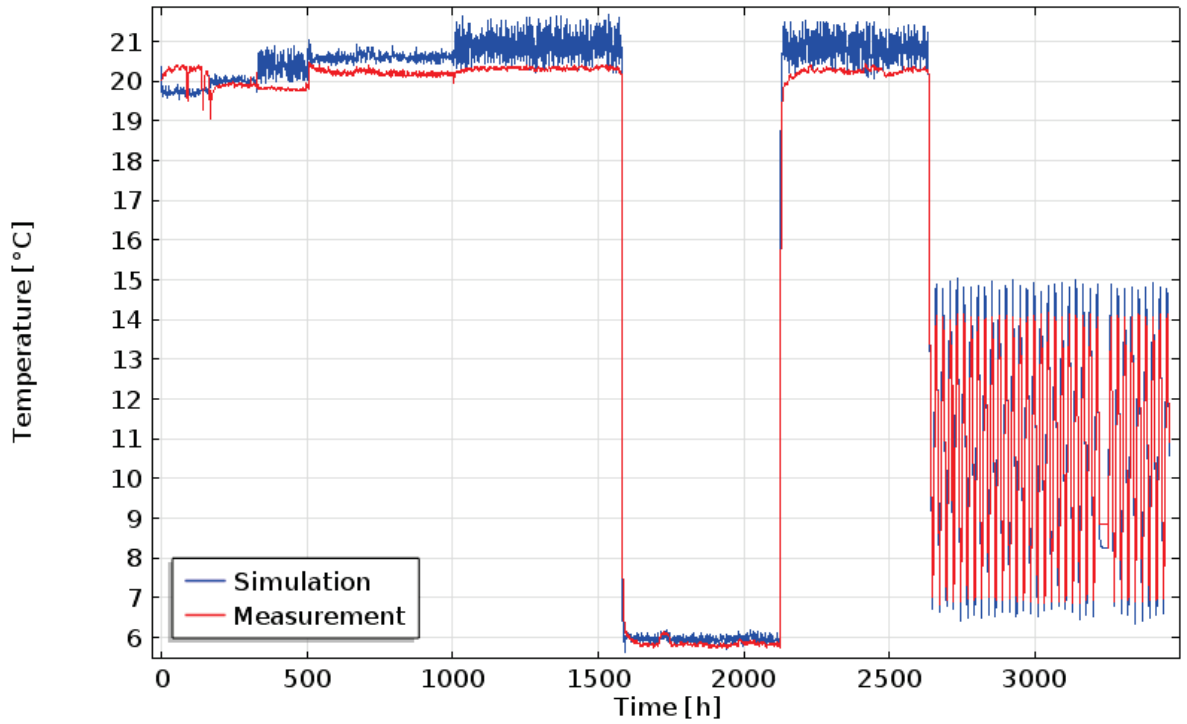

Figure 4.34: Temperature [°C] at the depth 7 mm of wall configuration 4.

HAM-BC 2015 generates reasonable results at the location of 7 mm in wall configuration 4 for both the temperature simulation as the relative humidity simulation. Before 500 hours, the measurements show peaks, but these are not implemented into the simulation to prevent the singularity error.

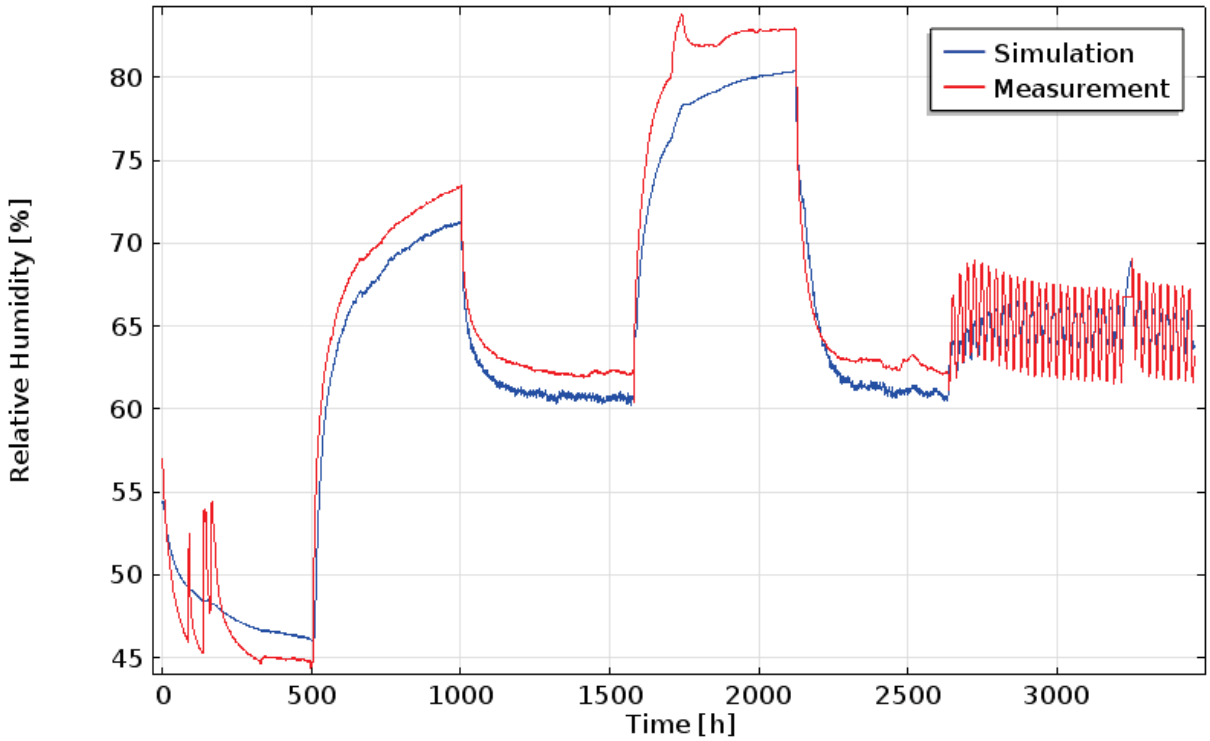

Figure 4.35: Relative Humidity [%] at the depth 7 mm of wall configuration 4.

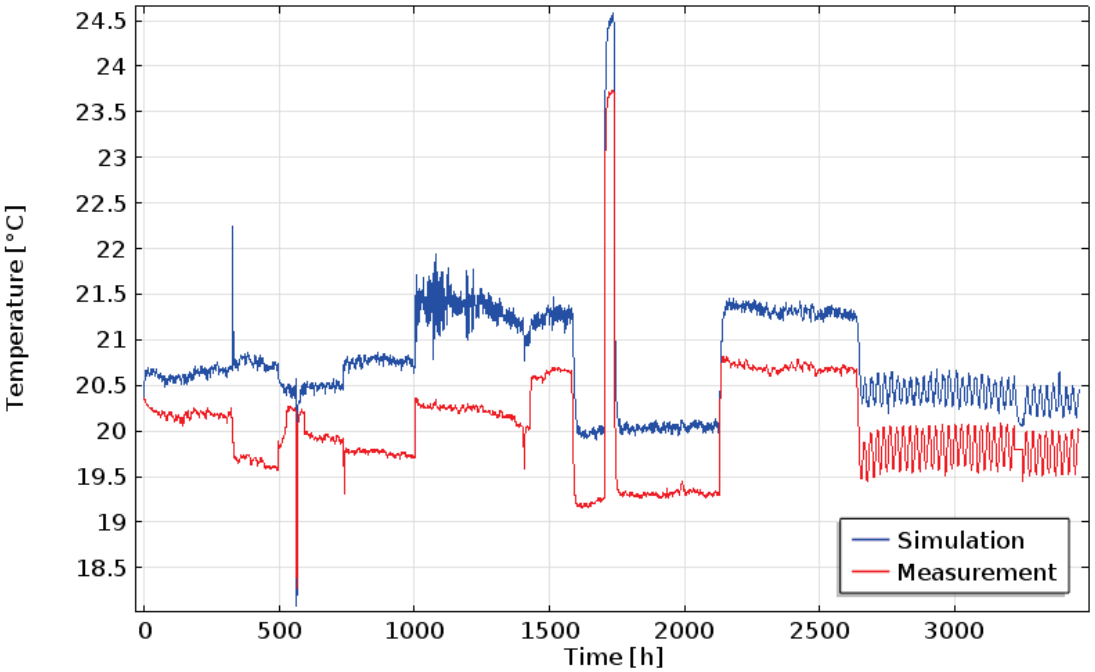

Figure 4.36: Temperature [°C] at the depth 167 mm of wall configuration 4.

The simulation results for the relative humidity from location 167 mm – figure 4.37 – deviates largely from the measurements. The main reason is that [Rafidiarison et al. 2015] mentions strange values for the water vapor diffusion resistance factor of the Oriented Strand Board (OSB), namely 46 (dry cup) and 27 (wet cup). According to the material database of Delphin, the water vapor diffusion resistance factor is in the range of 287 and 376. The vapor diffusion resistance factor dependent on the relative humidity from the Delphin-material *OSB Board* was used minus 95, because this generated the best results. Moreover, the moisture permeability is also used from *OSB Board* multiplied with 20, because this lead to the most accurate results.

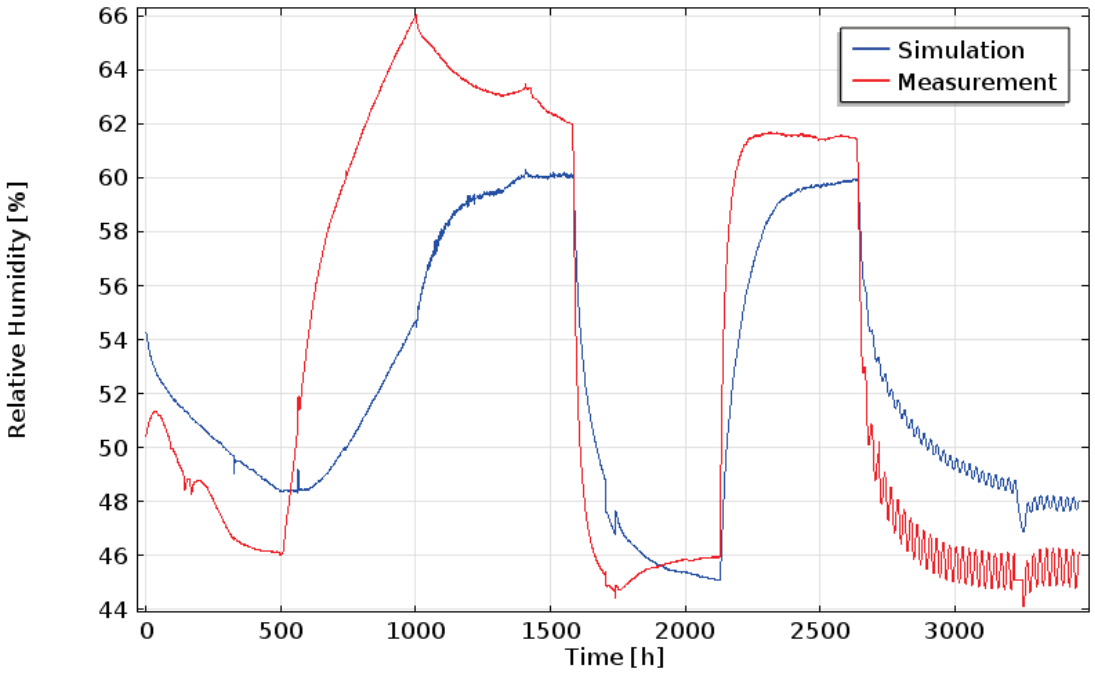

Figure 4.37: Relative Humidity [%] at the depth 167 mm of wall configuration 4.

4.3 Validation with dataset from historical building in Estonia

This section is about the empirical validation of HAM-BC 2015 with the dataset from measurements in a historical school building in the city Kohtla-Järve in Estonia. The measurements are described in [Klõšeiko et al. 2015] and the dataset was made available by the authors. The measurement of the historical school in Estonia occurred from 15/05/2012 to 01/10/2013.

There were some issues with the measurement of the outdoor temperature; and therefore, the authors of [Klõšeiko et al. 2015] also sent the measurements of the weather station in Jõhvi for approximate 9.400 hours. Only the first 9.400 hours are simulated and compared with the measured data. For the outdoor temperature and relative humidity mostly the data from the weather station in Jõhvi is used. This weather station is at approximate 10 kilometers distance from the school building. The solar irradiation used in the simulation model is measured at the weather station in Narva. It is assumed that only diffuse solar irradiation reaches the monitored wall, because the monitored wall is directed to the north. All the weather data were provided by the authors of [Klõšeiko et al. 2015]. The weather data consist of several gaps, which were filled with values of the nearest existing values. The most important gaps in the data are mentioned in Annex E.

The estimation of the horizontal wind-driven rain is made with the use of the vertical rain flux, wind speed and wind direction from the weather station in Jõhvi. The estimation of the wind-driven rain is described in the manual of HAM-BC 2015 – which can be found in Annex A. In Annex E, the environmental data used in the simulations of the historical school building in Estonia are shown.

Figure 4.38: Photographs of the building, received from the authors of [Klõšeiko et al. 2015].

The wall-configurations are:

- Reference wall: original wall without internal insulation
- Calcium silicate (CaSi) with a thickness of 50 mm
- Autoclaved aerated concrete (AAC) with a thickness of 60 mm
- Polyurethane board with capillary-active channels (IQ-T) with a thickness of 50 mm
- Polyisocyanurate (PIR) with a thickness of 30 mm

The temperature and relative humidity between the original wall and the insulation is measured with the sensor Rotronic HC 2 SC05, while the temperature at the internal surface of the wall is measured with Hukseflux HFP01. [Klõšeiko et al. 2015]

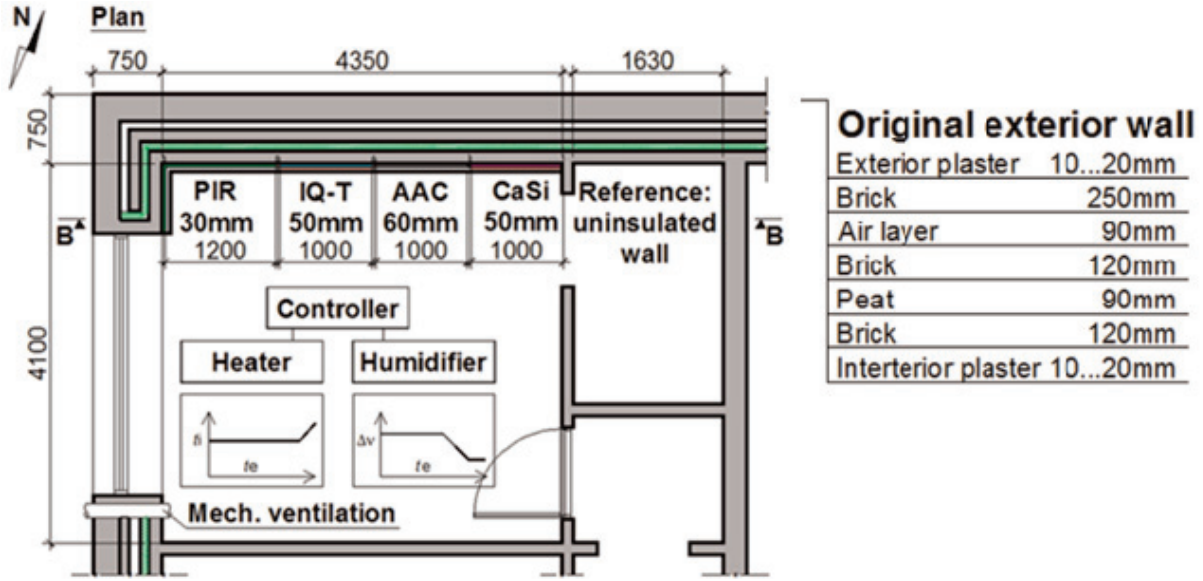

Figure 4.39: Floor plan of the room with the monitored walls. Source: [Klõšeiko et al. 2015]

Errors occurred which terminated the simulations, when using the material properties of the article in the BL-coefficients. This was caused due to the fact that the article gives only the values of the moisture retention curve at the RH-values 33%, 75% and 93%. Simulations with the Delphin-materials did not generate these errors, because the Delphin material database gives 100 values for the moisture retention curve. Therefore, the results are from the simulations with the material properties from Delphin.

First the simulation results are compared with the measured data at several locations. In this chapter, for the reference wall the outdoor and indoor surface temperature are shown, while for the others the temperature and relative humidity are shown at the interface between the old existing indoor plaster and the applied insulation material. More graphs are shown in Annex E. As shown in this chapter, the damage indicators are determined for each wall configuration, which makes it possible to show which insulation materials leads to a less risk on damage.

The graphs show the simulation result and the measured result by the sensors in het middle of the construction. [Klõšeiko et al. 2015] also measured near the ceiling. The %RMSE was not determined due to the large amount of missing values in the dataset.

Reference Wall

The indoor and outdoor surface temperature of the reference wall were measured and used to compare with the simulation. The results shown for the reference wall is simulated with the simple convection method. It must be mentioned that the reference wall is in a different room of the other walls which were insulated. The indoor temperature is measured at the room with the extra insulated walls instead at the reference wall. The heating is in that room; therefore, the temperature in the room of the reference wall is probably lower than the heated room.

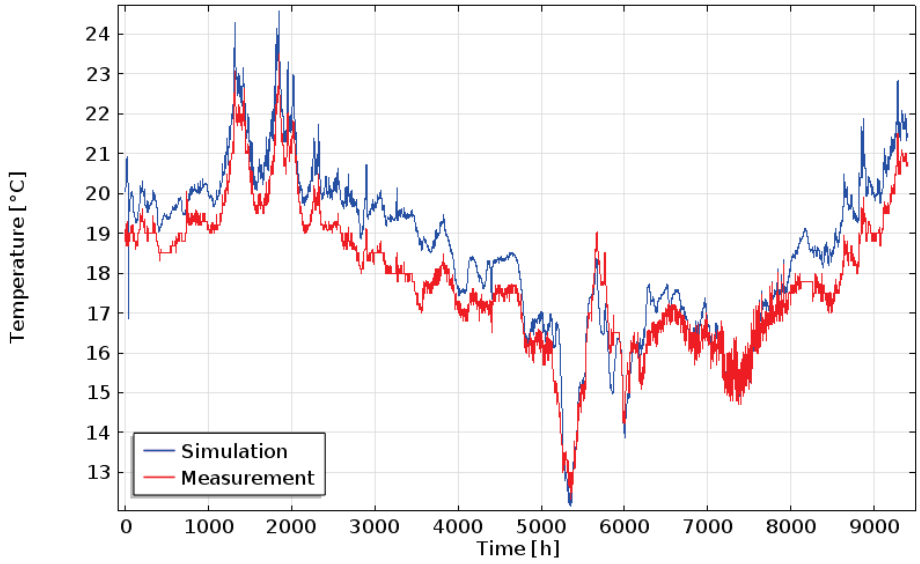

Figure 4.40: Simulated and measured indoor surface temperature [°C] of the reference wall.

In figure 4.40, the simulated and measured indoor surface temperature is shown of the reference wall. The deviation between the measurement and simulation can be caused by the fact that the reference wall is located in another room from where the indoor temperature was measured, which is located next to another not-heated and insulated room.

The simulated temperature at the external surface is depicted in figure 4.41. The outdoor surface temperature of each simulated configuration does not differ much from each other. The graphs of the external surface temperature of the other configurations are shown in Annex E.

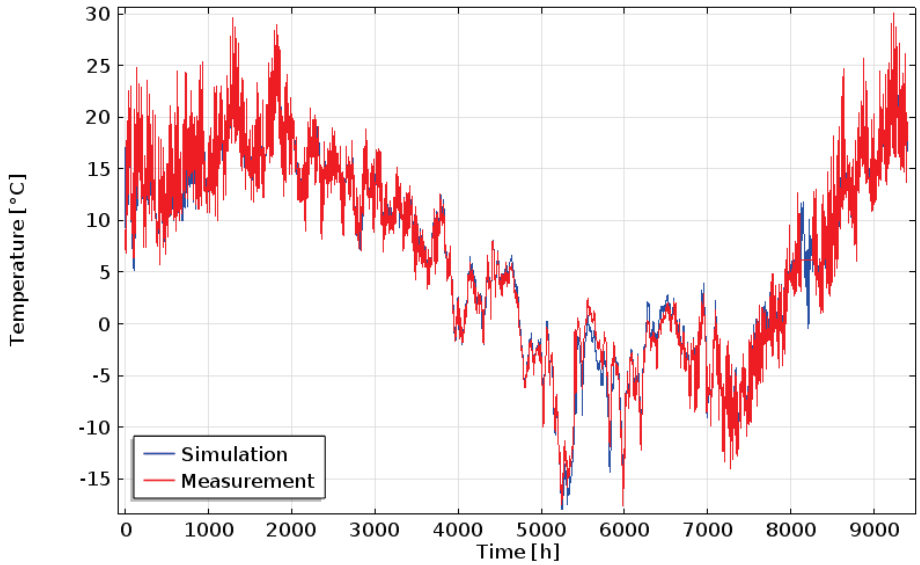

Figure 4.41: Simulated and measured outdoor surface temperature [°C] of the Reference Wall.

CaSi-configuration

The simulation model with the sophisticated convection method generated the best results in the case of the CaSi-configuration. The temperature at the interface of the insulation material and the existing construction is shown in figure 4.42, and the relative humidity on the same location in figure 4.43.

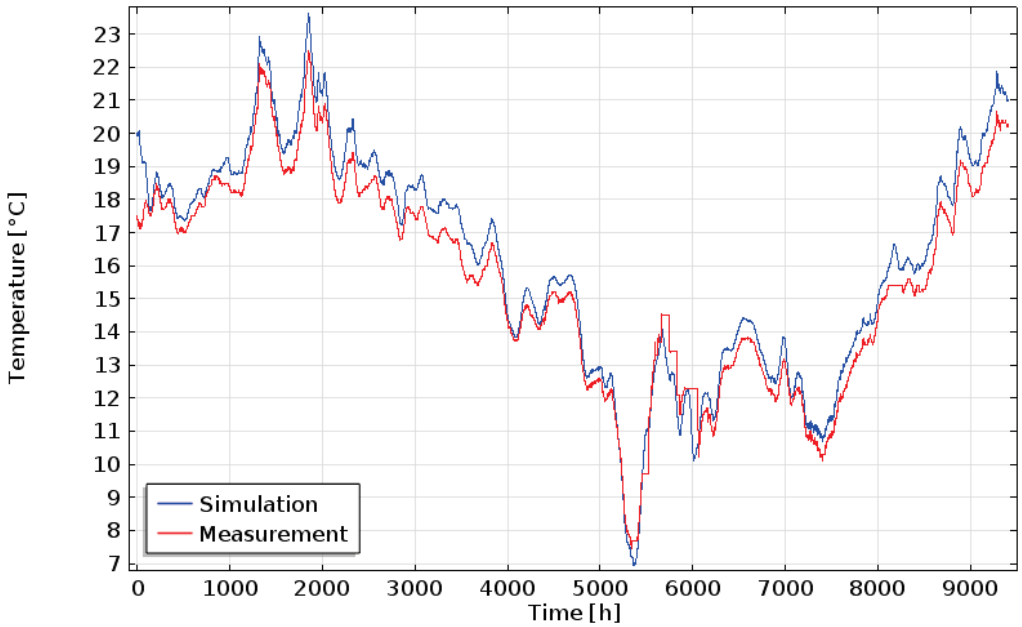

Figure 4.42: Simulated and measured temperature [°C] at the interface of the CaSi-configuration.

The simulated temperature at the interface between the old existing construction and the newly applied insulation has a good correspondence – with the exception of the first part which is caused by the used initial value of the simulation.

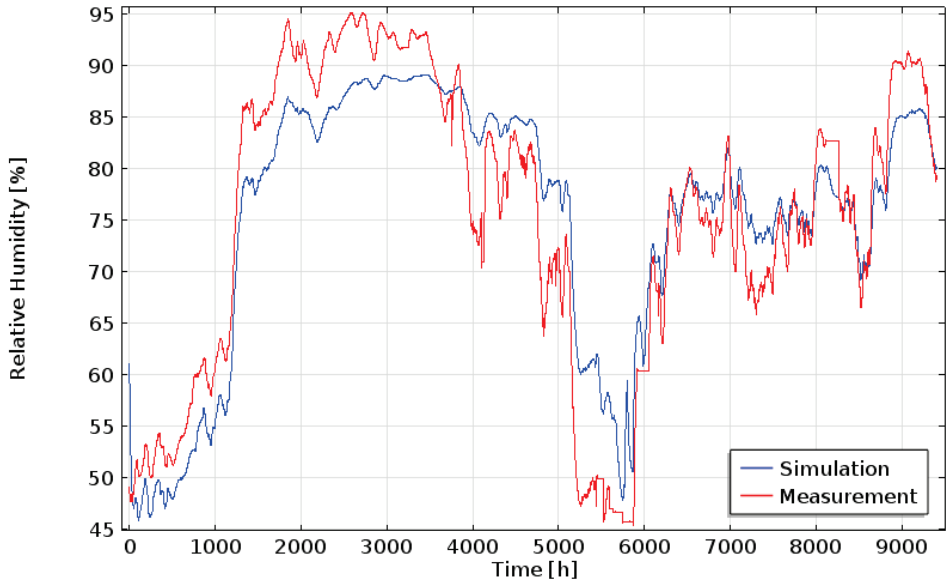

Figure 4.43: Simulated and measured relative humidity [%] at the interface of the CaSi-configuration.

As usual, the simulated RH differs more from the measured value than the simulated temperature. The simulated RH shows largely the same trend as the measurements.

AAC-configuration

The simulation model with the simple convection method generated the best results for the AAC-configuration. The temperature at the interface of the insulation material and the existing construction is shown in figure 4.44, while the relative humidity on the same location in figure 4.45.

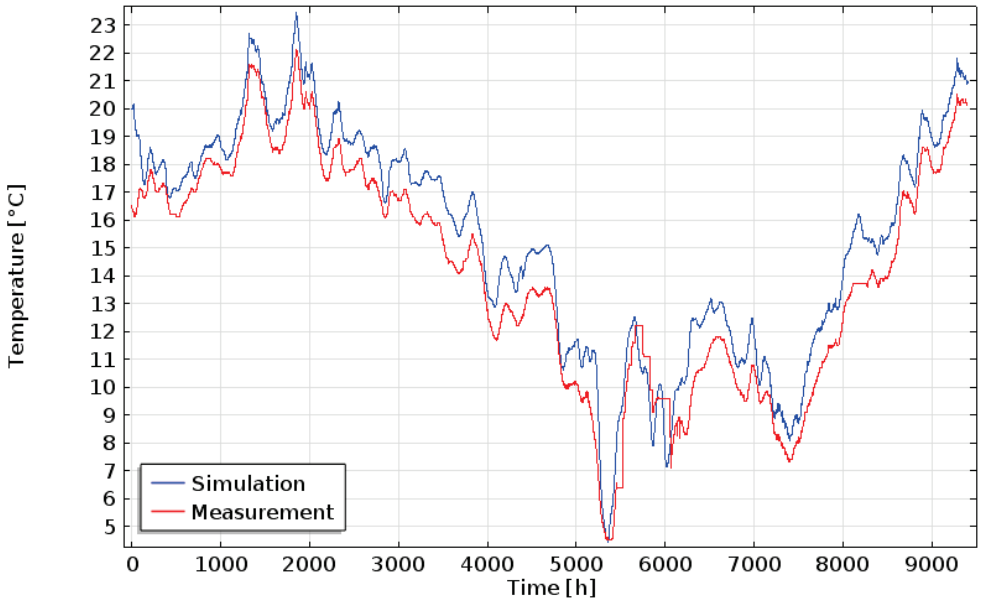

Figure 4.44: Simulated and measured temperature [°C] at the interface of the AAC-configuration.

The relative humidity at the interface of the AAC-configuration is depicted in figure 4.45. This shows that HAM-BC 2015 generates the same trend, but with large deviations. The maximum error is approximate 10%. This is a large shortcoming, because of this large deviation in the area of RH 90% to 100%, both the condensation time and possible the wood decay criteria are underestimated. The possible causes of this large deviation could be the material properties from Delphin.

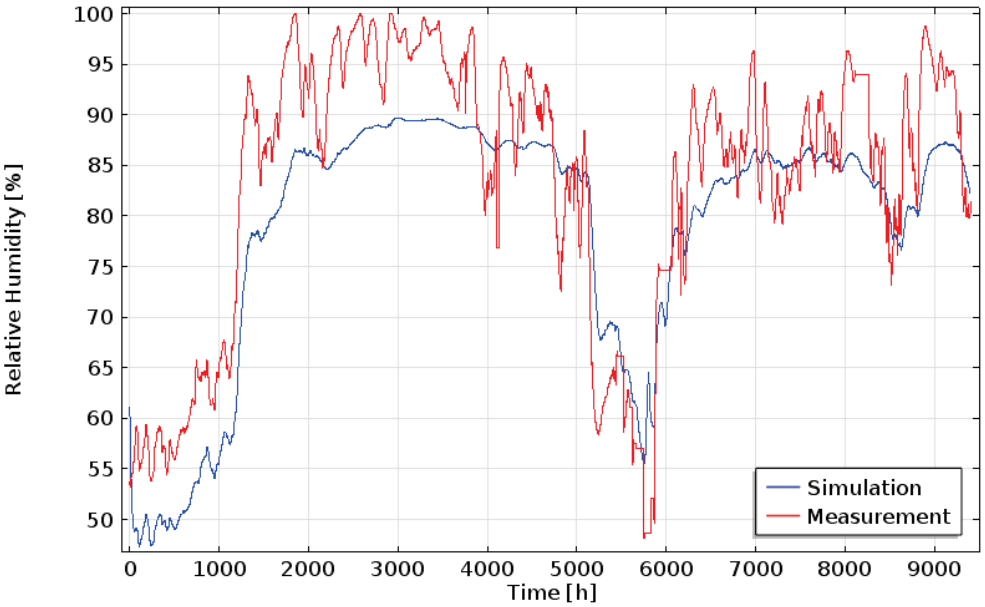

Figure 4.45: Simulated and measured relative humidity [%] at the interface of the AAC-configuration.

IQ-T-configuration

The results from the simulation model with the sophisticated convection method generated better results than the model with the simple convection method for the IQ-T-configuration. The temperature and relative humidity at the interface of the insulation material and the existing construction is shown in figure 4.46 and figure 4.47.

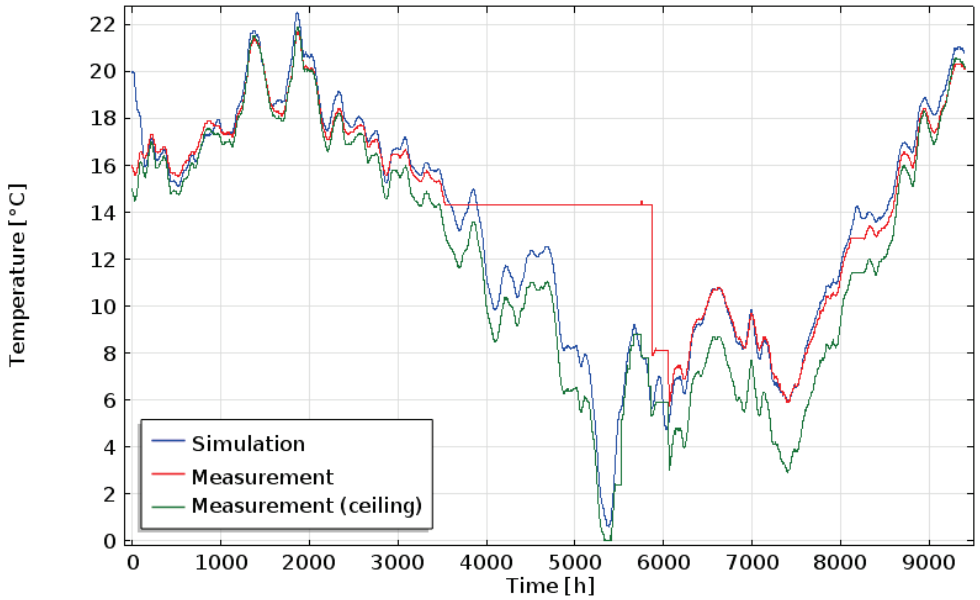

Figure 4.46: Simulated and measured temperature [°C] at the interface of the IQ-T-configuration.

The simulated temperature at the interface is compared with the measured data. The red line is the measurement in the middle of the IQ-T-configuration, which has a large interval with missing data. Therefore, the measurement at the interface near the ceiling is also shown in the graph. Figure 4.46 shows that the simulated temperature is similar as the measurement in the middle, while the area of the missing values is almost the same trend as the measurement near the ceiling. Around 5388 hours the temperature at the interface is near 1°C, when the outdoor temperature was approximate -20°C.

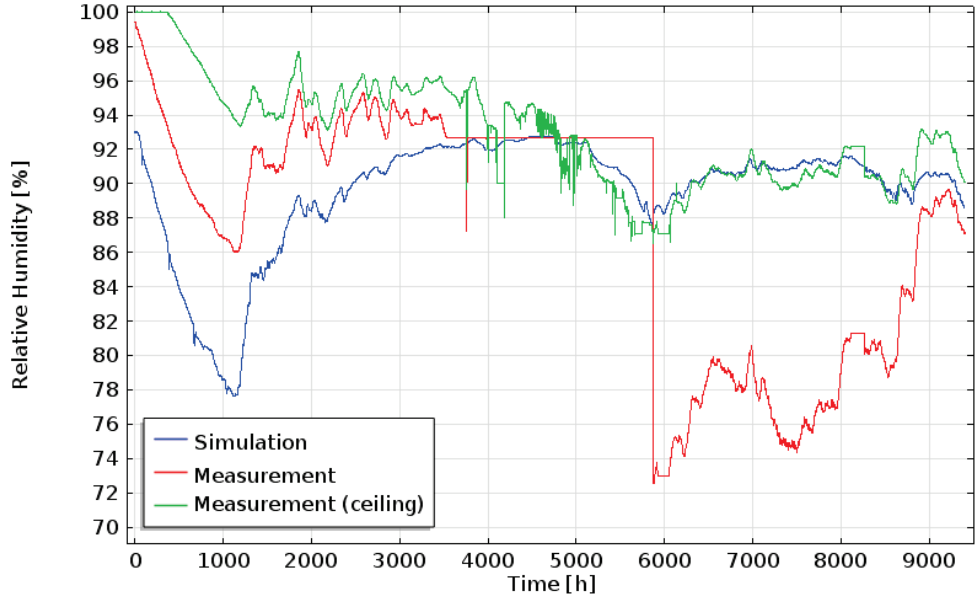

Figure 4.47: Simulated and measured relative humidity [%] at the interface of the IQ-T-configuration.

The simulated relative humidity at the interface differs largely from the measurements. It is assumed that the relative humidity measurement in the middle of the wall (red line) after approximate 3500 hours is not trustworthy. The simulation shows the same trend as the measurements near the ceiling (green line). The initial value of the simulation is lower than the measurements; however, when using a higher initial value in COMSOL this generated an error which terminated the simulation.

PIR-configuration

The simulation model with the sophisticated convection method generated better results for the PIR-configuration than the model with the simple convection method. The temperature and the relative humidity at the interface of the insulation material and the existing construction are shown in figure 4.48 and 4.49.

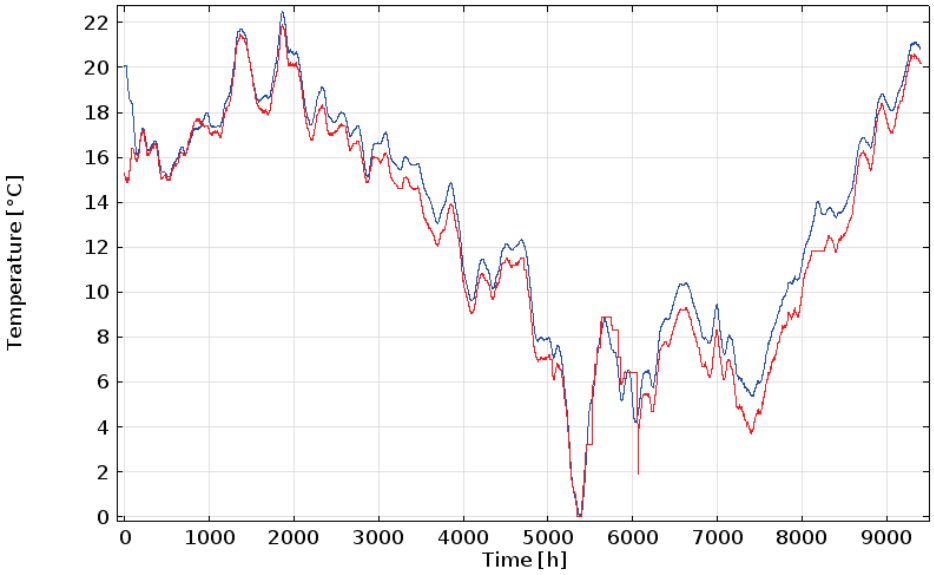

Figure 4.48: Simulated and measured temperature [°C] at the interface of the PIR-configuration.

The simulated temperature at the interface corresponds quite well with the measured data, with the biggest deviation of 2°C.

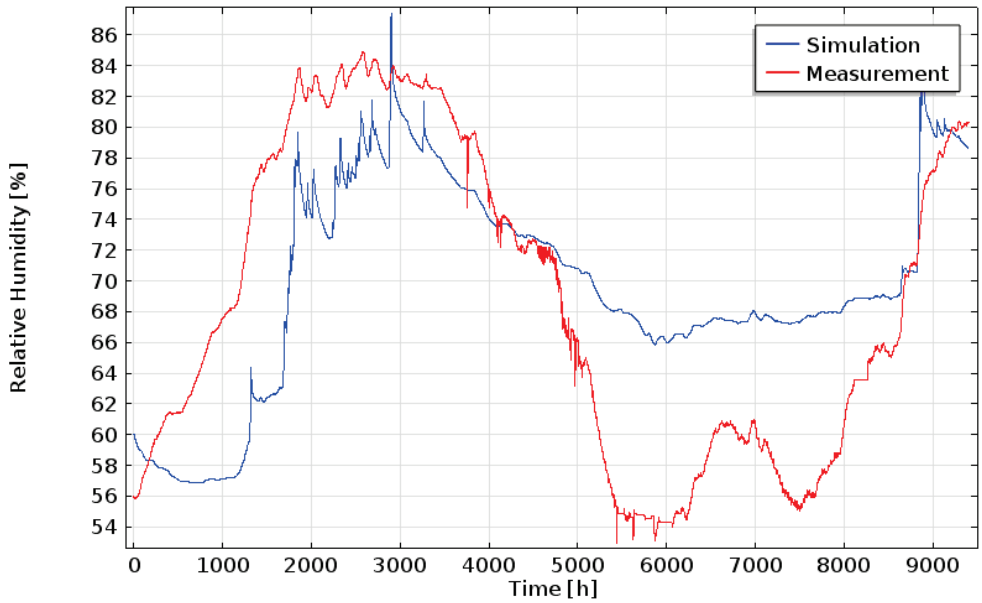

Figure 4.49: Simulated and measured relative humidity [%] at the interface of the PIR-configuration.

Instead of the temperature at the interface, the simulated relative humidity differs largely from the measured data. It even does not follow the trend. The material-database of Delphin did not contain the material properties of PIR, which probably is the reason for this large deviation. Sometimes it even differs 10%.

Possible causes for the deviations

An explanation of the large deviation between the simulation results and the measured data could be the fact that not all material properties were known, for example the air permeability and moisture permeability. Also the air permeability of the air cavity used by Delphin generated simulation results which deviate largely from the measurements.

Certain factors were disregarded or neglected in the simulations. The effect of buoyancy on the convection is not taken into account by HAM-BC 2015 and also the effect of gravity on the air flux (equation 3.4) and moisture transport by capillary suction (equation 3.32) is not taken into account. The geometry was simplified by the fact that the masonry was simulated as one single homogeneous material, whereas the bricks and the mortars were considered to have the same material properties. However, according to [Vereecken 2013], the simulating of masonry as separate bricks and mortar layers did not lead to significant other results as simulating masonry as a homogenous layer of bricks.

Also, the interface resistance at the interface of two materials was not taken into account, which is created by the fact that the surface pores of the two different materials do not perfectly adjoining and adjacently each other. [Vereecken 2013] states that the interface resistance for heat and moisture – *i.e.* the interface between two different materials – has an insignificant influence on the temperature and moisture gradient and can be neglected. The simulation model assumes that each material is homogeneous and the effects of gravity on the moisture content were not taken into account.

Also, the weather data is used from a weather station which was located Jõhvi, which was approximate 10 kilometers from the building. Probably, the trees in the neighborhood of the monitored wall could cause some deviations with the measured value at the weather station. One weakness is that the relative humidity of the external surface was not determined, because otherwise it would be possible to validate the simulation of the rain.

Damage Indicators

The results from the damage indicators are shown in table 4.6. The percentage of condensation depicts the percentage of time that in the total structure is a location where the relative humidity is above 99%. It is chosen to use 99% as damage indicator, because of inaccuracies of boundary conditions and round off errors and deviation of the measurement of which the moisture retention curve.

The percentage that the mold growth criteria are met, are based on a RH-threshold of 80%. The values of wood decay are depicted red, because they are determined for peat, which is not a wood type material. Peat cannot rot, because it is per definition already rotten. The wood decay indicator is determined to test the indicator. Wood decay occurs when the surface relative humidity exceeds 95% and/or the mass moisture content exceeds 0.2 kg/kg. The peat is enclosed between two brick walls, but it is assumed that the criterion of surface relative humidity is still valid. According to [Klõšeiko et al. 2015], the specific density of the peat is 150 kg/m^3.

The total freeze-thaw-cycles has the criteria that the temperature below 0°C. The effective freeze-thaw-cycles have the criteria: temperature below 0°C and capillary moisture content higher than 91 volume percent. The capillary moisture content of the plaster is 75 kg/m^3 and the masonry has a moisture content of 13 kg/m^3, which is based on the material properties given by [Klõšeiko et al. 2015].

Each salt has a different critical RH-value. The two salts which cause the most severe physical damage are chosen. These have the critical RH-percentages of 65% and 90%. The factor of salinity is not taken into account. The damage indicator assumes that the salt in the wall crystallizes and dissolves instantly, which means if the RH comes from 64% to 66%, instantly back to 64% it is still considered as a crystallization-dissolution-cycle.

Table 4.6: Damage indicators determined for all five insulation configurations. The wood decay indicator is depicted red, since it is determined for peat and not for wood.

Damage Indicators	Ref	CaSi	AAC	IQ-T	PIR
Percentage Condensation [%]	86.65	87.72	86.54	88.58	86.69
Percentage Mold Growth [%]	23.48	19.52	19.46	17.63	17.47
Amount of Wood Decay [h]	0	0	0	6666	0
Total freeze-thaw-cycles (plaster)	36	36	36	35	36
Effective freeze-thaw-cycles (plaster)	0	0	0	0	0
Total freeze-thaw-cycles (brick)	36	36	36	35	36
Effective freeze-thaw-cycles (brick)	36	36	36	35	36
Crystallization-dissolution-cycles 65 RH indoor	68	57	52	66	65
Crystallization-dissolution-cycles 90 RH indoor	40	24	25	34	35
Crystallization-dissolution-cycles 65 RH outdoor	174	181	185	181	176
Crystallization-dissolution-cycles 90 RH outdoor	179	172	158	180	173

The wood decay indicator for IQ-T differs significantly from the other configurations. The RH-distribution through the construction of each configuration is shown in Annex E.

The results in table 4.6 confirm that it is not sufficient to investigate only the material at the outside for frost damage, because the material behind the external material could have a lower capillary moisture content; and therefore, can be more vulnerable for effective freeze-thaw-cycles than the external material.

As is shown in table 4.6, the mold growth damage indicator is the highest at the reference wall, which was as expected. The appliance of insulation leads to a higher temperature and lower relative humidity at the indoor surface, because the insulated configurations have a higher thermal resistance than the reference wall without insulation. The Mollier-diagram of the indoor surface of the reference wall is depicted in figure 4.50. In figure 4.51, the same values are plotted in the graph with the isopleths for mold growth according to [Viitanen and Ojanen 2007] and [Hens 1999].

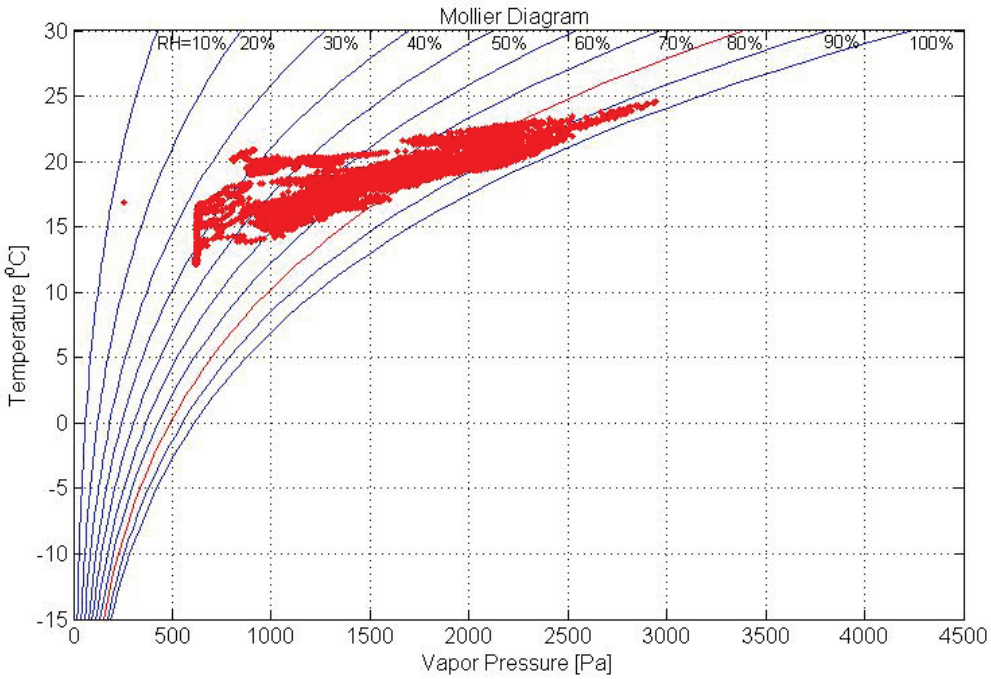

Figure 4.50: Mollier-diagram of the indoor surface of the Reference Wall. Each red point is from one time step. The x-axes depict the surface vapor pressure [Pa] and the y-axes describe the surface temperature [°C]. The lines are the RH, of which the line of RH 80% is depicted red, because that is the RH-threshold for mold growth.

According to a steady state calculation with an outside temperature of -20°C and an indoor temperature of 20°C, the temperature ratio of the Reference Wall is 0.905. This means that the value of the temperature ratio exceeds the minimum requirement of 0.65. According to the temperature ratio method, there is as a low risk on mold growth. However, this contradicts the findings derived from HAM-BC 2015, because the requirements for mold growth are valid for 24% of the time. The negative evaluation of the temperature ratio in this case, is in accordance with the research of [Vereecken 2013], which founds empirically that wall samples with a sufficient high temperature ratio endured mold growth on the surface.

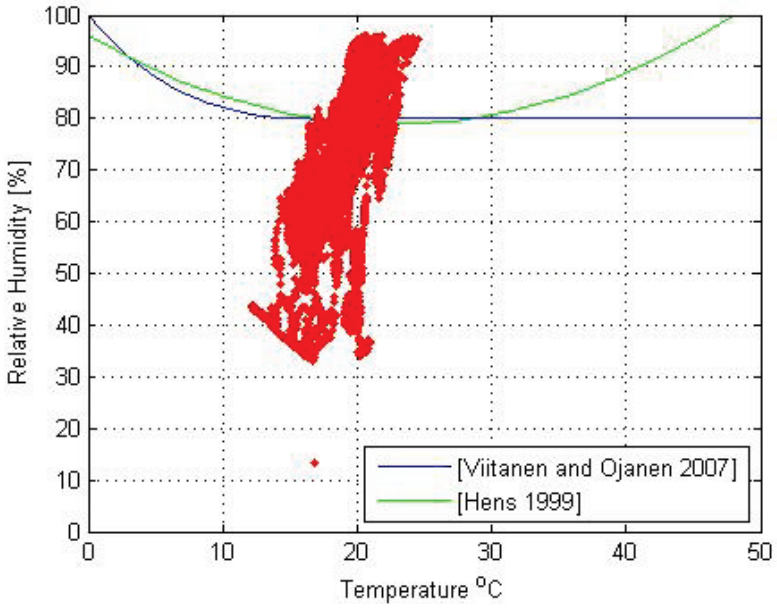

Figure 4.51: Isopleths of mold growth according to [Viitanen and Ojanen 2007] and [Hens 1999] of the Reference Wall. Each red dot is one hourly time step. The x-axes describe the surface temperature [°C] and the y-axes depict the relative humidity [%].

5. Conclusion and Recommendations

Insulating historical buildings can result in damage, such as: condensation, mold growth and wood decay, frost damage, salt damage and thermal cracks. These problems occur mainly because the drying process of the existing construction is affected by insulating the construction, especially when the insulation is applied at the indoor side of the construction.

The hygrothermal simulation model HAM-BC 2015 has been developed and equipped with damage indicators related to damage as a result of insulating historical buildings. The term "*indicators"* is used, because essential and crucial mechanism in the field of physics and biology are excluded, with the result that the model cannot predict damage precisely. Missing mechanisms or variables are for example: substrate quality for fungi, amount of fungi spores; ice volume expansion, salinity and tensile strength of materials. The damage indicators for each damage type are:

Condensation is indicated with the percentage of the time that the relative humidity exceeds 99%. The value 99% is chosen instead of 100% to cope with the inaccuracy of the model and the input.

Mold growth is indicated by the percentage of the time that the relative humidity of the indoor surface exceeds the 80%. Wood decay is indicated by the amount of simulation time steps that the relative humidity at the wood surface exceeds the 95% or when the moisture content of the wood exceeds the 20 mass percent.

Frost damage is indicated by the amount of effective freeze-thaw-cycles ($T \leq 0°C \cap w_{cap} \geq$ 91% volume). Also, the total amount of freeze-thaw cycles ($T \leq 0°C$) is determined.

The indicator for salt damage is the amount of crystallization-dissolution cycles for the sulfates $MgSO_4$ and $MgSO_4$, which have respectively 65% and 90% as critical relative humidity. Sulfates are chosen because these are main causes for physical salt damage.

Validation

HAM-BC 2015 is validated by three means, namely with the HAMSTAD-benchmarks; empirical validation with the dataset of [Rafidiarison et al. 2015]; and also empirical validation with the measured data from a historical school building measured by [Klõšeiko et al. 2015].

HAM-BC 2015 produces results which are in compliance with the results from the simulation models of the HAMSTAD-benchmarks.

The empirical validation with the dataset of [Rafidiarison et al. 2015] proves that in the cases of the wall configurations consisting of one material, HAM-BC 2015 produces reliable results. The wall configurations consisting of more materials, give less accurate results of relative humidity. In all cases, the simulated temperature by HAM-BC 2015 was accurate.

The empirical validation of HAM-BC 2015 with the dataset of [Klõšeiko et al. 2015] demonstrated that the temperature results were trustworthy for all configurations. However, the simulation of the relative humidity generated less accurate results for the IQ-T-configuration and the PIR-configuration. Nevertheless, the simulation of the relative humidity simulation for CaSi-configuration and AAC-configuration generated similar values and trends as the measured data. Probably these deviations occurred because of imprecise material data.

However, inherent model shortcomings cannot be excluded for certain. The damage indicators determined for the historical school building in Estonia lead to the conclusion that the growth conditions of mold was decreased due to the insulating, but the percentage of condensation in the whole construction and the amount of freeze-thaw cycles stayed more or less constant. The salt damage indicators showed large differences between the several insulation configurations.

The hygrothermal simulation model of the manual HAM-BC 2015 generates trustworthy results when sufficient information about the material properties was available.

Recommendations

Improvements or additions to the model

The difference between the simulations and the measurements in the two empirical validation studies may be caused by the calculation method of convection. It is recommended to improve the current sophisticated convection method. A more sophisticated transient convection model may require the internal air pressure and the external air pressure – instead of only the air pressure difference over the construction. Other improvements are the appliance of the buoyancy effect or using the equations of Delphin or the equations described in [Li 2008] and [Dos Santos et al. 2009].

HAM-BC 2015 disregards the effect of gravity in the calculation of the air flux and in Darcy's law. It is recommended to determine the importance of gravity in these equations. In the case that gravity has a significant effect, than it is recommended to implement gravity in a new HAM-BC version.

HAM-BC 2015 assumes that 100% of the rain flux is absorbed, which is not the case in reality. It is recommended to find and implement an absorption coefficient.

Another recommendation is the application of rising damp into the model. It is advised to add the explanation in the appendix of a new HAM-BC version. The boundary conditions related to moisture transport in HAM-BC 2015 have the dimension [kg/(m^2·s)]. However, the appliance of rising damp boundary conditions must also be empirical validated.

Another recommended extension for HAM-BC is the ability to simulate salt migration in constructions, because the current salt damage indicators are too superficial due to the fact that the salt content is not determined. Salt damage only occurs at a certain salinity level.

Another recommendation is the development of a separate manual for simulating the swelling and shrinking of a material related to thermal cracks.

Material properties

The absence of air permeability values was a recurring problem. Therefore, the creation of a database with air permeability of materials is recommended, which was also recommended by [Uittenbosch 2012] and [Voerman 2013].

A recommendation for future studies with the goal for creating a dataset for empirical validation of hygrothermal simulation models is to determine the moisture retention curve of the materials more precise – *i.e.* at more relative humidity values. In case of the school building in Estonia, the imprecise moisture retention curve from [Klõšeiko et al. 2015] caused errors which terminated the simulation. Also, the imprecise moisture retention curve of

[Rafidiarison et al. 2015] caused large deviations. Furthermore, it is advised to determine the moisture permeability k_m of the materials in such studies, because the effect of capillary suction can have a large influence on the results.

Possible research uses for HAM-BC 2015

This report has the development of HAM-BC 2015 as a goal in itself; however, the hygrothermal simulation model could be used as a tool for gaining understanding between the uses of different insulation materials. The damage indicators make it possible to compare different insulation solutions with each other. For example, a choice of a standard masonry wall in a historical building, and investigate which insulation measures and solution generates the lowest values for the damage indicators. Also, case studies about insulating buildings or construction nodes can be simulated.

Another use for HAM-BC 2015 could be the simulation of *reference details,* such as the so-called *SBR-details* in the Netherlands. The SBR-details mentions for some details the temperature ratio. As mentioned in chapter 2, the temperature ratio is not reliable. HAM-BC 2015 determines a better damage indicator for mold growth, and additional indicators about condensation, wood decay, frost damage and salt damage can be determined with HAM-BC 2015.

6. References

Aarle van, M.A.P. 2013. *Hygrothermische simulatie van vorstschade in metselwerk: Effecten van klimaatverandering.* Graduation thesis. Eindhoven: Technische Universiteit Eindhoven.

Adan O.C.G. and Samson R.A. 2011. *Fundamentals of mold growth in indoor environments and strategies for healthy living*. Wageningen Academic Publishers. 2011. e-ISBN: 978-90-8686-722-6.

Aelenei D. and Henriques F.M.A. 2008. *Analysis of the condensation risk on exterior surface of building envelopes*. Energy and Buildings 40 (2008) 1866-1871.

Al-Homaud M.S. 2004. *Performance characteristics and practical applications of common insulation material*. Building and Environment 40 (2005) 353-366.

Barreira E. and de Freitas V.P. 2007. *Evaluation of building materials using infrared thermography*. Construction and Building Materials 21 (2007) 218-224.

Belleghem van M., Steeman M., Janssens A., De Paepe M. 2014. *Drying behaviour of calcium silicate*. Construction and Building Materials 65 (2014) 507-517.

Bellia L. and Minichiello F. 2003. *A simple evaluator of building envelope moisture condensation according to an European Standard*. Building and Environment 38 (2003) 457-468.

Bekke ter T. 2001. *Vochttransport in monumentaal metselwerk*. Graduation thesis. FAGO. Eindhoven University of Technology.

Blocken B., Carmeliet J. 2004. *A review of wind-driven rain research in building science*. Journal of Wind Engineering and Industrial Aerodynamics 92 (2004) 1079-1130.

Boos P. and Giergiczny Z. 2010. *Testing the frost resisting of concrete with different cement types.* Building and Environment 82 (2014) 27-41.

Bos A.F. and Hesselink M. 1996. *Huiszwam een ware ramp!*. Biologiewinkel rapport 37. Rijksuniversiteit Groningen. ISBN 90 367 0438 3.

Budaiwi I., El-Diasty R. and Abdou A. 1999. *Modelling of moisture and thermal transient behaviour of multi-layer non-cavity walls*. Building and Environment 34 "(1999) 537-551.

Cai H. and Liu X. 1998. *Freeze-thaw durability of concrete ice formation process in pores.* Cement and Concrete Research, Vol. 28, No. 9, pp. 1281-1287, 1998.

Camuffo D. and Giorio R. 2002. *Quantitive evaluation of water deposited by dew on monuments*. Boundary-Layer Meteorology 107: 655-672, 2003.

Capozzoli A., Gorrino A. and Corrado V. 2013. *A building thermal bridges sensitivity analysis*. Applied Energy 107 (2013) 229-243.

Clarke J.A., Johnstone C.M., Kelly N.J., McLean R.C., Anderson J.A., Rowan N.J. and Smith J.E. 1999. *A technique for the prediction of the conditions leading to mould growth in buildings.* Building and Environment 34 (1999) 515-521.

D'Agostino D. and Congedo P.M. 2014. *CFD modeling and moisture dynamics implications of ventilation scenarios in historical buildings.* Building and Environment 79 (2014) 181-193.

Delgado J.M.P.Q., de Freitas V.P., Guimarães A.S. and Ferreira C. 2013. *Controlled relative humidity in crawl spaces: a new treatment methodology*. Structural Survey, Vol. 31 Iss 2 pp. 139 - 156.

Dos Santos G.H., Mendes N. and Philippi P.C. 2009. *A building corner model for hygrothermal performance and mould growth risk analyses.* International Journal of Heat and Mass Transfer 52 (2009) 4862-4872.

Fassina V., Favaro M., Naccari A. and Pigo M. 2002. *Evaluation of compatibility and durability of a hydraulic lime-based plaster applied on brick wall masonry of historical buildings affected by rising damp phenomena*. Journal of Cultural Heritage 3 (2002) 45-51.

Freitas de V.P., Abrantes V. and P. Crausse. 1996. *Moisture Migration in Building Walls - Analysis of the Interface Phenomena*. Building and Environment, Vol. 31, No. 2, pp. 99-108, 1996.

Gentilini C., Franzoni E., Bandini S. and Nobile L. 2012. *Effect of salt crystallisation on the shear behaviour of masonry walls. An experimental study*. Construction and Building Materials 37 (2012) 181-189.

Hagentoft, C.E. 2002. *Final report: Methodology of HAM-modeling, Report R-02:8.* Gothenburg, Department of Building Physics, Chalmers University of Technology.

Harris S.Y. 2001. *Building Pathology: deterioration, diagnostics, and intervention*. New York: John Wiley and Sons, 2001.

Hees van R.P.J. and Brocken H.J.P. 2004. *Damage development to treated brick masonry in a long-term salt crystallisation test*. Construction and Building Materials 18 (2004) 331-338.

Hendry A.W. 2001. *Masonry walls materials and construction*. Construction and Building Materials 15 (2001). 323-330.

Hens H. L.S.C. 1999. *Fungal Defacement in Buildings: A Performance Related Approach*. HVAC&R Research, 5:3, 265-280.

Hens H., Janssens A., Depraetere W., Carmeliet J. and Lecompte J. 2007. *Brick Cavity Walls: A Performance Analysis Based on Measurements and Simulations*. Journal of Building Physics 2007 31: 95.

Isaksson T., Thelandersson S., Ekstrand-Tobin A. and Johansson P. 2010. *Critical conditions for onset of mould growth under varying climate conditions*. Building and Environment 45 (2010) 1712-1721.

Johansson S., Wadsö L. and Sandin K. 2010. *Estimation of mould growth levels on rendered façades based on surface relative humidity and surface temperature measurements.* Building and Environment 45 (2010) 1153-1160.

Johansson P., Ekstrand-Tobin A., Svensson T. and Bok G. 2012. *Laboratory study to determine the critical moisture level for mould growth on building materials.* International Biodeterioration & Biodegradation 73 (2012) 23-32.

Klaassen R.K.W.M., 2014. *Speed of bacterial decay in waterlogged wood in soil and open water*. International Biodeterioration & Biodegradation 86 (2014) 129-135.

Klõšeiko P., Arumägi E. and Kalamees T. 2015. *Hygrothermal performance of internally insulated brick wall in cold climate: A case study in a historical school building.* Journal of Building Physics 2015, Vol. 38(5) 444-464.

Koniorczyk M. and Gawin D. 2008. *Heat and Moisture Transport in Porous Building Materials Containing Salt*. Journal of Building Physics 2008 31: 279.

Kruschwitz J. and Bluhm J. 2005. *Modeling of ice formation in porous solids with regard to the description of frost damage*. Computational Materials Science 32 (2005) 407-417.

Kubik J. and Kucharczyk A. 2008. *Salt solution flows in walls of monumental buildings.* Verlag für Architektur und technische Wissenschaften GmbH & Co. KG, Berlin · Bauphysik 30 (2008), Heft 6.

Künzel H. and Kiessl K. 1997. *Calculation of heat and moisture transfer in exposed building components*. Int. J. Heat Mass Transfer. Vol.40, No. 1, pp. 15-167, 1997.

Li Q. 2008. *Development of a Hygrothermal Simulation Tool (HAM-BE) for Building Envelope Study.* Concordia University. Montreal, Quebec. Canada.

Lisø K.R., Kvande T., Hygen H.O., Thue J.V. and Harstveit K. 2006. *A frost decay exposure index for porous, mineral building materials.* Building and Environment 42 (2007) 3547-3555.

Magrini A. (editor). 2014. *Building refurbishment for energy performance*. Springer Cham Heidelberg New York Dordrecht London. ISBN 978-3-319-03074-6 (eBook).

Meeusen J. 2006. *Na-isolatie van spouwmuren*. Universiteit Gent Faculteit Ingenieurswetenschappen. 2006.

Menetrez M.Y. and Foarde K.K. 2003. *Research and Development of Prevention and Control Measures for Mold Contamination*. Indoor and Built Environment 2004 13: 109.

Merillou N., Merillou S., Galin E. and Ghazanfarpour D. 2012. *Simulating How Salt Decay ages buildings*. IEEE Computer Graphics and Applications.

Monumentenwacht Nederland. 2014. *Informatieblad Energie besparen in historische gebouwen*. 2014.

Morelli M. and Svendsen S. 2013. *Investigation of interior post-insulated masonry walls with wooden beam ends*. Journal of Building Physics 2013 36: 265.

Mudarri D. and Fisk W.J. 2007. *Public health and economic impact of dampness and mold*. Indoor Air 2007; 17: 226-235.

Mumovic D., Ridley I., Oreszczyn T. and Davies M. 2006. *Condensation risk: comparison of steady-state and transient methods*. Building Serv. Eng. Res. Technol. 27.3 (2006) pp. 219-233.

Nasraoui M., Nowik W. and Lubelli B. 2009. *A comparative study of hygroscopic moisture content, electrical conductivity and ion chromatography for salt assessment in plasters of historical buildings.* Construction and Building Materials 23 (2009) 1731-1735.

Nielsen K.F., Holm G., Uttrup L.P. and Nielsen P.A. 2004. *Mould growth on building materials under low water activities. Influence of humidity and temperature on fungal growth and secondary metabolism.* International Biodeterioration & Biodegradation 54 (2004) 325-336.

Pakkala T.A., Köliö A, Lahdensivu J. and Kiviste M. 2014. *Durability demands related to frost attack for Finnish concrete buildings.* Building and Environment 82 (2014) 27-41.

Papadopoulos A.M., Avgelis A. and Santamouris M. 2003. *Energy study of a medieval tower, restored as a museum*. Energy and Buildings 35 (2003) 951-961.

Pavlik Z. and Černý R. 2008. *Experimental assessment of hygrothermal performance of an internal thermal insulation*. Energy and Buildings 40 (2008) 673-678.

Pavlikova M, Pavlik Z, Keppert M and Černy R, 2011. *Salt transport and storage parameters of renovation plasters and their possible effects on restored buildings' walls.* Construction and Building Materials 25 (2011) 1205-1212.

Pel L., Huinink H., Kopinga K., van Hees R.P.J. and Adan O.C.G. 2004. *Efflorescence pathway diagram understanding salt weathering*. Construction and Building Materials 18 (2004) 309-313.

Qiu X. 2003. *Moisture transport across interfaces between building materials*. Concordia University. Montreal, Quebec. Canada.

Rafidiarison H., Rémond R., Mougel E. *Dataset for validating 1-D heat and mass transfer models within building walls with hygroscopic materials*, Building and Environment, Volume 89, July 2015, Pages 356-368, ISSN 0360-1323.

Ramos N.M.M., Delgado J.M.P.Q., Barreira E. and Freitas de V.P. 2010. *Hygrothermal Numerical Simulation: Application in Moisture Damage Prevention*. Numerical Simulations – Examples and Applications in Computational Fluid Dynamics, Angermann L., (Ed.), Intech, Rijeka, Croatia, 97-122.

Russell B. *Human Knowledge: Its scope and limits.* page 475. Fourth Impression 1961.

Schellen H.L., Ankersmit B., Neuhaus E. and Martens M.H.J. 2008. *Het 'verantwoorde' binnenklimaat; In monumenten met een museale functie.* TVVL Magazine 6/2008.

Schellen H.L. and Stappers M.H.J. 2008. *Monument isoleren: complex en lastig karwei*. Energie NR3 MET 2008.

Schellen H.L. 2010. *Klimaat en behaaglijkheid in monumentale gebouwen; Klimaatmaatregelen bedenken vanuit het begrijpen van het gebouw.* Reader BK 6010; Maart 2010. Technische Universiteit Delft; Faculteit Bouwkunde.

Scherer G.W. 2004. *Stress from crystallization of salt.* Cement and Concrete Research 34 (2004) 1613-1624.

Scherer G.W. 2006. *Internal stress and cracking in stone and masonry.* M.S. Konsta-Gdoutos, (ed.), Measuring, Monitoring and Modeling Concrete Properties, 633-641. 2006.

Schijndel, A.W.M. van 2006. *Heat, Air and Moisture Construction modeling using COMSOL with MatLab*. Modeling guide version 1.0, Proceedings of the COMSOL Users Conference 2006 Eindhoven.

Sedlbauer. K. 2001. *Prediction of mould fungus formation on the surface of and inside building components*. (Dissertation) 2001. Fraunhofer Institute for Building Physics.

Singh J., Yu C. and Kim J.T. 2010. *Building Pathology, Investigation of Sick Buildings -- Toxic Moulds*. Indoor and Built Environment 2010 19: 40.

Singh J., Yu C. and Kim J.T. 2011. *Building Pathology - Toxic Mould Remediation*. Indoor and Built Environment 2011 20:36.

Small B.M. 2003. *Creating Mold-Free Buildings: A Key to Avoiding Health Effects of Indoor Mold*s. Archives of Environmental Health: An International Journal, 58:8, 523-527.

Stappers M.H.J. and Schellen H.L. 2011. *Na-isoleren van historische gebouwen.* In H. van de Ven, T. Hermans & A.M. Postel (Eds.), *Duurzaam erfgoed: duurzaamheid, energiebesparing en monumenten* Houten; Amersfoort: Terra; Rijksdienst voor het Cultureel Erfgoed.

Stazi F., Di Perna C. and Munafo P. 2009. *Durability of 20-year-old external insulation and assessment of various types of retrofitting to meet new energy regulations*. Energy and Buildings 41 (2009) 721-731.

Steeman H.J., Van Belleghem M., Janssens A., De Paepe M. 2009. *Coupled simulation of heat and moisture transport in air and porous materials for the assessment of moisture related damage*. Building and Environment 44 (2009) 2176-2184.

Theoulakis P. and Moropoulou A. 1997. *Microstructural and mechanical parameters determining the susceptibility of porous building stones to salt decay*. Construction and Building Materials, Vol. 11, No. 1, pp. 65-71, 1997.

Uittenbosch S. 2012. *Risico van inwendige condensatie in een externe scheidingsconstructie*. (Graduation report) Building Physics and Services. Eindhoven University of Technology.

Vereecken E. and Roels S. 2012. *Review of mould prediction models and their influence on mould risk evaluation*. Building and Environment 51 (2012) 296-310.

Vereecken E. 2013. *Hygrothermal analysis of interior insulation for renovation projects*. phD Dissertation December 2013. KU Leuven.

Viitanen H. and Ojanen T. 2007. *Improved Model to Predict Mold Growth in Building Materials.* In: Thermal Performance of the Exterior Envelopes of Whole Buildings X-Proceedings CD, 2-7 December 2007, Clearwater Beach, USA, ASHRAE, DOE, ORNL.

Viitanen H., Vinha J., Salminen K., Ojanen T., Peuhkuri R, Paajanen L. and Lähdesmäki K. 2010. *Moisture and Bio-deterioration Risk of Building Materials and Structures*. Journal of Building Physics 2010 33: 201.

Voerman B. 2013. *De thermohygrische prestatie van uitwendige scheidingsconstructies van herbestemd historisch (monumentaal) erfgoed*. Master thesis 2012/2013. Unit Building Physics and Services. Eindhoven University of Technology.

Vololonirina O., Coutand M., Perrin B. 2014. *Characterization of hygrothermal properties of wood-based products – Impact of moisture content and temperature.* Construction and Building Materials 63 (2014) 223-233.

Voronina V., Pel L., Sawdy A. and Kopinga K. 2013. *The influence of osmotic pressure on poulticing treatments for cultural heritage objects*. Materials and Structures (2013) 46:221-231.

Vrána T. and Björk F. 2009. *Frost formation and condensation in stone-wool insulations*. Construction and Building Materials 23 (2009) 1775-1787.

Vydra V. 2007. *Degradation risk assessment of external envelopes: A practical engineering approach*. Building and Environment 42 (2007) 344-348.

Watt D. and Colston B. 2000. *Investigating the effects of humidity and salt crystallisation on medieval masonry*. Building and Environment 35 (2000) 737-749.

De Wit M.H. 2009. *Heat, Air and Moisture in Building Envelopes.* Unit Building Physics and Services. Eindhoven University of Technology.

Zagorskas J., Zavadskas E.K., Turskis Z., Burinskiené M., Blumberga A. and Blumberga D. 2014. *Thermal insulation alternatives of historic brick buildings in Baltic Sea Region*. Energy and Buildings 78 (2014) 35-42.

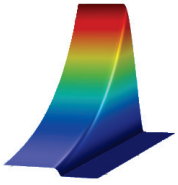

7. Annex

Annex A – HAM-BC 2015

Annex A has its own page numbering, because the manual HAM-BC 2015 is a stand-alone document. The page numbering of the main text starts again in Annex B.

Annex B – Transformation of formulas to the LPc-method

The equations discussed in the main text of this report are transformed into the subdomain equations of the LPc-model. This is an English translation of Annex A of [Uittenbosch 2012].

Heat

The heat equation includes the conductive heat flux, latent heat and the heat flux by convection:

$$(\rho \cdot c + c_l \cdot w)\frac{\partial T}{\partial t} = \operatorname{div} \lambda \cdot \operatorname{grad} T + L \cdot \operatorname{div}\frac{\delta_a}{\mu} \cdot \operatorname{grad} p_v - L \cdot 0.62 \cdot 10^{-5} \cdot \vec{g_a} \cdot \operatorname{grad} p_v - c_p \cdot \vec{g_a} \cdot \operatorname{grad} T$$

The parts which include the latent heat in the equation require the right potential:

$$L\left(\operatorname{div}\frac{\delta_a}{\mu} - 0.62 \cdot 10^{-5} \cdot \vec{g_a}\right) \cdot \frac{\partial(\varphi \cdot p_{sat}(T))}{\partial x}$$

$$L\left(\operatorname{div}\frac{\delta_a}{\mu} - 0.62 \cdot 10^{-5} \cdot \vec{g_a}\right)\left(\varphi \cdot \frac{p_{sat}(T)}{\partial x} + p_{sat}(T) \cdot \frac{\partial \varphi}{\partial x}\right)$$

$$L\left(\operatorname{div}\frac{\delta_a}{\mu} - 0.62 \cdot 10^{-5} \cdot \vec{g_a}\right)\left(\varphi \cdot \frac{p_{sat}}{\partial T} \cdot \frac{\partial T}{\partial x} + p_{sat}(T) \cdot \frac{\partial \varphi}{\partial x}\right)$$

$$L\left(\operatorname{div}\frac{\delta_a}{\mu} - 0.62 \cdot 10^{-5} \cdot \vec{g_a}\right)\left(\varphi \cdot \frac{p_{sat}}{\partial T} \cdot \frac{\partial T}{\partial x} + p_{sat}(T) \cdot \frac{\partial \varphi}{\partial p_c} \cdot \frac{\partial p_c}{\partial x}\right)$$

$$L\left(\operatorname{div}\frac{\delta_a}{\mu} - 0.62 \cdot 10^{-5} \cdot \vec{g_a}\right)\left(\varphi \cdot \frac{p_{sat}}{\partial T} \cdot \frac{\partial T}{\partial x} + p_{sat}(T) \cdot \frac{\partial \varphi}{\partial p_c} \cdot \frac{\partial p_c}{\partial x}\right)$$

$$\rightarrow p_v = p_{sat} \cdot \exp\left(\frac{-p_c}{\rho_w \cdot R_v \cdot T}\right)$$

$$\rightarrow \varphi = \exp\left(\frac{-p_c}{\rho_w \cdot R_v \cdot T}\right) \Rightarrow p_c = \rho_w \cdot R_v \cdot T \cdot ln\,(\varphi)$$

$$\rightarrow \frac{\partial \varphi}{\partial p_c} = \frac{1}{\rho_w \cdot R_v \cdot T} \cdot \exp\left(\frac{-p_c}{\rho_w \cdot R_v \cdot T}\right)$$

$$\rightarrow \frac{\partial \varphi}{\partial p_c} = \frac{1}{\rho_w \cdot R_v \cdot T} \cdot \exp\left(\frac{-\rho_w \cdot R_v \cdot T \cdot ln\,(\varphi)}{\rho_w \cdot R_v \cdot T}\right)$$

$$\rightarrow \frac{\partial \varphi}{\partial p_c} = \frac{-\varphi}{\rho_w \cdot R_v \cdot T}$$

$$L\left(\operatorname{div}\frac{\delta_a}{\mu} - 0.62 \cdot 10^{-5} \cdot \vec{g_a}\right)\left(\varphi \cdot \frac{p_{sat}}{\partial T} \cdot \frac{\partial T}{\partial x} - p_{sat}(T) \cdot \frac{\varphi}{\rho_w \cdot R_v \cdot T} \cdot \frac{\partial p_c}{\partial x}\right)$$

$$\rightarrow \frac{\partial \varphi}{\partial p_c} = \frac{-\varphi}{\rho_w \cdot R_v \cdot T}$$

$$L\left(\operatorname{div}\frac{\delta_a}{\mu} - 0.62 \cdot 10^{-5} \cdot \vec{g_a}\right)\varphi \cdot \frac{p_{sat}}{\partial T}\frac{\partial T}{\partial x} - L\left(\operatorname{div}\frac{\delta_a}{\mu} - 0.62 \cdot 10^{-5} \cdot \vec{g_a}\right) \cdot p_{sat}(T)\frac{\varphi}{\rho_w R_v T} \cdot \frac{\partial p_c}{\partial Lp_c} \cdot \frac{\partial Lp_c}{\partial x}$$

$$\rightarrow Lp_c = \log_{10}(p_c)\ , \quad p_c = 10^{Lp_c}$$

$$\rightarrow \frac{\partial p_c}{\partial Lp_c} = 10^{Lp_c} \cdot \log_{10}(10)$$

$$\rightarrow \frac{\partial p_c}{\partial Lp_c} = 10^{Lp_c} \cdot 2.3026$$

The above equations are implemented in the heat flux equation:

$$(\rho\, c + c_l\, w)\frac{\partial T}{\partial t} = \operatorname{div}\lambda \cdot \operatorname{grad} T + L \cdot \operatorname{div}\frac{\delta_a}{\mu}\cdot\varphi\frac{\partial p_{sat}}{\partial T}\cdot \operatorname{grad} T - L\cdot\operatorname{div}\frac{\delta_a}{\mu}\cdot p_{sat}(T)\cdot\frac{\varphi}{\rho_w R_v T}\cdot\frac{\partial p_c}{\partial Lp_c}$$
$$\cdot \operatorname{grad} Lp_c - L\cdot 0.62\cdot 10^{-5}\cdot\vec{g_a}\cdot\varphi\cdot\frac{\partial p_{sat}}{\partial T}\cdot\operatorname{grad} T + L\cdot 0.62\cdot 10^{-5}\cdot\vec{g_a}\cdot p_{sat}(T)$$
$$\cdot\frac{\varphi}{\rho_w R_v T}\cdot\frac{\partial p_c}{\partial Lp_c}\cdot\operatorname{grad} Lp_c - c_p\cdot\vec{g_a}\cdot\operatorname{grad} T$$

The equation is made more compact by using brackets:

$$(\rho\, c + c_l\, w)\frac{\partial T}{\partial t} = \left(\operatorname{div}\lambda + L\left(\operatorname{div}\frac{\delta_a}{\mu} - 0.62\cdot 10^{-5}\cdot\vec{g_a}\right)\varphi\cdot\frac{\partial p_{sat}}{\partial T} - c_p\cdot\vec{g_a}\right)\operatorname{grad} T$$
$$+ L\left(\operatorname{div}\frac{-\delta_a}{\mu} + 0.62\cdot 10^{-5}\cdot\vec{g_a}\right)\cdot p_{sat}(T)\cdot\frac{\varphi}{\rho_w R_v T}\cdot\frac{\partial p_c}{\partial Lp_c}\cdot\operatorname{grad} Lp_c$$

Moisture transport

The same mathematical transformation is done for the potential of the moisture flux:

$$\frac{\partial w}{\partial t} = \operatorname{div}\frac{\delta_a}{\mu}\cdot\operatorname{grad} p_v - 0.62\cdot 10^{-5}\cdot\vec{g_a}\cdot\operatorname{grad} p_v + \operatorname{div}(-k_m)\cdot\operatorname{grad}(p_c + \rho_w\cdot g\cdot z)$$

The storage term at the left side of the equation is changed to the equivalent with the potential Lpc:

$$\frac{\partial w}{\partial p_c}\cdot\frac{\partial p_c}{\partial Lp_c}\cdot\frac{\partial Lp_c}{\partial t} = \operatorname{div}\frac{\delta_a}{\mu}\operatorname{grad} p_v - 0.62\cdot 10^{-5}\cdot\vec{g_a}\operatorname{grad} p_v + \operatorname{div}(-k_m)\operatorname{grad}(p_c + \rho_w\cdot g\cdot z)$$

The water vapor transport by diffusion and convection in the equation receives the Lp_c as potential:

$$\operatorname{div}\frac{\delta_a}{\mu}\operatorname{grad} p_v - 0.62\cdot 10^{-5}\cdot\vec{g_a}\operatorname{grad} p_v$$

$$\left(\operatorname{div}\frac{\delta_a}{\mu} - 0.62\cdot 10^{-5}\cdot\vec{g_a}\right)\operatorname{grad} p_v$$

$$\left(\operatorname{div}\frac{\delta_a}{\mu} - 0.62\cdot 10^{-5}\cdot\vec{g_a}\right)\operatorname{grad} p_v$$

$$\left(\operatorname{div}\frac{\delta_a}{\mu} - 0.62\cdot 10^{-5}\cdot\vec{g_a}\right)\varphi\cdot\frac{p_{sat}}{\partial T}\cdot\frac{\partial T}{\partial x} - \left(\operatorname{div}\frac{\delta_a}{\mu} - 0.62\cdot 10^{-5}\cdot\vec{g_a}\right)p_{sat}(T)\frac{\varphi}{\rho_w R_v T}\cdot\frac{\partial p_c}{\partial Lp_c}\cdot\frac{\partial Lp_c}{\partial x}$$

When the equation is inserted into the water vapor transport equation, this leads to:

$$\frac{\partial w}{\partial p_c}\cdot\frac{\partial p_c}{\partial Lp_c}\cdot\frac{\partial Lp_c}{\partial t} = \left(\operatorname{div}\frac{\delta_a}{\mu} - 0.62\cdot 10^{-5}\cdot\vec{g_a}\right)\varphi\cdot\frac{\partial p_{sat}}{\partial T}\operatorname{grad} T$$
$$-\left(\operatorname{div}\frac{\delta_a}{\mu} - 0.62\cdot 10^{-5}\cdot\vec{g_a}\right)p_{sat}(T)\cdot\frac{\varphi}{\rho_w R_v T}\cdot\frac{\partial p_c}{\partial Lp_c}\operatorname{grad} Lp_c + \operatorname{div}(-k_m)\cdot\frac{\partial p_c}{\partial Lp_c}\operatorname{grad} Lp_c$$

The equation is made more compact by using brackets:

$$\frac{\partial w}{\partial p_c}\cdot\frac{\partial p_c}{\partial Lp_c}\cdot\frac{\partial Lp_c}{\partial t} = \left(\operatorname{div}\frac{\delta_a}{\mu} - 0.62\cdot 10^{-5}\cdot\vec{g_a}\right)\varphi\cdot\frac{\partial p_{sat}}{\partial T}\operatorname{grad} T$$
$$+\left(\left(\left(-\operatorname{div}\frac{\delta_a}{\mu} + 0.62\cdot 10^{-5}\cdot\vec{g_a}\right)p_{sat}(T)\cdot\frac{\varphi}{\rho_w R_v T}\cdot\frac{\partial p_c}{\partial Lp_c}\right) - \operatorname{div} k_m\cdot\frac{\partial p_c}{\partial Lp_c}\right)\operatorname{grad} Lp_c$$

Annex C – Additional information and results from HAMSTAD

Additional information and results are given from the simulations of the five HAMSTAD-benchmarks with HAM-BC 2015. The additional information includes the boundary conditions and material properties.

HAMSTAD 1

The sealing layer is not simulated, but the effect of the layer is implemented by giving the boundary conditions related to moisture the value zero. Also the construction is air-tight; and therefore, the convective heat and moisture transport has no influence on the heat and moisture transport. The boundary conditions are transient and the simulation is 5 years.

Boundary conditions

h_e = 25 W/(m^2K) h_i = 7 W/(m^2K) β_e = 0 s/m β_i = 2e-8 s/m

Initial conditions load bearing material: w = 145 kg/m^3 T = 10°C
Insulation layer material: w = 0.065 kg/m^3 T = 10°C

Material properties

Material A: Load Bearing Material

Special density * specific heat capacity = 1824000

Moisture content (w) in [kg/m^3] dependent on capillary pressure (Pc) in [Pa]
146/((1+(8*10^-8*Pc)^1.6)^0.375)

Thermal conductivity coefficient (λ) in [W/(m·K)] related to moisture content (w) in [kg/m^3].
1.5+15.8*w/1000

Vapor permeability (δ_v) in [s] related to temperature (Tk) in [K] and moisture content (w) in [kg/m^3].
(Mw/(R*Tk))*(26.1*10^-6/200)*(1-w/146)/(0.503*(1-w/146)^2+0.497)

Moisture permeability (k_m) in [s] related to moisture content (w) in [kg/m^3]
exp(-39.2619+0.0704*(w-73)-1.74*10^-4*(w-73)^2-2.7953*10^-6*(w-73)^3-1.15*10^-7*(w-73)^4+2.5969*10^-9*(w-73)^5)

Material B: Insulation Material

Special density * specific heat capacity = 73900

Moisture content (w) in [kg/m^3] dependent on capillary pressure (Pc) in [Pa]
900/((1+(2*10^-4*Pc)^2)^0.5)

Thermal conductivity coefficient (λ) in [W/(m·K)] related to moisture content (w) in [kg/m^3].
0.033+0.59*w/1000

Vapor permeability (δ_v) in [s] related to temperature (Tk) in [K] and moisture content (w) in [kg/m^3].
(Mw/(R*Tk))*(26.1*10^-6/9.6)*(1-w/900)/(0.503*(1-w/900)^2+0.497)

Moisture permeability is zero

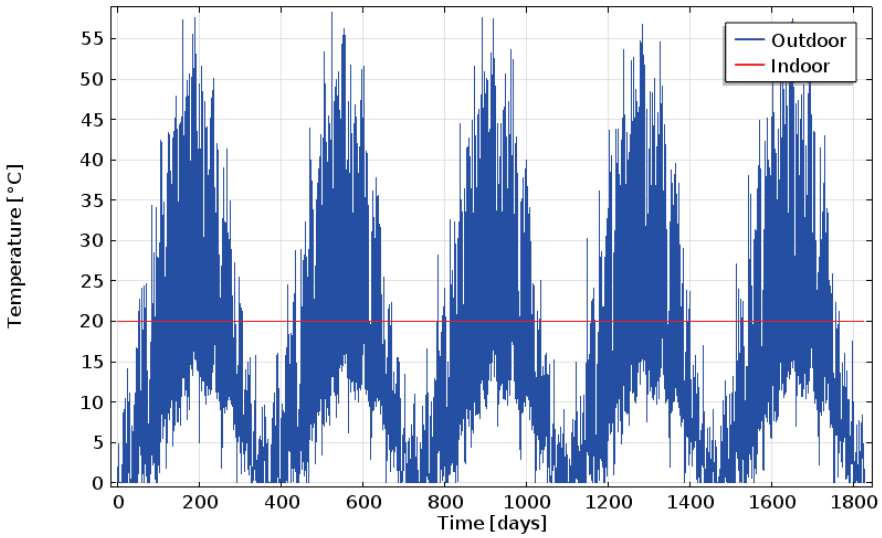

C.1: Outdoor and indoor temperature [^{o}C]

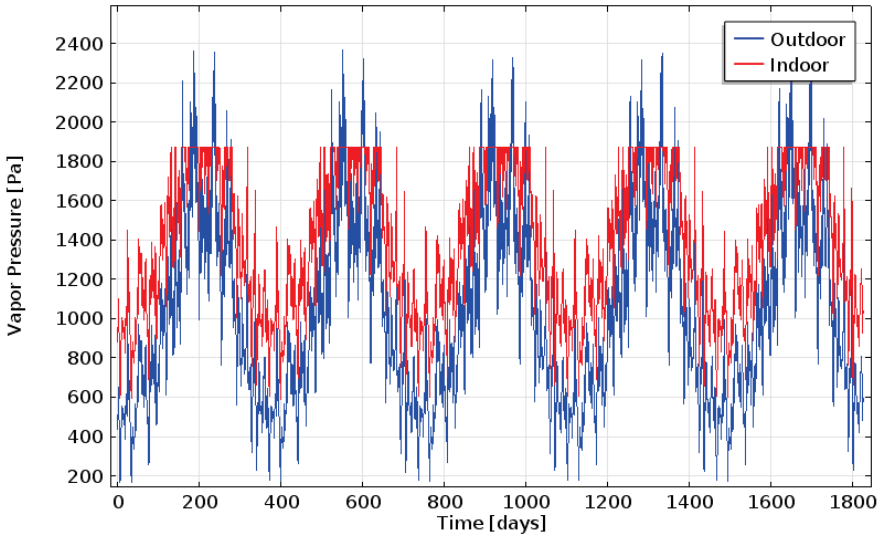

C.2: Outdoor and indoor vapor pressure [Pa]

Results

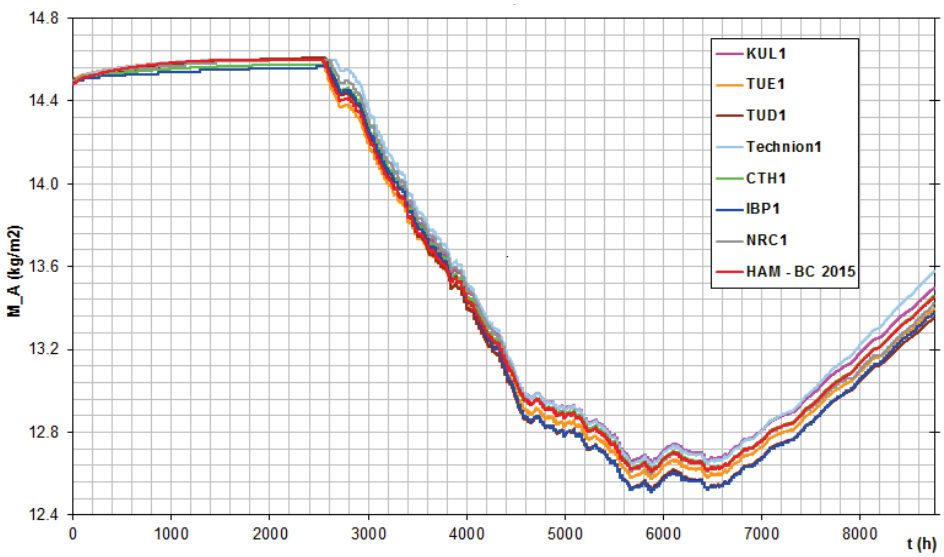

Figure C.3: Total moisture content [kg/m^{3}] of the load bearing material in the first year.

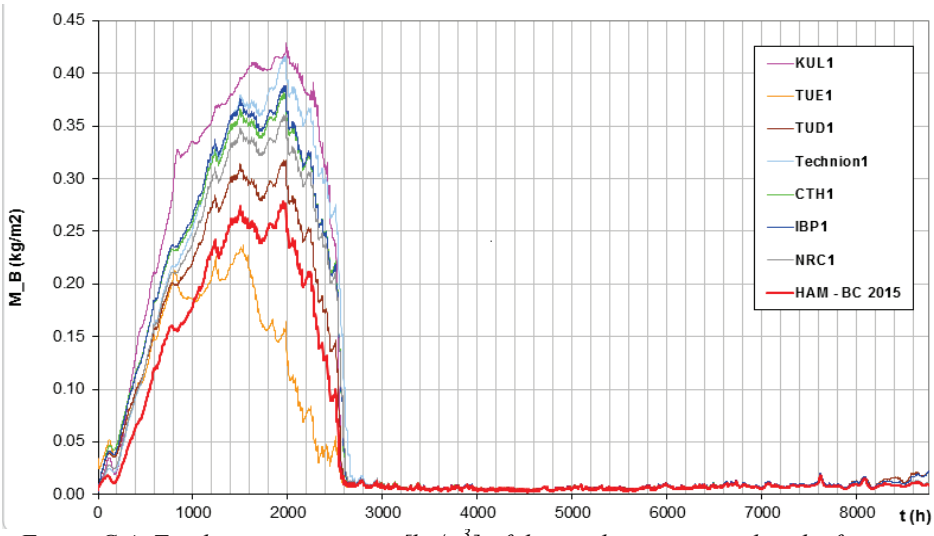

Figure C.4: Total moisture content [kg/m^3] of the insulation material in the first year.

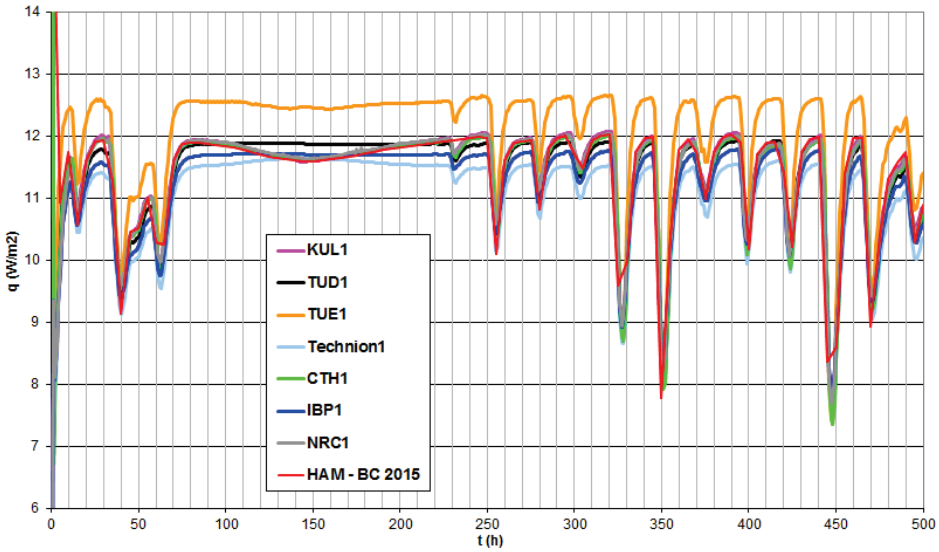

Figure C.5: Heat flux at the inside of the construction of the first 500 hours of the first year.

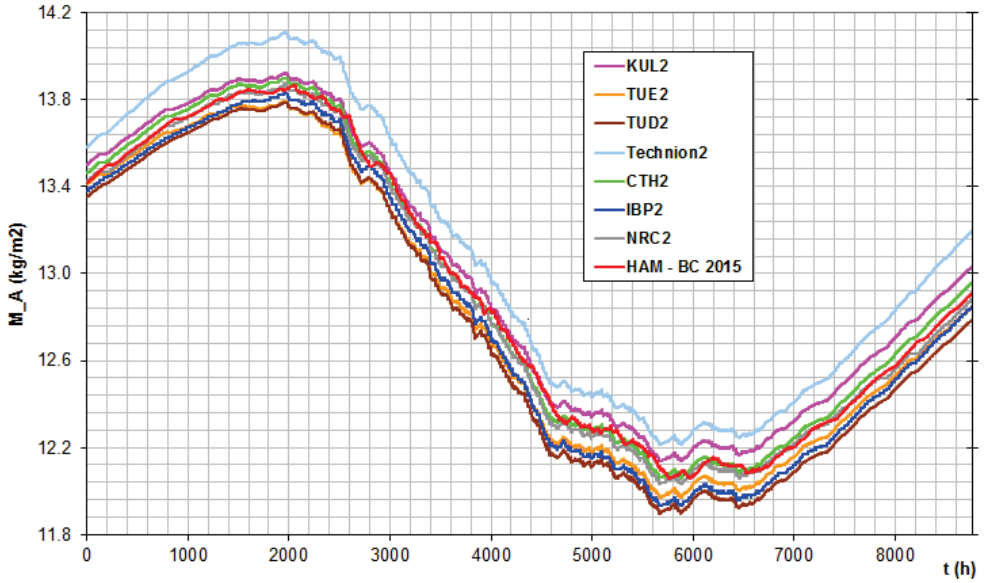

*Figure C.6: Total moisture content [kg/m^3] of the load bearing material in the **second** year.*

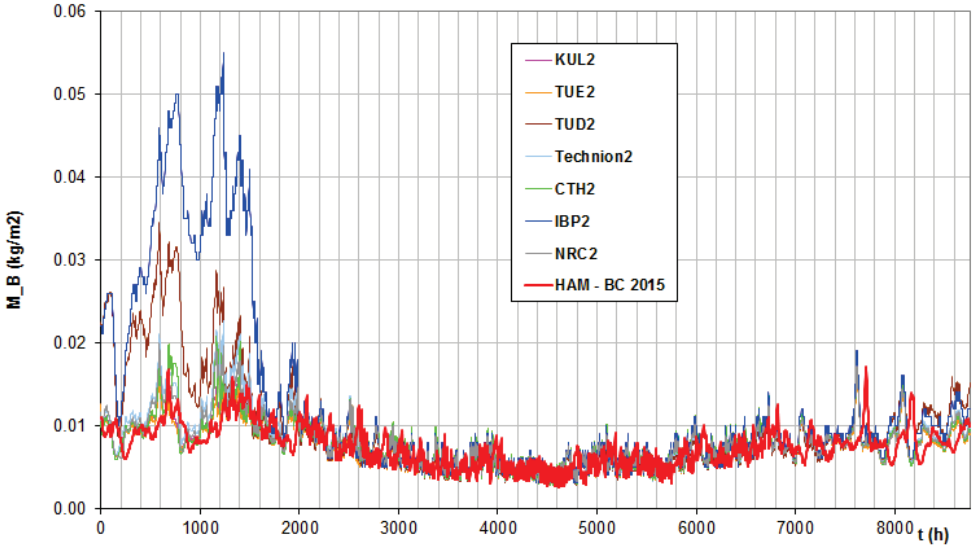

Figure C.7: Total moisture content [kg/m^3] of the insulation material in the second year.

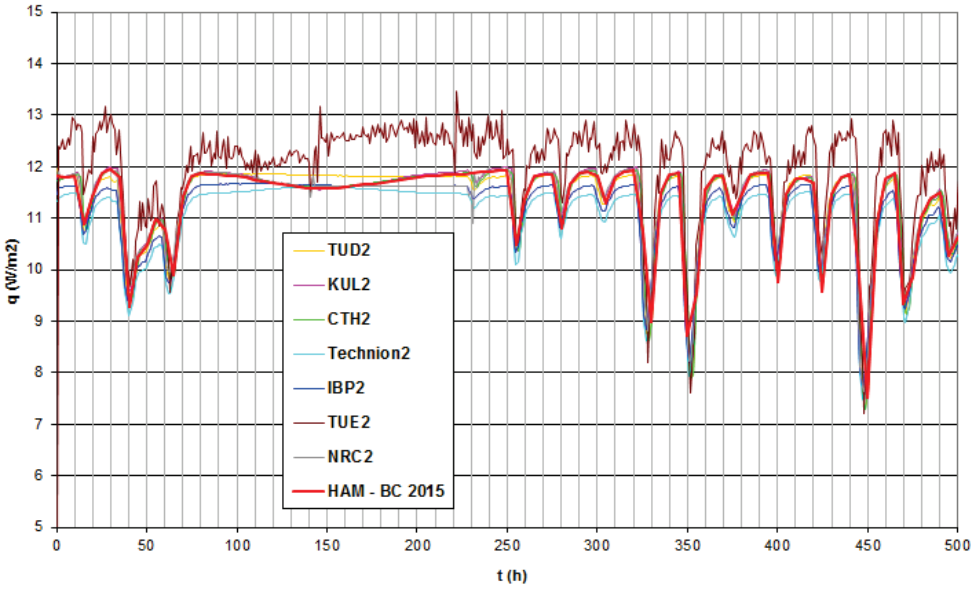

Figure C.8: Heat flux at the inside of the construction of the first 500 hours of the second year.

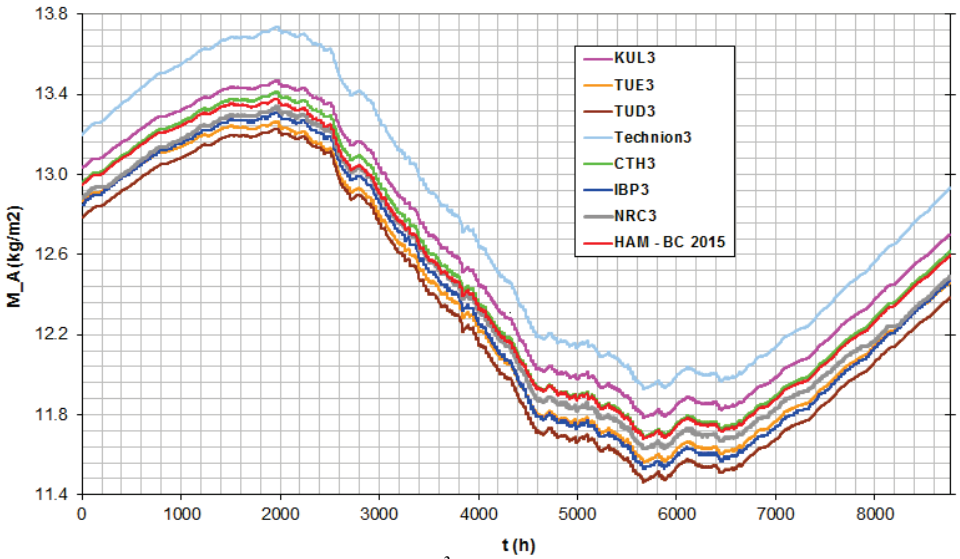

*Figure C.9: Total moisture content [kg/m^3] of the load bearing material in the **third** year.*

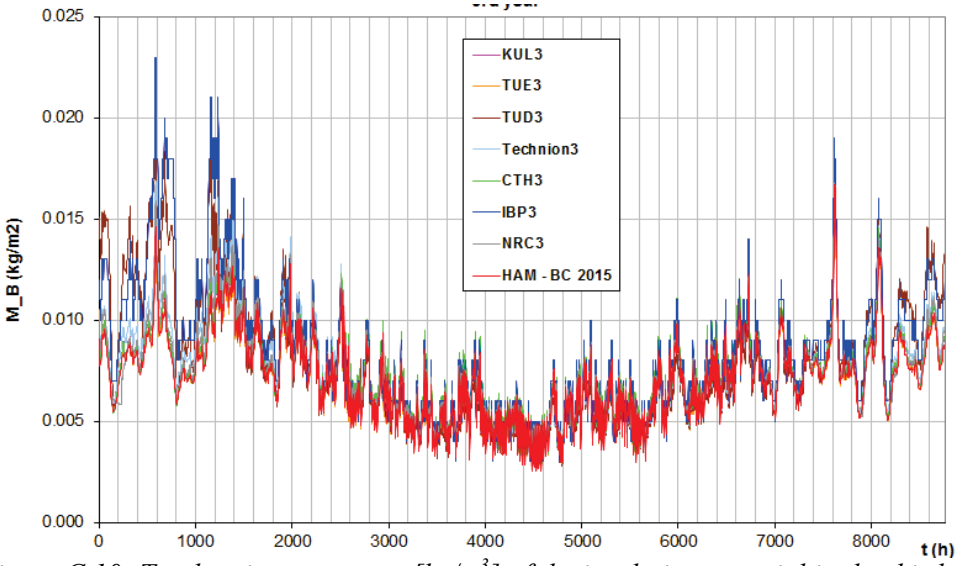

Figure C.10: Total moisture content [kg/m^3] of the insulation material in the third year.

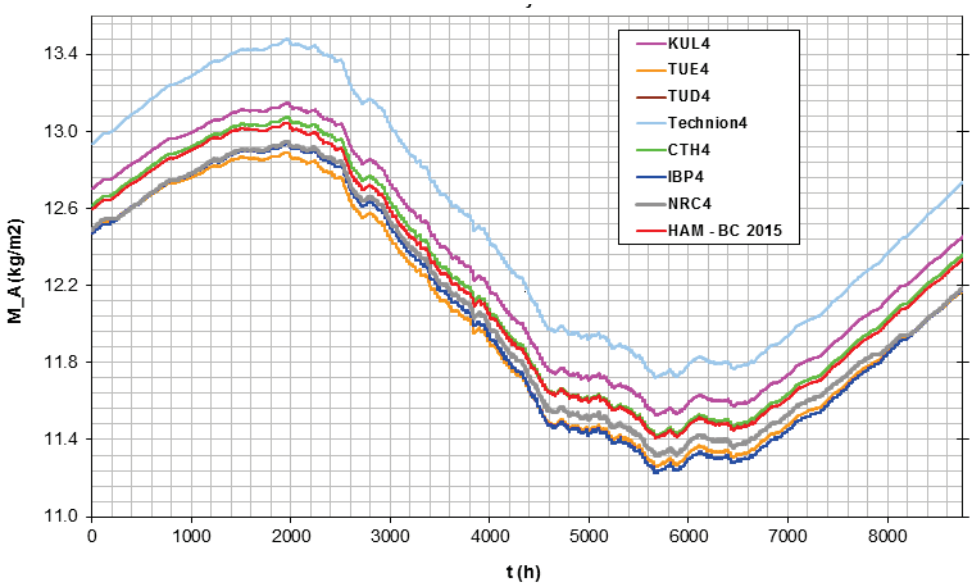

*Figure C.11: Total moisture content [kg/m^3] of the load bearing material in the **fourth** year.*

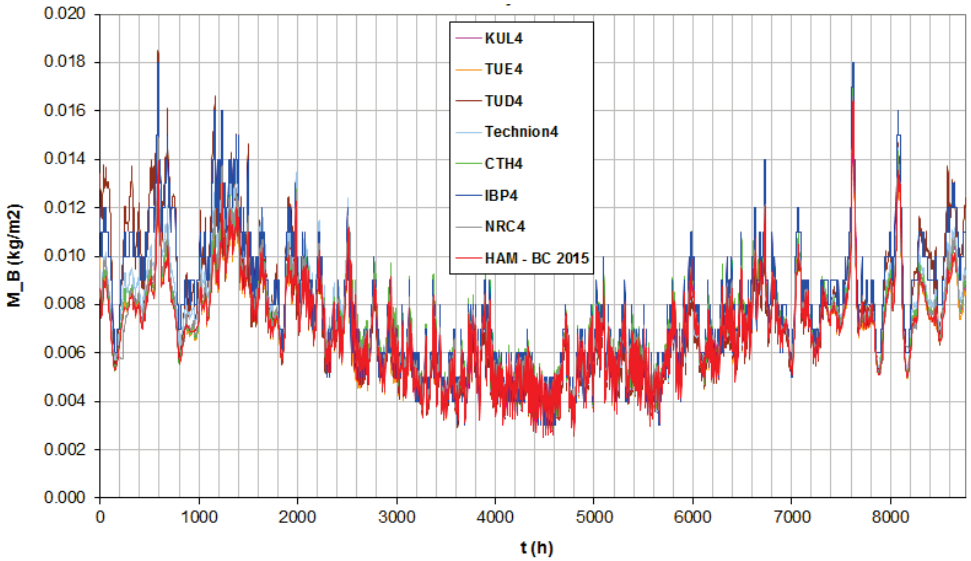

Figure C.12: Total moisture content [kg/m^3] of the insulation material in the fourth year.

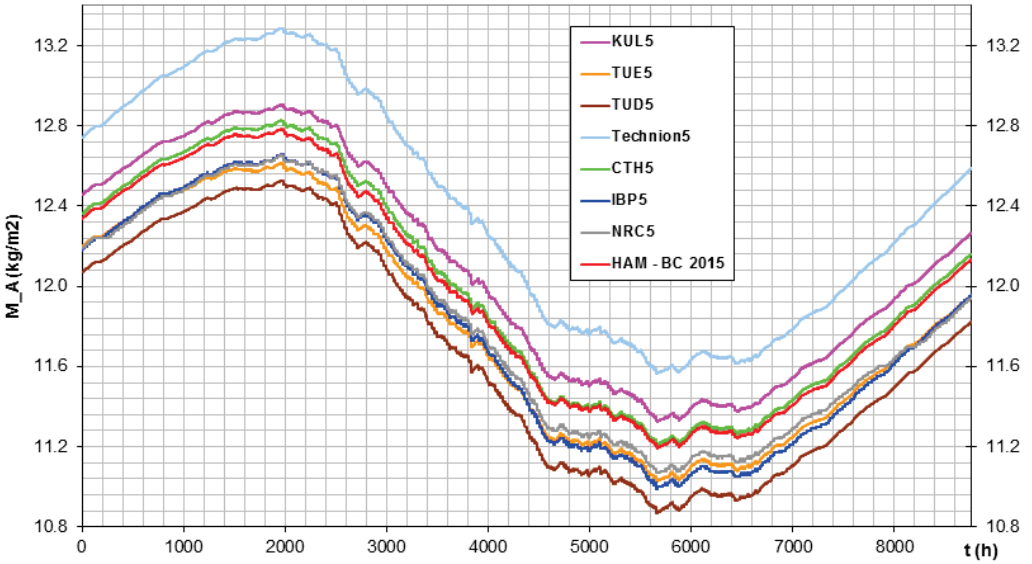

*Figure C.13: Total moisture content [kg/m^3] of the load bearing material in the **fifth** year.*

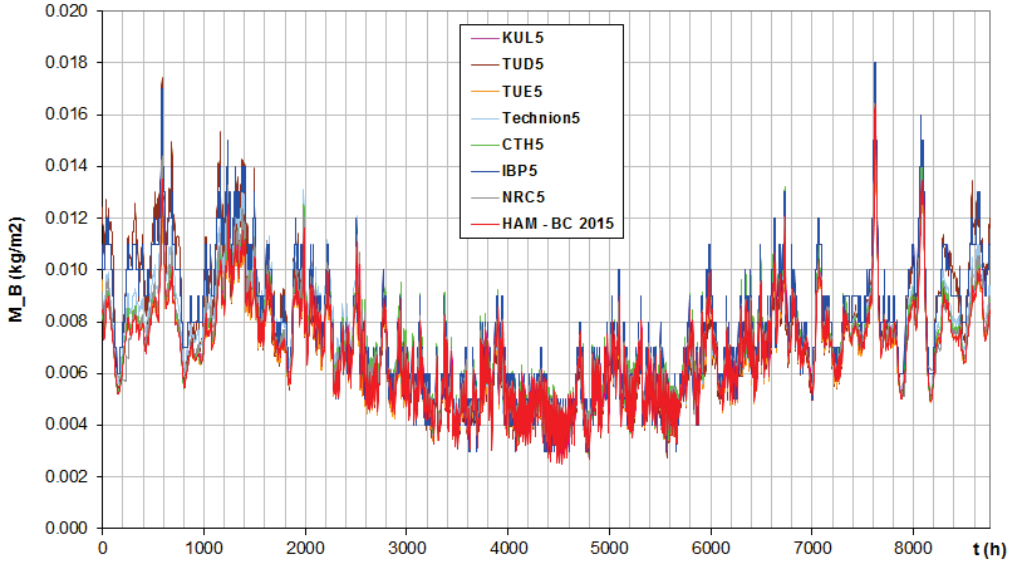

Figure C.14: Total moisture content [kg/m^3] of the insulation material in the fifth year.

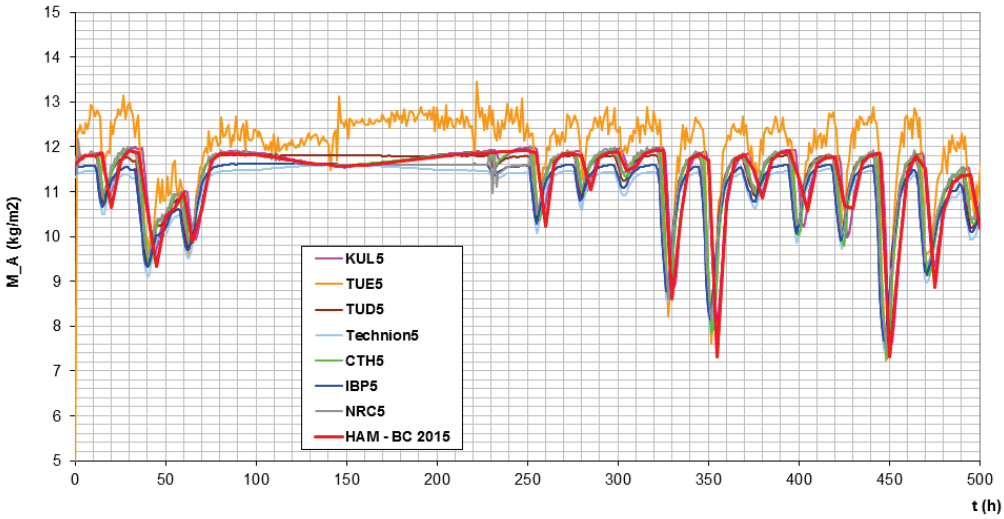

Figure C.15: Heat flux at the inside of the construction of the first 500 hours of the fifth year.

HAMSTAD 2

The benchmark 2 is about an isotherm drying process of a material with the hickness 200 mm. The initial conditions are 293 Kelvin and a relative humidity of 85%. There is a sudden drop of the air humidity, which is done by a step function in COMSOL by which the relative humidity at the inside and outside reaches a constant value. The internal boundary conditions when it become constant are 293K and 65%. The external side has the boundary conditons of 293K and 45% RH. The simulation time is 1000 hours.

Boundary conditions

h_i = 25 W/(m^2·K) h_e=25 W/(m^2·K) β_e = 1e-3 s/m β_i = 1e-3 s/m

Material properties

Initial conditions: RH = 95% and T = 20°C

Specific density = 525 kg/m^3
Specific heat capacity = 800 J/(kg·K)
Thermal conductivity = 0.15 W/(m·K)
Vapor permeability = 1·10^{-15} s

Moisture content (w) in [kg/m^3] dependent on relative humidity (φ) in [-] at 293.15K.
116/((1-(1/0.118)*ln(φ))^0.869)

Moisture permeability for capillary suction (K) in [s] related to temperature (Tk) in [K] and moisture content (w) in [kg/m^3]
-(6*10^-10)/(-(7275400*(116/w)^(0.1507)*Tk)/(w^2))

See main text for results.

HAMSTAD 3

The effect of convection on heat and moisture transport inside the material is simulated with HAMSTAD-benchmark 3. In this benchmark a single-layer lightweight construction with a thickness of 200 mm is simulated. The boundary conditions are constant, with the exception of the air pressure difference between outside and inside. First there is infiltration of air, caused by a pressure difference of 30 Pa, which at day 20 will be changed linearly to -30 Pa, which value is reached at day 21, *i.e.* to an exfiltration by an air pressure difference of 30 Pa. The complete description of the benchmark is given in [Hagentoft 2002].

The material properties are:

Initial temperature = 293.15 K
Initial relative humidity = 95%

Specific density = 212 kg/m^3
Specific heat capacity = 1000 J/(kg·K)

Moisture content (w) in [kg/m^3] dependent on capillary pressure (Pc) in [Pa]
871*((0.41/((1+(0.006*(Pc/(1000*9.81)))^2.4883)^(1-(1/2.4883))))+((0.59/((1+(0.012*(Pc/(1000*9.81)))^2.3898)^(1-(1/2.3898))))))

Thermal conductivity coefficient (λ) in [W/(m·K)] related to moisture content (w) in [kg/m^3].
0.06+0.56*(w/1000)

Vapor permeability (δ_v) in [s] related to temperature (Tk) in [K] and moisture content (w) in [kg/m^3].
(Mw/(R*Tk))*((26.1e-6/5.6)*(((1-(w/871))/(((1-0.2)*((1-(w/871))^2))+0.2))))

Moisture permeability for capillary suction (K) in [s] related to moisture content (w) in [kg/m^3]
exp(-46.245+294.506*(w/1000)-1439*((w/1000)^2)+3249*((w/1000)^3)-
3370*((w/1000)^4)+1305*((w/1000)^5))

Air permeability (k_a) = 3e-5 [s]

The data for creating the graphs have a time step of 24 hours. The results given in this report are made with the simplified convection method of HAM-BC 2015.

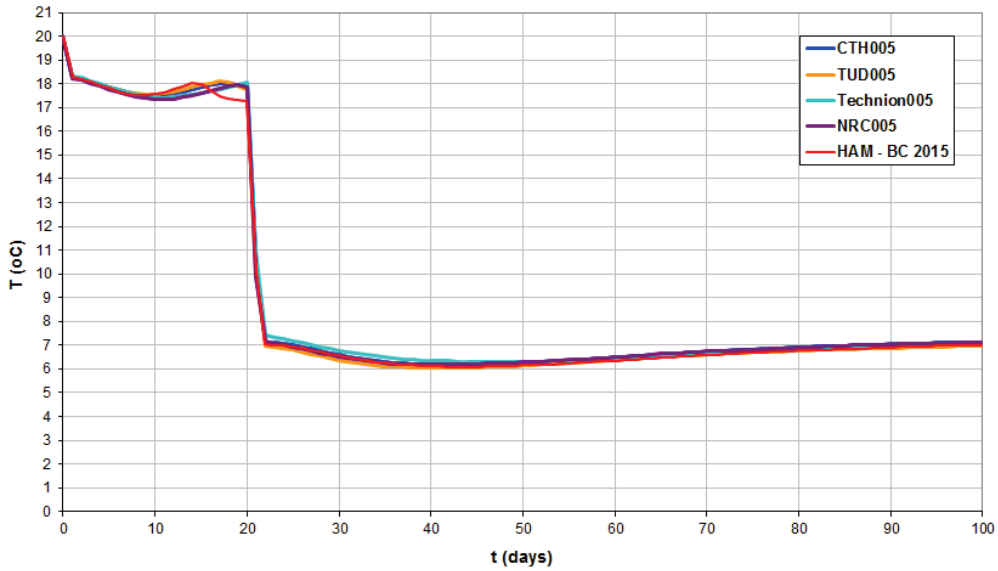

Figure C.16: Temperature distribution [^{o}C] related to time [days] at 0.05 m.

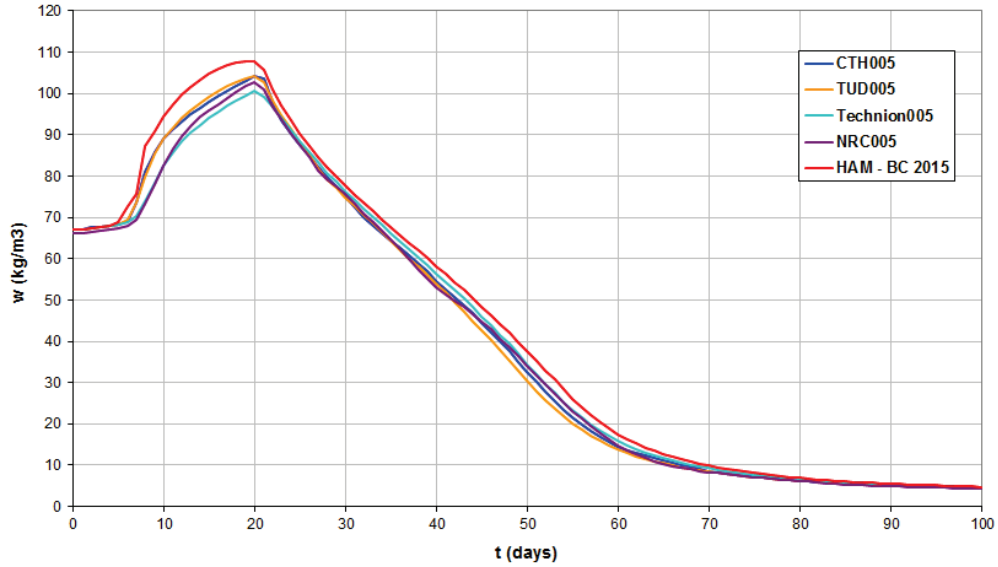

Figure C.17: Moisture content [kg/m^3] related to time [days] at 0.05 m.

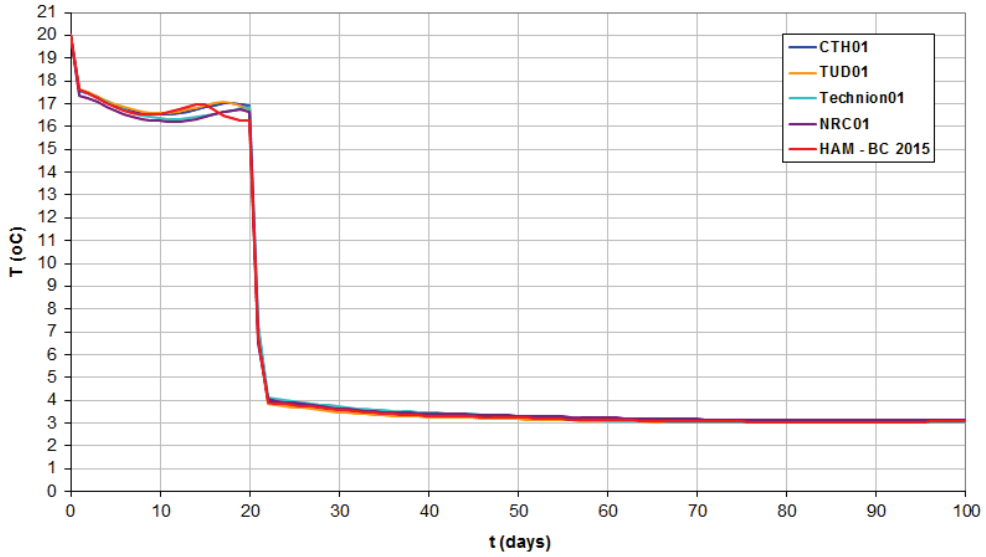

Figure C.18: Temperature distribution [^{o}C] related to time [days] at 0.10 m.

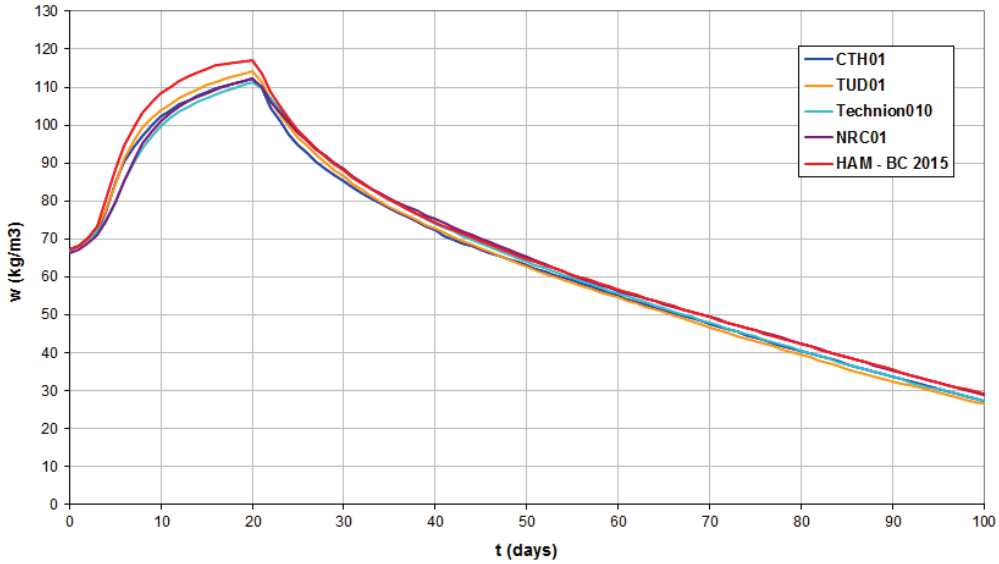

Figure C.19: Moisture content [kg/m^3] related to time [days] at 0.10 m.

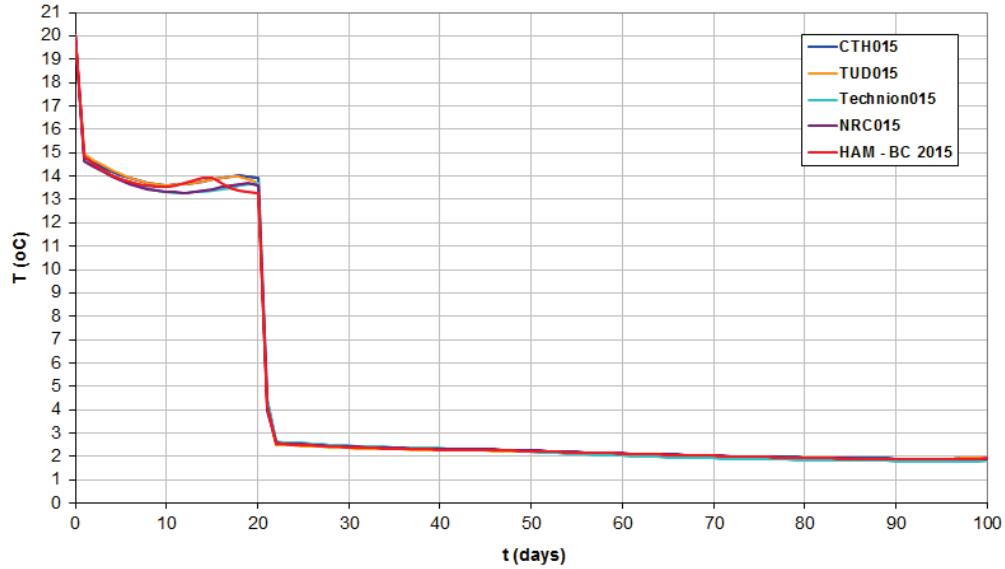

Figure C.20: Temperature distribution [^{o}C] related to time [days] at 0.15 m.

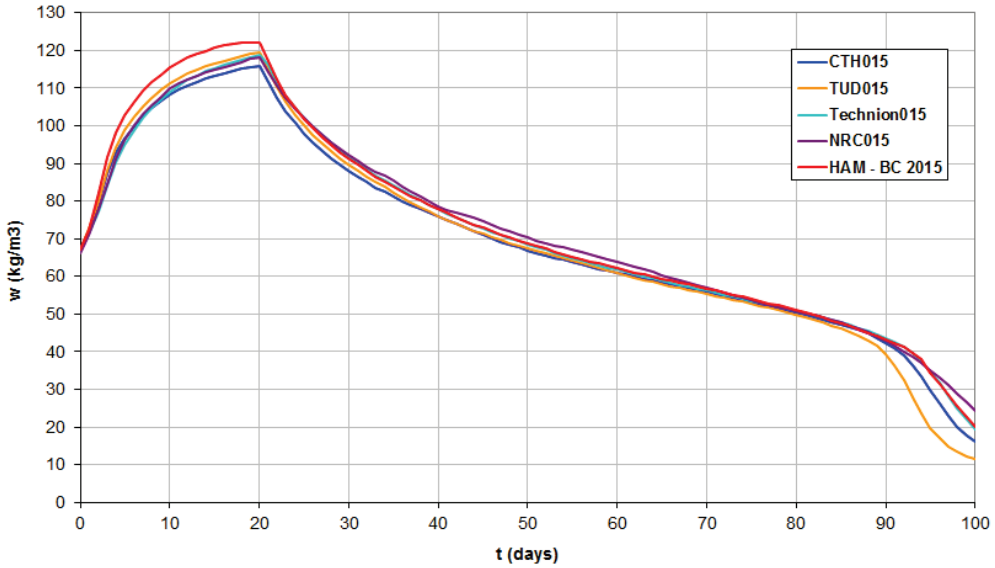

Figure C.21: Moisture content [kg/m^3] related to time [days] at 0.15 m.

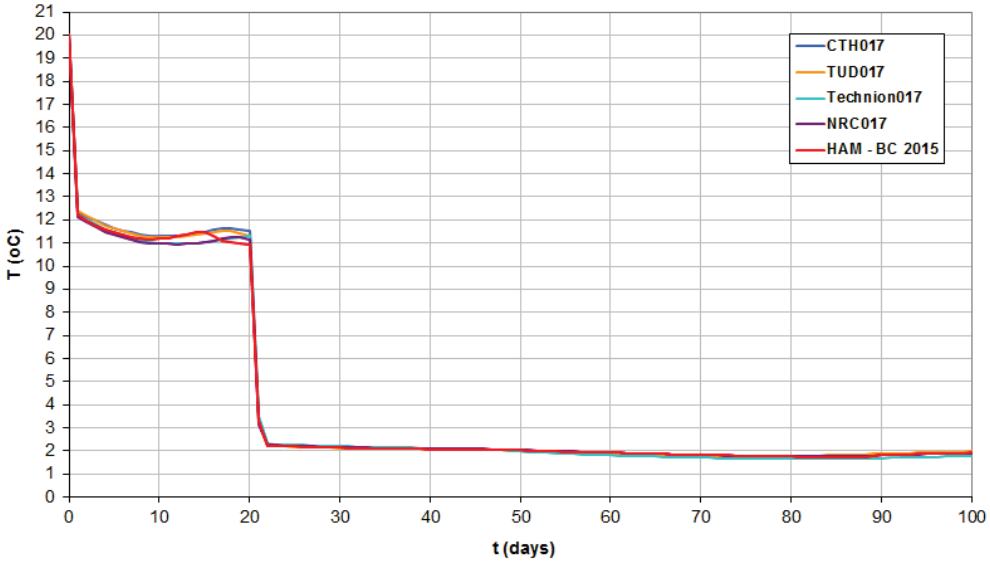

Figure C.22: Temperature distribution [^{o}C] related to time [days] at 0.17 m.

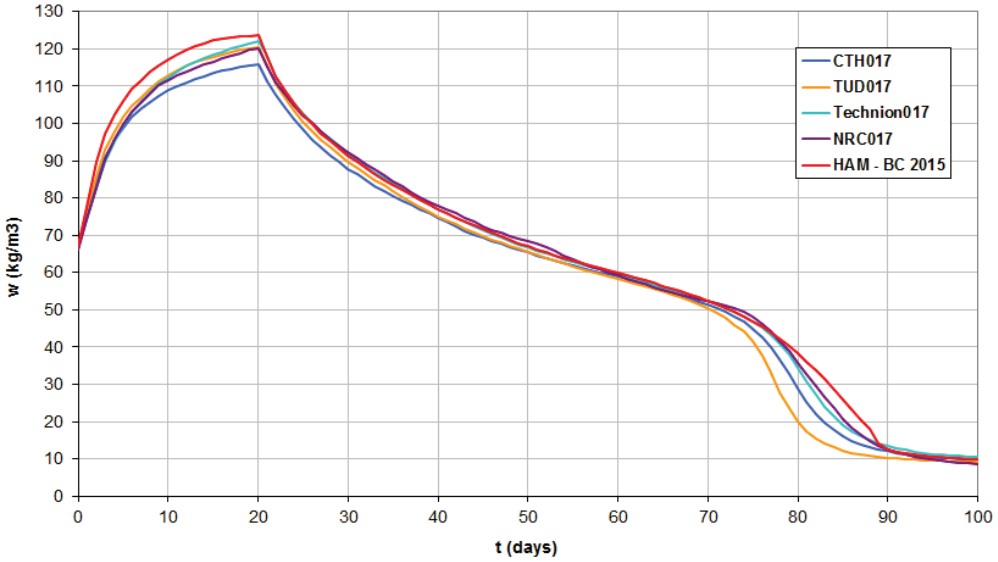

Figure C.23: Moisture content [kg/m^3] related to time [days] at 0.17 m.

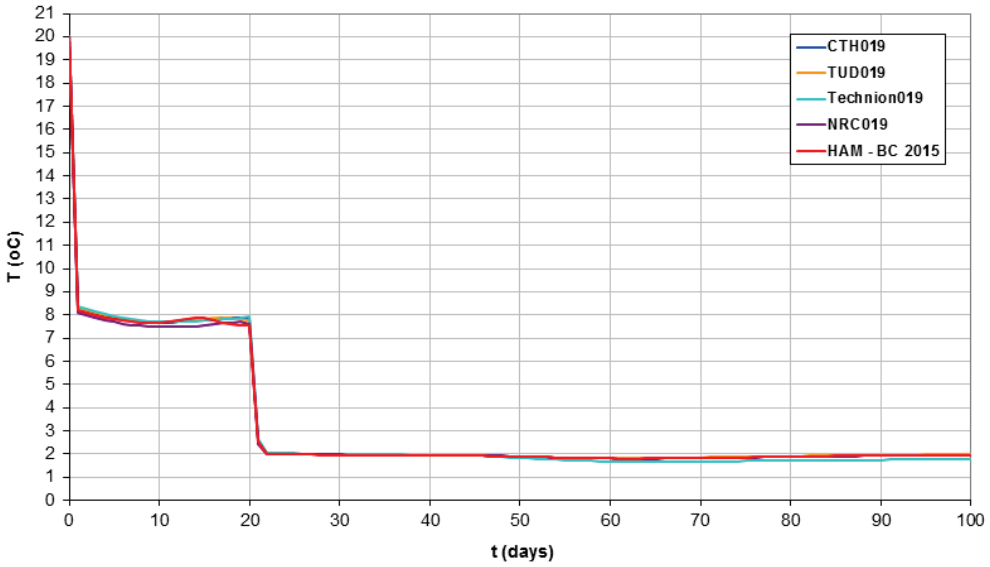

Figure C.24: Temperature distribution [^{o}C] related to time [days] at 0.19 m.

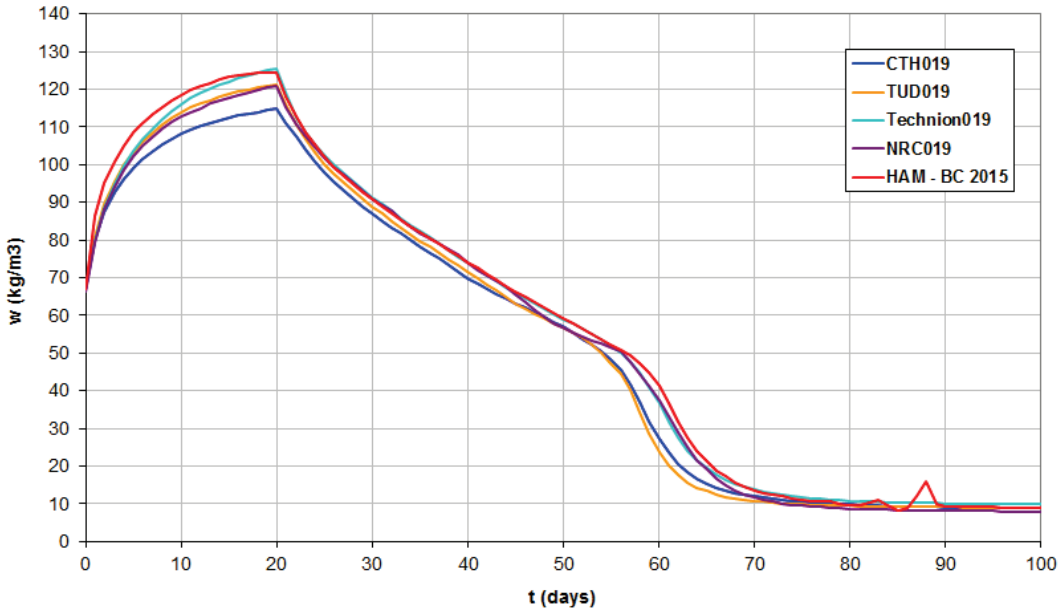

Figure C.25: Moisture content [kg/m^3] related to time [days] at 0.19 m. The peak between 85 and 90 days is caused by the time step of 24 hours.

HAMSTAD 4

The benchmark 4 is about a wall with plaster at the inside. The external surface is submitted to solar irradiation and wind-driven rain. The structure is considered perfectly airtight; and therefore, no convection heat and moisture transport occurs. The initial values for the construction are the temperature of 298K and relative humidity of 60%.

Material properties

Material A: Outer skin

Specific density = 2005 kg/m^3
Specific heat capacity = 840 J/(kg·K)

Moisture content (w) in [kg/m^3] dependent on capillary pressure (Pc) in [Pa]
157*(0.3*(1+(1.25e-5*Pc)^1.65)^((1-1.65)/1.65)+0.7*(1+(1.8e-5*Pc)^6)^((1-6)/6))

Thermal conductivity coefficient (λ) in [W/(m·K)] related to moisture content (w) in [kg/m^3].
0.5+0.0045*w

Vapor permeability (δ_v) in [s] related to temperature (Tk) in [K] and moisture content (w) in [kg/m^3].
(Mw/(R*Tk))*(((26.1e-6)/30)*(((1-(w/157))/((0.503*((1-(w/157))^2))+0.497))))

Moisture permeability for capillary suction (K) in [s] related to capillary pressure (Pc) in [Pa]
K = from a given table

Material B: Inside Finishing material
Specific density =790 [kg/m^3]
Specific heat capacity = 870 [J/(kg·K)]

Moisture content (w) in [kg/m^3] dependent on capillary pressure (Pc) in [Pa]
209*(1*(1+(2e-6*Pc)^1.27)^((1-1.27)/1.27))

Thermal conductivity coefficient (λ) in [W/(m·K)] related to moisture content (w) in [kg/m^3].
0.2+0.0045*w

Vapor permeability (δ_v) in [s] related to temperature (Tk) in [K] and moisture content (w) in [kg/m^3].
(Mw/(R*Tk))*(((26.1e-6)/3)*(((1-(w/209))/((0.503*((1-(w/209))^2))+0.497))))

Moisture permeability for capillary suction (K) in [s] related to moisture content (w) in [kg/m^3]
exp(-33+0.0704*(w-120)-1.742e-4*(w-120)^2-2.7953e-6*(w-120)^3-1.1566e-7*(w-120)^4+2.5969e-9*(w-120)^5)

The indoor temperature is constant 20^{o}C and the external ambient temperature – thus without solar irradiation – is constant 10^{o}C. The external vapor pressure is constant 1150 Pa.

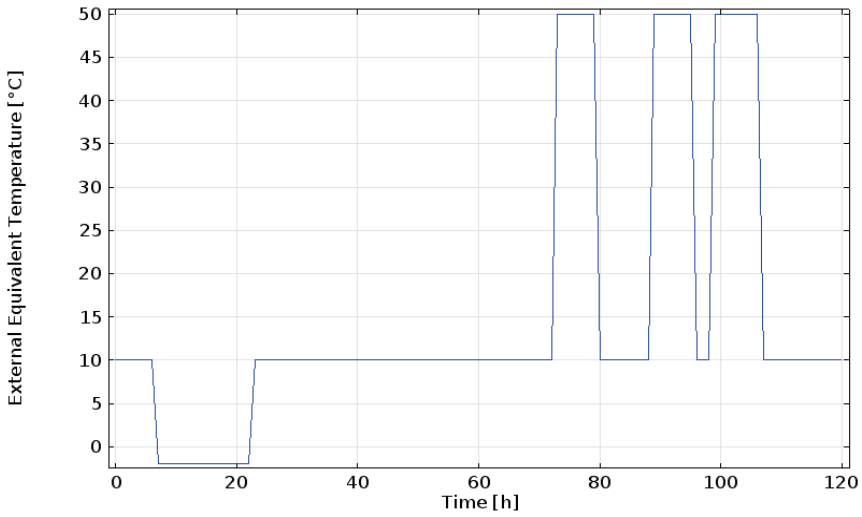

Figure C.26: External equivalent temperature [^{o}C] related to the time in hours.

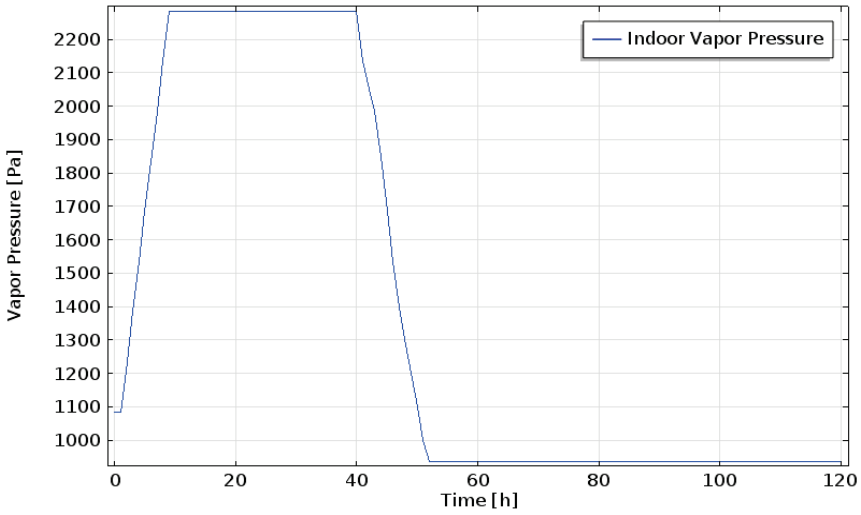

Figure C.27: Indoor vapor pressure [Pa] related to time [h].

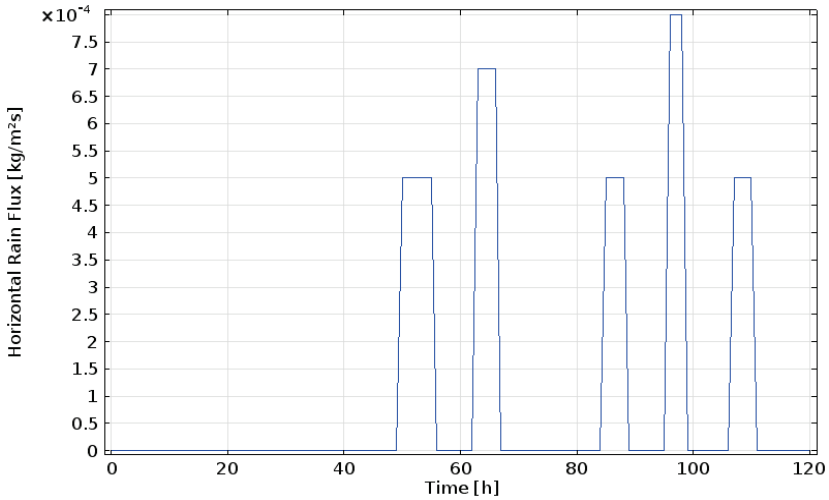

Figure C.28: Horizontal wind-driven rain flux on the external surface in [kg/(m^2·s)] over time in hours.

Results

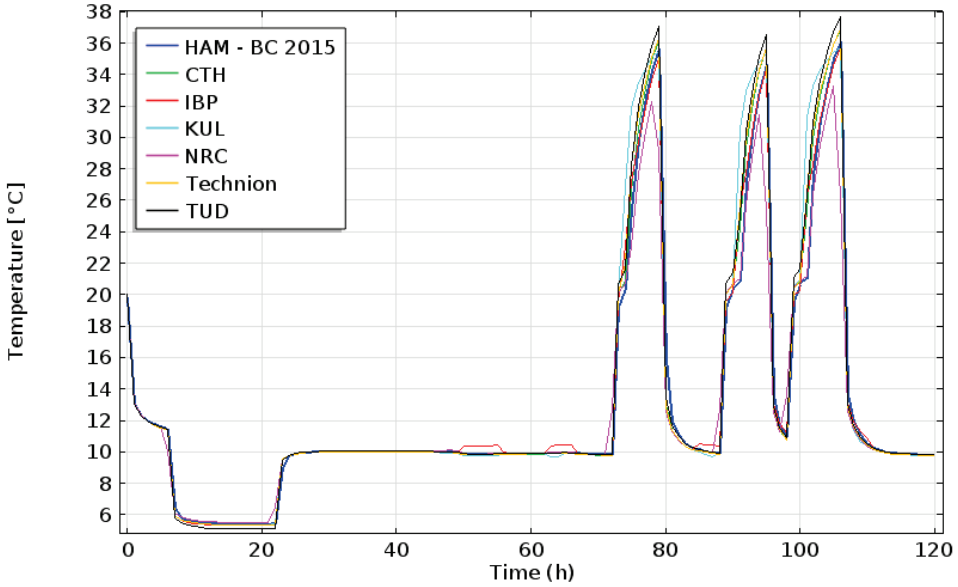

Figure C.29: Temperature [^{o}C] related to time [hours] at the external surface of the construction.

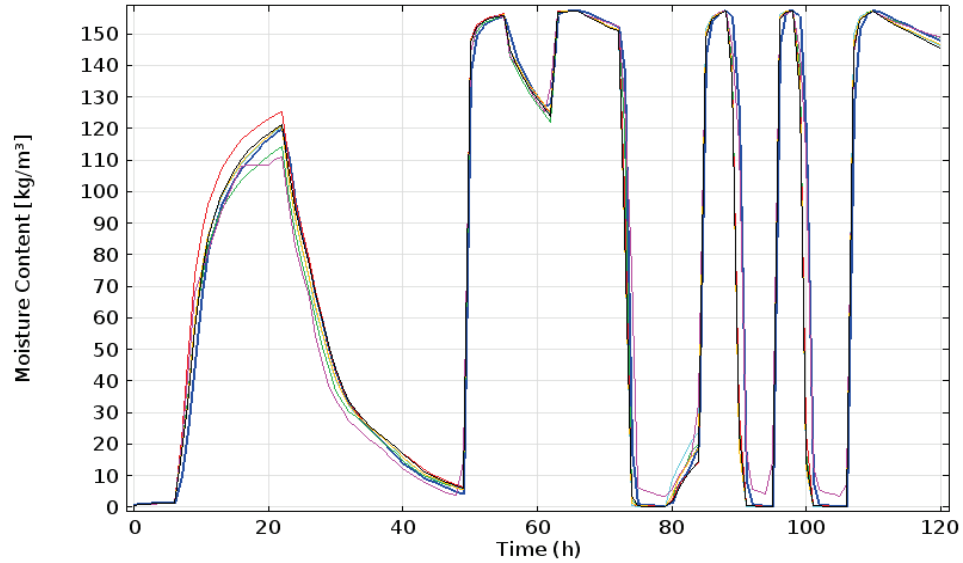

Figure C.30: Moisture content [kg/m^3] related to time [hours] at the external surface.

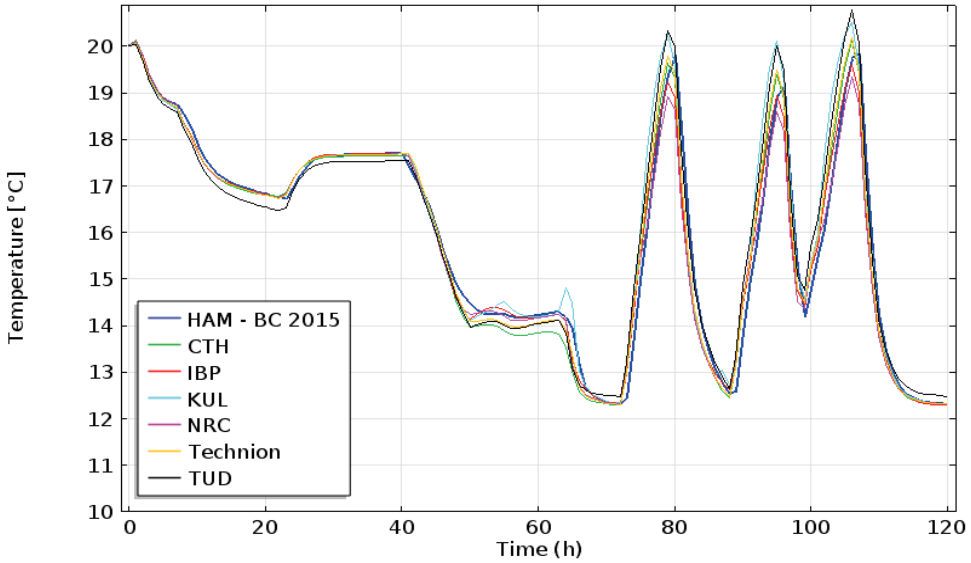

Figure C.31: Temperature [^{o}C] related to time [hours] at the internal surface of the construction.

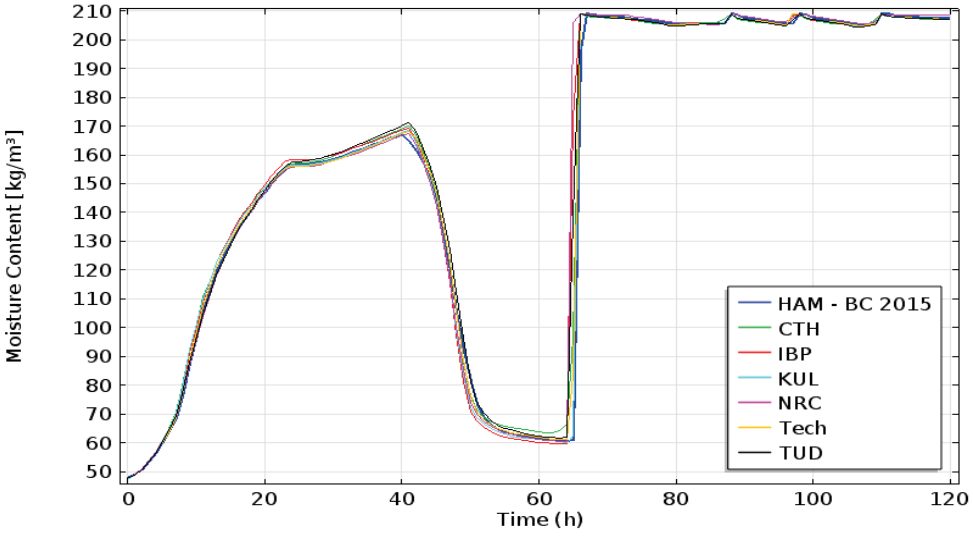

Figure C.32: Moisture content [kg/m^3] related to time [hours] at the internal surface.

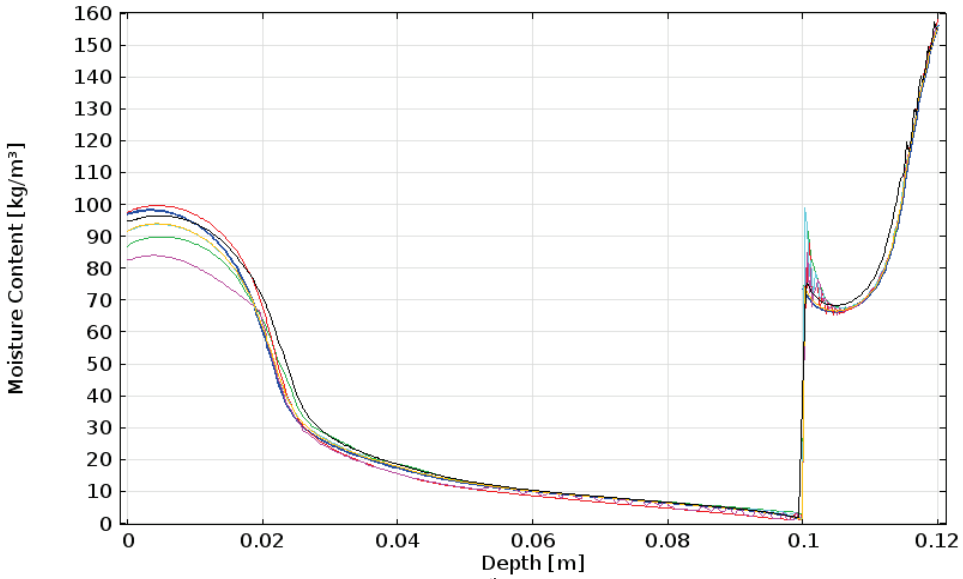

Figure C.33: Moisture content [kg/m^3] related to depth [m] on 24 hours.

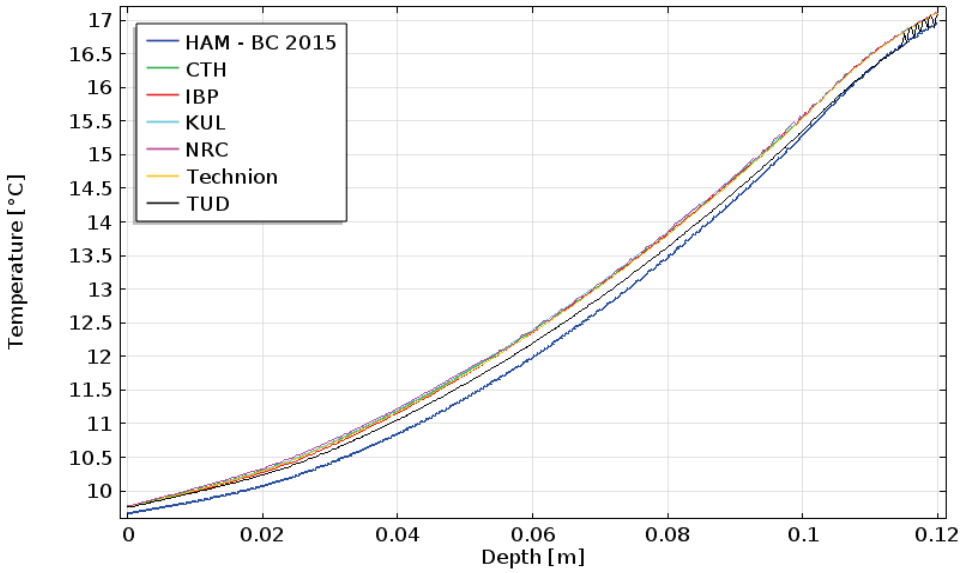

Figure C.34: Temperature [^{o}C] related to depth [m] on 24 hours.

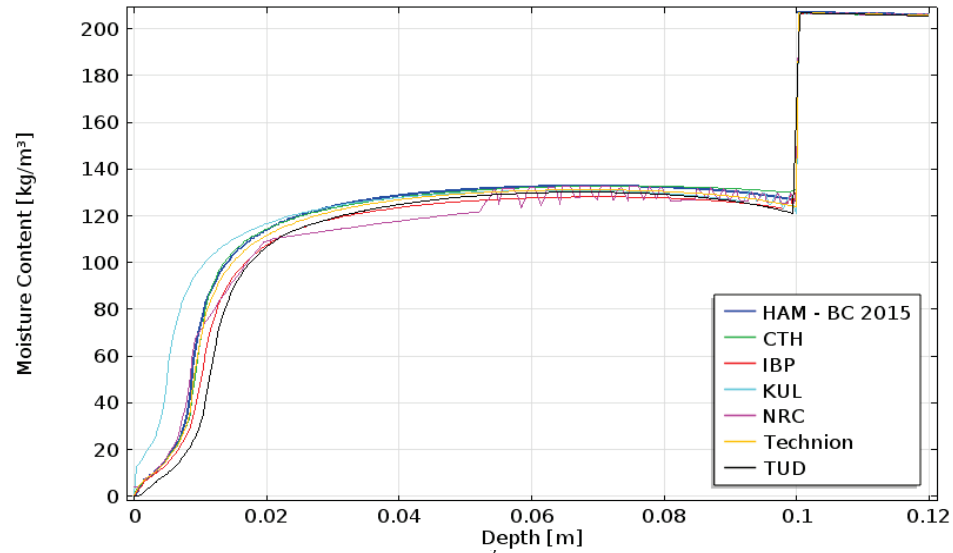

Figure C.35: Moisture content [kg/m^3] related to depth [m] on 78 hours.

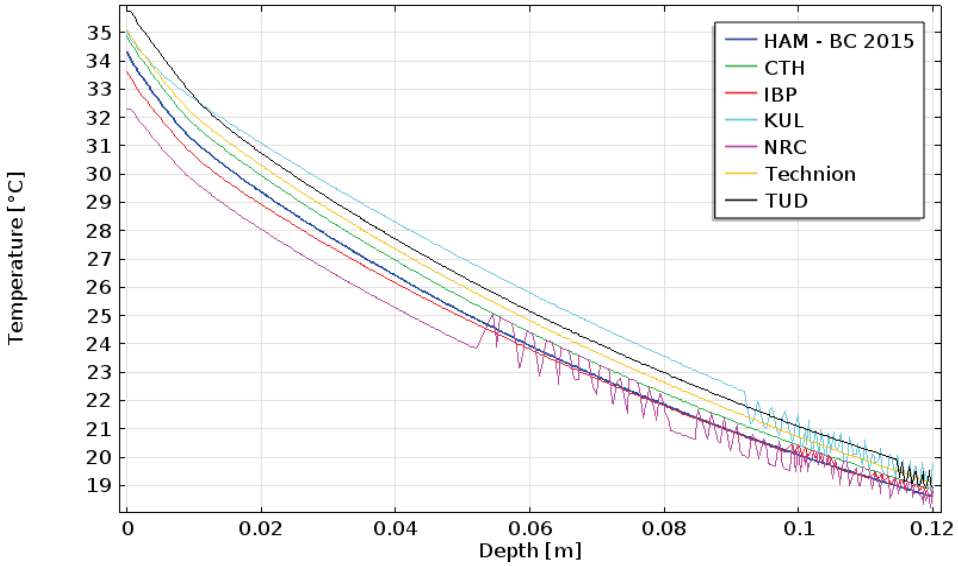

Figure C.36: Temperature [^{o}C] related to depth [m] on 78 hours.

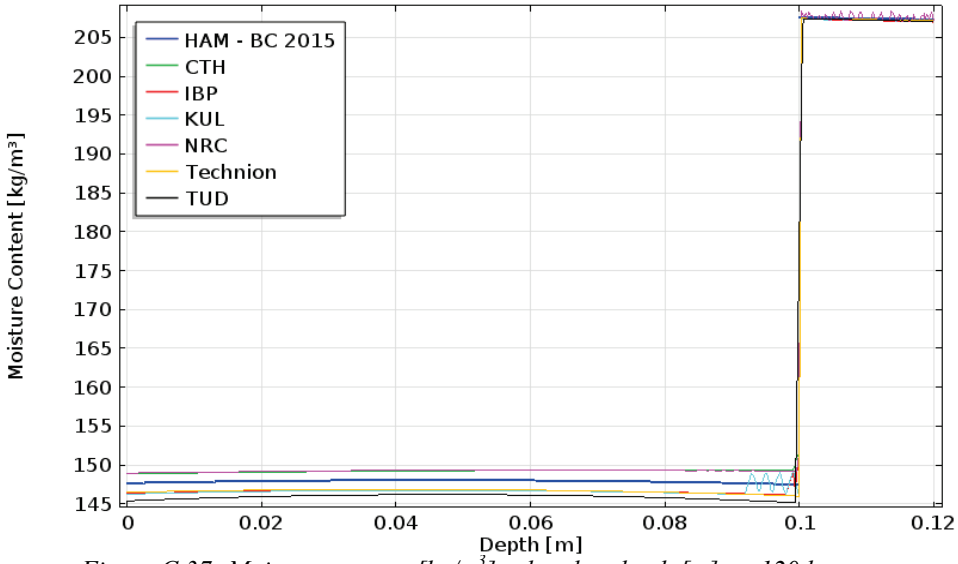

Figure C.37: Moisture content [kg/m^{3}] related to depth [m] on 120 hours.

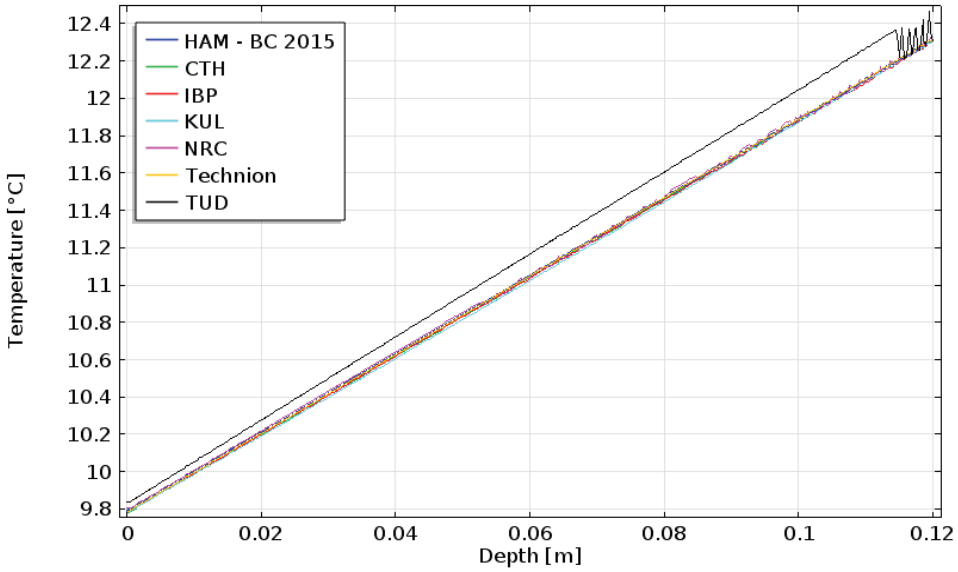

Figure C.38: Temperature [^{o}C] related to depth [m] on 120 hours.

HAMSTAD 5

Material A: Brick at the outside

Specific density = 1600 [kg/m^3]
Specific heat capacity = 1000 [J/(kg·K)]

Moisture content (w) in [kg/m^3] dependent on capillary pressure (Pc) in [Pa]
373.5*(0.46/(1+(0.47*(Pc/(1000*9.81)))^1.5)^m1)+ 373.5*(0.54/(1+(0.2*(Pc/(1000*9.81)))^3.8)^m2)
With m1 = 1-1/1.5 and m2 = 1-1/3.8

Thermal conductivity coefficient (λ) = 0.682 [W/(m·K)]

Vapor permeability (δ_v) in [s] related to temperature (Tk) in [K] and moisture content (w) in [kg/m^3].
(Mw/(R*Tk))*((26.1*10^-6/7.5)*((1-(w/373.5))/((1-0.2)*((1-(w/373.5))^2)+0.2)))

Moisture permeability for capillary suction (K) in [s] related to moisture content (w) in [kg/m^3]
exp(-36.484+461.325*(w/1000)-5240*((w/1000)^2)+2.907e4*((w/1000)^3)-
7.41e4*((w/1000)^4)+6.997e4*((w/1000)^5))

Material B: Mortar

Specific density = 230 [kg/m^3]
Specific heat capacity = 920 [J/(kg·K)]

Moisture content (w) in [kg/m^3] dependent on capillary pressure (Pc) in [Pa]
700*(0.2/(1+(0.5*(Pc/(1000*9.81)))^1.5)^m1)+700*(0.8/(1+(0.004*(Pc/(1000*9.81)))^3.8)^m2)
With m1 = 1-1/1.5 and m2 = 1-1/3.8

Thermal conductivity coefficient (λ) in [W/(m·K)] related to moisture content (w) in [kg/m^3].
0.6+0.56*(w/1000)

Vapor permeability (δ_v) in [s] related to temperature (Tk) in [K] and moisture content (w) in [kg/m^3].
(Mw/(R*Tk))*(26.1e-6/50)*((1-(w/700)/(((1-0.2)*(1-(w/700))^2)+0.2)))

Moisture permeability for capillary suction (K) in [s] related to moisture content (w) in [kg/m^3]
exp(-40.425+83.319*(w/1000)-175.961*((w/1000)^2)+123.863*((w/1000)^3)

Material C: Inside insulation

Specific density = 212 [kg/m^3]
Specific heat capacity = 1000 [J/(kg·K)]

Moisture content (w) in [kg/m^3] dependent on capillary pressure (Pc) in [Pa]
871*(0.41/(1+(0.006*(Pc/(1000*9.81)))^2.5)^m1)+871*(0.59/(1+(0.012*(Pc/(1000*9.81)))^2.4)^m2)
With: m1 = 1-1/2.5 and m2 = 1-1/2.4

Thermal conductivity coefficient (λ) in [W/(m·K)] related to moisture content (w) in [kg/m^3].
0.06+0.56*(w/1000)

Vapor permeability (δ_v) in [s] related to temperature (Tk) in [K] and moisture content (w) in [kg/m^3].
(Mw/(R*Tk))*(26.1e-6/5.6)*((1-(w/871)/(((1-0.2)*(1-(w/871))^2)+0.2)))

Moisture permeability for capillary suction (K) in [s] related to moisture content (w) in [kg/m^3]
exp(-46.245+294.506*(w/1000)-1439*((w/1000)^2)+3249*((w/1000)^3)-
3370*((w/1000)^4)+1305*((w/1000)^5))

Annex D – Additional data and results related to the climate chamber in France

Additional data and results from the empirical validation of HAM-BC 2015 with the measured dataset of [Rafidiarison et al. 2015] are shown in this annex. The tables with %RMSE and Maximum Error are shown in the main text. In table D.1, the material properties given by [Rafidiarison et al. 2015] are shown.

Wood Fibreboard								
Thermal conductivity W/(m·K)	(0.28·H+(0.108·T + 38))/1000							
Water vapor resistance factor	Dry cup				Wet cup			
μ	6				2			
Dry bulk density kg/m3	150							
Sorption isotherm at 20 °C	RH (%)		0	22.5	43	66	93	97
	MC (%)	Adsorption	0	3.2	5.6	8.6	15	23.93
		Desorption	0	4	6.87	9.8	19.07	23.13
Heat capacity (J/kg·K)	1600 + 4185·H							
External lime plaster								
Thermal conductivity (W/(m·K)	0.087							
Water vapor resistance factor	RH (%): 40-75 at 23 °C							
μ	31							
Dry bulk density kg/m3	1300							
Sorption isotherm at 20 °C	RH (%)		0	13	29	44	58	73	87
	MC (%)	Adsorption	0	0.11	0.16	0.2	0.26	0.36	0.65
		Desorption	0	0.26	0.32	0.38	0.44	0.53	0.65
Heat capacity (J/kg·K)	850							
Oriented Strand Board (OSB)								
Thermal conductivity (W/(m·K)	((0.018·T - 0.072)·θthetam + (0.27·T+89))/1000							
Water vapor resistance factor	Dry cup				Wet cup			
μ	46				27			
Dry bulk density kg/m3	590							
Sorption isotherm at 20 °C	RH (%)		0	22.5	43	66	93	97
	MC (%)	Adsorption	0	3.58	5.77	8.87	16.27	27.75
		Desorption	0	5.1	8.53	12.4	21.18	24.25
Heat capacity (J/kg·K)	1700							

Table D1: Material data from [Rafidiarison et al. 2015].

Probably there is a typing error about the thermal conductivity coefficient of the plaster material. The article stated that the thermal conductivity coefficient was 0.87 mW/(m·K); however, in the simulation the value 0.087 W/(m·K) is used.

According to [Rafidiarison et al. 2015], the water vapor resistance factor of the Oriented Strand Board (OSB) – as shown in table D1 – are 46 (dry cup) and 27 (wet cup). It is assumed that this is a typing error after comparing with the information of the material properties of OSB in Delphin. It is assumed to be 46 and 270.

For each wall configuration, the initial values in COMSOL for the logarithmic capillary pressure (LPc) and temperature (T) are determined by using the first values in the Excel-sheets of the center of the respective wall configuration.

The surface coefficients about heat transfer and moisture transfer were not determined by [Rafidiarison et al. 2015]; therefore, the values of these surface coefficients were "fine-tuned" by simulating with several values and choosing the values which generated the best results in the graphs of the surface temperatures and surface relative humidity. The used surface coefficients are shown in table D2.

	Wall 1	**Wall 2**	**Wall 3**	**Wall 4**
$\mathbf{h_e}$	20	16	19	19
$\mathbf{h_i}$	10	7	6	4
$\mathbf{\beta_e}$	5.8382e-8	5.8382e-8	5.8382e-9	5.8382e-9
$\mathbf{\beta_i}$	1.8382e-8	5.8382e-7	5.8382e-9	5.8382e-9

Table D2: Surface coefficients of each wall configurations about the external surface heat transfer coefficient (h_e) in [W/(m^2·K)], internal surface heat transfer coefficient (h_i) in [W/(m^2K)], external surface vapor transfer coefficient (β_e) in [s/m] and internal surface vapor transfer coefficient (β_i) in [s/m].

Each wall configuration is further discussed by giving first the boundary conditions; the changes made in the measured data; and the results at each point for the temperature and relative humidity.

The wind velocities in the two chambers are measured, but these are not used in the simulation models. The velocity in both rooms was in the range 0 to 0.17 m/s.

The air pressure difference between the two chambers is shown in figure D.1.

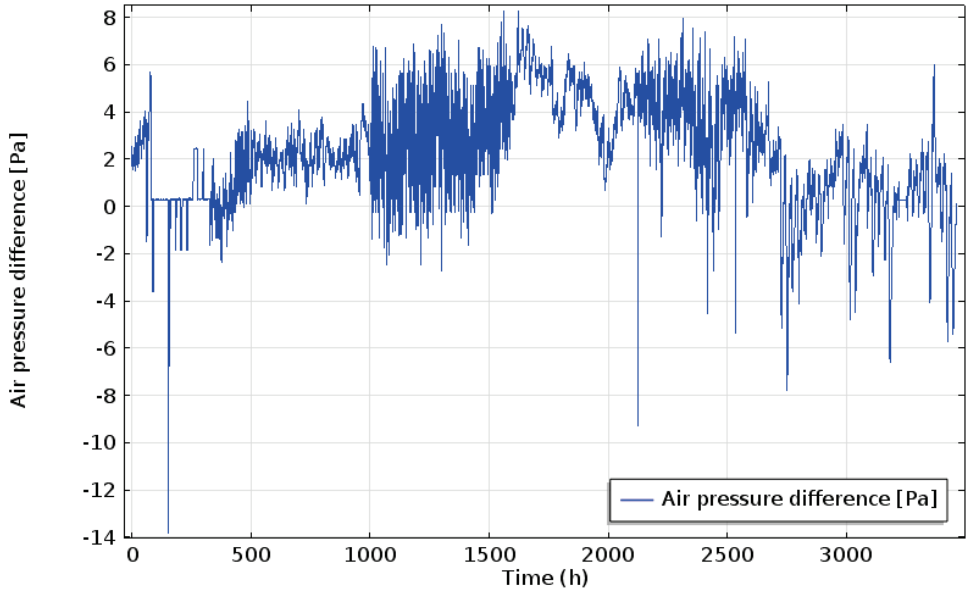

Figure D.1: Air pressure difference between the two chambers in [Pa]. A positive value means that the air flows from the outer chamber to the inner chamber.

Wall configuration 1 (sophisticated convection method)

The indoor temperature is at the interval 1704 hour to 1739 hour is changed from 24°C to 19.3°C to prevent the singularity error. At the same interval the internal vapor pressure is changed from around 1900 Pa to 1300 Pa. Also at the interval 3223 hour to 3249 hour the measured relative humidity at point x=60 mm is changed from 29.31% to 59%.

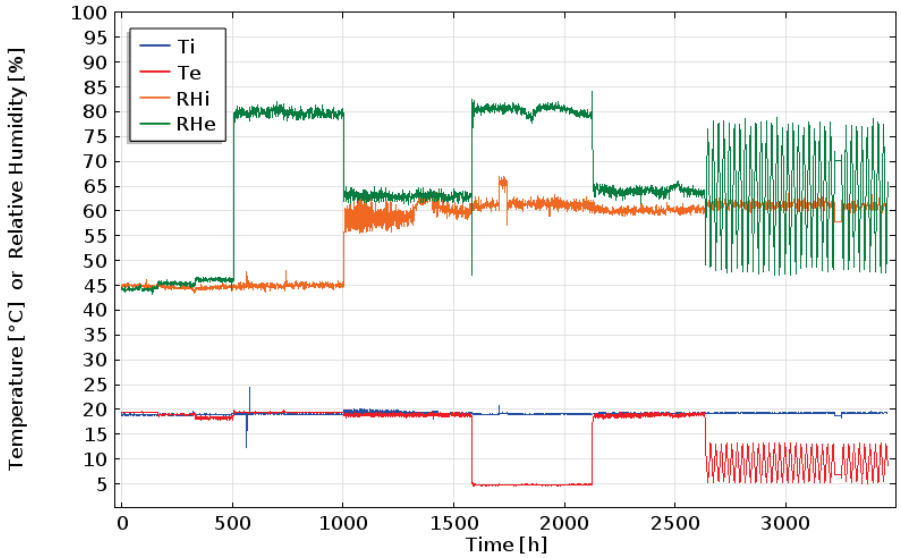

Figure D.2: Climate data measured at wall configuration 1 with indoor temperature (Ti), external temperature (Te), indoor relative humidity (RHi) and external relative humidity (RHe).

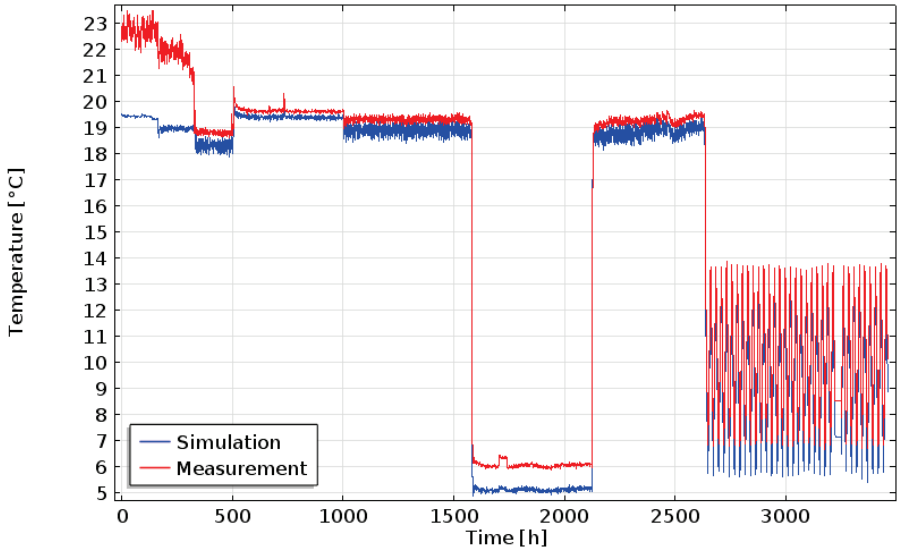

Figure D.3: Temperature [°C] at the external surface of wall configuration 1.

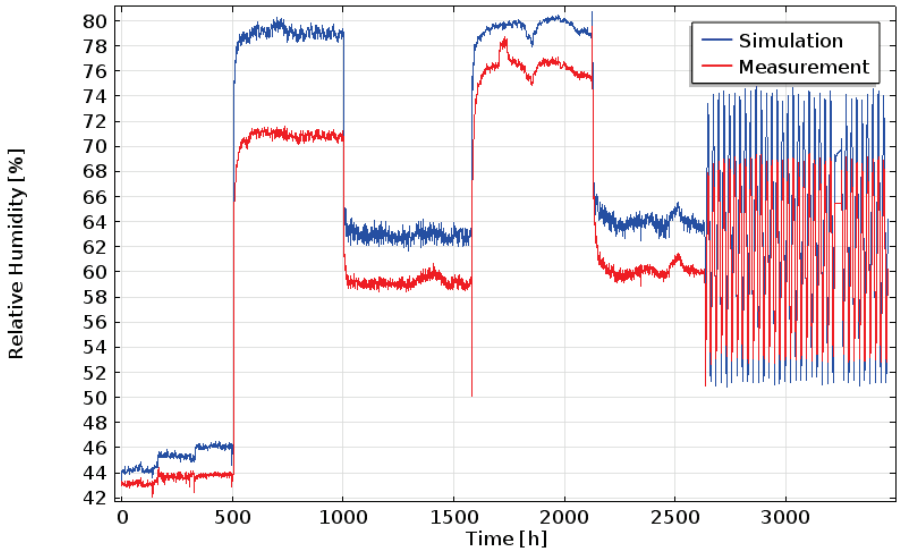

Figure D.4: Relative humidity [%] at the external surface of wall configuration 1.

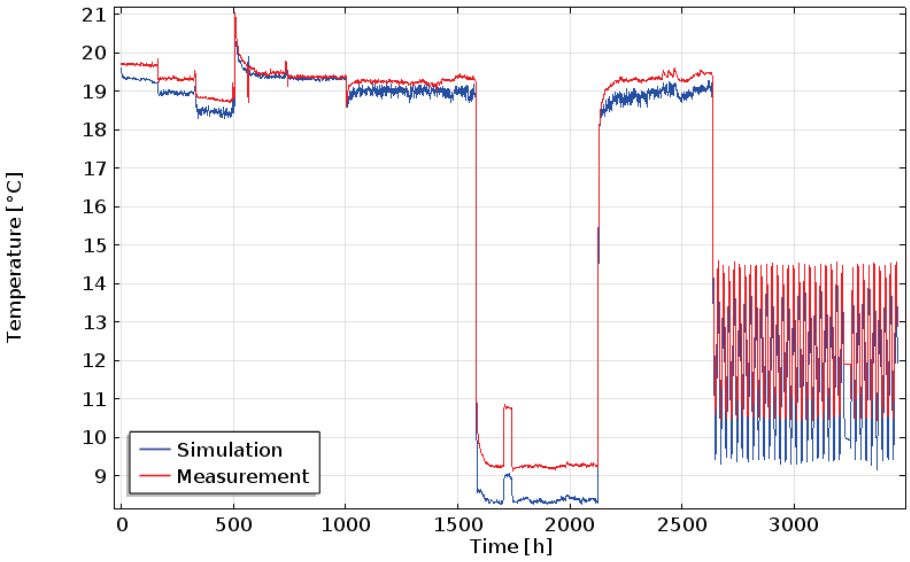

Figure D.5: Temperature [°C] at the depth 20 mm of wall configuration 1.

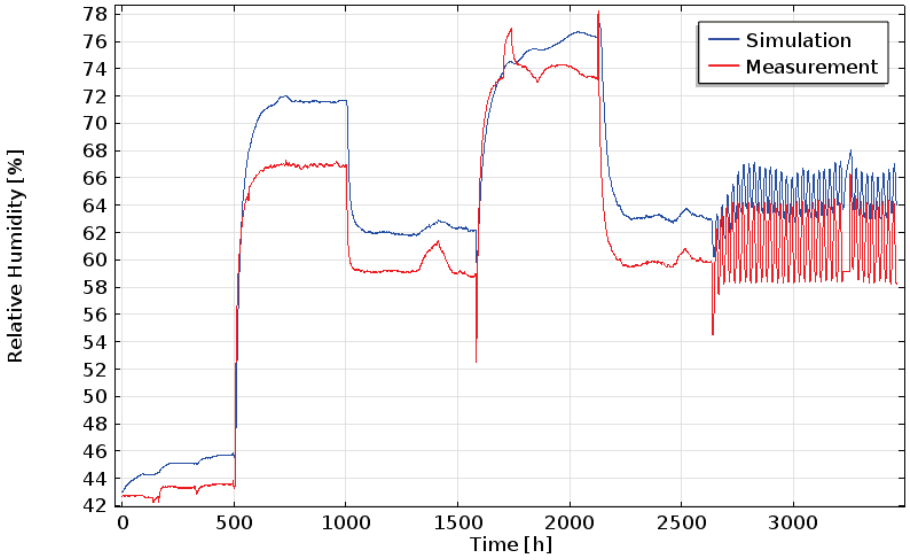

Figure D.6: Relative humidity [%] at the depth 20 mm of wall configuration 1.

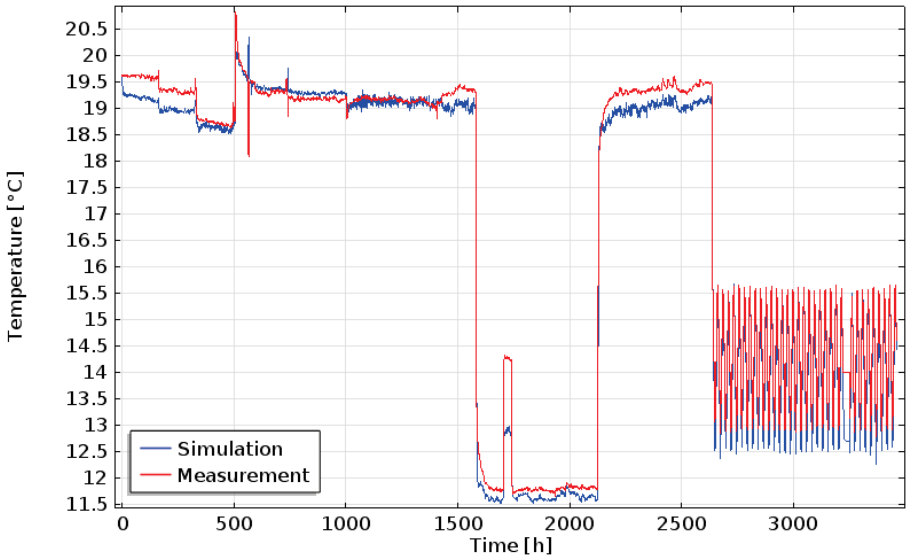

Figure D.7: Temperature [°C] at the depth 40 mm of wall configuration 1.

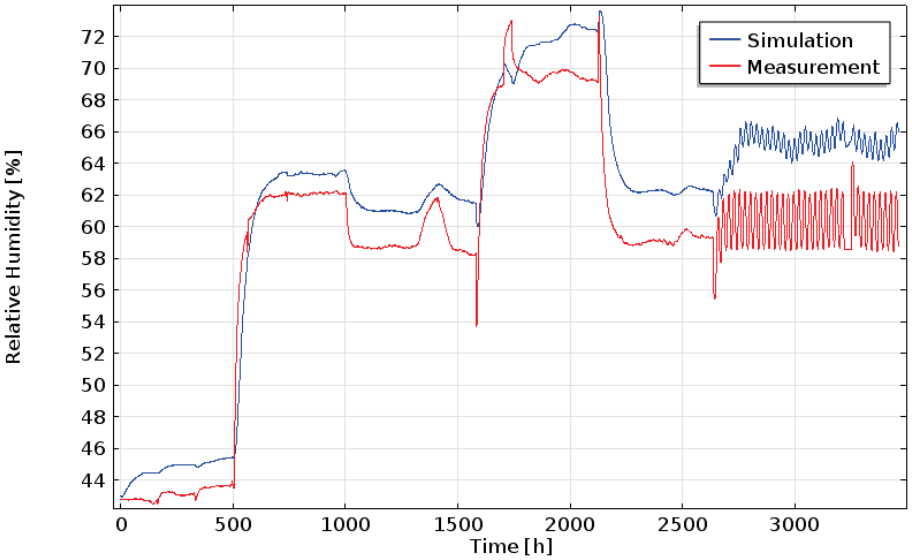

Figure D.8: Relative humidity [%] at the depth 40 mm of wall configuration 1.

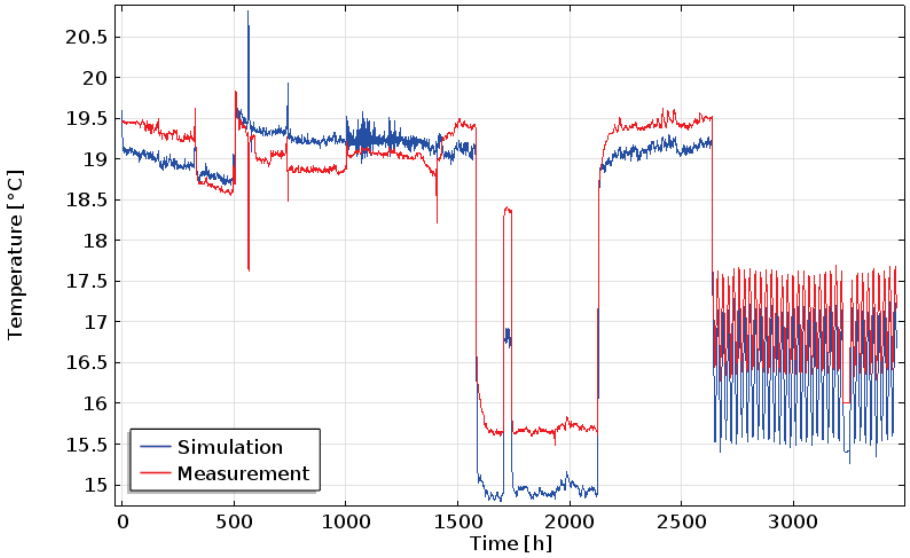

Figure D.9: Temperature [°C] at the depth 60 mm of wall configuration 1.

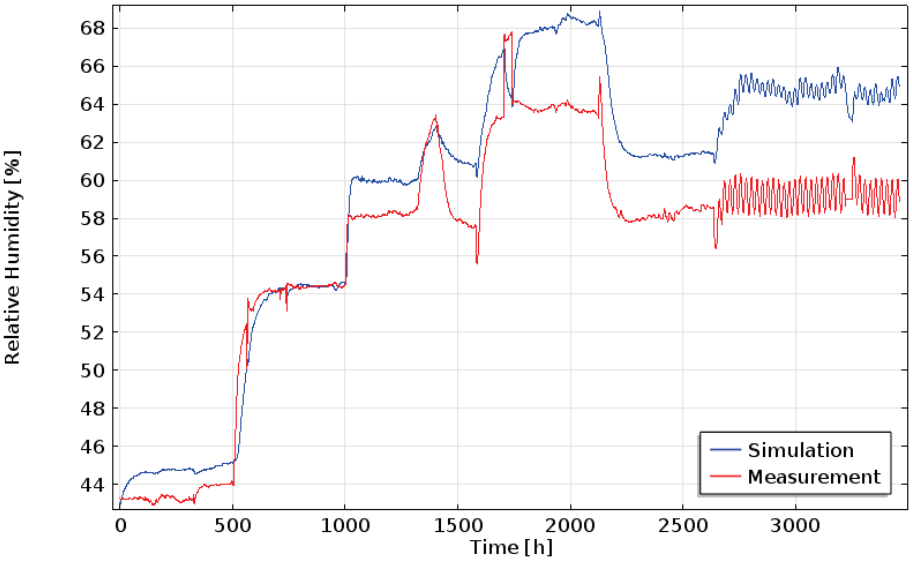

Figure D.10: Relative humidity [%] at the depth 60 mm of wall configuration 1.

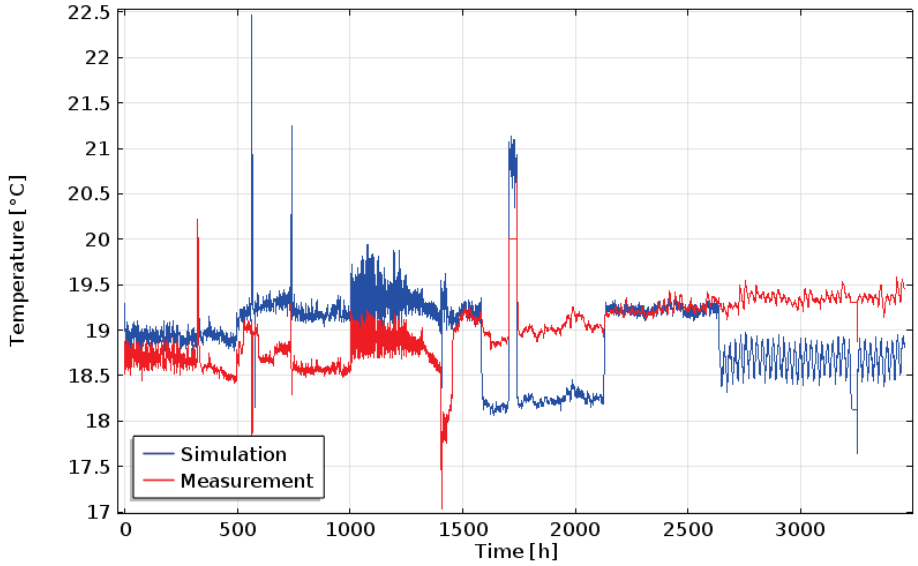

Figure D.11: Temperature [°C] at the internal surface of wall configuration 1.

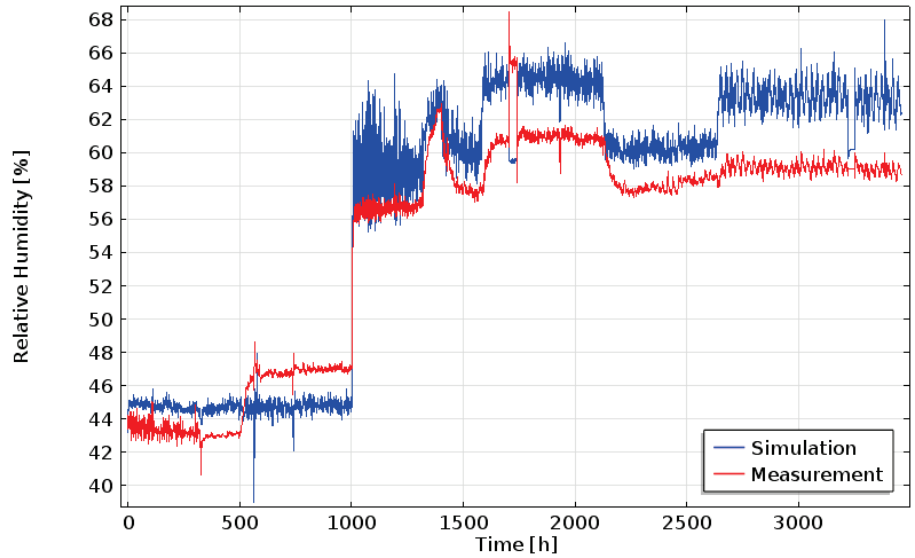

Figure D.12: Relative humidity [%] at the internal surface of wall configuration 1.

Wall configuration 2 (simple convection method)

The values of relative humidity for the internal chamber are missing between 1703 hour and 1745 hour, which is filled with the value 59%. Also the internal vapor pressure was missing values at this time interval, which were filled with the value 1300 Pa. The values for the relative humidity at the internal surface are missing values between 525 hour and 590 hour, which are filled with the value 44%. The same dataset for the relative humidity at the internal surface misses values between 1911 hour and 2080 hour, which are filled with 58%. At 3233 hour and 3250 hour there was a sudden drop from 58% to 28%, were the 28% is changed to 58%. The temperature dataset at location 0.04 m inside the material is missing values in the time slot 524 hour to 564 hour, which is filled with the value 20°C. The relative humidity at the same location (0.04 m) misses values between 525 hour and 564 hour, which are filled with 56%. At the data of the internal temperature between 1703 hour and 1739 hour, the temperature suddenly dropped below zero from 19°C to around -19°C – which are changed to 19°C. At 1911 hour and 2080 hour at the measured temperature at the material surface suddenly dropped from 19°C to 9°C, whereby these values were 9.46°C, which are changed to 19°C.

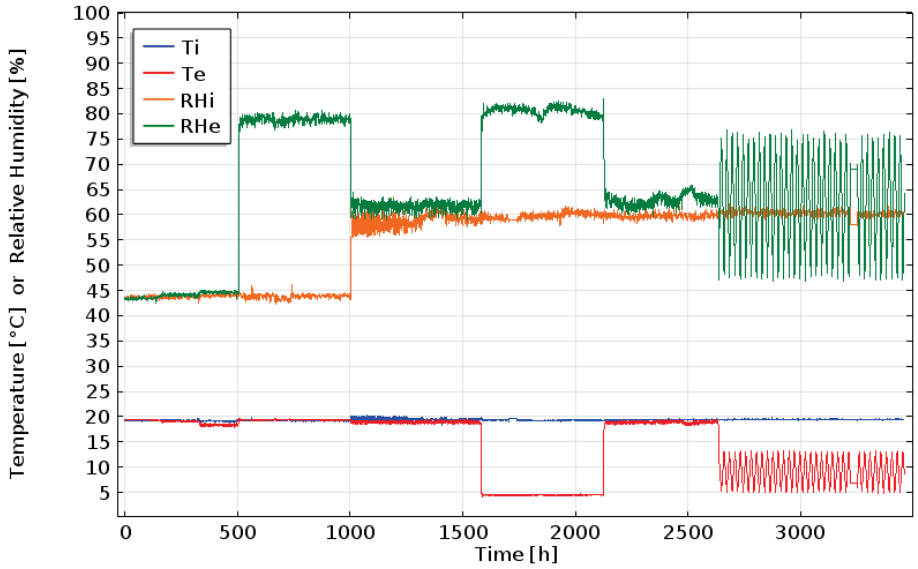

Figure D.13: Climate data measured at wall configuration 2 with indoor temperature (Ti), external temperature (Te), indoor relative humidity (RHi) and external relative humidity (RHe).

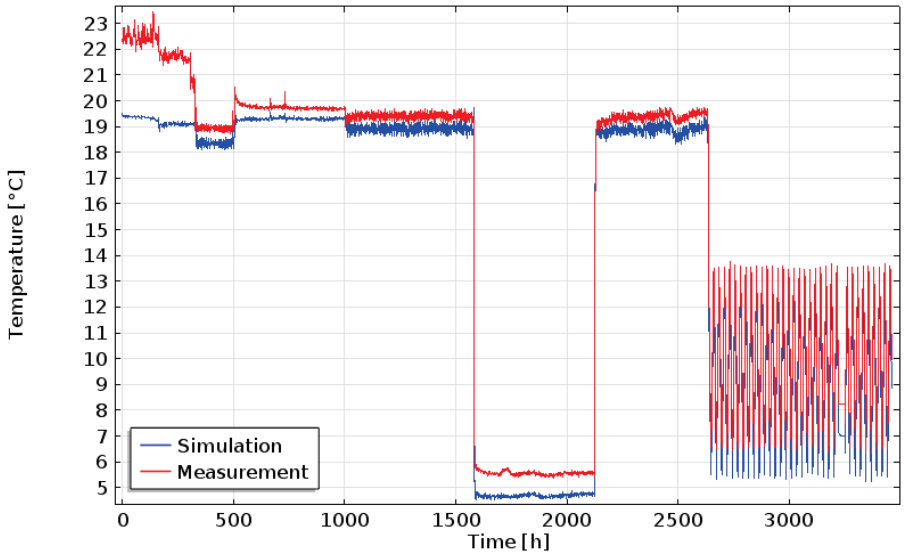

Figure D.14: Temperature [°C] at the external surface of wall configuration 2.

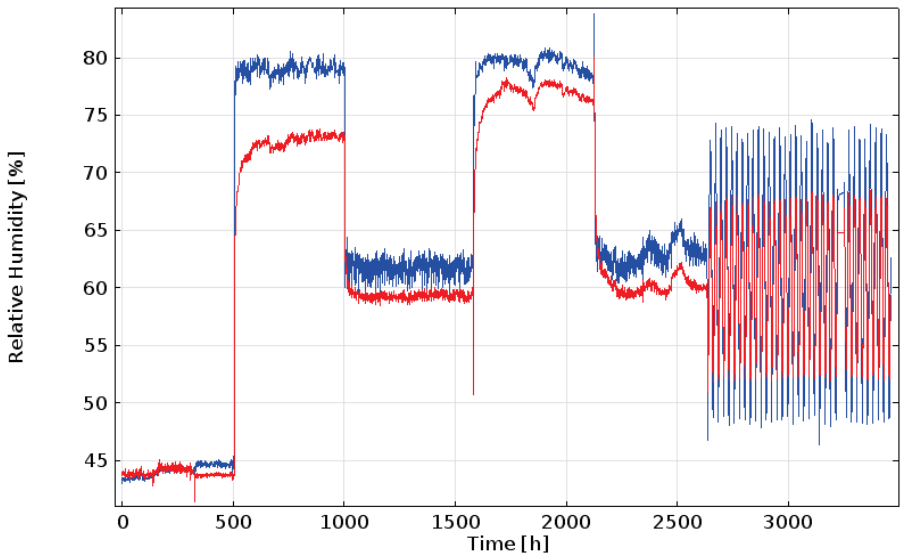

Figure D.15: Relative humidity [%] at the external surface of wall configuration 2.

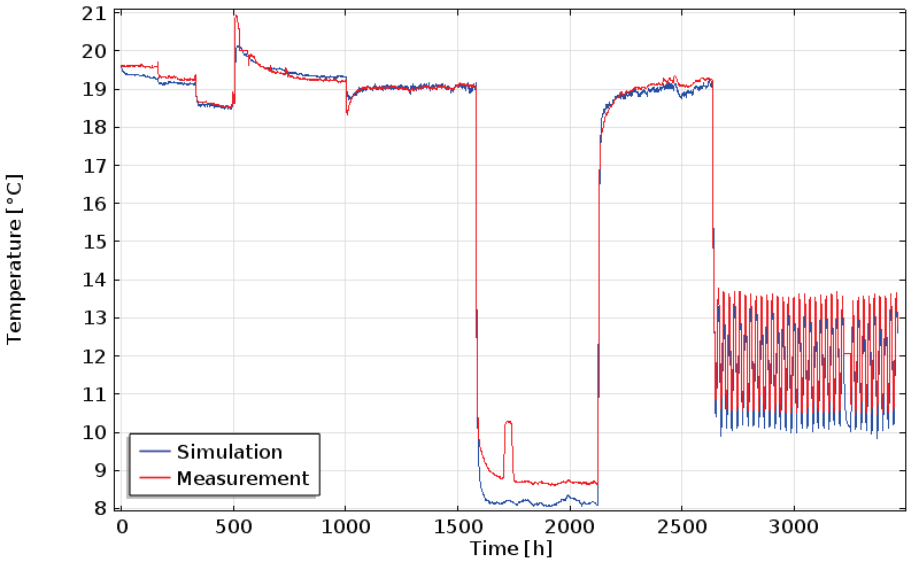

Figure D.16: Temperature [°C] at the depth 40 mm of wall configuration 2.

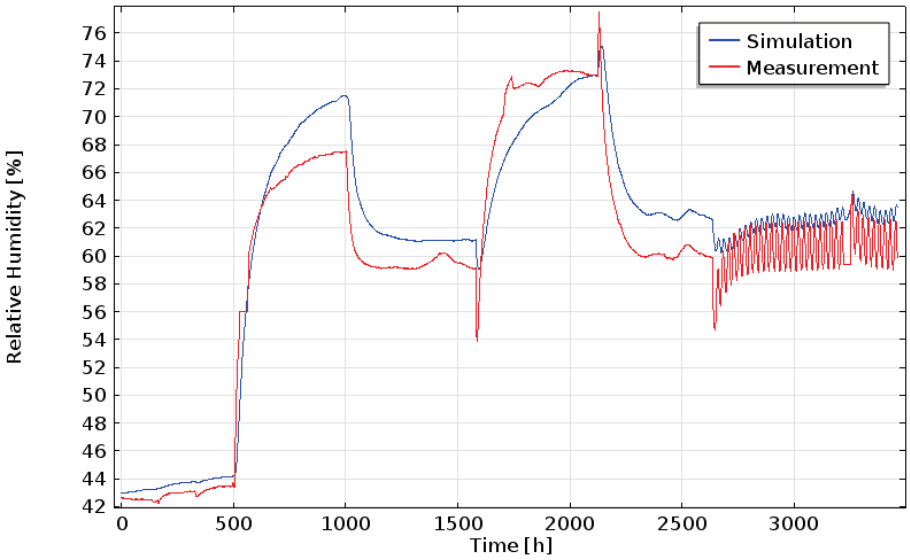

Figure D.17: Relative humidity [%] at the depth 40 mm of wall configuration 2.

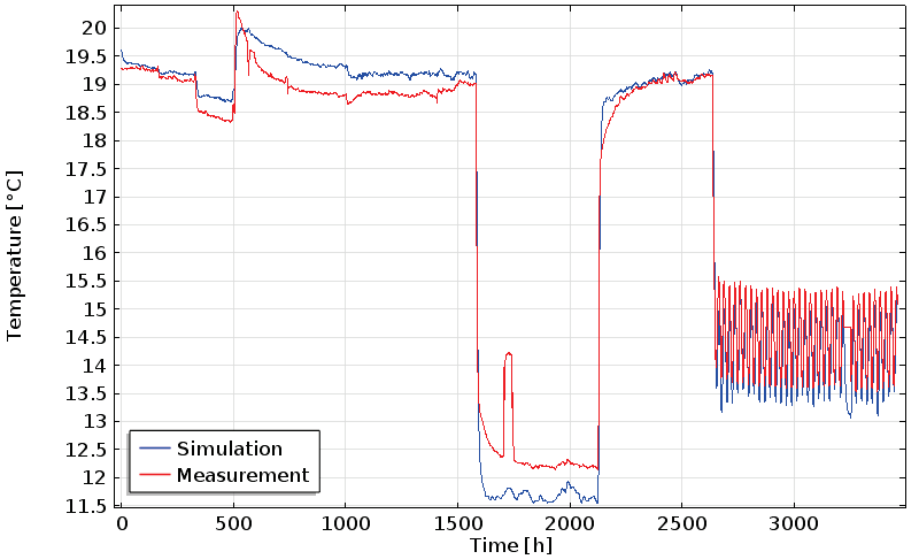

Figure D.18: Temperature [°C] at the depth 80 mm of wall configuration 2.

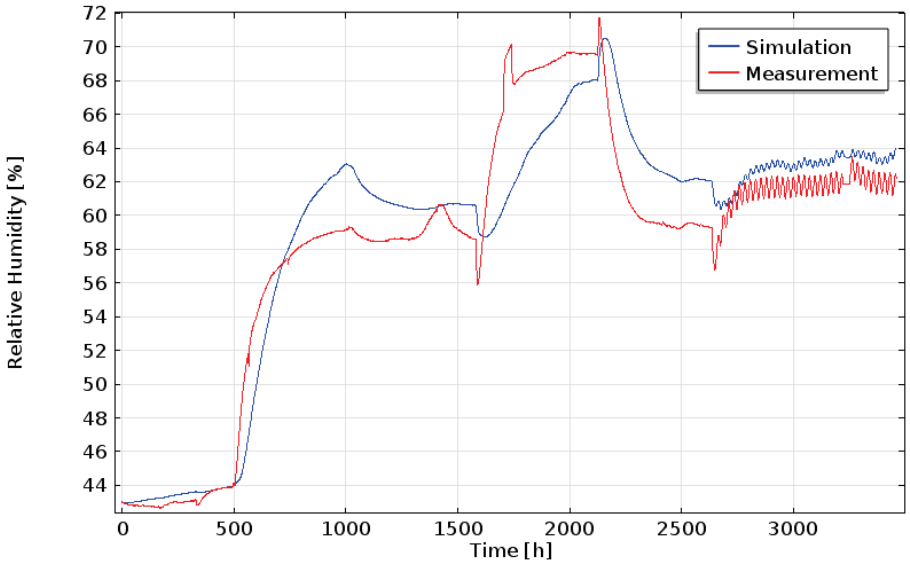

Figure D.19: Relative humidity [%] at the depth 80 mm of wall configuration 2.

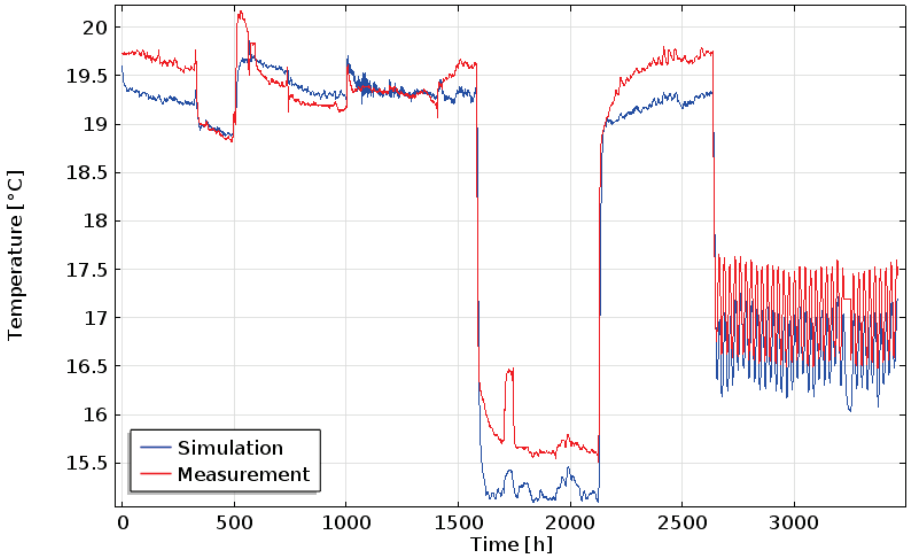

Figure D.20: Temperature [°C] at the depth 120 mm of wall configuration 2.

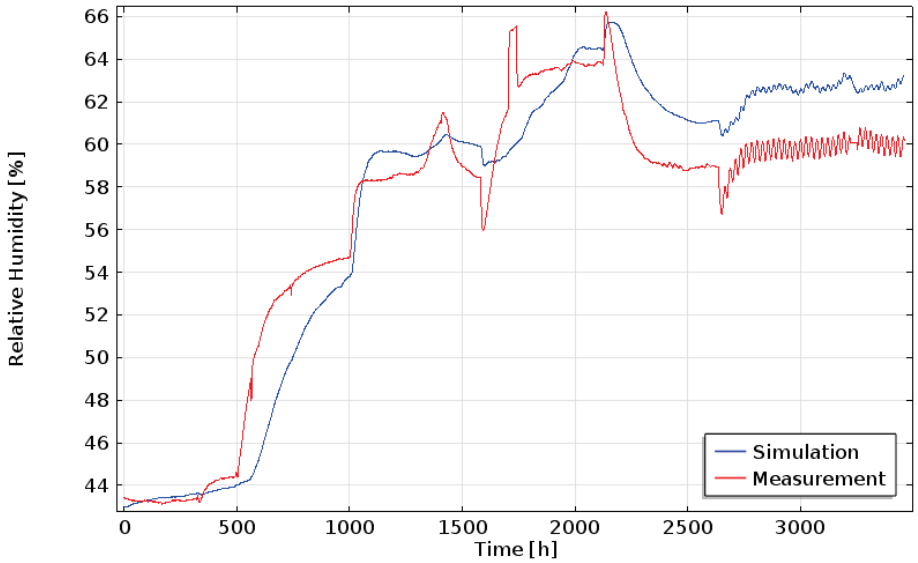

Figure D.21: Relative humidity [%] at the depth 120 mm of wall configuration 2.

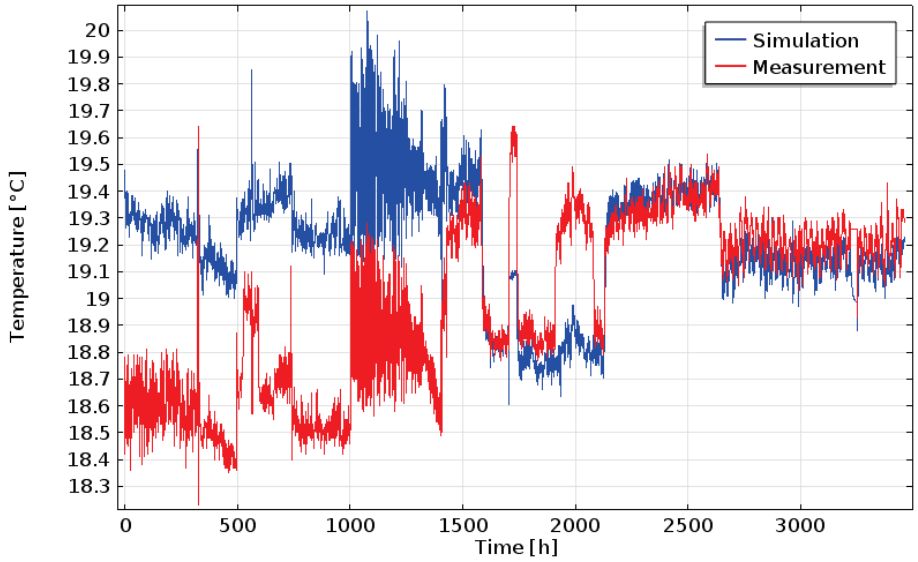

Figure D.22: Temperature [°C] at the internal surface of wall configuration 2.

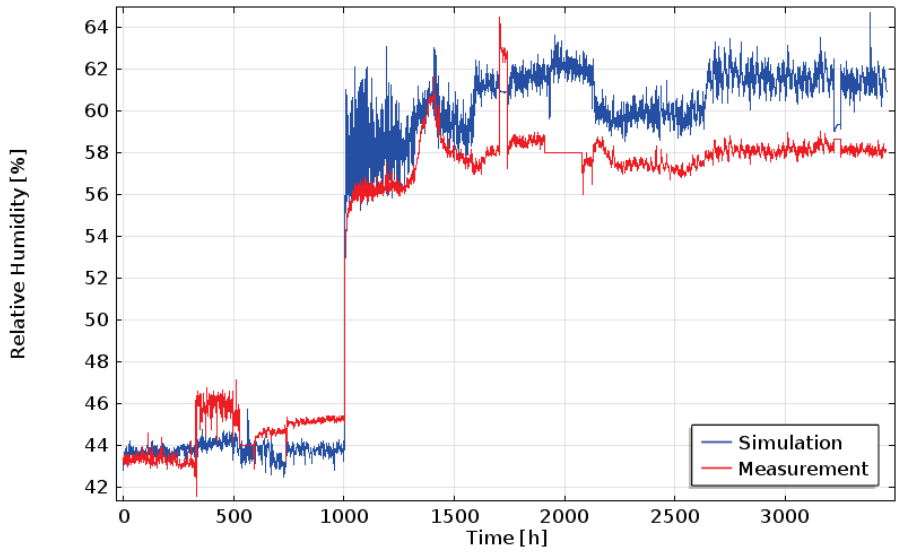

Figure D.23: Relative humidity [%] at the internal surface of wall configuration 2.

Wall configuration 3 (simple convection method)

The sensor measuring the temperature, vapor pressure and relative humidity indoors, has on certain interval strange and unreliable results. On interval 3223 hour to 3250 hour, the indoor RH is changed from 55.5% to 61%, the vapor pressure from constant 1329 Pa to constant 1550 Pa and the temperature from 20.38°C to 21°C. This was necessary, because otherwise it leads to errors and the aborting of the calculation in COMSOL. The liquid permeability for the materials is not known. For the plaster, the *Lime plaster fine* with a specific density of 1500 kg/m^3, specific heat capacity of 850 J/(kg·K) and a vapor diffusion factor of 51 from Delphin is used.

There was a singularity-error, because of the sudden increase at 2128 hour. This problem is solved by making at the interval between 2122 hour and 2128 hour a linear and slower slope with steps of 100 Pa for external vapor pressure and a slope of 2°C for the external temperature.

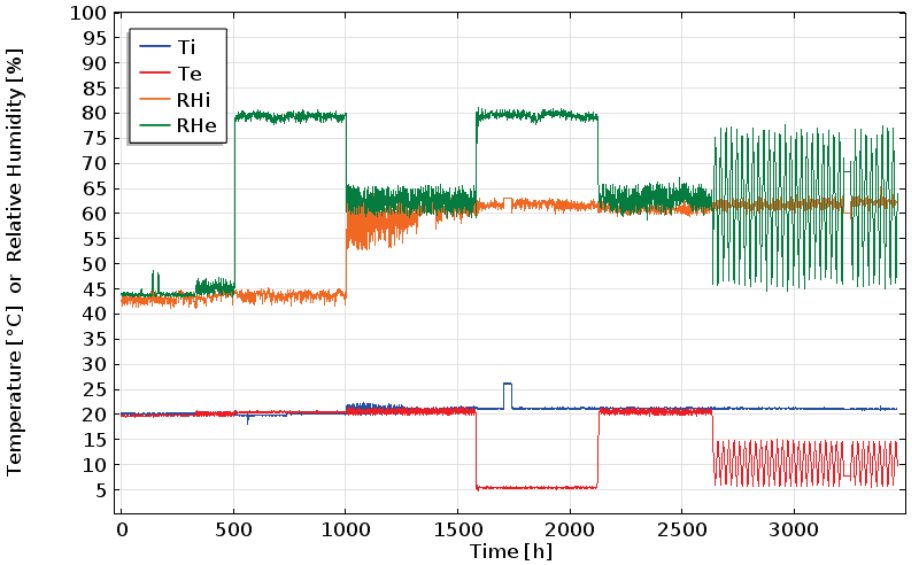

Figure D.24: Climate data measured at configuration 3 with indoor temperature (Ti), external temperature (Te), indoor relative humidity (RHi) and external relative humidity (RHe).

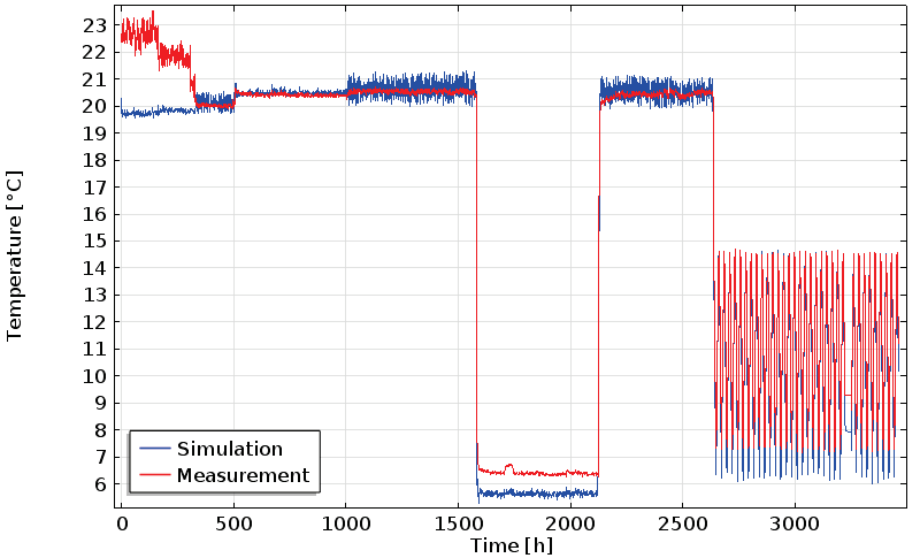

Figure D.25: Temperature [°C] at the external surface of wall configuration 3.

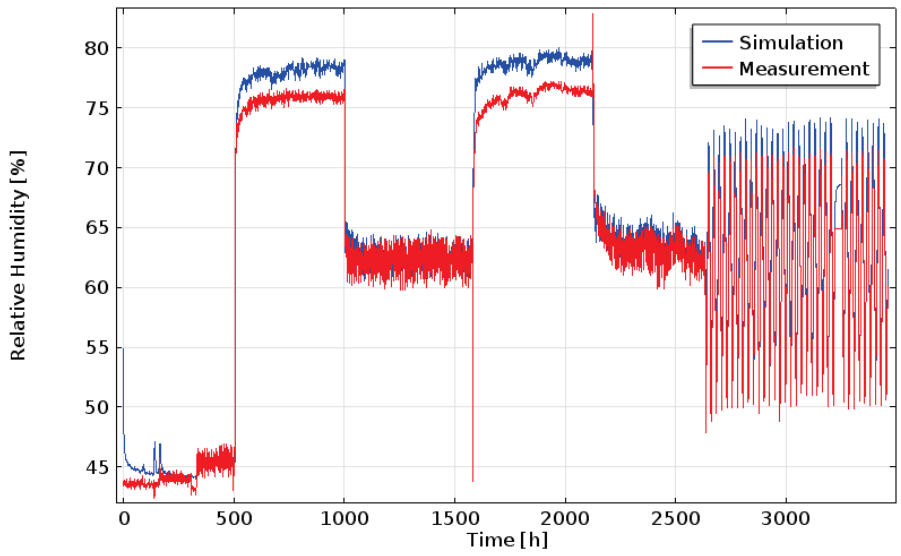

Figure D.26: Relative humidity [%] at the external surface of wall configuration 3.

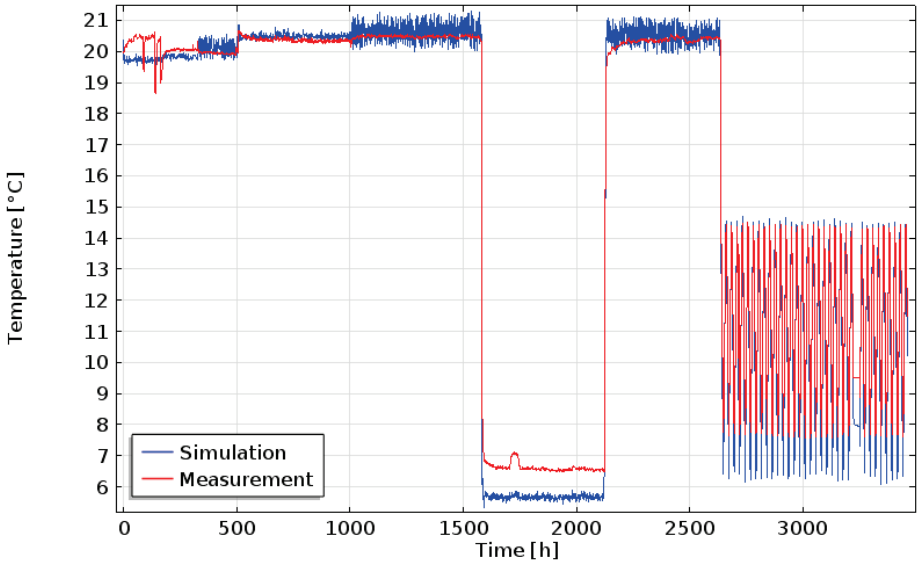

Figure D.27: Temperature [°C] at the depth 7 mm of wall configuration 3.

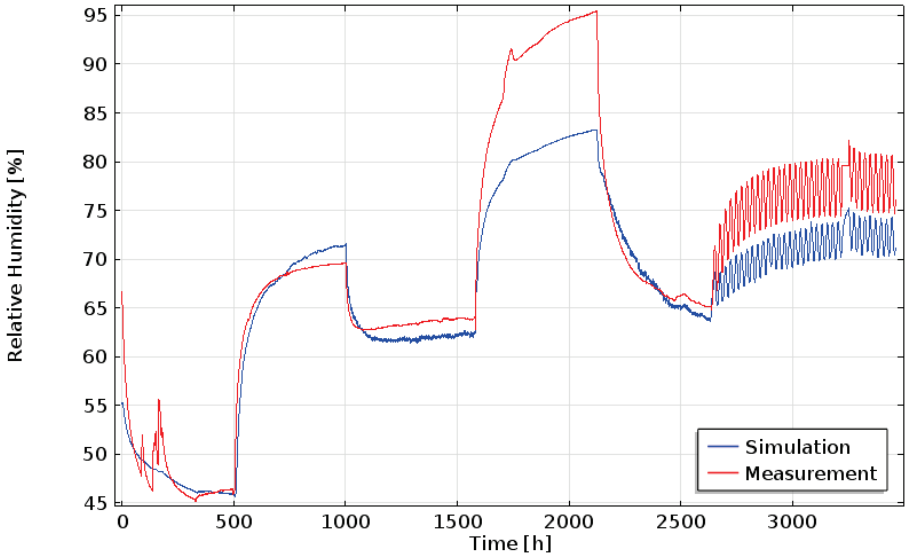

Figure D.28: Relative humidity [%] at the depth 7 mm of wall configuration 3.

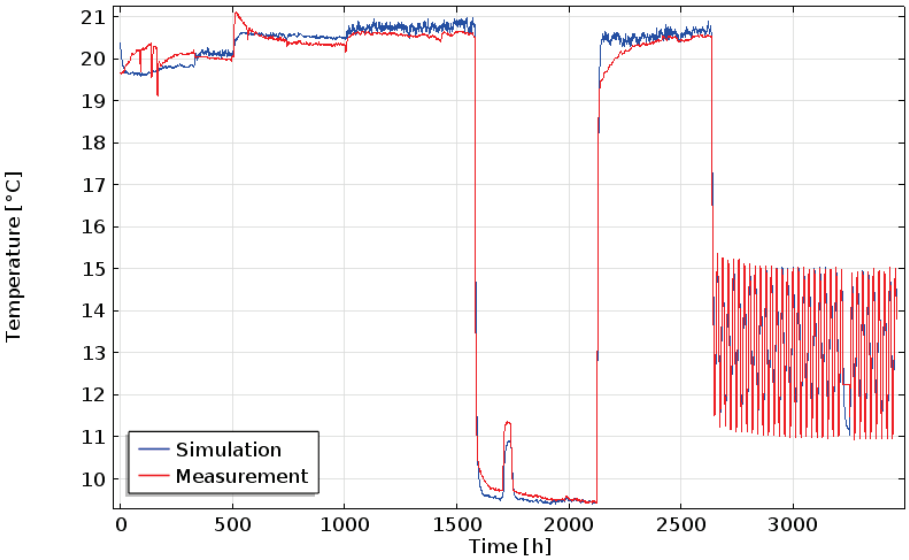

Figure D.29: Temperature [°C] at the depth 47 mm of wall configuration 3.

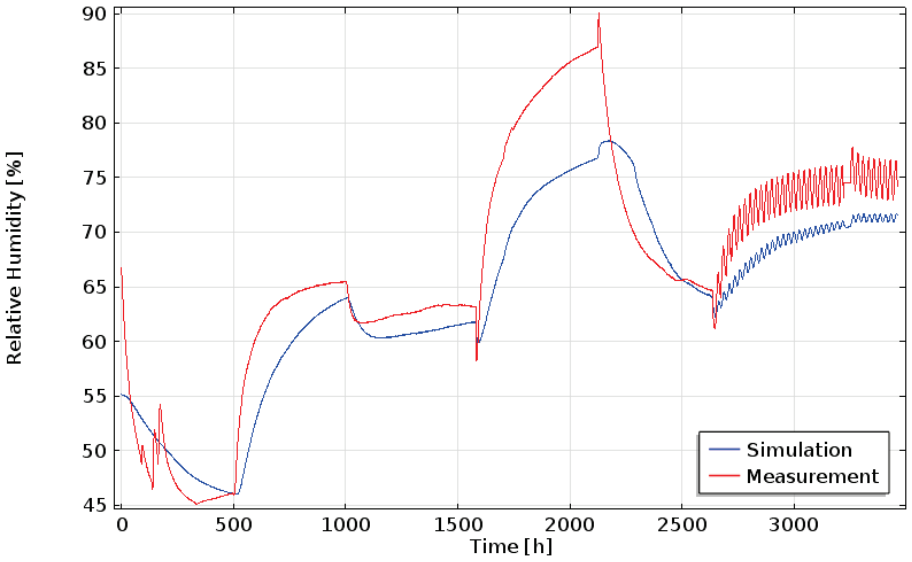

Figure D.30: Relative humidity [%] at the depth 47 mm of wall configuration 3.

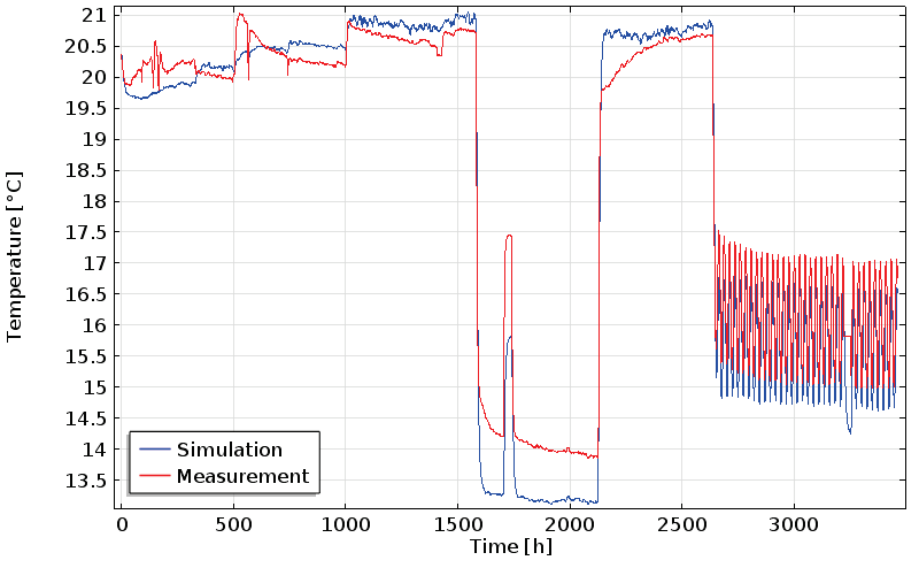

Figure D.31: Temperature [°C] at the depth 87 mm of wall configuration 3.

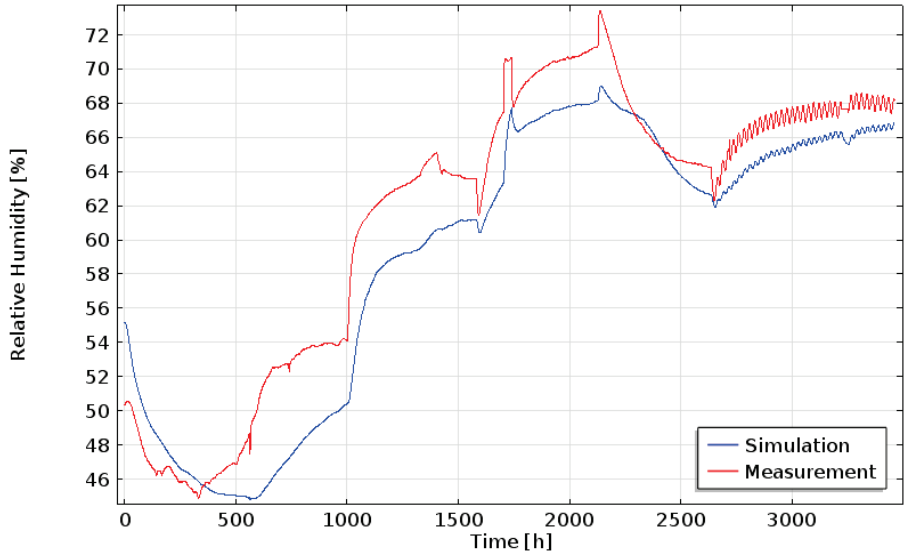

Figure D.32: Relative humidity [%] at the depth 87 mm of wall configuration 3.

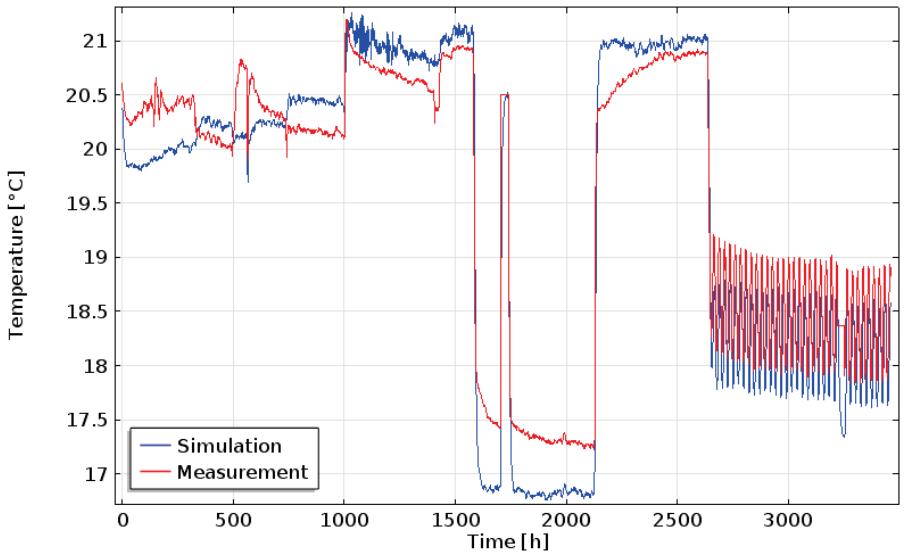

Figure D.33: Temperature [°C] at the depth 127 mm of wall configuration 3.

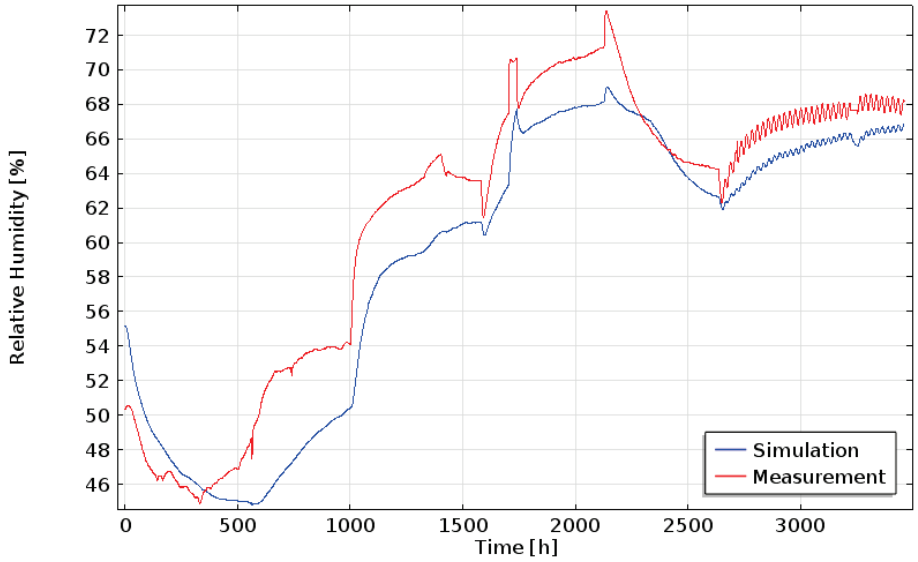

Figure D.34: Relative humidity [%] at the depth 127 mm of wall configuration 3.

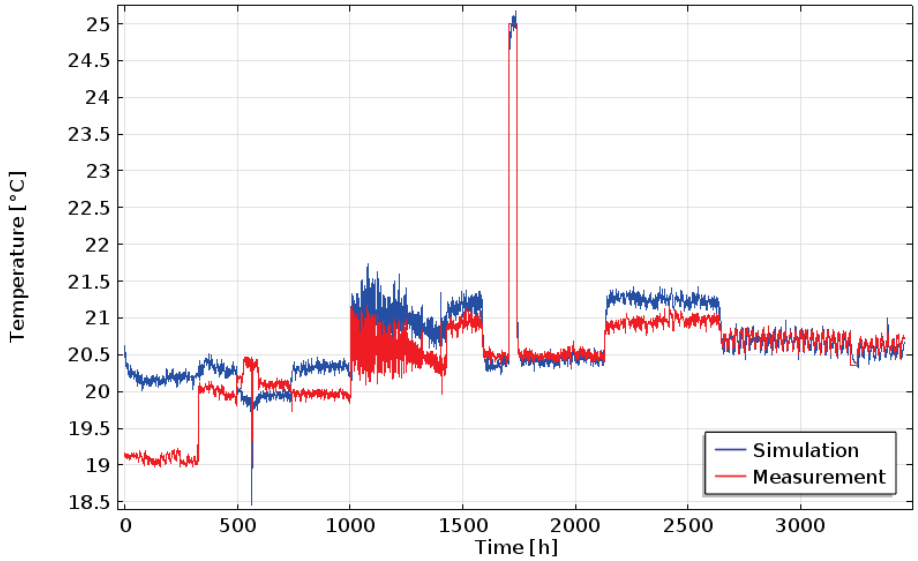

Figure D.35: Temperature [°C] at the indoor surface of wall configuration 3.

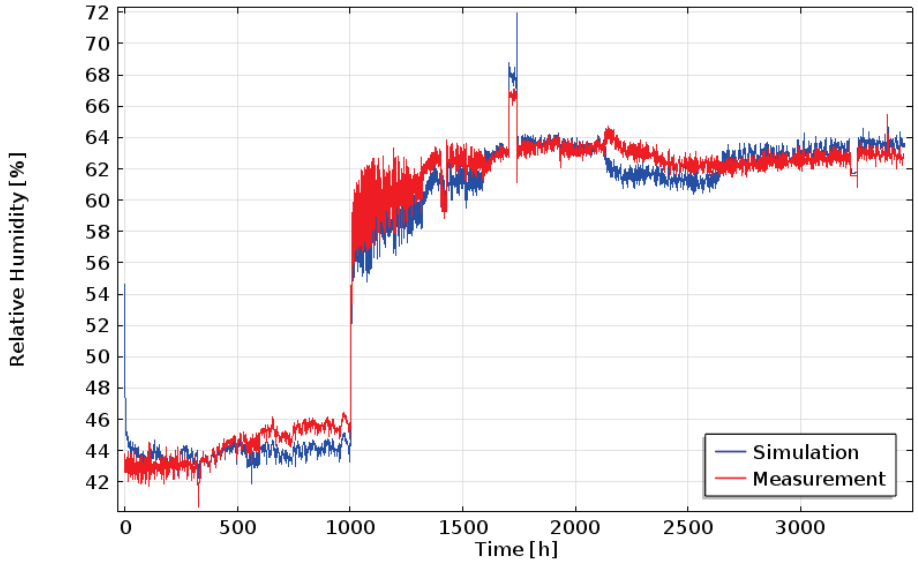

Figure D.36: Relative humidity [%] at the indoor surface of wall configuration 3.

Wall configuration 4 (sophisticated convection method)

The air permeability of exterior coating is 1e-8 s and the air permeability of the OSB is 1e-7 s.

In the data of the indoor vapor pressure (Pi) at 3223 hour to 3250 hour the value is large deviating from the rest with a constant value of 1332 Pa. This is change to 1550 Pa. Also several peaks consisting of one á 2 values are flattened out.

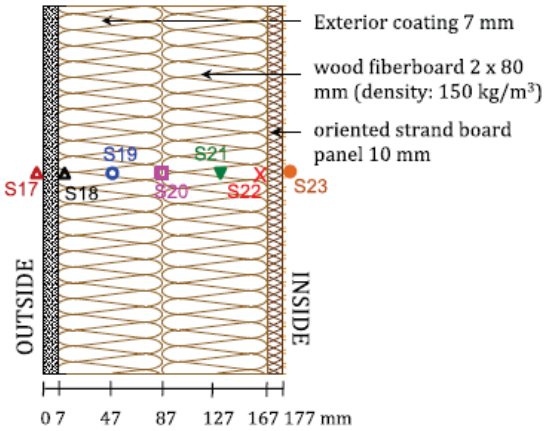

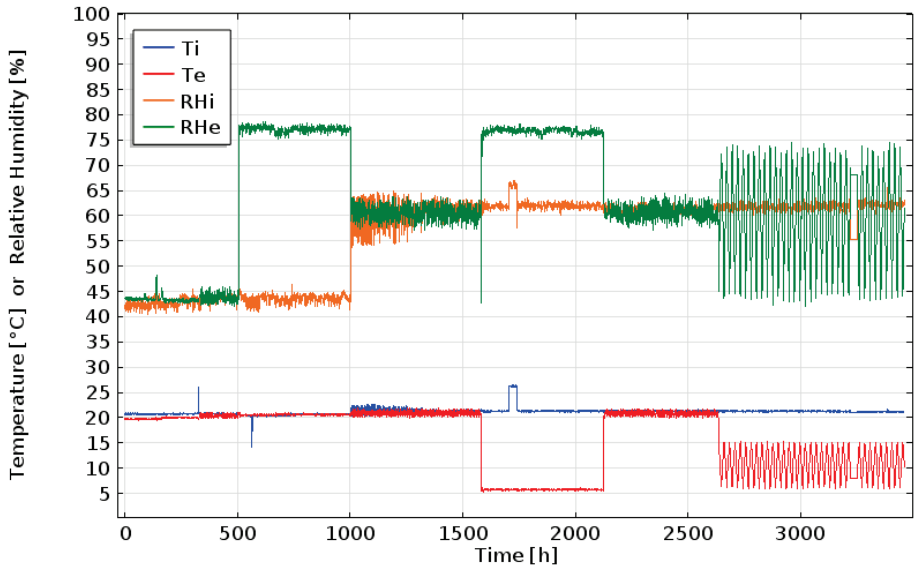

Figure D.37: Climate data measured at configuration 4 with indoor temperature (Ti), external temperature (Te), indoor relative humidity (RHi) and external relative humidity (RHe).

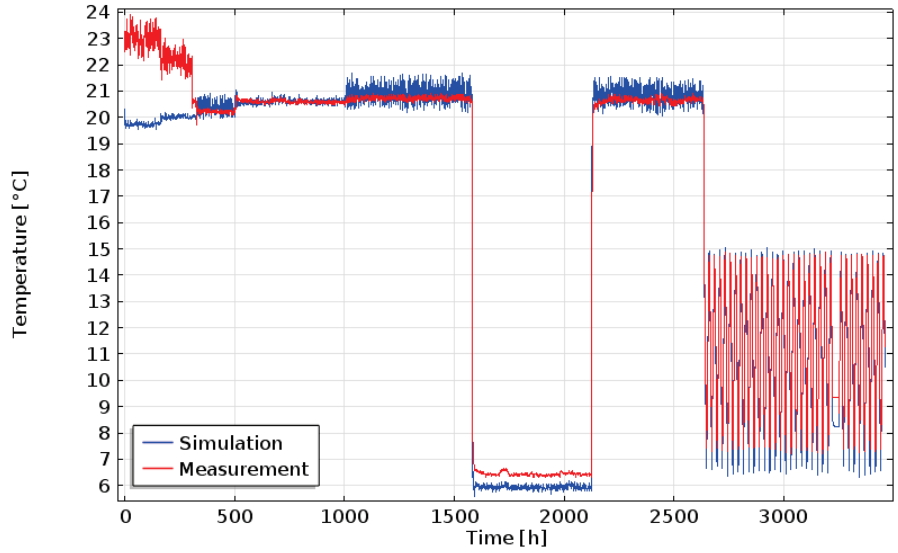

Figure D.38: Temperature [°C] at the external surface of wall configuration 4.

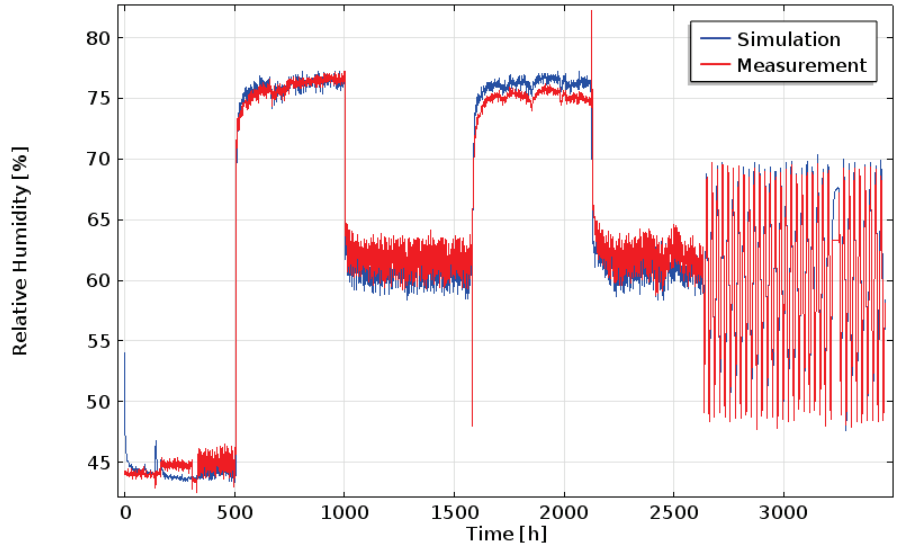

Figure D.39: Relative humidity [%] at the external surface of wall configuration 4.

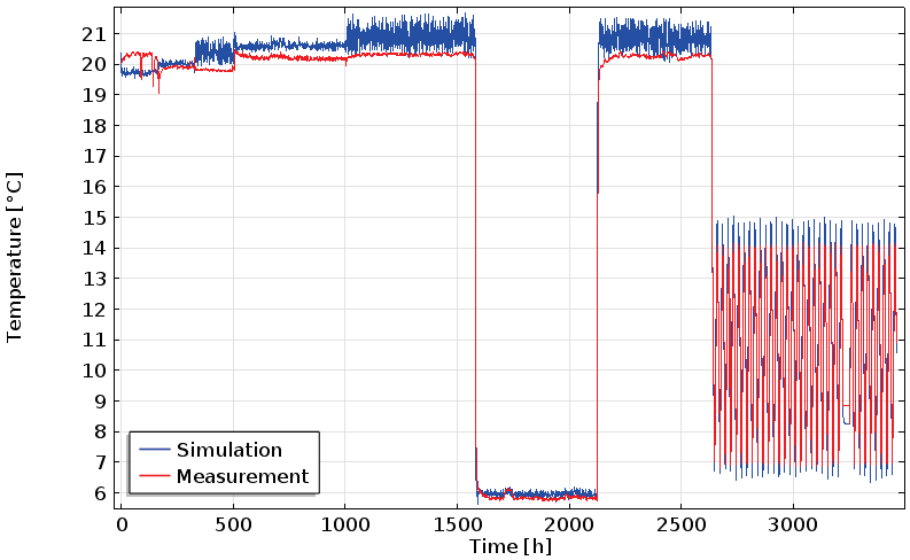

Figure D.40: Temperature [°C] at the depth 7 mm of wall configuration 4.

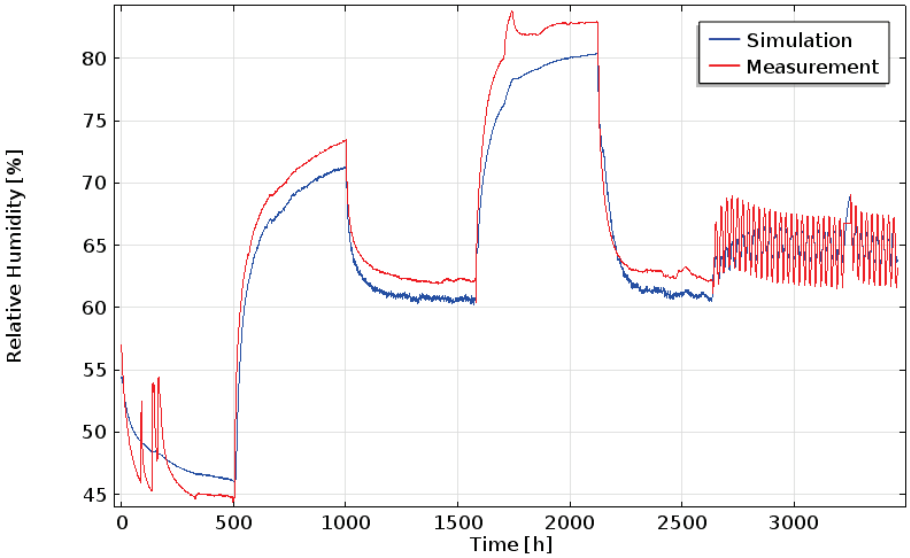

Figure D.41: Relative humidity [%] at the depth 7 mm of wall configuration 4.

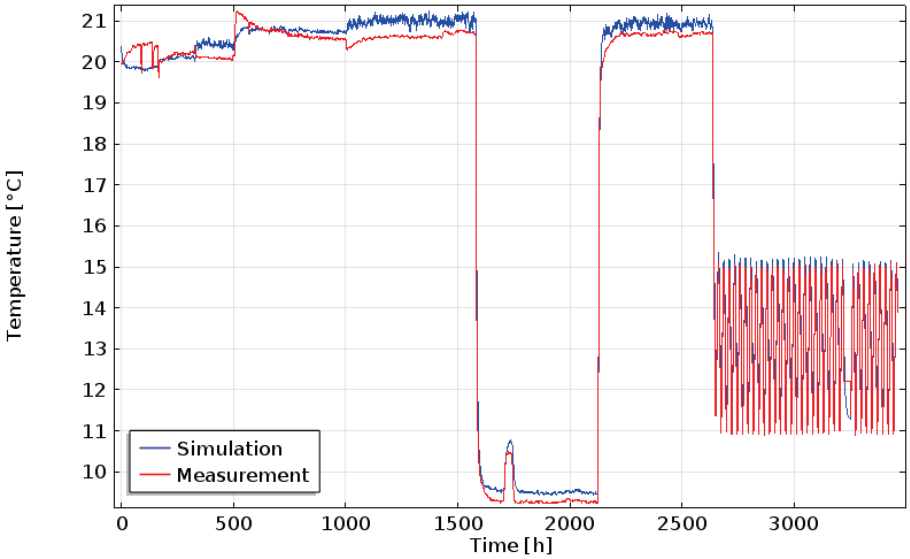

Figure D.42: Temperature [°C] at the depth 47 mm of wall configuration 4.

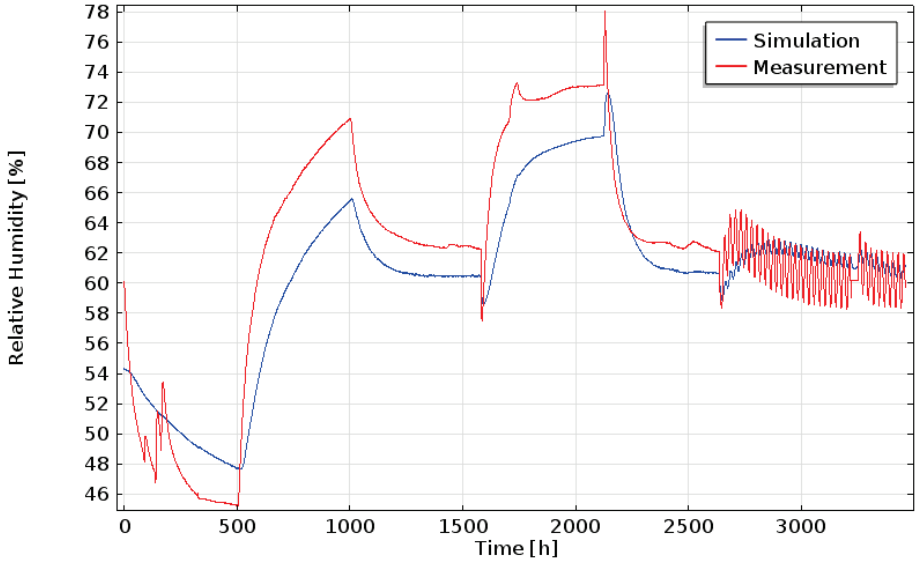

Figure D.43: Relative humidity [%] at the depth 47 mm of wall configuration 4.

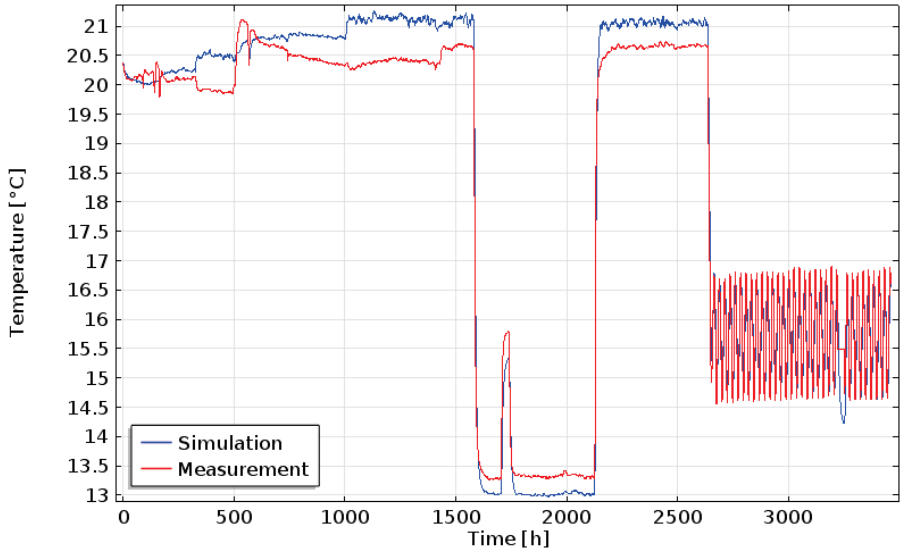

Figure D.44: Temperature [°C] at the depth 87 mm of wall configuration 4.

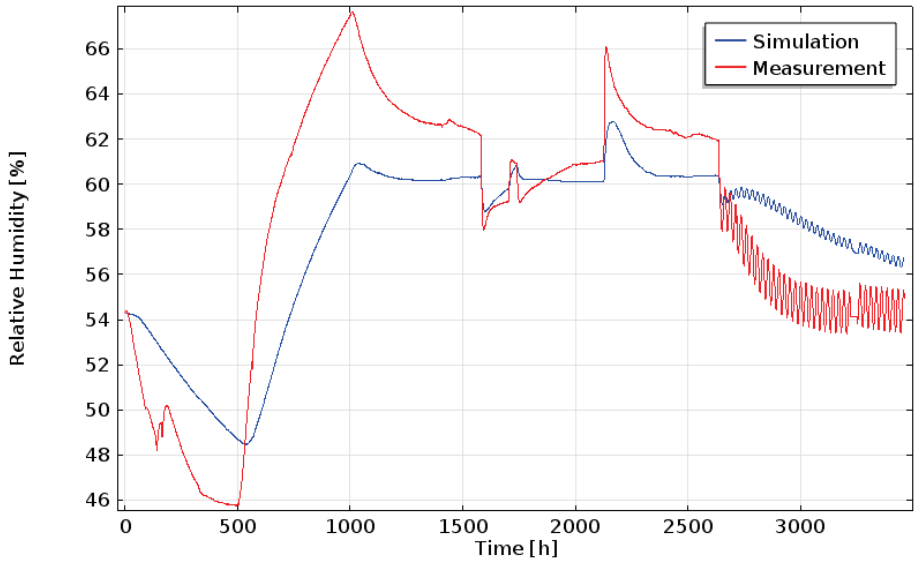

Figure D.45: Relative humidity [%] at the depth 87 mm of wall configuration 4.

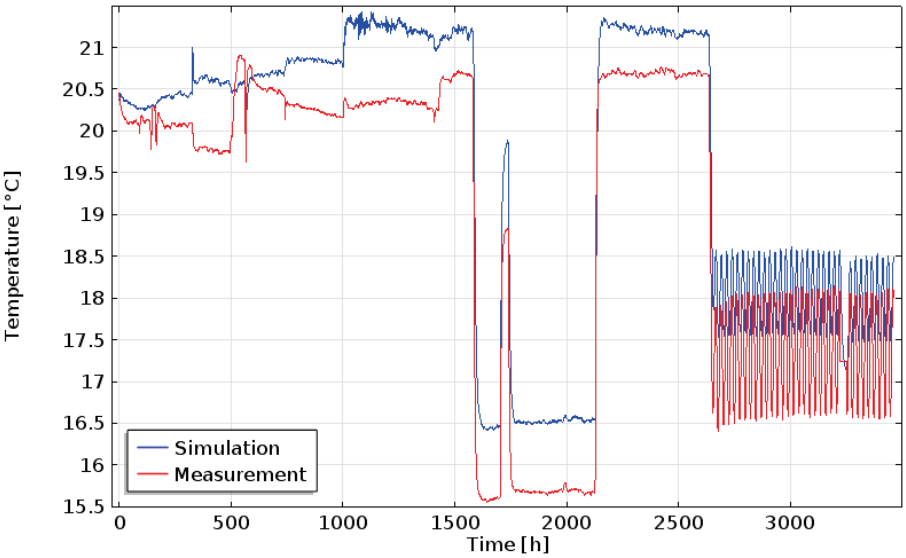

Figure D.46: Temperature [°C] at the depth 127 mm of wall configuration 4.

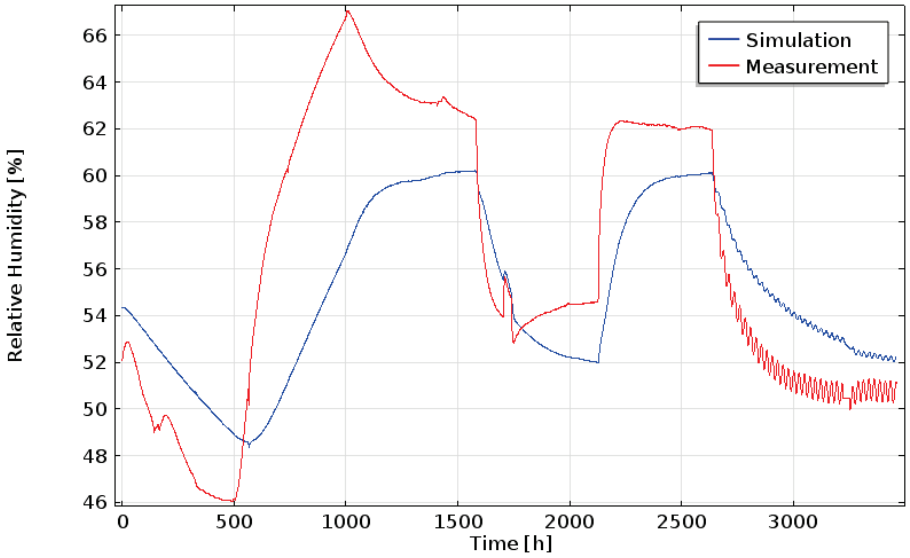

Figure D.47: Relative humidity [%] at the depth 127 mm of wall configuration 4.

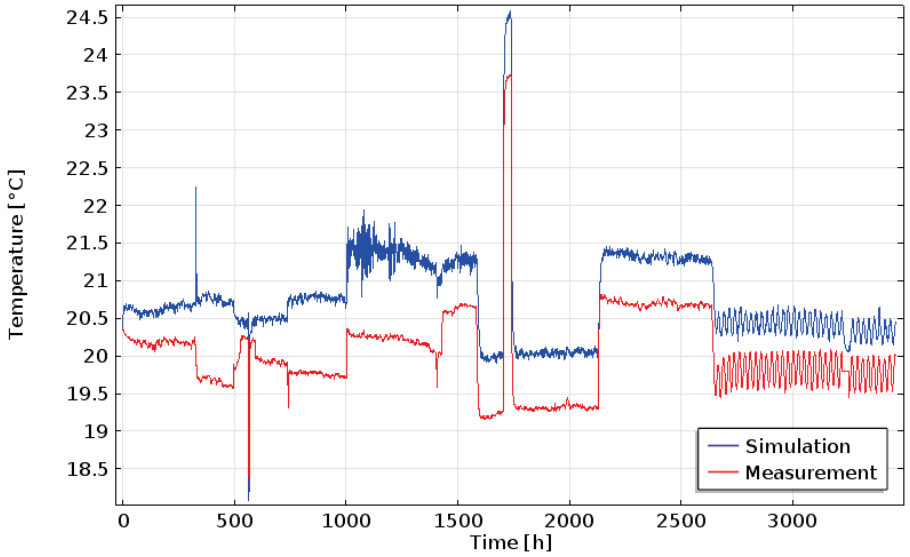

Figure D.48: Temperature [°C] at the depth 167 mm of wall configuration 4.

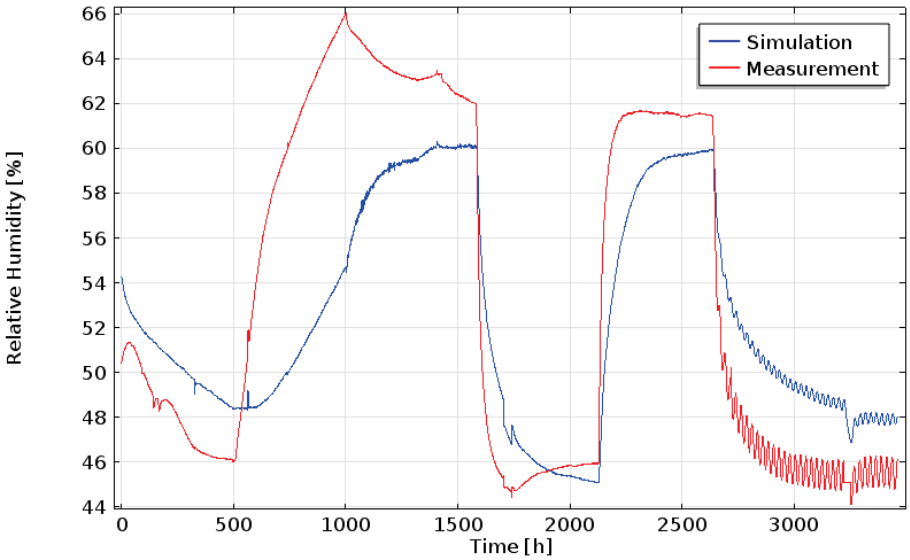

Figure D.49: Relative humidity [%] at the depth 167 mm of wall configuration 4.

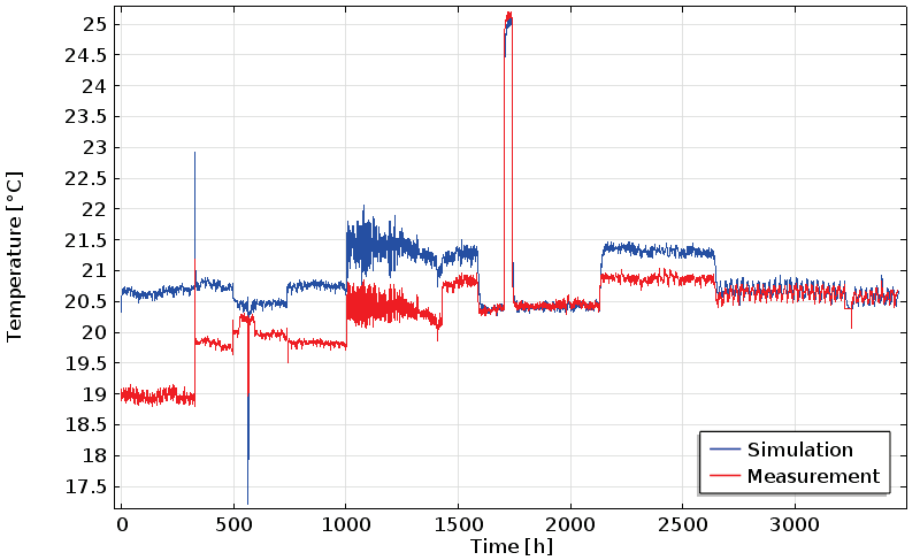

Figure D.50: Temperature [°C] at the indoor surface of wall configuration 4.

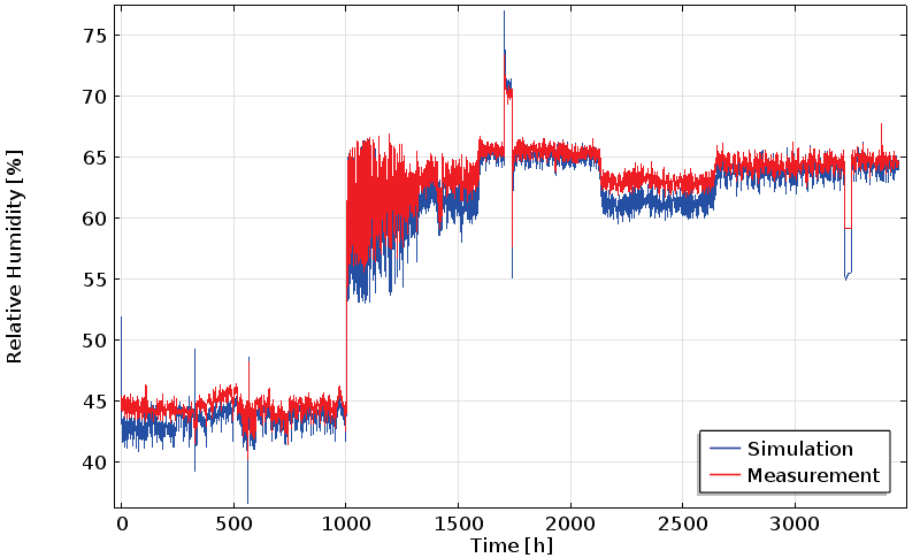

Figure D.51: Relative humidity [%] at the indoor surface of wall configuration 4.

Annex E – Additional data and results related to the school building in Estonia

In the measurement values there were some missing values, because the electricity supply to the sensors did not function during certain time slots. The gaps of the datasets were filled with values of the nearest existing values. The biggest gaps in the data are:

* The indoor temperature between 8123 hours and 8267 hours is missing and filled with 21°C.
* At the same time slot of the indoor relative humidity these values are filled with 59%.
* At the same time slot at the air pressure difference, it is used 0 Pa.
* The values of 695 hours and 852 hours the indoor RH were missing and filled with 50%.
* The time slots between 18/04/2013 at 11:00 and 24/04/2013 at 12:00 of all parameters were missing.

The existing wall consists of bricks, plasters and peat; while the later applied insulation materials are Polyisocyanurate (PIR), Polyurethane board with capillary-active channels (IQ-T), Autoclaved Aerated Concrete (AAC) and Calcium Silicate (CaSi). The material properties can be found in tables E.1 and E.2.

Table E.1: Material properties of the exterior plaster, brick, peat and interior plaster from [Klõšeiko et al. 2015] and the heat capacity from Delphin.

Exterior Plaster					
Dry bulk density kg/m3	1270				
	RH (%)	0	33	75	≥93
Thermal conductivity W/(m·K)		0.55	0.56	0.58	0.59
Moisture content [kg/m3]			11	57	75
Water vapor resistance factor μ		12	12	14	14
Heat capacity (J/kg·K)	950				
Brick					
Dry bulk density kg/m3	1800				
	RH (%)	0	33	75	≥93
Thermal conductivity W/(m·K)		0.7	0.7	0.7	0.71
Moisture content [kg/m3]			4.8	6.4	13
Water vapor resistance factor μ		25	25	25	26
Heat capacity (J/kg·K)	788				
Peat					
Dry bulk density kg/m3	150				
	RH (%)	0	33	75	≥93
Thermal conductivity W/(m·K)		0.09	0.09	0.09	0.09
Moisture content [kg/m3]			9.1	18	42
Water vapor resistance factor μ		2	2	2	2
Heat capacity (J/kg·K)	850				
Interior Plaster					
Dry bulk density kg/m3	1800				
	RH (%)	0	33	75	≥93
Thermal conductivity W/(m·K)		0.82	0.82	0.83	0.83
Moisture content [kg/m3]			2.3	9.2	25
Water vapor resistance factor μ		12	12	13	13
Heat capacity (J/kg·K)	850				

Table E.2: Material properties of PIR, IQ-T, AAC and CaSi from [Klõšeiko et al. 2015] and the heat capacity from Delphin.

PIR					
Dry bulk density kg/m3	35				
	RH (%)	0	33	75	≥93
Thermal conductivity W/(m·K)		0.02	0.02	0.021	0.022
Moisture content [kg/m3]			0.49	0.96	4.4
Water vapor resistance factor μ		400	400	400	400
Heat capacity (J/kg·K)	1400				
IQ-T					
Dry bulk density kg/m3	49				
	RH (%)	0	33	75	≥93
Thermal conductivity W/(m·K)		0.029	0.029	0.029	0.03
Moisture content [kg/m3]			0.27	0.35	1.4
Water vapor resistance factor μ		51	51	51	51
Heat capacity (J/kg·K)	1400				
AAC					
Dry bulk density kg/m3	126				
	RH (%)	0	33	75	≥93
Thermal conductivity W/(m·K)		0.045	0.046	0.047	0.054
Moisture content [kg/m3]			1.3	3.4	16
Water vapor resistance factor μ		6	6	6	6
Heat capacity (J/kg·K)	1081				
CaSi					
Dry bulk density kg/m3	297				
	RH (%)	0	33	75	≥93
Thermal conductivity W/(m·K)		0.067	0.071	0.075	0.077
Moisture content [kg/m3]			16	21	26
Water vapor resistance factor μ		11	11	11	11
Heat capacity (J/kg·K)	1155				

The material properties from the material database of Delphin are used for the simulations, because that has led to the best results. In many cases, these material data were multiplied or divided by a value to get a better compliance with the material information in [Klõšeiko et al. 2015]. These are implemented in the Matlab-files.

No information about the air cavity is given in [Klõšeiko et al. 2015]; therefore, the material properties of the air cavity from the material-database of Delphin are used. The Delphin-database of materials gives the value 0.1 kg/(s·m·Pa) as air permeability for an air cavity. However, this value generates with the simple convection method always an error and stops the simulation. In the sophisticated convection method, this value generates big deviations with the measurements. Therefore, the air permeability of the air cavity is assumed 0.001 kg/(s·m·Pa).

Boundary conditions

The internal surface coefficient of heat transfer (h_i) is 5 W/(m^2·K) and the internal surface coefficient of vapor transfer (β_i) is 1.8382e-7 kg/(m^2·s·Pa). The external surface coefficient of heat transfer (h_e) is 20 W/(m^2·K) and the external surface coefficient of vapor transfer (β_e) is 5.8823e-8 kg/(m^2·s·Pa). The following graphs depict the boundary conditions used in the simulation.

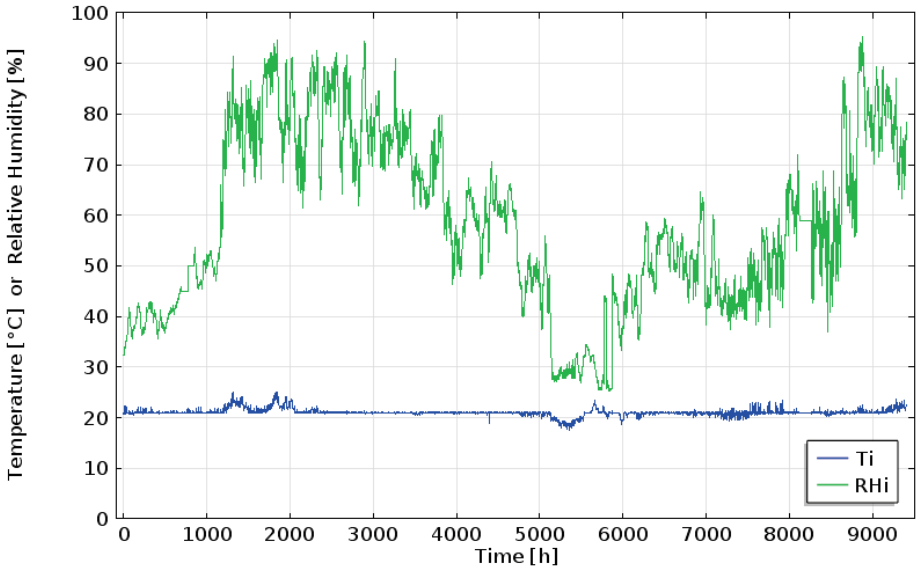

Figure E.1: Indoor temperature (Ti) and indoor relative humidity (RHi).

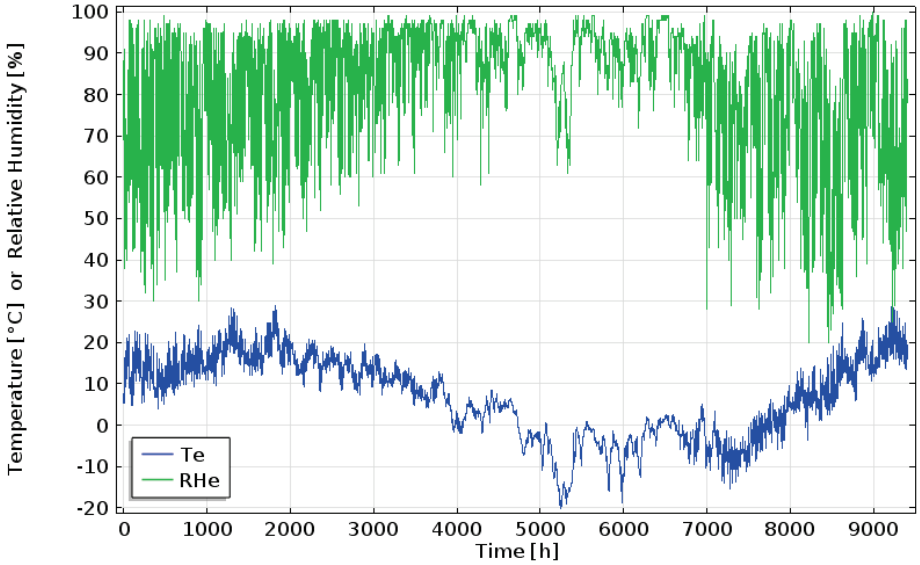

Figure E.2: Outdoor temperature (Ti) and outdoor relative humidity (RHi).

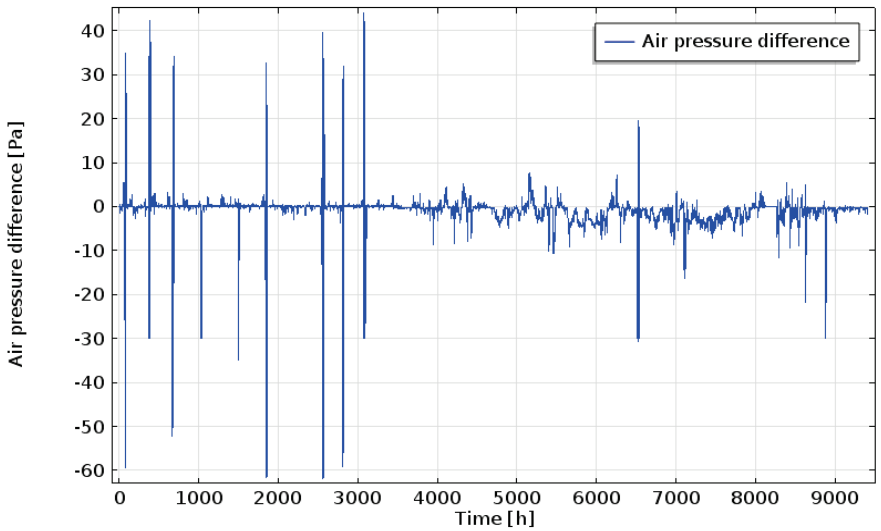

Figure E.3: Air pressure difference [Pa] between indoor and outdoor.

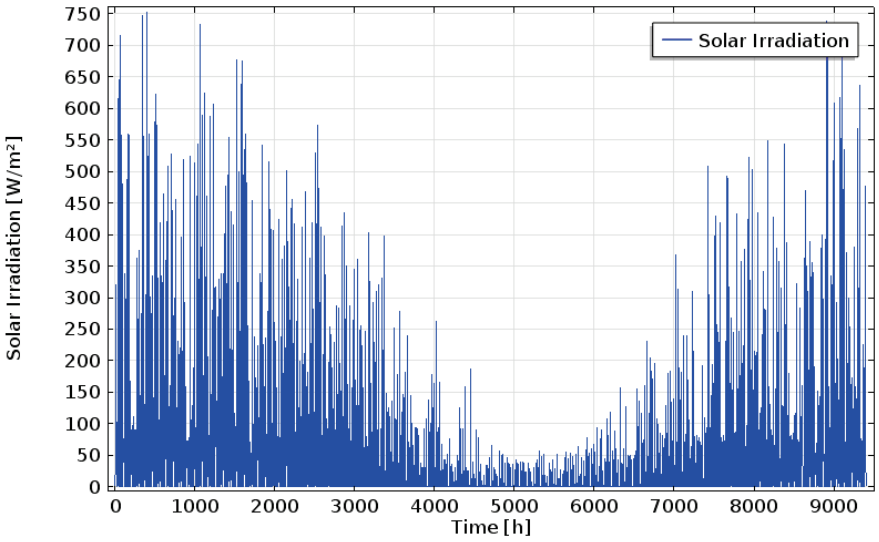

Figure E.4: Diffuse solar irradiation used in the simulation model.

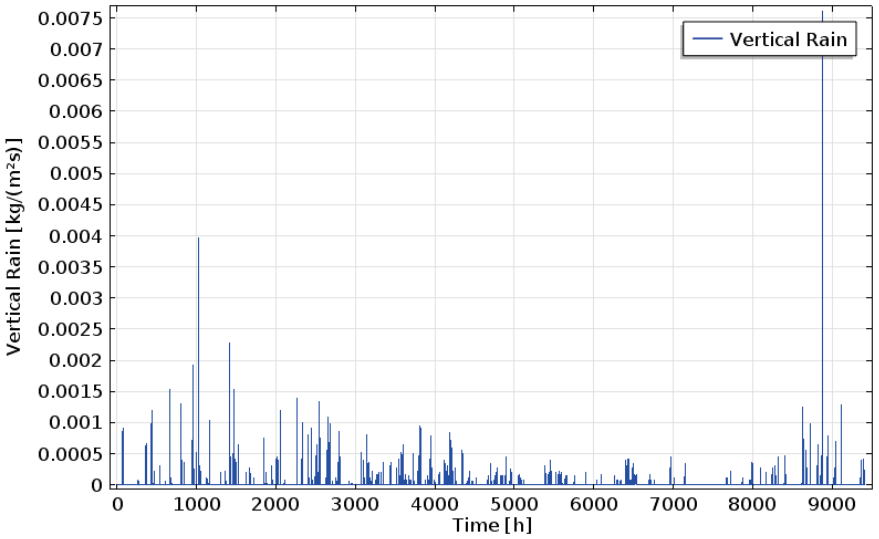

Figure E.5: Total vertical rain flux on a horizontal plane measure by the weather station in Narva.

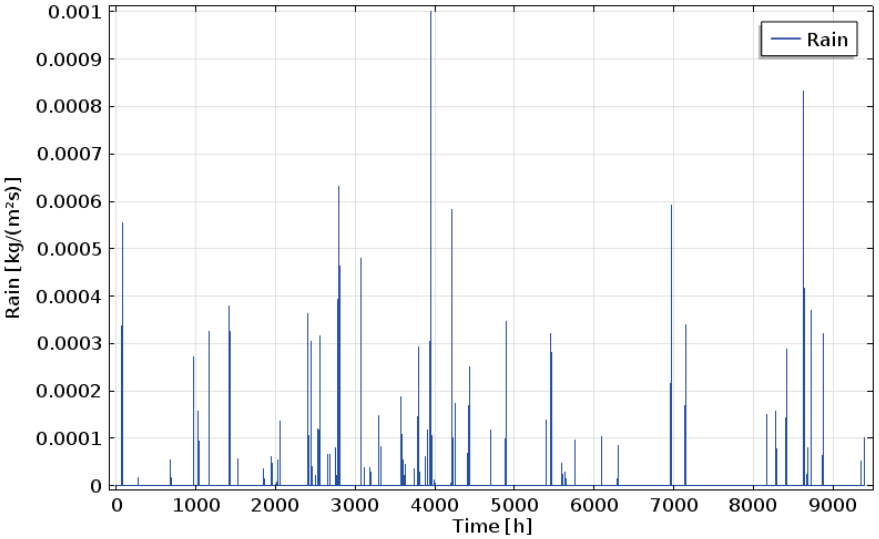

Figure E.6: Estimated horizontal wind-driven rain on the test wall.

Reference Wall (simple convection method)

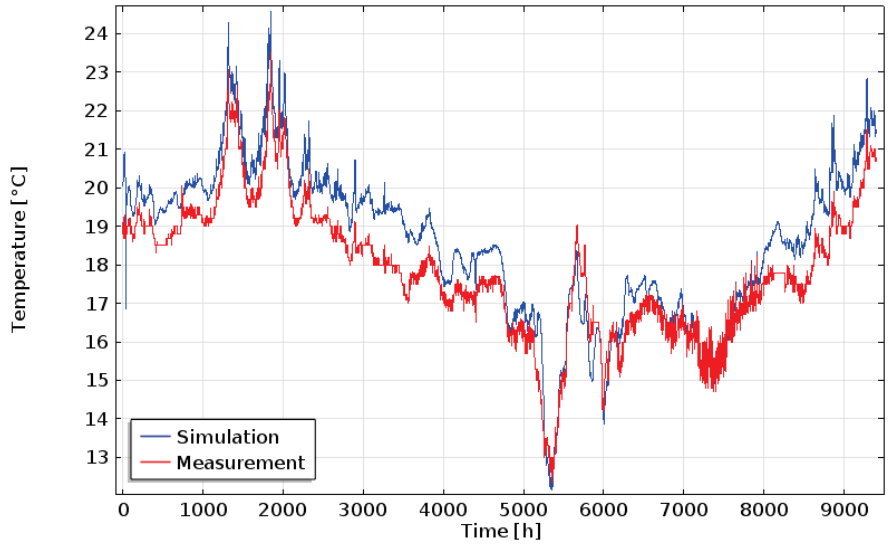

Figure E.7: Simulated and measured indoor surface temperature [°C] of the Reference wall.

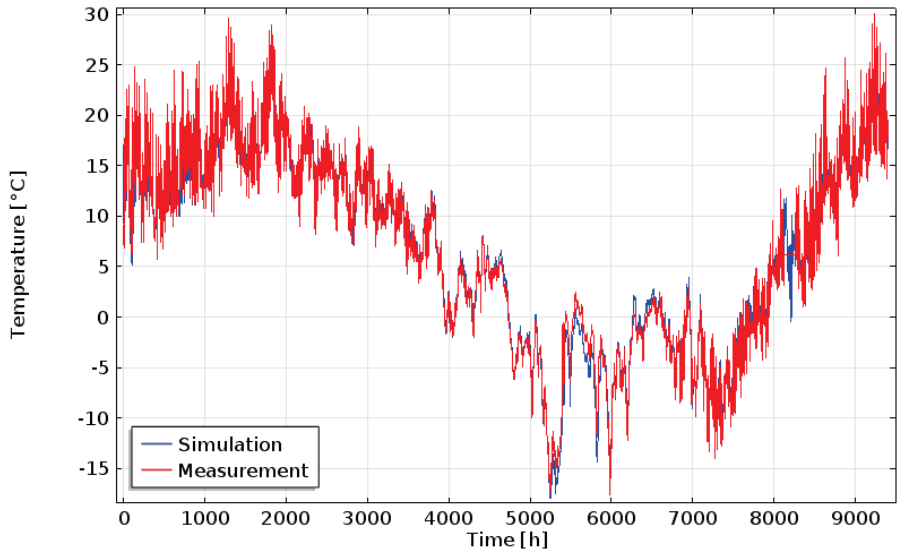

Figure E.8: Simulated and measured outdoor surface temperature [°C] of the Reference wall.

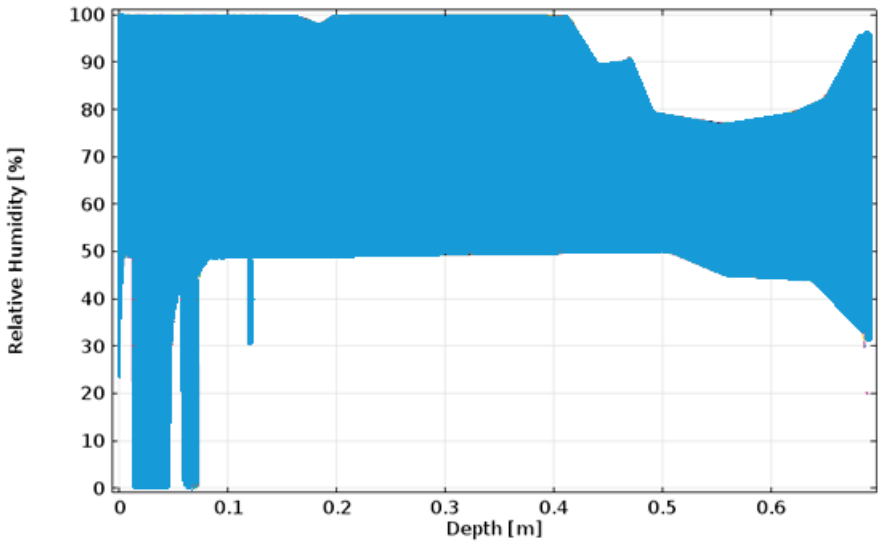

*Figure E.9: Simulated relative humidity range over depth of Reference Wall **including rain**.*

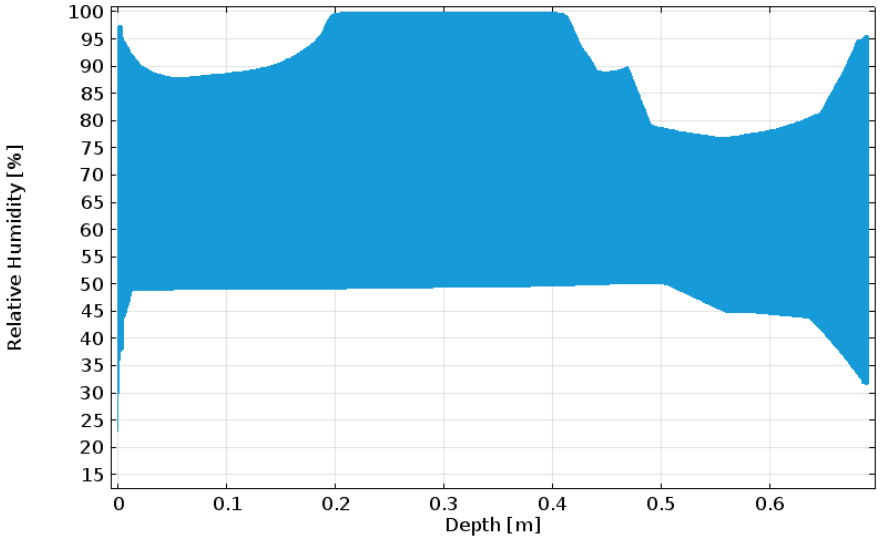

*Figure E.10: Simulated relative humidity range of the Reference Wall **without rain**.*

Temperature Ratio of the reference wall

The thermal resistance of the reference wall is determined with the material properties given by [Klõšeiko et al. 2015]. The thermal resistance of the cavity is assumed 0.17 (m^2·K)/W, in accordance with [Wit 2009].

$$R_l = \frac{1}{h_e} + \sum\left(\frac{d}{\lambda}\right) + \frac{1}{h_i} = \frac{1}{20} + \frac{0.01}{0.59} + \frac{0.25}{0.70} + 0.17 + \frac{0.12}{0.70} + \frac{0.09}{0.09} + \frac{0.12}{0.70} + \frac{0.01}{0.83} + \frac{1}{5} = 2.15$$

$$T_{si} = T_i - \frac{1/h_i}{R_l} \cdot \Delta T = 20 - \frac{0.20}{2.15} \cdot (20 - -20) = 16.19$$

$$f = \frac{T_{si} - T_e}{T_i - T_e} = \frac{16.19 - -20}{20 - -20} = 0.905$$

CaSi-configuration (sophisticated convection method)

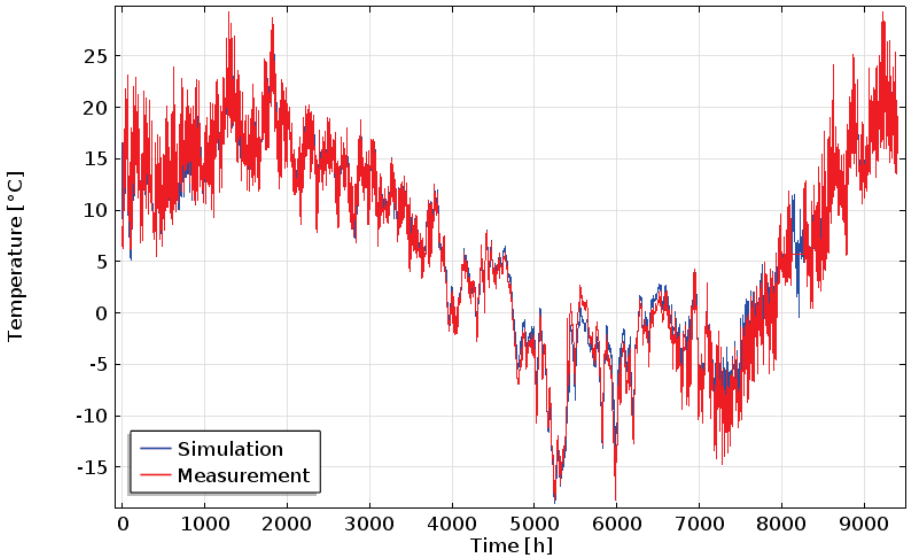

Figure E.11: Simulated and measured outdoor surface temperature [°C] of the CaSi-configuration.

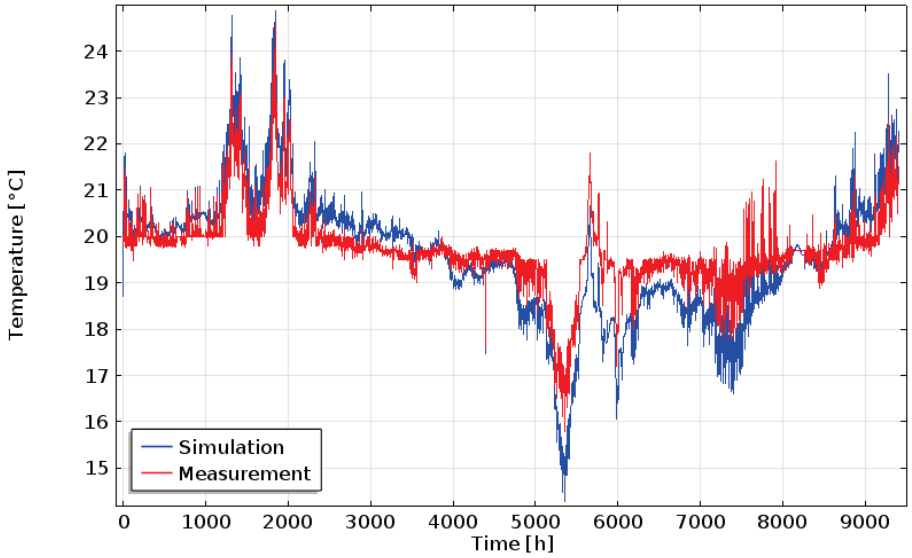

Figure E.12: Simulated and measured indoor surface temperature [°C] of the CaSi-configuration.

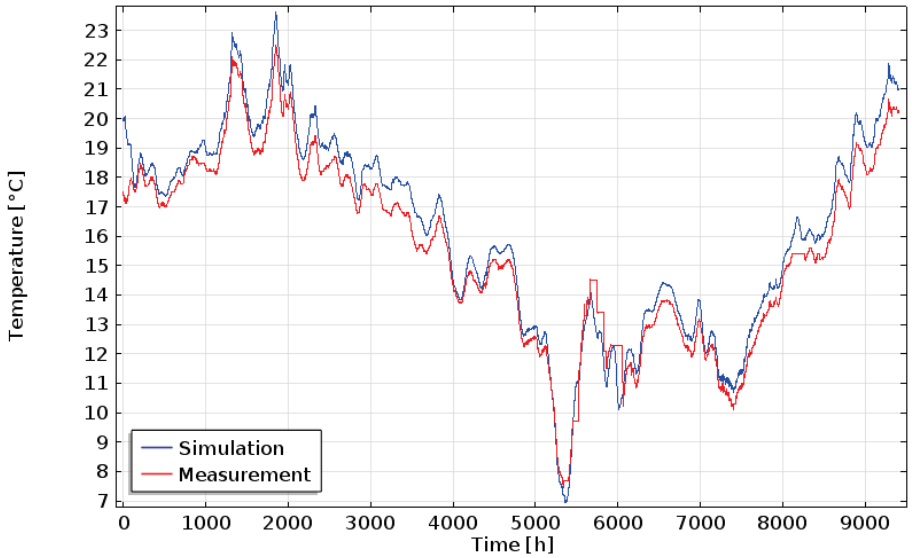

Figure E.13: Simulated and measured temperature [°C] at the interface of the CaSi-configuration.

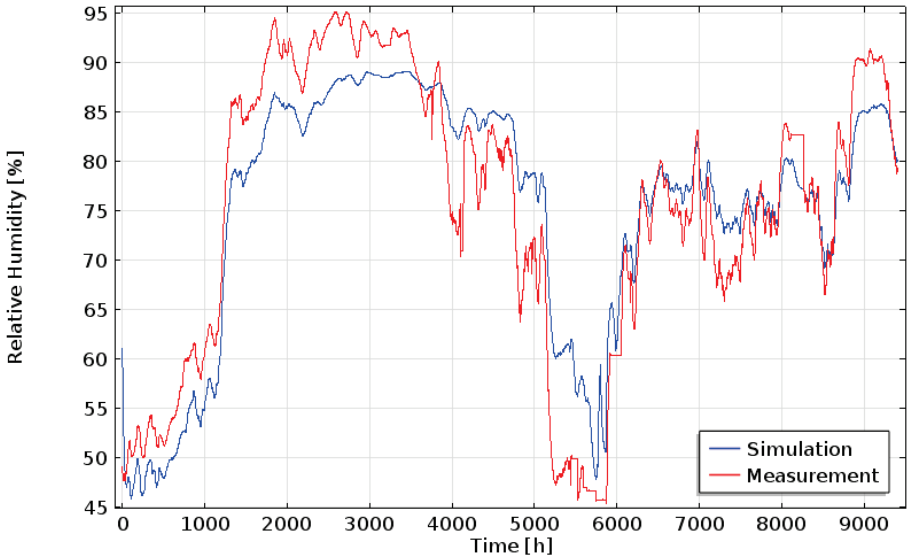

Figure E.14: Simulated and measured relative humidity at the interface of the CaSi-configuration.

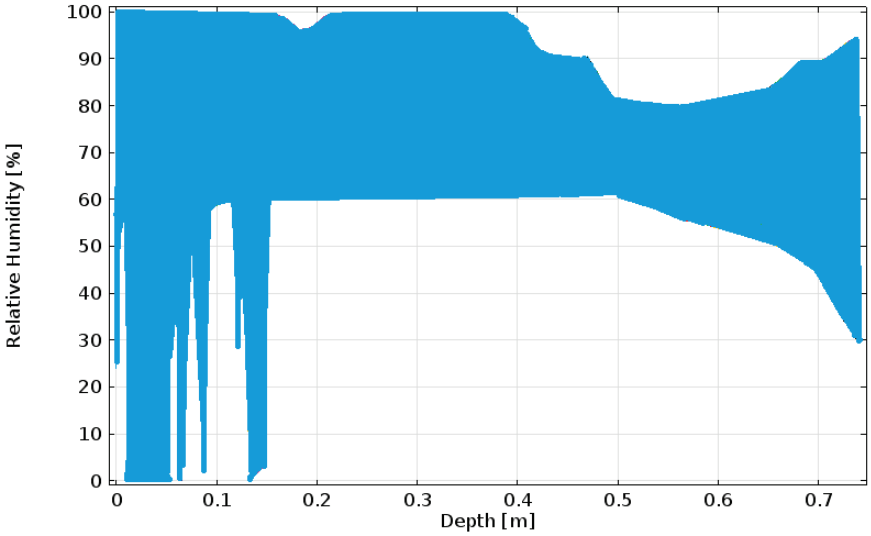

Figure E.15: Simulated relative humidity range of the CaSi-configuration when rain is included. Instability caused by rain, which caused a relative humidity of zero.

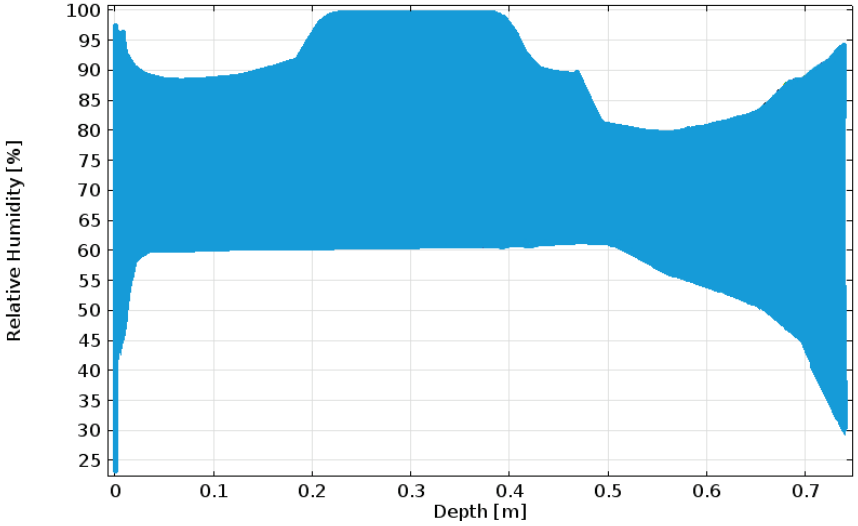

Figure E.16: Simulated relative humidity range of the CaSi-configuration ***without rain****.*

AAC-configuration (simple convection method)

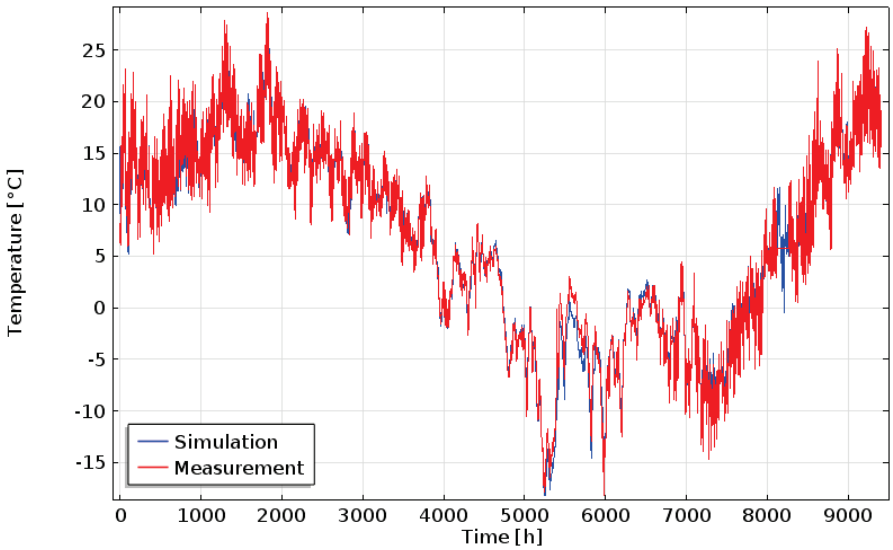

Figure E.17: Simulated and measured outdoor surface temperature [°C] of the AAC-configuration.

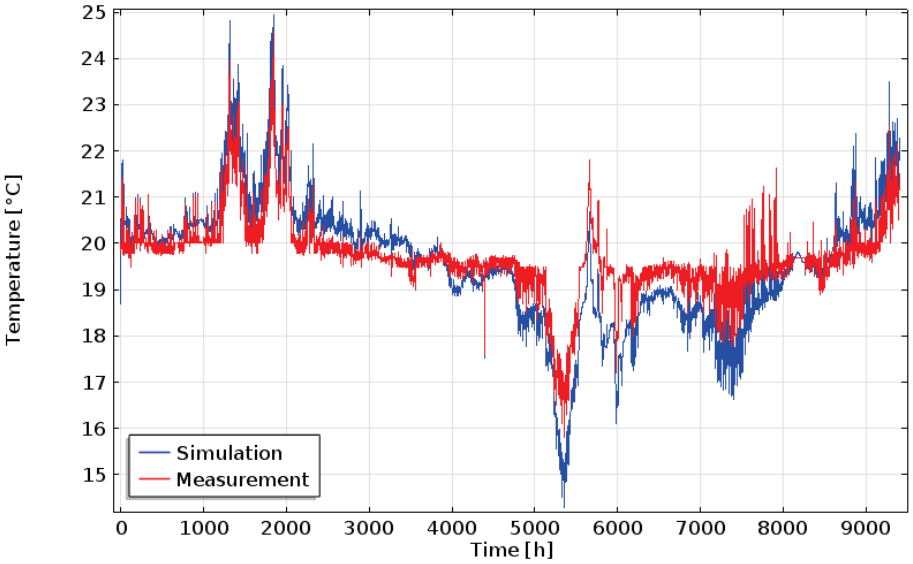

Figure E.18: Simulated and measured indoor surface temperature [°C] of the AAC-configuration.

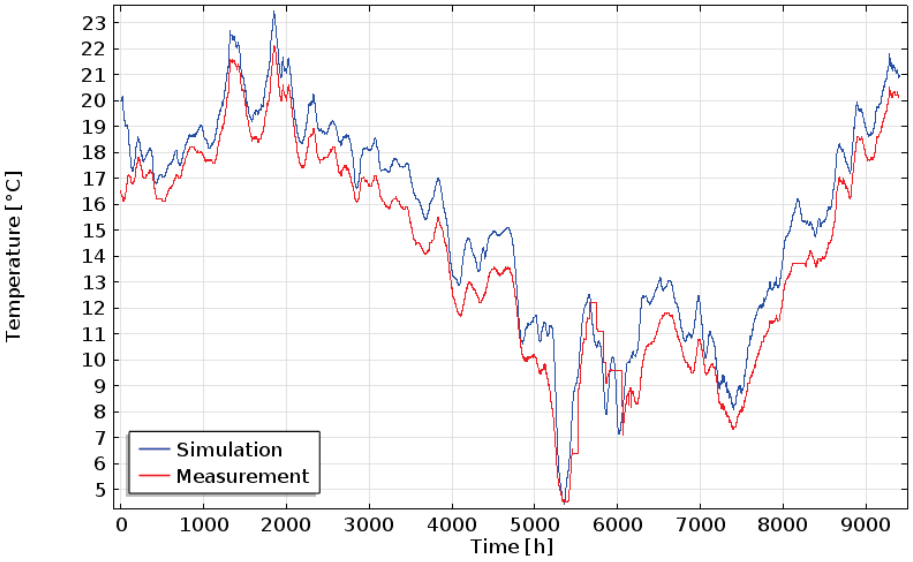

Figure E.19: Simulated and measured temperature [°C] at the interface of the AAC-configuration.

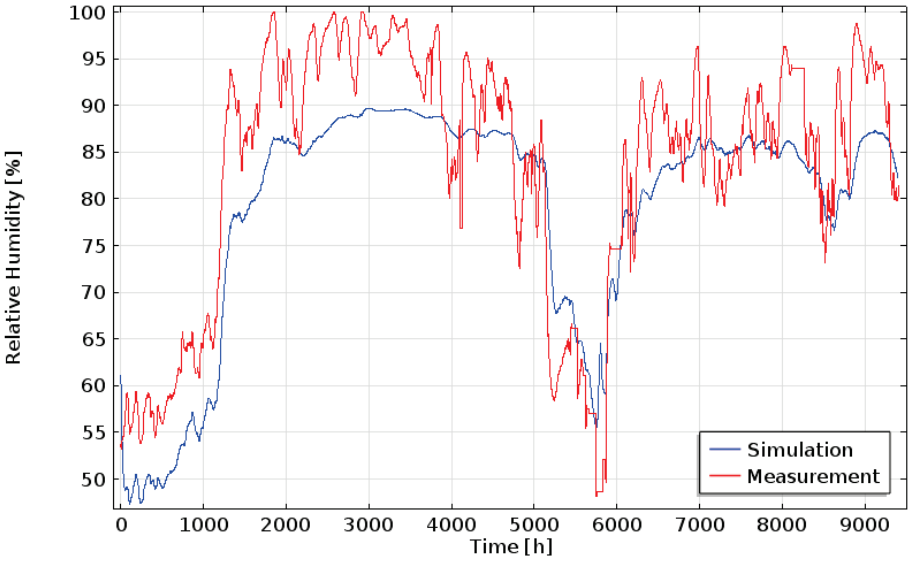

Figure E.20: Simulated and measured relative humidity [%] at the interface of the AAC-configuration.

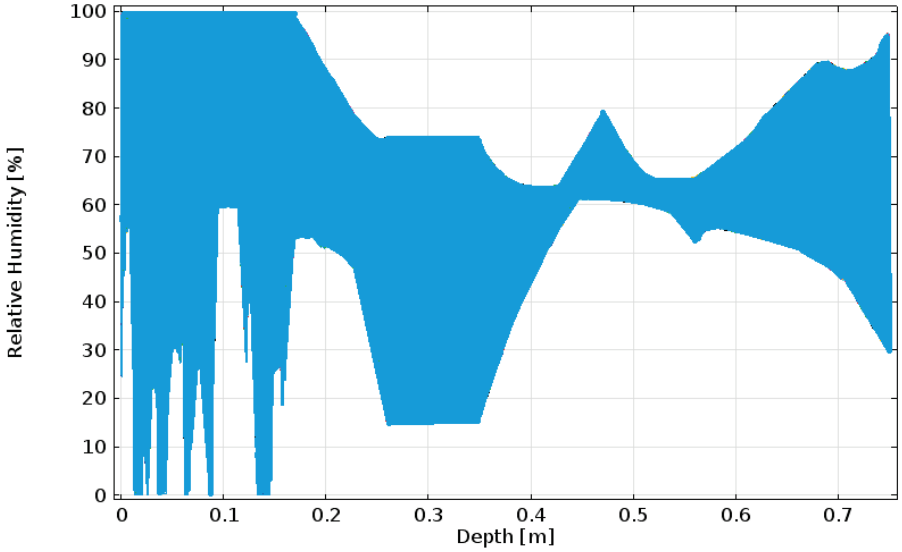

*Figure E.21: Simulated relative humidity range of the AAC-configuration **including rain**.*

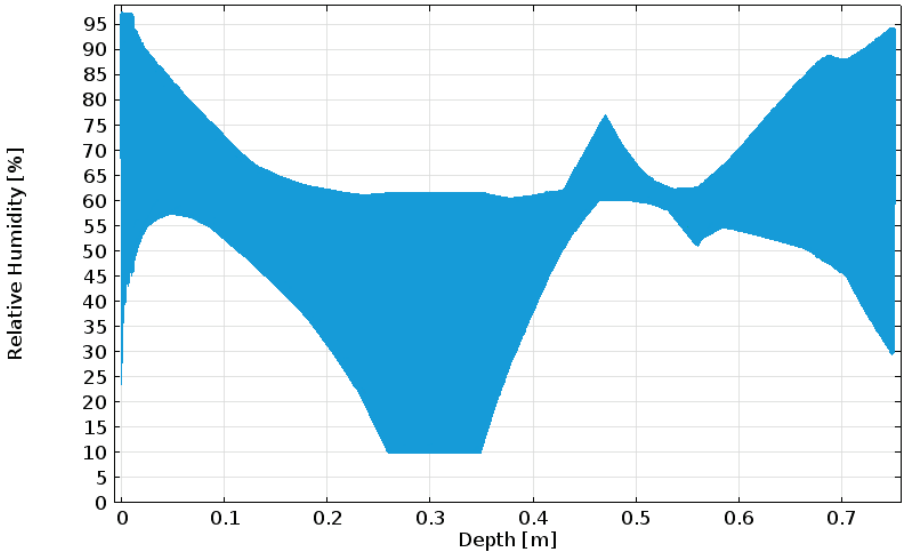

*Figure E.22: Simulated relative humidity range of the AAC-configuration **without rain**.*

IQ-T-configuration (sophisticated convection method)

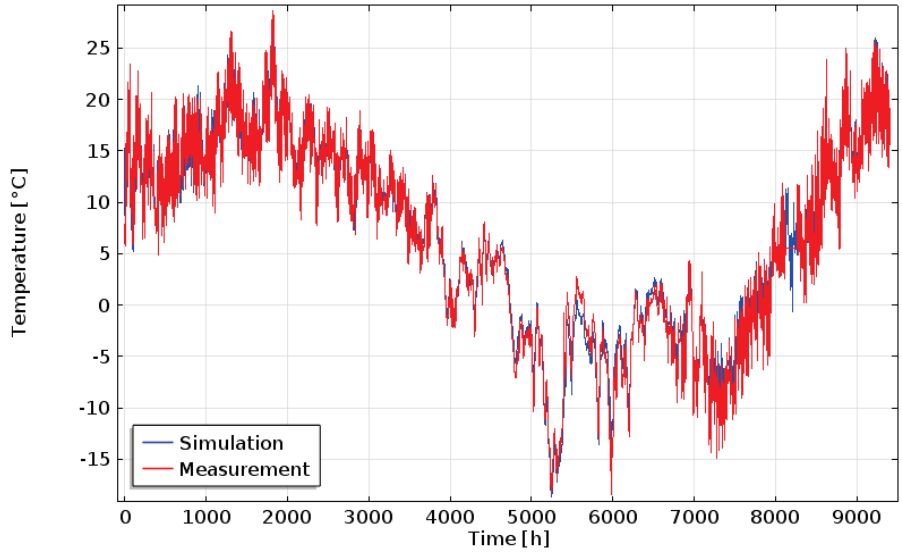

Figure E.23: Simulated and measured outdoor surface temperature [°C] of the IQ-T-configuration.

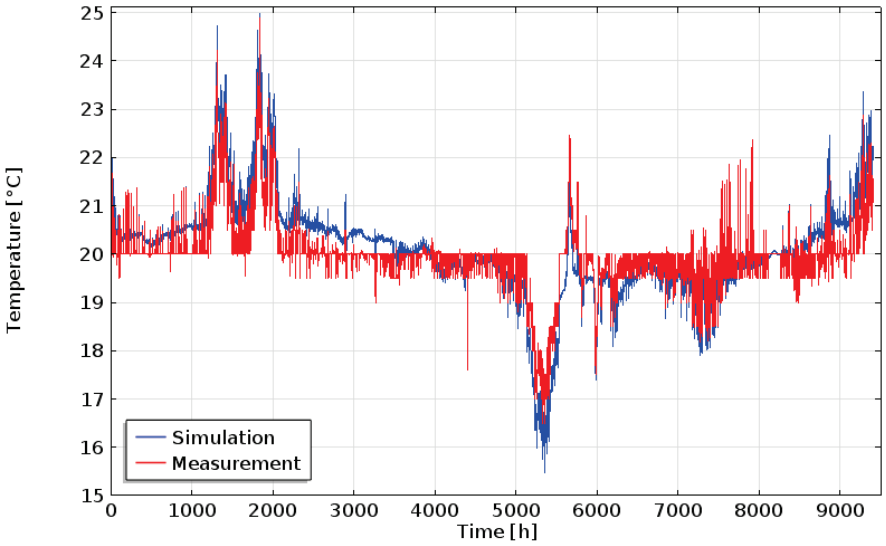

Figure E.24: Simulated and measured indoor surface temperature [°C] of the IQ-T-configuration.

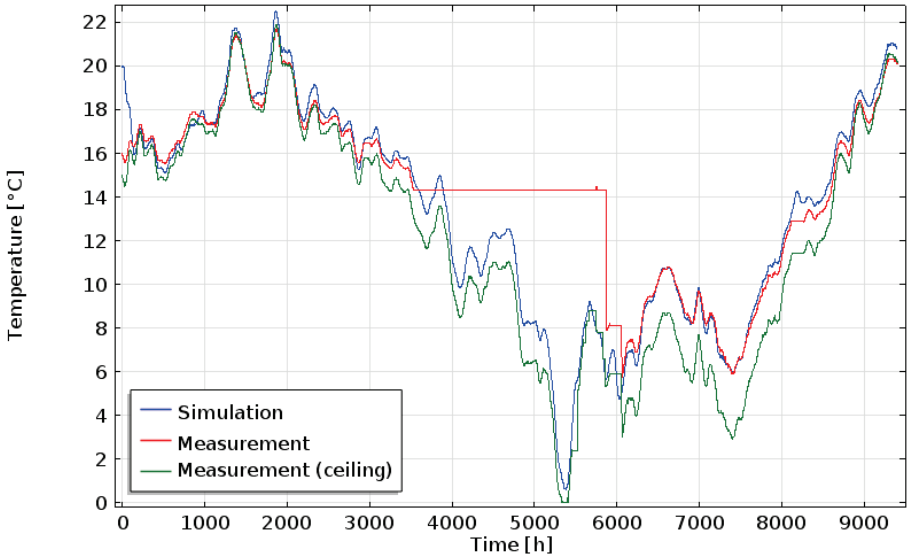

Figure E.25: Simulated and measured temperature [°C] at the interface of the IQ-T- configuration.

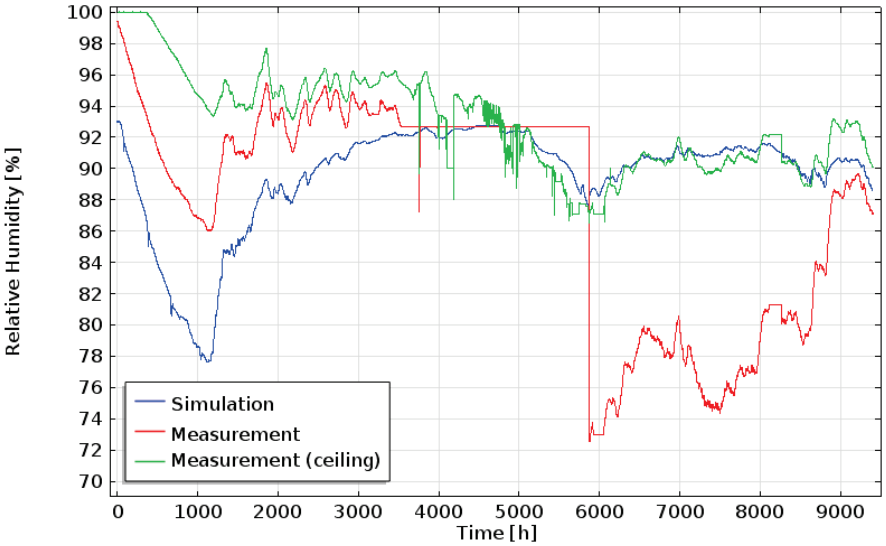

Figure E.26: Simulated and measured relative humidity at the interface of the IQ-T-configuration.

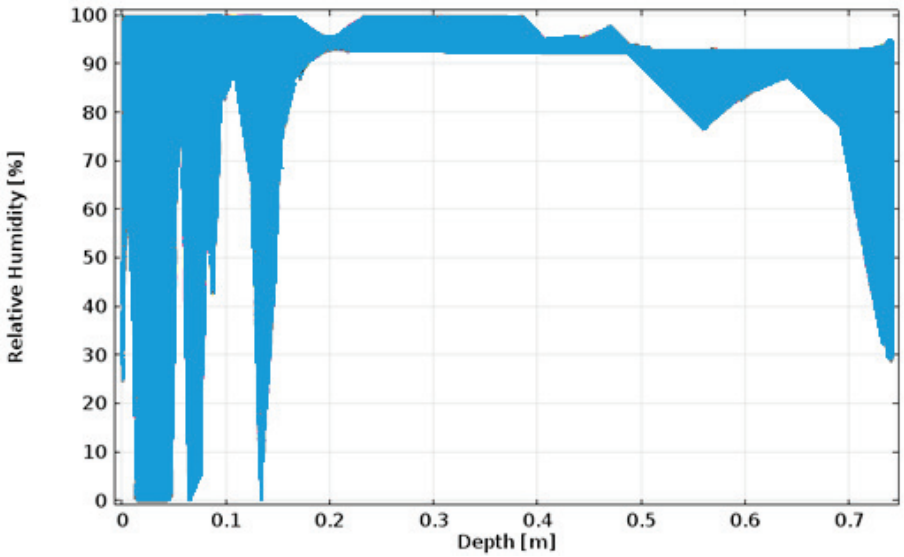

*Figure E.27: Simulated relative humidity range of the IQ-T-configuration **including rain**.*

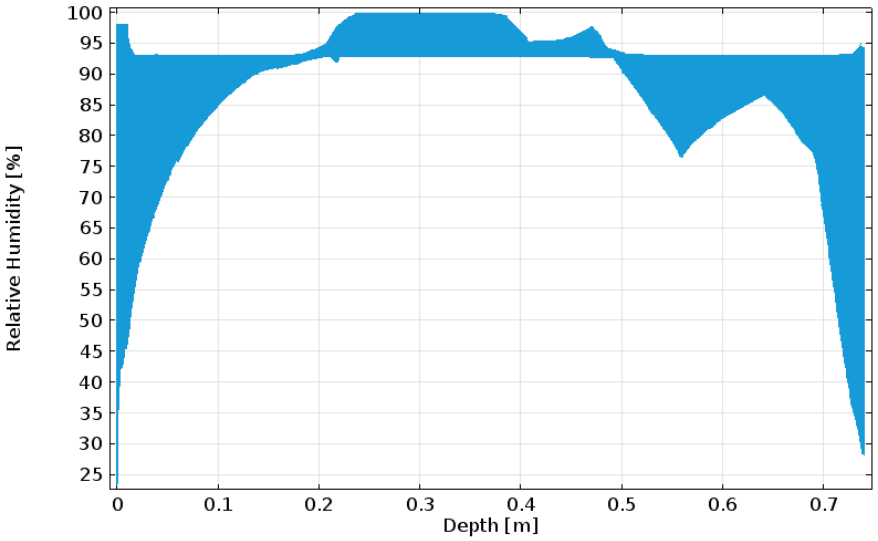

*Figure E.28: Simulated relative humidity range of the IQ-T-configuration **without rain**.*

PIR-configuration (sophisticated convection method)

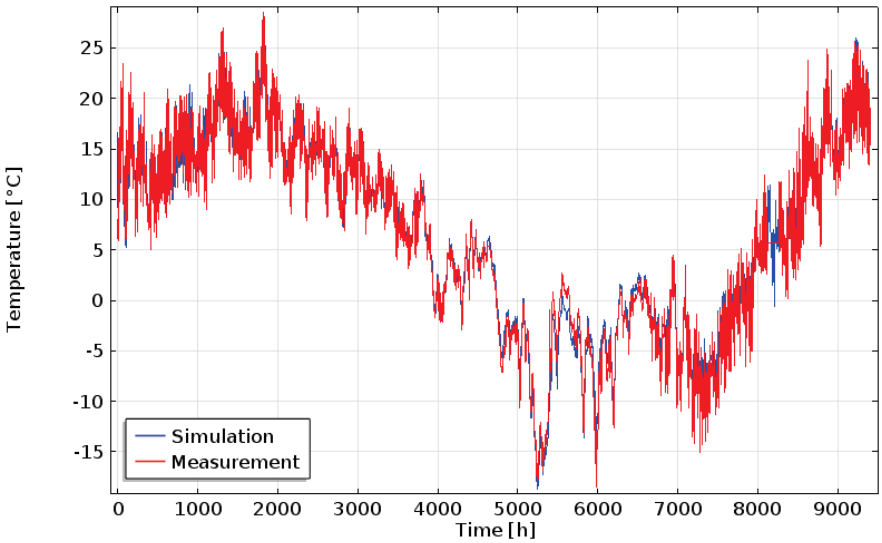

Figure E.29: Simulated and measured outdoor surface temperature [°C] of the PIR-configuration.

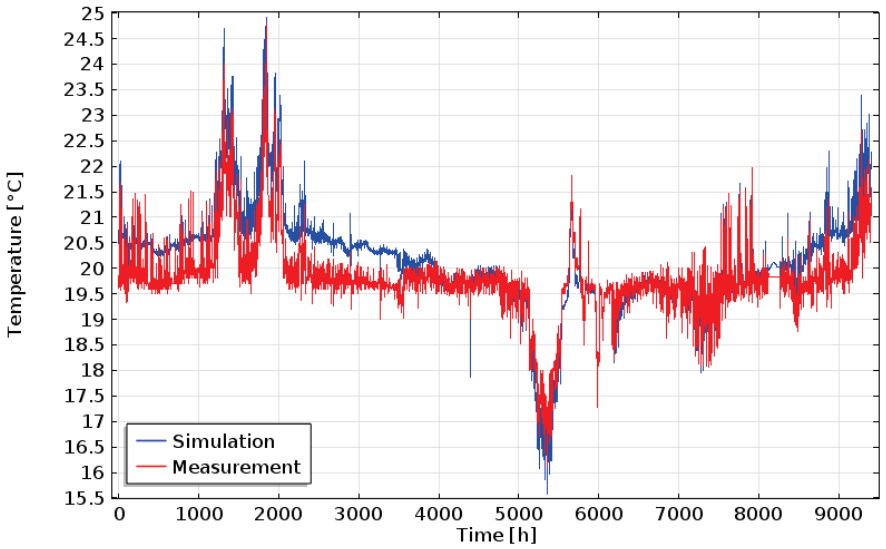

Figure E.30: Simulated and measured indoor surface temperature [°C] of the PIR-configuration.

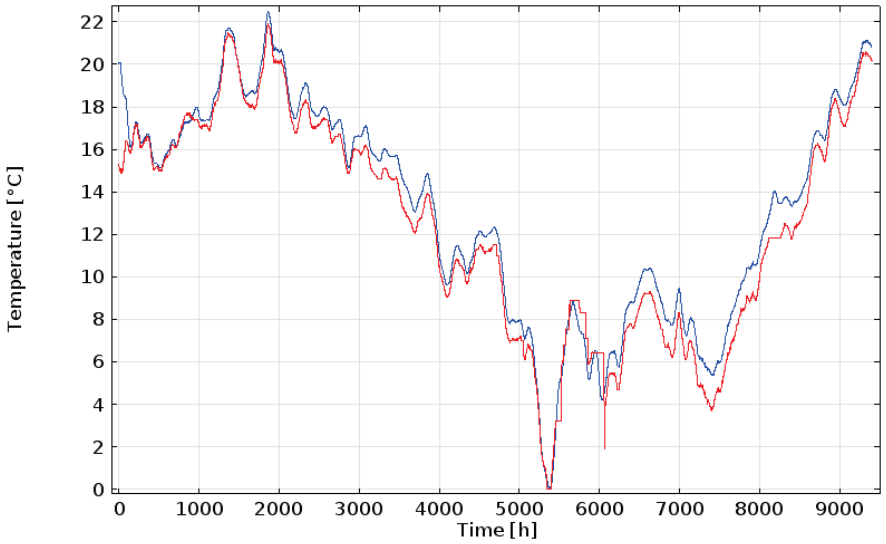

Figure E.31: Simulated and measured temperature [°C] at the interface of the PIR-configuration.

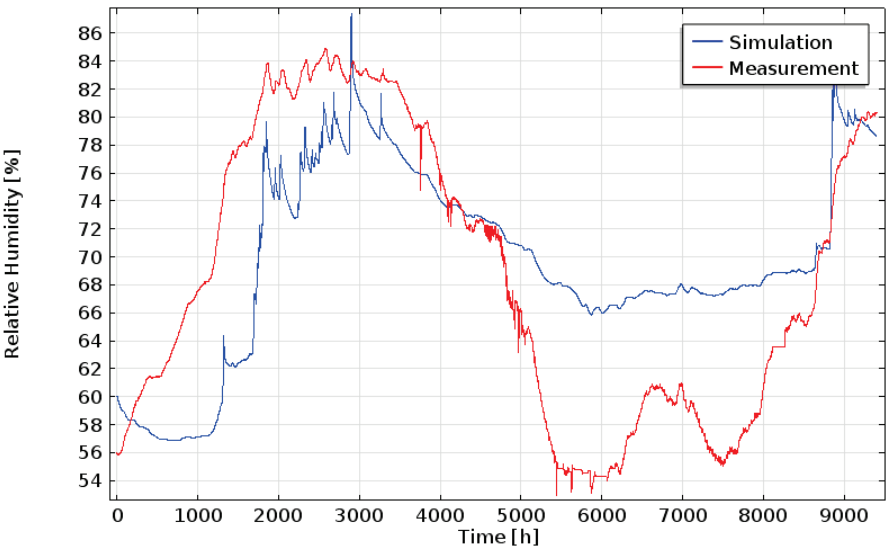

Figure E.32: Simulated and measured relative humidity [%] at the interface of the PIR-configuration.

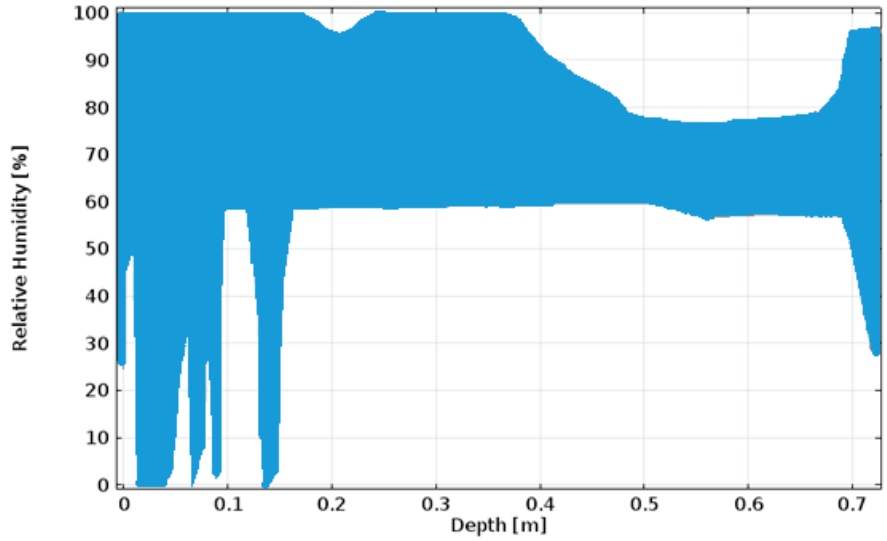

*Figure E.33: Simulated relative humidity range over depth of the PIR-configuration **including rain**.*

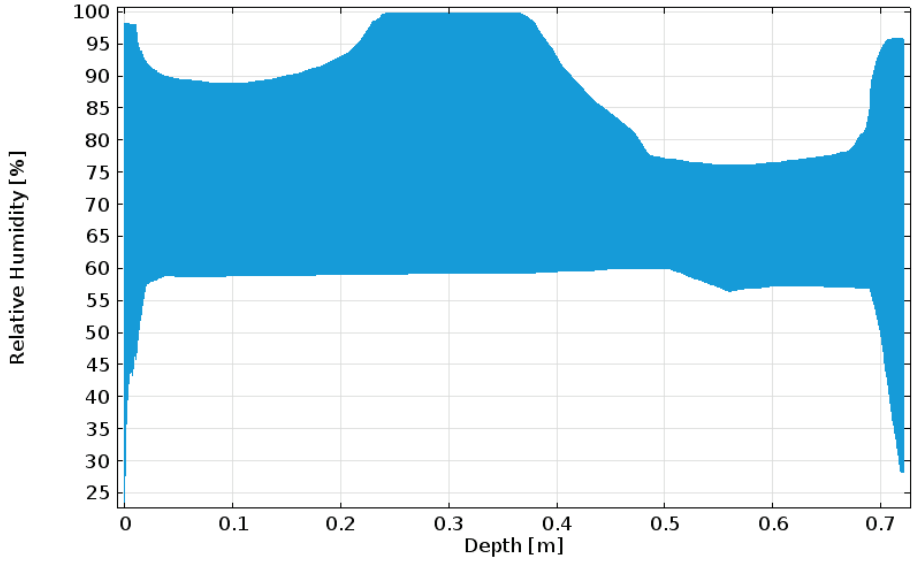

*Figure E.34: Simulated relative humidity range over depth of the PIR-configuration **without rain**.*